De la toupie sphérique à la toupie asymétrique

Maud Rotger

Laboratoire de Physique de l'Université de Bourgogne
UMR CNRS 5027

Habilitation à Diriger des Recherches

présentée par

Maud ROTGER

DE LA TOUPIE SPHERIQUE A LA TOUPIE ASYMETRIQUE

Soutenue le 17 décembre 2004, devant la commission d'examen composée de :

A. Perrin	Directeur de Recherches CNRS (Université Paris-Sud, Orsay)	*Rapporteur*
D. Bermejo	Professeur (Instituto de Estructura de la Materia, Madrid)	*Rapporteur*
J. Demaison	Directeur de Recherches CNRS (Université de Lille 1, Lille)	*Rapporteur*
A. Barbe	Professeur (Université de Reims Champagne-Ardenne, Reims)	*Examinateur*
J.-P. Bellat	Professeur (Université de Bourgogne, Dijon)	*Examinateur*
H.-R. Jauslin	Professeur (Université de Bourgogne, Dijon)	*Examinateur*
G. Millot	Professeur (Université de Bourgogne, Dijon)	*Examinateur*

Remerciements

Je tiens à remercier l'ancien directeur H. Berger et l'actuel directeur J.-P. Champion pour leur accueil au sein de ce laboratoire, initialement Laboratoire de Spectromètrie Moléculaire et Instrumentation Laser, devenu depuis 1995 Laboratoire de Physique de l'Université de Bourgogne.

J'adresse mes plus vifs remerciements à H.-R. Jauslin pour son chaleureux accueil au sein de l'équipe "Spectroscopie et Dynamique Moléculaire" ainsi qu'à tous les autres membres de ce groupe.

Plus particulièrement, j'ai beaucoup interagi ces dernières années avec V. Boudon et M. Loëte, mes proches collaborateurs. Je les remercie tous les deux pour leurs conseils et leur soutien constant. Je tiens aussi à remercier Ch. Wenger pour son aide en informatique.

Je remercie R. Saint-Loup et M. Chapuis pour m'avoir aidé à la mise en place de certaines expériences ainsi que les électroniciens S. Pernot et B. Sinardet.

Au cours de ces nombreuses années, j'ai demandé toutes sortes de services aux personnels de l'atelier de mécanique du Laboratoire et je les remercie tous de m'avoir aidée de leur mieux et souvent très rapidement. Une intention particulière à André Javelle, Pierre Michaux et Jean-Marc Müller.

Merci à W. Raballand (stagiaire de DEA puis thésard) dont le travail a permis la mise en place d'une nouvelle thématique.

Ce travail est aussi le fruit de nombreuses collaborations avec des expérimentateurs et des théoriciens. Il n'a été possible que grâce à l'aide de nombreux spectroscopistes et chimistes nationaux (D. Avignant, J. Demaison, J.-M. Flaud, F. Herlemont, J.-M. Simon, ...) et internationaux (J. Breidung, H. Bürger, A. Fayt, M. Quack, W. Thiel, ...) et mille excuses à ceux que j'ai oublié de citer.

Finalement, je remercie les membres de ce jury et plus particulièrement les rapporteurs. Je suis très flattée de la présence de tous dans ce jury.

Table des matières

Première partie

Introduction

Ce rapport d'habilitation présente une synthèse de mes activités de recherche au cours des quatorze dernières années. En effet, à la rentrée 1990, j'ai été nommée Maître de Conférences au laboratoire et me suis tournée vers la spectroscopie expérimentale après une thèse portant sur les cavités lasers. J'ai donc effectué une reconversion thématique avant d'entamer de véritables recherches en spectroscopie.

La deuxième partie de ce document est un *curriculum vitæ* qui résume mes activités d'enseignement et de recherche. En enseignement, j'essaie de faire ressortir l'investissement personnel tant sur le plan pédagogique (rédaction de fascicules, mise en place de nouveaux cours, ...) que sur le plan de la gestion de l'enseignement (coordinatrice du L2, co-responsable des emplois du temps de L2, responsabilités de TP, ...). En recherche, je retrace mon parcours scientifique en insistant sur les étapes préliminaires qui m'ont permis d'ouvrir des voies nouvelles (toupies quasi-sphériques et molécules piégées dans des solides) tout en m'appuyant sur les compétences dijonnaises. Je termine en citant toutes les collaborations nationales et internationales que ce travail m'a permis d'établir et qui m'ont beaucoup enrichie sur le plan scientifique.

Les troisième, quatrième et cinquième parties de ce rapport sont dédiées aux sujets de recherche et à la présentation des résultats. La troisième partie est essentiellement expérimentale et retrace le début de mon activité en spectroscopie. Les deux autres parties exposent les nouvelles voies principalement théoriques que j'ai personnellement explorées. La dernière partie débutée depuis la rentrée 2002 est encore peu détaillée ici. D'une façon générale, ces activités sont un mélange de théorie et d'expériences. L'ensemble de ces résultats est présenté ici sous la forme de treize articles que je considère comme les plus représentatifs de mon activité de recherche (période 1991–2004). Mon apport personnel le plus important a été sur la thématique des toupies quasi-sphériques. Il s'agissait aussi bien d'crire les différents modèles, que de mettre au point les programmes que de tester les prédictions sur des données expérimentales. Ce fut un travail ardu du fait de ma formation essentiellement expérimentale mais néanmoins passionnant. La thématique sur les molécules piégées dans les solides a été confiée essentiellement à W. Raballand. Elle n'en est qu'à ses débuts, notamment avec l'étude de l'effet Stark dans les molécules asymétriques. C'est une voie inter-disciplinaire avec des possibilités d'applications nombreuses notamment en dépollution de l'air. Ces deux nouvelles voies s'appuient sur les techniques dijonnaises utilisées depuis longtemps au laboratoire et sans lesquelles ce travail n'aurait pu voir le jour. Il s'agit essentiellement de tout ce qui a été développé théoriquement à Dijon au sujet des toupies sphériques et dont ce travail est une extension.

Enfin, la dernière partie récapitule l'ensemble de ma production scientifique. J'y distingue les articles dans des revues à comité de lecture (P), les actes de colloques (A), les conférences invitées (I), les posters présentés lors de colloques (C), les communications orales présentées lors de colloques (O) et enfin les séminaires (S).

Deuxième partie

Curriculum Vitæ

I – Etat civil

Nom, Prénom : Rotger-Languereau, Maud.
Née le : 29 Décembre 1964 à Montbard (21).
Nationalité : Française.
Situation familiale : Mariée, trois enfants.
Adresse : 7bis, Place Darcy, Bât. C, F-21000 DIJON.

II – Fonction et coordonnées professionnelles

Fonction : Maître de Conférences, classe normale.
Section CNU : 30.
Section CNRS : 04.

Unité d'affectation : UMR 5027,
Laboratoire de Physique de l'Université de Bourgogne (LPUB),
(Directeur : Pr. Jean-Paul Champion).

Adresse : LPUB, 9 Av. A. Savary, B.P. 47 870, F-21078 DIJON Cedex.
Téléphone : +33 (0)3 80 39 59 67.
Fax : +33 (0)3 80 39 59 71.
E-mail : `Maud.Rotger@u-bourgogne.fr`
Page Web : `http://www.u-bourgogne.fr/LPUB`

III – Formations et emplois occupés

1. Septembre 1986 – Septembre 1987 : Diplôme d'ingénieur (ENSI CAEN) et DEA de Physique "Instrumentation et Commande", mention AB

2. Septembre 1987 – Février 1990 : Thèse

Bourse BDI. Vacataire au Laboratoire SMIL de l'Université de Bourgogne.

3. Depuis Octobre 1990 : MCf à l'Université de Bourgogne

Maître de Conférences au Laboratoire SMIL puis LPUB de l'Université de Bourgogne.

4. Août 1996 – Janvier 1997 : Stage postdoctoral

Groupe du Pr. Martin Quack,
Laboratorium für Physikalische Chemie,
Ecole Polytechnique Fédérale (ETH) de Zürich (Suisse).

Sujet : Spectroscopie en jet moléculaire supersonique d'hexafluorures métalliques (WF_6, ReF_6).

IV – Titres et diplômes universitaires

DEA de Physique "Instrumentation et Commande" :

Mars 1987 – Septembre 1987, au Laboratoire Central de Recherches de Thomson-Corbeville (Orsay).

Mention assez bien.

Sujet : Cartographie par photoluminescence de lasers semi-conducteurs.

Thèse de doctorat :

Soutenue le 16 février 1990 au Laboratoire de Spectronomie Moléculaire et d'Instrumentation Laser (Dijon).

Mention très honorable.

Directeur de thèse : Pr. H. Berger.

Sujet : Contribution à l'Etude d'un Laser Nd-YAG Industriel de Puissance. Réalisation d'un Lambdamètre pour Lasers Impulsionnels.

V – Enseignement

Dans un premier temps, je résume ci-après brièvement mon activité d'enseignement.

Depuis ma nomination, j'ai effectué un service d'environ 192 heures par an pour un public allant de la première année de DEUG A à la Licence de Physique/Licence de Sciences Physiques, pour des étudiants de la première à la troisième année d'Ecole d'Ingénieurs (ESIREM, Dijon) ainsi que pour des étudiants en deuxième année de DEUG B. Mon activité est focalisée essentiellement autour de quatre thèmes : l'Optique, l'Electromagnétisme, la Propagation d'Ondes et la Mécanique des Fluides. J'ai mis en place ou remanié plusieurs fascicules de TP en Optique et en Electromagnétisme et je donne un cours de Propagation et de Mécanique des Fluides approprié aux étudiants de DEUG B2/ST2 (bio-physique et géophysique). Je suis coordinatrice pour la Physique de l'année de L2 et je participe à l'élaboration des emplois du temps de L2 toutes matières confondues.

En 1er cycle à l'UFR Sciences, Technologies, Santé de l'Université de Bourgogne :

- **Responsable** des **TD** et **TP** d'optique en DEUG A 2ème année de 1994 à 1997.
- **Responsable** des **TD** et **TP** d'électromagnétisme en DEUG A 2ème année de 2000 à 2003.
- Enseignante en TD d'électromagnétisme et/ou d'optique en DEUG A 2ème année.

En 1er cycle à l'UFR Sciences Vie de l'Université de Bourgogne :

- **Responsable** du **cours** et des **TD** de mécanique des fluides en DEUG B 2ème année depuis la rentrée 1998.

En 1er cycle à l'UFR Sciences Terre de l'Université de Bourgogne :

- **Responsable** du **cours** et des **TD** de mécanique des fluides et de propagation en DEUG ST 2ème année depuis la rentrée 2004.

En 2eme cycle à l'UFR Sciences, Technologies, Santé de l'Université de Bourgogne :

- Enseignante et **responsable** des **TD** et **TP** d'optique en 2ème année de l'école d'ingénieurs FIRST/ESIREM de 1991 à 1997.
- Enseignante des **TD** et **TP** de thermodynamique en licence de Physique et physique et applications de 1997 à 1999.
- Enseignante de **TD (optique et propagation)** et de **TP** de Physique en Licence de Sciences Physiques de 2000 à 2004.

Je donne ci-après plus de détails sur mon activité d'enseignement au cours de ces quinze dernières années.

A ma nomination, j'ai effectué l'essentiel de mon enseignement dans le domaine de l'optique en premier et second cycle. Très vite, en 1991, avec la création de l'école d'ingénieurs FIRST, j'ai pris en charge la mise en place de nouvelles expériences en deuxième et troisième année. En tout, six nouveaux TP ont été testés, installés et ont donné lieu à la rédaction d'énoncés. En deuxième année, les expériences portent sur :

- L'optique géométrique (étude d'un objectif photographique et notions sur la biréfringence).
- Les communications à fibres optiques (couplage optique de sources infrarouge vers fibres et multiplexage en longueurs d'onde).
- L'interférométrie holographique (comparaison expérience-théorie de la déformée d'une poutre encastrée).
- Le laser à gaz (mise en place d'une cavité laser He-Ne et caractérisation du faisceau).

Un fascicule d'une cinquantaine de pages a été réalisé. Les deux expériences mises en place en troisième année font partie d'un module plus important qui s'inscrivait alors dans le cadre de l'option Optique de l'école. Il s'agit d'une expérience d'initiation à un programme de calculs optiques (logiciel Solord de la société Optis) et d'une expérience sur les fibres optiques en tant que capteurs de pression et de température.

A la rentrée 1994, j'ai été également responsable des TD et TP d'optique de 2ème année de DEUG A. A l'initiative du Pr. G. Millot, une nouvelle expérience portant sur l'interféromètre de Michelson a été installée et à cette occasion, le fascicule a été largement remanié. Dans ce module, les enseignants étaient nombreux et j'ai toujours fait en sorte que chaque intervenant puisse effectuer son travail dans les meilleures conditions possibles. Avec la réforme du DEUG A, le fascicule a été à nouveau modifié. J'ai abandonné cette responsabilité de TP en 1997 car je suis partie six mois en stage postdoctoral à l'Ecole Polytechnique Fédérale de Zürich.

A la rentrée 1998, j'ai pris en charge le cours magistral de physique pour les deuxième année de DEUG B, qui étaient alors au nombre d'environ 250 étudiants. Depuis 1999, j'ai également des groupes de TD et de TP afin de pouvoir mieux connaître les réactions des étudiants vis-à-vis de ce que je leur enseigne.

Depuis l'année universitaire 2000/2001 et jusqu'à la rentrée 2003, j'ai été responsable des TD et TP d'électromagnétisme. Une nouvelle partie de TP portant sur les bobines de Helmoltz a été mise en place. D'autre part, des TP existants et portants sur les interféromètres de Fabry-Pérot et de Michelson ont été dupliqués. Deux TP ont été re-rédigés et un fascicule de TD a été réalisé.

Depuis la rentrée 2001, je m'occupe des emplois du temps de deuxième année avec deux collègues chimistes.

Depuis Janvier 2003, je suis membre élue du conseil de l'UFR Sciences, Technologies, Santé.

Cette année, j'ai entrepris un enseignement de cours magistral (niveau L2) spécifique aux géologues dans les domaines de la mécanique des fluides, de la propagation et des mathématiques.

Encadrement de stagiaires de TER

- 2003–2004 : Jean-Baptiste Mime, étudiant en Licence de Physique, Analyse de la bande ν_{12} de l'éthylène par spectroscopie infrarouge.
- 2001–2002 : Nicolas Benoit, étudiant en Licence de Physique, enregistrement du spectre d'absorption par diode laser de la bande ν_8 de SF_5Cl.
- 2001–2002 : Raphaël Bouillet et Aline Devaivre, étudiants en Licence de Sciences Physiques, rédaction du TP sur la propagation dans une ligne à retard.
- 2001–2002 : Catherine Gaudin et Caroline Boirot, étudiantes en Licence de Sciences Physiques, rédaction du TP sur les interféromètres de Michelson et de Fabry-Pérot.
- 1999–2000 : Christelle Nivot et Carine Robert, étudiantes en Licence de Sciences Physiques, recensement et réalisation de pages web sur l'enseignement de la thermodynamique.

VI – Parcours scientifique

1. Thématiques abordées

Les trois paragraphes suivants résument brièvement les travaux scientifiques effectués après ma thèse (1990–2004). Je tiens à signaler ici que n'ayant pas continué sur mon sujet de thèse après ma nomination, je me suis initiée à la spectroscopie moléculaire et j'ai travaillé essentiellement à l'émergence de sujets nouveaux dans ce domaine ainsi qu'à la mise en place de nouvelles collaborations.

• LPUB (1990 – 1994)

A la rentrée 1990, j'ai été nommée à Dijon au laboratoire de Spectronomie Moléculaire et Instrumentation Laser (aujourd'hui Laboratoire de Physique de l'Université de Bourgogne). Pendant trois ans, avec l'aide de B. Lavorel, je me suis initiée à la spectroscopie moléculaire dans les milieux dilués. J'ai débuté mes recherches dans ce domaine par la mise en place, à partir du dispositif Raman déjà existant, d'un nouveau dispositif de Spectroscopie Raman Photoacoustique (ou PARS). Puis, des études sur CF_4 et SiH_2D_2 m'ont permis de réaliser d'autres expériences telles que la spectroscopie CARS polarisée ainsi que celle en configuration croisée dans le plan (dite BOXCARS). Ces travaux ont été suivis par des attributions et analyses, d'une part sur CF_4 par un étudiant (A. Tabyaoui) alors en thèse avec le Pr. H. Berger, et d'autre part sur SiH_2D_2 par nos collègues parisiens M. Bétrencourt et J.-C. Deroche (attributions) par moi-même (analyse) et aussi grâce aux calculs *ab initio* de J. Breidung et W. Thiel.

• LPUB (1994 – 1997)

A partir de 1994, à mon initiative et sur suggestion du Pr. H. Berger, je me suis plus particulièrement impliquée sur l'aspect expérimental de deux projets :

- La spectroscopie des hexafluorures à nombre impair d'électrons.
- La spectroscopie des états vibrationnellement excités du silane.

En ce qui concerne le premier sujet, il s'avère que l'étude des radicaux ou espèces présentant une sous-couche électronique incomplète est un domaine de recherche au carrefour de plusieurs thèmes, à savoir : la chimie de composés très réactifs, l'astrophysique, la physique des interfaces et la physique fondamentale (théorie des groupes, ...).

Les hexafluorures de métaux de transition (iridium, rhénium, platine, ...) constituent des exemples très intéressants de ce type d'espèces. Du point de vue bibliographique, la spectroscopie de ces composés est assez mal connue et aucune bande vibrationnelle dans un état électronique dégénéré n'avait encore été résolue en rotation. D'autre part, l'étude de ces molécules est importante car ce sont les seuls composés gazeux des métaux en question, ce qui intéresse notamment les industriels pour des dépôts en phase vapeur (tungstène sur silicium, ou rhénium sur acier par exemple). Avec V. Boudon (qui a effectué sa thèse sous la direction des Pr. J. Moret-Bailly et F. Michelot), nous nous sommes plus particulièrement intéressés dans un premier temps à la spectroscopie de l'hexafluorure d'iridium, IrF_6. Sa synthèse a été réalisée par le Pr. D. Avignant du Laboratoire de Chimie des Solides de l'Université de Clermont-Ferrand. Les processus de synthèse, de purification et de conservation du gaz dans des cuves en quartz scellées ont été parfaitement maîtrisés. Deux premières études à basse résolution ont été réalisées sur cette molécule :

- Spectroscopie d'absorption dans le proche infrarouge, le visible et l'ultraviolet à l'aide de spectrophotomètres commerciaux.
- Spectroscopie par diffusion Raman spontanée, en collaboration avec Mr. A.T. Nguyen de la société Jobin Yvon à Longjumeau.

L'analyse et l'interprétation de ces spectres a été achevée et a fait l'objet de trois publications. Nous avons pu analyser des spectres de ReF_6 et partiellement analyser des spectres de OsF_6. Les spectres de PtF_6, très complexes, n'ont pas encore pu être analysés.

Nous avons par ailleurs mis en place à Dijon deux dispositifs spectroscopiques à haute résolution dans le visible (absorption saturée – testée sur une cuve à iode – et simple absorption avec multiples

passages). Ceux-ci utilisaient notamment un laser à colorant en anneau. De nouveaux essais de spectroscopie d'absorption saturée dans le visible, cette fois avec multiples passages ont été effectués, en collaboration avec le Pr. W.A. Kreiner de l'Abteilung Chemische Physik – Gruppe Laseranwendungen de l'Université d'Ulm (Allemagne). Cependant, ces techniques ne permettent pas de résoudre la structure rovibronique de molécules aussi lourdes.

Dans le but d'obtenir des spectres résolus en rotation, une collaboration a été mise en place avec Mr. A. Jourdan de la société COMURHEX à Pierrelatte (fournisseur de WF_6 et de ReF_6) et le Pr. M. Quack de l'Ecole Polytechnique Fédérale de Zürich (Suisse), pour la réalisation de spectres par jet moléculaire supersonique, et par transformée de Fourier, de la bande fondamentale ν_3 de WF_6 et de ReF_6. Des études diode laser ont complété ce travail et ont fait l'objet de mon stage postdoctoral.

J'ai également co-encadré (avec B. Morel et D. Darfeuille) le stage Ingénieur d'Emmanuelle Gallois à la Société Comurhex (Pierrelatte). Ce travail portait sur la détection de polluants gazeux par voie spectroscopique (spectromètre à transformée de Fourier).

Le deuxième projet a été mené en étroite collaboration avec l'équipe "Matériaux pour l'Optique" du laboratoire. Ainsi, en septembre 1995, j'ai co-encadré avec Benoît Boulanger (chargé de recherches CNRS) un stagiaire de DEA (O. Mauguin). Ce travail concernait la mise en place d'une source laser infrarouge impulsionnelle obtenue par différence de fréquences dans un cristal de KTP. Elle devait servir de source pompe pour la réalisation de spectres par double résonance infrarouge-infrarouge de la région à trois quanta d'excitation sur les modes d'élongation de la molécule de silane. Ce projet a malheureusement du être abandonné sur décision du directeur de laboratoire.

• ETH (Zürich) (1996-97)

J'ai effectué un séjour postdoctoral d'environ six mois dans le groupe du Pr. M. Quack à Zürich dans le but d'enregistrer pour la première fois des spectres résolus en rotation de la molécule ReF_6. Dans un premier temps, nous avons enregistré des spectres à transformée de Fourier et jet sur la molécule WF_6 puis ensuite, nous avons remis en place l'expérience diode laser et jet pour enregistrer des portions de spectres des molécules WF_6 et ReF_6. Bien évidemment, les expériences de confirmation de ces résultats ont été faites ensuite par V. Boudon seul car il me fallait rentrer à Dijon pour assurer mes heures d'enseignement (un service sur 6 mois).

La collaboration avec le Pr. Martin Quack de l'Ecole Polytechnique Fédérale de Zürich (Suisse) se poursuit et a donné lieu à un article sur la bande ν_3 de WF_6 et de ReF_6. Je travaille toujours avec V. Boudon, qui a été nommé à la rentrée 1997 Chargé de Recherche CNRS au laboratoire.

• LPUB (depuis 1997)

De retour à Dijon, j'ai récupéré le matériel diode laser auparavant utilisé par Mr. Jean Cadot, collègue souhaitant arrêter ses activités de recherche, pour mettre à profit l'expérience acquise à Zürich. C'est ainsi qu'avec Emmanuelle Gallois (stagiaire DEA de 97 à 98 sous ma responsabilité), nous avons mis en place une expérience d'absorption à diode laser. Nous nous sommes plus particulièrement intéressées à la molécule SF_5Cl. Cette molécule pourrait par exemple être dissociée par champ laser intense, ce qui permettrait ainsi d'obtenir le radical SF_5 très utilisé en chimie. Mais au préalable une bonne connaissance des niveaux rovibrationnels est nécessaire, d'où l'interêt de la spectroscopie d'absorption infrarouge. J'ai développé sur ma propre initiative ce sujet à la fois sur le plan expérimental et théorique avec le soutien de V. Boudon et du Pr. M. Loëte. J'ai en effet écrit un modèle basé sur le formalisme tensoriel qui permet de calculer le spectre d'absorption infrarouge et Raman de SF_5Cl. Ce travail a donné lieu à deux publications. L'ensemble a été informatisé et constitue une chaîne de programmes FORTRAN 77 nommée C_{4v}TDS (C_{4v} Top Data System). J'ai aussi mis en place des programmes d'ajustements pour déterminer les paramètres rovibrationnels des diverses bandes d'absorption de cette molécule. Ce type d'étude peut s'étendre à d'autres molécules de type XY_5Z telles que IOF_5, SF_5Br, SeF_5Cl, SeF_5Br, ...

Au cours de l'année 2000, j'ai tout d'abord confronté le modèle pour les toupies symétriques du groupe C_{4v} de type XY_5Z avec le spectre expérimental de l'ensemble de la diade ν_1/ν_8 de la molécule

SF_5Cl. Il s'agit d'un spectre FTIR enregistré sur ma demande dans le groupe du Pr. Hans Bürger à Wuppertal (Allemagne). J'ai encadré sur cette thématique le stage DEA de Armelle Decrette.

L'analyse de la diade a été menée à bien et a ainsi permis la validation du modèle théorique (article paru au JMS). Les perspectives d'analyse sont nombreuses car c'est une molécule peu étudiée à haute résolution. La partie informatique concernant le calcul de spectre d'absorption infrarouge et la chaîne de programmes d'ajustements ont été standardisés par notre ingénieur informaticien Ch. Wenger. Une page Web (http://www.u-bourgogne.fr/LPUB/c4vTDS.html) permet le chargement de ces programmes. Un article sur ce sujet est paru au JQSRT en 2002.

Depuis peu, je travaille aussi sur la molécule quasi-sphérique SO_2F_2. En effet, les modèles classiques (pour toupies asymétriques) ne permettent pas par exemple l'analyse de la diade ν_4/ν_5, il s'avère donc intéressant de construire un nouveau modèle basé sur la réorientation de T_d vers C_{2v} et utilisant l'expérience acquise pour C_{4v}. Les parties théorique et informatique ont été achevées fin 2000. En 2002/03, la validation du modèle a été faite sur un spectre rotationnel pur de cette molécule, spectre enregistré à Lille dans le groupe de J. Demaison. Une publication au JMS en 2003 a finalisé cette étude sur le niveau de base. Des liens entre analyse "classique" et tensorielle ont été faits. L'analyse de la triade de cette molécule est en cours.

Mon travail actuel vise donc à étendre à d'autres catégories de molécules (symétriques et asymétriques) le modèle toupie sphérique utilisé de longue date au laboratoire. Récemment, du point de vue expérimental, des enregistrements de spectres de la molécule SF_5Cl par diode laser ont été réalisés grâce au dispositif décrit ci-dessus et ont donné lieu à un article et à un poster (stage TER de N. Benoit). Pour l'étude de molécules lourdes, la mise en place d'un jet fente supersonique est en cours. Des calculs *ab initio* sur cette molécule ont été entrepris par Natalia Zvereva-Loëte et vont donner lieu à une publication. Ces activités nouvelles au laboratoire ne n'empêchent pas de m'intéresser parfois à l'analyse de toupies sphériques (travail plus classique) telle que la molécule $^{80}SeF_6$ (article paru à Chem. Phys. Lett. en 2001).

Depuis février 2002, nous avons entrepris la mise en place d'une nouvelle thématique sur l'adsorption de molécules dans les zéolithes. C'est un travail en collaboration avec l'équipe " Adsorption dans des Solides Microporeux" du laboratoire LRRS de Dijon dirigé par G. Bertrand. Pour notre part, il s'agit d'interpréter grâce à un modèle quantique les spectres de molécules (par exemple, l'éthylène) piégées dans une zéolithe de type ZSM-5, donc en particulier de tenir compte de l'effet Stark en raison des champs électriques intenses présents dans ces solides. J'ai organisé le 26 Mai 2003 un atelier sur cette thématique financé par le réseau national SpecMo. J'ai participé à l'organisation d'une école d'été qui a eu lieu du 13 au 17 Septembre 2004 à Dijon avec la participation de spécialistes dans ce domaine dont en particulier T. Momose (Japon). Ce travail a donné lieu à un article au JMS en 2003 sur le formalisme pour la molécule isolée et un autre va être soumis prochainement sur l'effet Stark.

J'ajoute pour conclure que ces travaux ont nécessité de ma part un fort investissement personnel du fait que ma formation initiale et mes premiers travaux scientifiques ne portaient pas du tout sur la théorie. J'ai du me familiariser en particulier avec les techniques de théorie des groupes et de formalisme tensoriel, ce qui fut pour moi difficile mais extrêmement enrichissant.

2. Diffusion des résultats

- 25 publications dans des revues à comité de lecture.
- 1 acte de colloques ("proceedings" à comité de lecture).
- 2 conférences invitées.
- 38 contributions (orales ou posters) à des congrès.
- 1 séminaire dans un laboratoire étranger, 1 séminaire en entreprise.

La liste complète des travaux est fournie en annexe (partie VII).

3. Collaborations scientifiques locales

- Dr. Vincent Boudon (LPUB).
- Pr. Michel Loëte (LPUB).

- Christian Wenger (LPUB).
- Pr. Jean-Paul Champion (LPUB).
- Pr. Gérard Pierre (LPUB).
- Dr. Jean-Marc Simon (LRRS).

4. Collaborations scientifiques nationales et internationales

- Groupe de J. Demaison, Université de Lille 1, Lille.
- Groupe du Pr. Martin Quack, ETH Zürich (Suisse).
- Groupe du Pr. Hans Bürger, Université de Wuppertal (Allemagne).
- Dr. Jürgen Breidung et Pr. W. Thiel, Université de Mülheim (Allemagne).
- Dr. H.S.P. Müller et Pr. G. Winnewisser, Université de Cologne (Allemagne).
- Pr. H. Mäder, Université de Kiel (Allemagne).
- Groupe du Pr. Michel Herman, Université Libre de Bruxelles (Belgique).
- Pr. Daniel Avignant, Université Blaise Pascal (Clermont-Ferrand).
- Pr. Henry Selig, Université de Jérusalem (Israël).
- Pr. Dionisio Bermejo, Université de Madrid (Espagne).

5. Séjours de courte durée à l'étranger

- **Du 04/12 au 08/12 1995**, séjour à l'Abteilung Chemische Physik – Gruppe Laseranwendungenden, groupe du Pr. Welf Kreiner, Universität Ulm (Allemagne). Spectroscopie d'absorption saturée.
- **Du 27/04 au 03/05 1997**, séjour au Laboratorium für Physikalische Chemie, groupe du Pr. Martin Quack, ETH Zürich (Suisse). Spectroscopie par transformée de Fourier dans un jet supersonique de ReF_6. Séjour préparatoire au stage postdoctoral.

VII – Encadrement

1. Encadrement de thésard

– Depuis Septembre 2002, **co-direction** (avec le Pr. M. Loëte du LPUB) de Wilfried Raballand, sur la "*Spectroscopie rovibrationnelle de la molécule d'éthylène et applications à la molécule adsorbée dans les zéolithes*". Soutenance prévue en 2005.

2. Encadrements de stagiaires de DEA

– De Février à Juin 2002, encadrement d'un stagiaire de DEA, Wilfried Raballand, sur la "*Spectroscopie rovibrationnelle de la molécule d'éthylène*".

– De Février à Juin 2000, encadrement d'un stagiaire de DEA, Armelle Decrette, sur l'"*Analyse Rovibrationnelle de la diade ν_1/ν_8 de $SF_5{}^{35}Cl$*".

– De Février à Juin 1998, encadrement d'une stagiaire de DEA, Emmanuelle Gallois, sur la "*Spectroscopie d'absorption haute résolution par diode laser des bandes fondamentales ν_1 et ν_8 de SF_5Cl*".

– De Février à Juin 1996, encadrement d'un stagiaire de DEA, Olivier Mauguin, sur la "*Mise en place d'une source laser infrarouge par différence de fréquences dans KTP, en vue de la spectroscopie double résonance de SiH_4*".

VIII – Animation scientifique

1. Participation à l'organisation de colloques

– Participation à l'organisation du *12th Colloquium on High-Resolution Molecular spectroscopy* (HRMS Dijon, 9–13 Septembre 1991).

– Participation à l'organisation du *14th Colloquium on High-Resolution Molecular spectroscopy* (HRMS Dijon, 11–15 Septembre 1995).

– Participation à l'organisation du *16th Colloquium on High-Resolution Molecular spectroscopy* (HRMS Dijon, 6–10 Septembre 1999).

– Organisatrice de l'*Atelier sur la Spectroscopie de Molécules Piégées dans les Solides* organisée à Dijon le 26 mai 2003 par Maud Rotger dans le cadre du réseau SpecMo du CNRS.

– Participation à l'organisation du *18th Colloquium on High-Resolution Molecular spectroscopy* (HRMS Dijon, 8–12 Septembre 2003).

– Participation à l'organisation d'une école d'été intitulée *Molecules Trapped in Solids* du 13 au 17 septembre 2004 à Dijon.

IX – Responsabilités administratives et collectives

– Membre titulaire de la Commission de Spécialistes de Physique (29–30$^{\text{èmes}}$ sections) de l'Université de Reims Champagne - Ardenne.

– Membre élue au Conseil de l'UFR Sciences et Techniques.

Troisième partie

Spectroscopies Expérimentales

Troisième partie

Chapitre 1

Spectroscopie Photoacoustique et CARS

Publications P3, P4, P5, P11

1.1 Introduction

A ma nomination, je me suis tournée vers la spectroscopie qui était alors l'activité principale du laboratoire SMIL. J'ai fait mes premiers pas dans le domaine de la spectroscopie expérimentale avec B. Lavorel compte-tenu de mes compétences "Instrumentation et Mesures" acquises en école d'ingénieurs (ENSI CAEN).

1.2 Résultats

Dans un premier temps, nous avons effectué des essais de spectroscopie photoacoustique dans une cuve non résonante pour démontrer la bonne sensibilité de cette technique. Notre molécule test a été le dioxyde de carbone, CO_2. B. Lavorel m'a également initié à la spectroscopie CARS sur les bandes fondamentale et harmonique ν_1 et $2\nu_2$ de $^{12}CF_4$ qui ont été ensuite analysées par A. Tabyaoui.

Cependant, mon travail le plus important et le plus formateur pendant cette période a été l'étude expérimentale et l'analyse de la pentade (soit cinq niveaux vibrationnels en interaction de Coriolis) de la molécule asymétrique SiH_2D_2. Les bandes actives en infrarouge ont été enregistrées par Transformée de Fourier (Groupe du Pr. H. Bürger, Wuppertal) et la bande active en Raman a été enregistrée par spectroscopie CARS croisée dans le plan (technique BOXCARS) à Dijon avec l'aide de B. Lavorel. Cette étude a été un double challenge, d'une part du point de vue expérimental et d'autre part, du point de vue de l'analyse des spectres.

Expérimentalement, il a fallu mettre en place une expérience des plus sophistiquées afin d'enregistrer cette bande faible en intensité. Ensuite, l'analyse de cette pentade a pu être menée à bien grâce aux attributions de J.-C. Deroche et M. Betrencourt (Université d'Orsay) et grâce aussi aux programmes d'analyse et d'ajustements de H. M. Pickett (JPL, Pasadena, USA) et à l'aide précieuse de ce dernier. Une autre clé pour mener à bien l'analyse de cette pentade a été l'apport des calculs *ab initio* par J. Breidung qui a pu nous fournir de bonnes valeurs des constantes de Coriolis et du moment dipolaire. Il y avait sans aucun doute dans ce travail tous les ingrédients formateurs nécessaires pour me permettre de mener à terme bon nombre d'analyses spectroscopiques.

1.3 Perspectives

Cette première expérience spectroscopique m'a prouvé qu'un bon article devait associer à la fois de l'expérience et du traitement de données. J'en garderai aussi le souvenir d'une collaboration constructive avec H. Bürger, J. Breidung et V. Boudon. C'est sans aucun doute après cette étape très formatrice, que se sont ouvertes à moi de nouvelles voies en matière de spectroscopie.

1.4 Articles-clés

Sont reproduits ici les deux articles résumant le mieux mes premières activités en spectroscopie expérimentale et en analyse de données.

- [**P4 :** *J. Raman Spectrosc.*, **23**, 303–309 (1992)] présente les résultats expérimentaux obtenus en spectroscopie photoacoustique.
- [**P11 :** *J. Mol. Spectrosc.*, **192**, 294–308 (1998)] porte sur l'enregistrement de données Raman et l'analyse de la pentade de SiH_2D_2.

JOURNAL OF RAMAN SPECTROSCOPY, VOL. 23, 303–309 (1992)

High-Resolution Photoacoustic Raman Spectroscopy of Gases

M. Rotger,* B. Lavorel and R. Chaux
Laboratoire de Spectronomie Moléculaire et Instrumentation Laser, Université de Bourgogne, URA CNRS No. 777, 6 Bd Gabriel, 21000 Dijon, France

A high-resolution photoacoustic Raman spectroscopy experiment is described. The resolution achieved by using two single-mode pulsed lasers is about 0.0054 cm^{-1} (full width at half maximum intensity). The experiment was tested first on the $v_1/2v_2$ bands of CO_2 and gave an increase of at least about one order of magnitude in the signal-to-noise ratio with respect to stimulated Raman spectroscopy at low pressure (*ca.* 10 Torr ≈ 1.3 kPa). The sensitivity is also demonstrated by the study of the weak hot band $v_1 + v_2 - v_2$ of CO_2. In both cases, the experimental line shape is well reproduced by taking into account Doppler and collisional effects. A comparison with CARS spectra was also made.

INTRODUCTION

In the last 10–15 years, non-linear Raman techniques have allowed great improvements in the resolution of rotation–vibrational Raman spectra of gases.[1] Typically, an instrumental resolution of about 0.002 cm^{-1} can be achieved in stimulated Raman spectroscopy.[1] In many experiments, the resolution is mainly limited by Doppler broadening, which can be reduced by using molecular beam techniques.

The various methods of non-linear Raman spectroscopy have been reviewed[2,3] and some recent advances have been reported.[4,5] Among these methods, stimulated Raman spectroscopy (SRS) and coherent anti-Stokes Raman spectroscopy (CARS) are often used and have given many results on the Raman spectra of gases. Acoustic detection of the Raman process was first performed by Barrett and Berry[6] using continuous-wave (c.w.) laser sources. Pulsed lasers were then introduced for trace analysis using photoacoustic Raman spectroscopy (PARS).[7] Since then, only a few medium-resolution PARS experiments have been applied to some molecular gases.[8,9]

This paper reports experiments in which we combined the advantages of high-resolution spectroscopy using very narrow line-width lasers (*ca.* 0.004 cm^{-1}) and those of the photoacoustic detection of the stimulated Raman effect, namely high sensitivity and the possibility of recording pure rotational spectra without a Rayleigh line.

The experiment was tested on the $v_1/2v_2$ bands of CO_2 at low pressures. A comparison between CARS and PARS spectra was also made and led to some conclusions about the advantages and drawbacks of these two techniques.

THEORY

The coherent Raman processes are generated when two incident laser beams with frequencies ω_p (for the pump beam) and ω_s (for the Stokes beam) have a frequency difference equal to a Raman resonance of the molecule. A non-linear interaction between the beams and the molecule occurs through the third-order non-linear susceptibility $\chi^{(3)}(\omega_s)$ and leads to various third-order effects. Photoacoustic Raman spectroscopy is based on the detection of the energy deposited in a gas sample by the stimulated Raman process. This amount of energy is directly related to the change in power of the Stokes beam. If a and b are the lower and upper energy levels, respectively, of the Raman transition of the molecule, each molecule excited from level a to level b generates a Stokes photon which amplifies the Stokes beam. For focused Gaussian laser beams, the stimulated Raman gain g_s for the Stokes beam[7,10] is equal to (in the limit of small gain)

$$\frac{\Delta P_s(\omega_s)}{P_s(\omega_s)} = g_s = \frac{16\pi^2 cN\Delta\omega_p}{h\omega_s{}^3 n_s n_p}\left(\frac{d\sigma}{d\Omega}\right) \times L(\omega_p - \omega_s)P_p(\omega_p) \quad (1)$$

where N is the molecular density, Δ is the fractional population difference, $P_p(\omega_p)$ is the power of the pump beam, $P_s(\omega_s)$ is the power of the Stokes beam, $d\sigma/d\Omega$ is the differential Raman scattering cross-section, $L(\omega_p - \omega_s)$ is the line-shape function and n_s and n_p are refractive indices approximately equal to 1.

In the Lorentzian case,

$$L(\omega_p - \omega_s) = \frac{\Gamma}{[\omega_v - (\omega_p - \omega_s)]^2 + \Gamma^2}$$

where ω_v is the frequency of the Raman transition and Γ is the half width at half maximum intensity (HWHM).

The difference in energy in the Stokes beam is

$$\Delta E_s = \Delta P_s(\omega_s)T = \Delta n_s \hbar\omega_s \quad (2)$$

if we assume square laser pulses of duration T; Δn_s is the number of photons produced by the process. The number of molecules excited in the upper level is

$$\Delta n_v = \Delta n_s = \frac{\Delta P_s(\omega_s)T}{\hbar\omega_s} \quad (3)$$

0377–0486/92/050303–07 $05.00

Received 2 January 1992
Accepted 12 February 1992

The energy deposited in the process is therefore

$$\Delta U = \Delta n_v \hbar\omega_v = \frac{\omega_v}{\omega_s} \Delta P_s(\omega_s) T \tag{4}$$

Finally, taking into account Eqn (1):

$$\Delta U = \left(\frac{16\pi^2 c\omega_p}{\hbar n_s n_p}\right)[P_p(\omega_p)P_s(\omega_s)NT] \times \left[\frac{\omega_v \Delta}{\omega_s^4}\left(\frac{d\sigma}{d\Omega}\right)L(\omega_p - \omega_s)\right] \tag{5}$$

This expression and Eqn (7) in Ref. 7 differ by a factor $(2\pi c)^3$, which arises from the use here of wavenumbers rather than frequencies for all ωs. For a larger amplification factor, the exponential form of the Raman gain must be used.[7,11]

The relaxation of the vibrational energy of the excited molecules to translational kinetic energy through collisions leads to an increase in the translational internal energy U by ΔU. The corresponding pressure change can then be calculated by using the ideal gas equation of state, which gives[7]

$$\Delta P = \frac{(\gamma - 1)\Delta U}{V} \tag{6}$$

where γ is the specific heat ratio (C_p/C_v) and V is the effective volume of the cell.

If the characteristic time of collision relaxation, τ_{V-T}, is short compared with the thermal diffusion time constant, τ_D, the microphone detects a pressure change directly proportional to the thermal change in the gas. The envelope of the acoustic signal is a function of these two constants (τ_{V-T} and τ_D) and the pressure variation $p(t)$[8,12] is given by the equation

$$p(t) = p_0[1 - \exp(-t/\tau_{V-T})] \exp(-t/\tau_D) \tag{7}$$

where p_0 is a constant, τ_{V-T} is the vibrational–translational relaxation time constant and τ_D is the thermal diffusion time constant. τ_D is equal to[13] a^2/D, where a is the cell radius and D the thermal diffusivity factor, given by

$$D = \frac{K}{NC_V} \tag{8}$$

where K is the thermal conductivity, N is the gas density and C_V the specific heat capacity.

According to this relationship, τ_D is proportional and τ_{V-T} is inversely proportional to the gas density N. For CO_2 molecules, at low pressure (*ca.* 8 Torr $\approx$ 1 kpa) and cell radius $a = 0.3$ cm, we obtained $\tau_D \approx 8$ ms whereas $\tau_{V-T} \approx 0.7$ ms. The inequality $\tau_{V-T} < \tau_D$ is thus verified even at relatively low pressure.

In fact, the time dependence of the photoacoustic signal is much more complicated than would appear from Eqn (7). It results from a pressure-dependent excitation of various acoustic modes of the gas cell.[8,13]

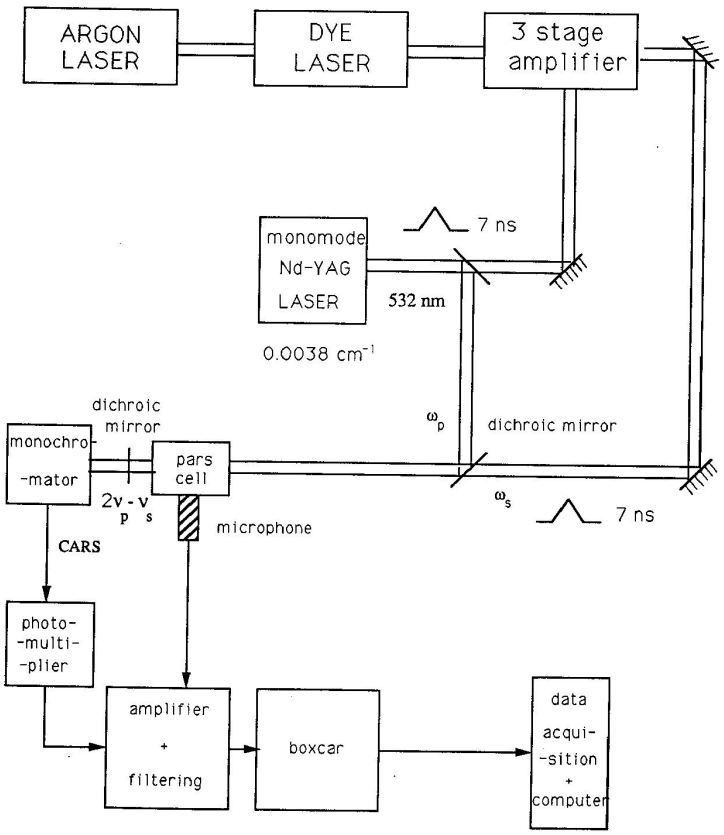

Figure 1. Schematic representation of the PARS–CARS experimental set-up.

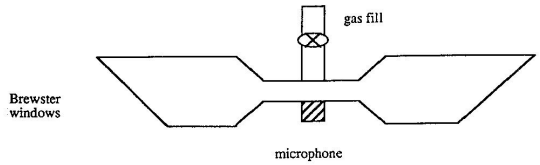

Figure 2. Cell used in PARS. Note the small volume near the microphone.

EXPERIMENTAL

The PARS experimental arrangement derives directly from the stimulated Raman set-up already described.[14] The main modification is the use of a frequency-doubled monomode Nd:YAG laser (Quanta-Ray Model GCR 3, 7 ns pulse duration, 25 Hz repetition rate) rather than a c.w. ion laser (argon or krypton laser) (Fig. 1). The second pulsed laser beam is a pulsed amplified c.w. tunable dye laser. The three-stage dye amplifier is pumped by the Nd:YAG laser. The two laser beams are mixed by means of a dichroic mirror and focused ($f = 250$ mm) in the PARS cell. This is shown schematically in Fig. 2. A condenser microphone (Brüel and Kjaer Model 4135, sensitivity 4 mV Pa^{-1}, 4 Hz–50 kHz frequency response) is inserted in the sample cell just in front of the beam focal point. The photoacoustic signal is then amplified (Brüel and Kjaer Model 2633, followed by a laboratory-made amplifier) and integrated by a boxcar in which the gate delay is adjusted to select only the first peak. A cut-off electronic filter removes frequencies up to 10 kHz. The gate width is 6 μs.

A typical oscillogram of a PARS signal is given in Fig. 3. A baseline subtraction has been performed but

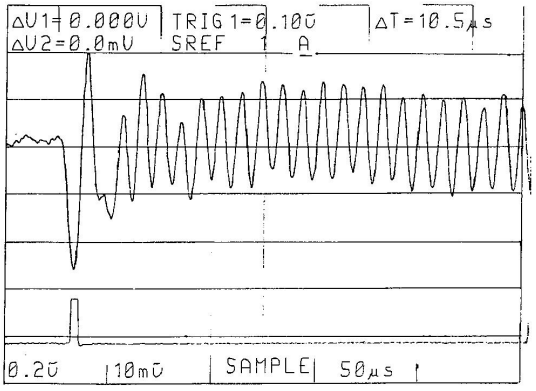

Figure 3. Oscillogram of the photoacoustic signal for CO_2 molecules at $P = 50$ Torr (6.6 kPa) and $T = 297$ K.

no improvement in the signal-to-noise ratio has been observed. The PARS profile is recorded in a data acquisition system associated with an IBM-PS/2 computer. The experimental resolution of this spectrum is limited only by the convoluted line width of the two lasers, which is nearly equal to 0.0038 cm^{-1} and leads to the value of 0.0054 cm^{-1} (FWHM).

The relative frequency calibration of the Raman spectra is ensured by a Michelson-type wavemeter which accurately measures the frequency of the tunable c.w. dye laser.[15] To achieve absolute frequency calibration, one needs to know the frequency of the Nd:YAG laser. This is first stabilized with a Fabry–Perot interferometer[16] during recordings, then its frequency is deduced from low-pressure spectra of oxygen Q-lines, or CO_2 Q-lines ($2\nu_2$ band or ν_1 band). A more accurate method of frequency measurement of the Nd:YAG or of other pulsed lasers by using a com-

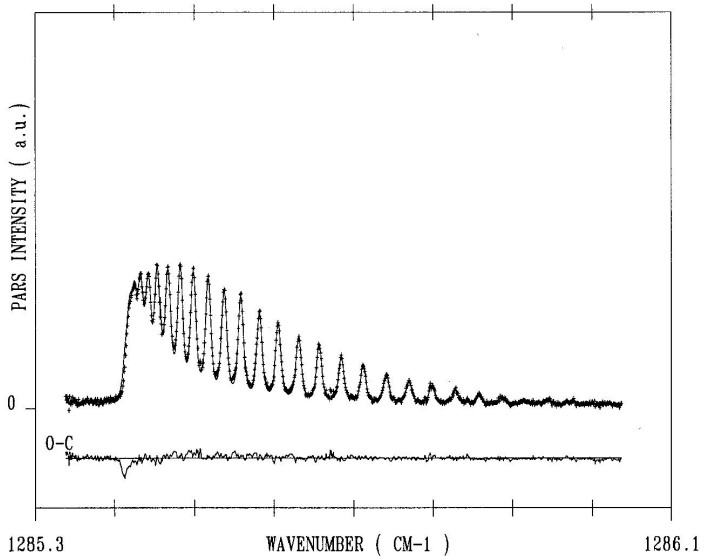

Figure 4. PARS spectrum of the $2\nu_2$ band of CO_2 at $P = 11$ Torr (1.6 kPa) and $T = 297$ K. $P_p = 400$ kW and $P_s = 100$ kW. Solid line, calculated spectra; +, experimental.

bination of Michelson and Fabry–Perot interferometers is being set up.

Simultaneously with the study of the PARS spectrum, the experimental arrangement enables us to record the corresponding CARS spectrum. This is done simply by optically filtering the CARS beam generated in the cell by means of dichroic mirrors and a monochromator and by directing it on a photomultiplier. Some comparisons between the two techniques have been performed in this way. In both techniques, particular attention must be given to the phenomena of saturation and Stark effects.[17–19]

The peak power of the two lasers was adjusted from 1 to 180 kW for the Nd:YAG laser and from 10 to 115 kW for the dye laser, depending on the band recorded. We observed saturation effects in some CARS spectra, whereas in PARS spectra recorded under identical conditions these effects were absent. We calculated the product of pump and probe laser powers in the case of two-photon saturation.[20] This product $(P_p P_s)_{SAT}$ is proportional to the square of the sample pressure: for the ν_1 band of CO_2 at $P \approx 1$ kPa, $P^2_{SAT} \approx 5 \times 10^7$ W^2, and for the $2\nu_2$ band of CO_2 at the same pressure, $P^2_{SAT} \approx 8 \times 10^7$ W^2. To avoid saturation effects in CARS spectra, we therefore decreased the input powers of both lasers as indicated in Figs 5 and 6.

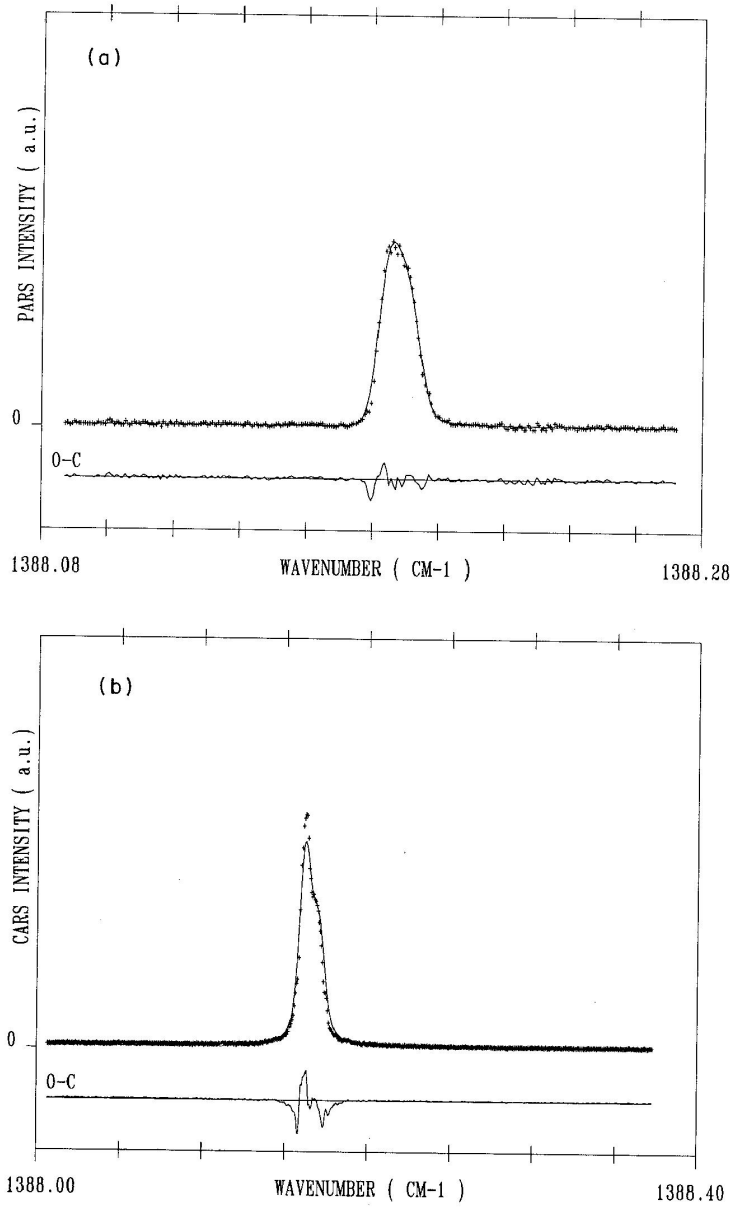

Figure 5. PARS and CARS spectra of the ν_1 band of CO_2 at $P = 16$ Torr (2.3 kPa) and $T = 297$ K. Solid lines, calculated spectra; +, experimental. (a) PARS, $P_p = 180$ kW, $P_s = 23$ kW; (b) CARS, $P_p = 1.1$ kW, $P_s = 6.8$ kW.

RESULTS

As a first test of the PARS experiment, we considered the Fermi diad $\nu_1/2\nu_2$ of CO_2 at room temperature (297 K) and at low pressure (*ca.* 1–4 kPa). These bands have recently been extensively studied by high-resolution stimulated Raman spectroscopy[21,22] and therefore were very suitable for an initial study using high-resolution PARS. Two spectra of the ν_1 and $2\nu_2$ bands are represented in Figs 5 and 6, respectively. The corresponding CARS spectra are also given. The signal-to-noise ratios of the two experiments are comparable but it must be noted that the CARS beam was attenuated to avoid saturation of the photomultiplier. The comparison between single-pass and multiple-pass cell SRS of the $2\nu_2$ band[23] shows that the PARS technique leads to a better signal-to-noise ratio than the single-pass SRS technique by about one order of magnitude at 1.3 kPa (Fig. 4). For this spectrum, each line has been adjusted separately in frequency and intensity. However, we must keep in mind that low pressure ($\leqslant 1.3$ kPa) is not favourable for detection of a PARS signal. The gain could be larger for higher pressures. The multiple-pass SRS experiment gives a greater enhancement of sensitivity at very low pressure.

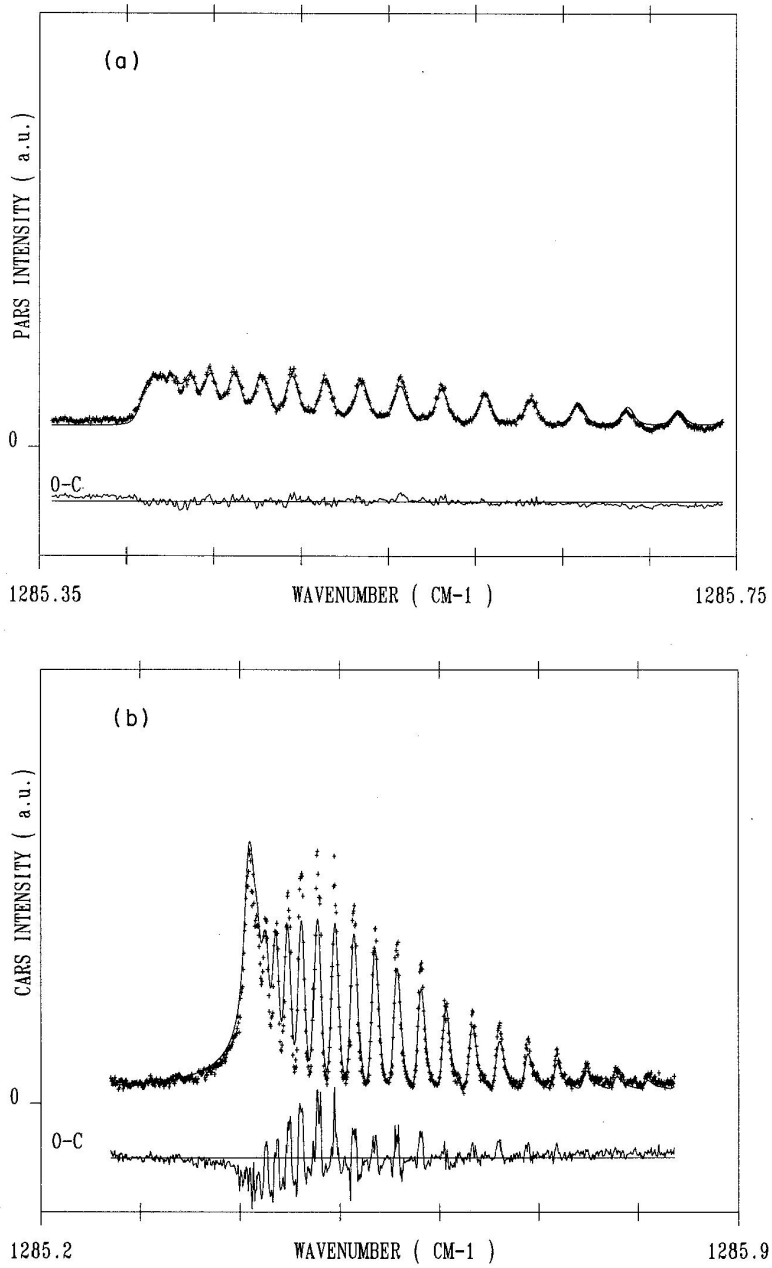

Figure 6. PARS and CARS spectra of $2\nu_2$ band of CO_2 at $P = 17$ Torr (2.4 kPa) and $T = 297$ K. Solid lines, calculated spectra; +, experimental. (a) PARS, $P_p = 180$ kW, $P_s = 115$ kW; (b) CARS, $P_p = 10.8$ kW, $P_s = 4.6$ kW.

The experimental PARS profiles were then fitted by calculated profiles. The least-squares fitting procedure is that described in Refs 21 and 22 and three main broadening sources were taken into account: the experimental apparatus function (Gaussian HWHM = 0.0027 cm^{-1}), the Doppler effect and the collisional line broadening. As in Refs 21 and 22, the collisional narrowing of the full band was also simultaneously modelled for the ν_1 and $2\nu_2$ bands through the ECS model for the rotational relaxation matrix. For these spectra, the adjusted parameters are a scale intensity factor, the baseline and a small frequency shift.

The agreement between the calculated and experimental PARS profiles (Figs 5 and 6) is good and similar to that obtained previously.[21,22] For CARS spectroscopy, we were not able to simulate accurately experimental profiles (Figs 5 and 6). This may be due to remaining saturation effects and to the more complicated line shape of this non-linear Raman technique, especially to the influence of the non-resonant susceptibility, χ_{NR}. It seems that CARS is much more sensitive than PARS to saturation.

As a further step, we recorded the Raman spectrum of the weak hot band $\nu_1 + \nu_2 - \nu_2$ in the 1409 cm^{-1} region (Fig. 7). Some lines were adjusted individually. To our knowledge, no high-resolution Raman spectrum of this band has been obtained previously.

The rotational line $S(12)$ of the ν_1 mode is superposed on this band. The energy diagram of the lower and upper states of this band with π_u symmetry is given in Fig. 8. Each J level undergoes an 'l-doubling' phenomenon, which is explained by the splitting of Σ^+(a) and Σ^-(s) states under the interaction of rotational and vibrational levels. Only the Σ^-(s) states are allowed by symmetry. Hence the $\nu_1 + \nu_2 - \nu_2$ hot band consists of two Q-branches corresponding to the c and d subsets of energy levels (Fig. 8): for c,

$$\nu(J) = \nu_0 + \Delta B_{(c)} J(J+1) - \Delta D_{(c)} J^2(J+1)^2 \quad (9)$$

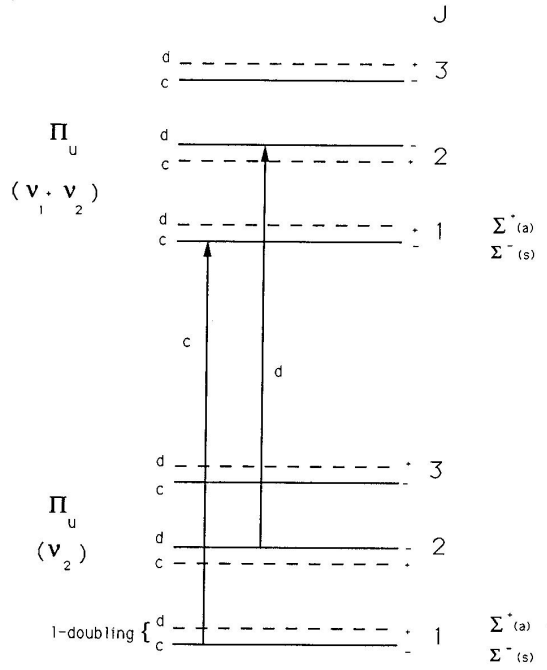

Figure 8. Vibration–rotational levels for π_u–π_u transition.

with $J = 1, 3, 5, 7, \ldots$, and for d,

$$\nu(J) = \nu_0 + \Delta B_{(d)} J(J+1) - \Delta D_{(d)} J^2(J+1)^2$$

with $J = 2, 4, 6, 8, \ldots$.

Frequencies and intensities were calculated using the available constants:[24] $\nu_0 = 1409.476$ cm^{-1}, $\Delta B_{(c)} = -2.263 \times 10^{-4}$ cm^{-1}, $\Delta B_{(d)} = 7.67 \times 10^{-5}$ cm^{-1}, $\Delta D_{(c)} = -7.8 \times 10^{-9}$ cm^{-1} and $\Delta D_{(d)} = -0.166 \times 10^{-7}$ cm^{-1}.

The nuclear statistical weight is the same for all

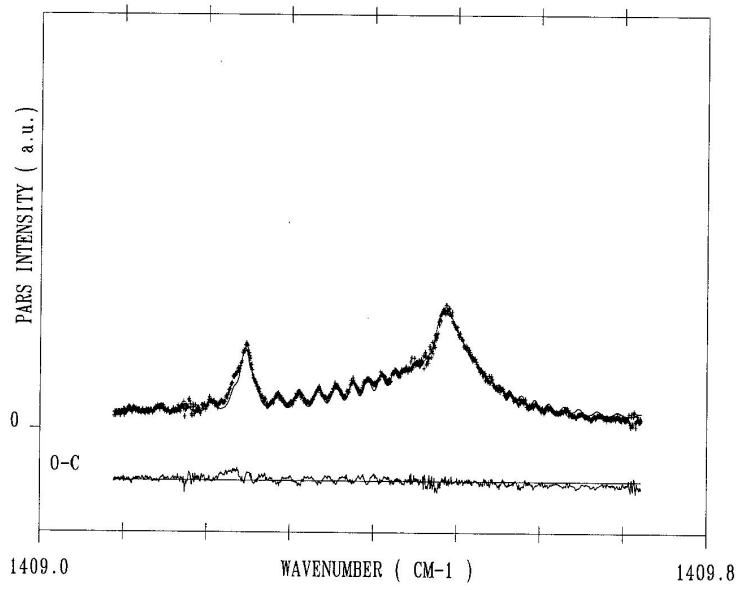

Figure 7. PARS spectrum of the hot band $\nu_1 + \nu_2 - \nu_2$ and the $S(12)$ line at $P = 30$ Torr (4 kPa) and $T = 297$ K. $P_p = 350$ kW and $P_s = 100$ kW. Solid line, calculated spectra; +, experimental.

levels. The calculated PARS profile is also shown in Fig. 7. It only takes into account the apparatus function, Doppler and collisional broadening. Good agreement between the observed and calculated PARS spectra is found.

DISCUSSION AND CONCLUSION

We have presented a high-resolution photoacoustic Raman experiment using two narrow-line pulsed lasers. The resolution achieved is about 0.0054 cm^{-1} (FWHM) and thus will allow the resolution of rotational—vibrational spectra of many gases. The sensitivity of the apparatus is fairly good, even at the low pressures required for high resolution, as demonstrated by the recording of the weak hot band $\nu_1 + \nu_2 - \nu_2$ of CO_2. Further enhancement of the sensitivity is expected with the help of an electret rather than a condenser microphone, and/or with a different design of the photoacoustic cell to concentrate the acoustic wave on the microphone. The main limitation encountered is a spurious absorption signal of the two beams by the gas itself, probably due to multi-photon absorption.[7]

In spite of this, we have obtained a spectrum of the $\nu_1 + \nu_2 - \nu_2$ band whose structure is well reproduced. We have also verified that the frequency line shape of the PARS signal led to the same agreement between calculated and observed profiles as in the case of SRS. Therefore, PARS is well suited for line-shape studies.

The simultaneously recorded CARS spectra show that CARS is even more sensitive at very low pressure, but the line shape seems to be more difficult to reproduce.

Finally, PARS, which is very easy to handle from the point of view of optics (just mixing and focusing of two lasers near a microphone), can provide very useful information about the Raman spectra of gases, especially for small Raman shifts as there is no signal at the Rayleigh line frequency. Attempts will be made to record high-resolution pure rotational Raman spectra of molecules for which no such spectra are available at present.

Acknowledgements

This research was supported by the Conseil Régional de Bourgogne. The authors are indebted to R. Saint-Loup for technical assistance.

REFERENCES

1. P. Esherick and A. Owyoung, in *Advances in Infrared and Raman Spectroscopy*, edited by R. J. Clark and R. E. Hester, Vol. 9, p. 130. Heyden, London (1982).
2. W. Kiefer and D. A. Long, *Non-Linear Raman Spectroscopy and Its Chemical Applications*. Reidel, Dordrecht (1982).
3. G. L. Eesley, *Coherent Raman Spectroscopy*. Pergamon Press, Oxford (1981).
4. H. W. Schrötter, H. Frunder, H. Berger, J. P. Boquillon, B. Lavorel and G. Millot, in *Advances in Non-Linear Spectroscopy*, edited by R. J. Clark and R. E. Hester, Chapt. 3, p. 97. Wiley, Chichester (1988).
5. H. W. Schrötter, H. Berger, J. P. Boquillon, B. Lavorel and G. Millot, *J. Raman Spectrosc.* **21**, 781 (1990).
6. J. J. Barrett and M. J. Berry, *Appl. Phys. Lett.* **34**, 144 (1979).
7. D. R. Siebert, G. A. West and J. J. Barrett, *Appl. Opt.* **19**, 1, 53 (1980).
8. A. M. Brodnikowskii, V. P. Zharov and N. I. Koroteev, *Sov. J. Quantum Electron.* **15**, 12,1600 (1985).
9. A. B. Duval, D. A. King, R. Haines, N. R. Isenor and B. J. Orr, *J. Raman Spectrosc.* **17**, 177 (1986).
10. A. Owyoung, *IEEE Quantum Electron.* **14**, 192 (1978).
11. G. A. West, *Rev. Sci. Instrum.* **54**, 797 (1983).
12. V. N. Bagratashvili, Z. P. Zharov and V. V. Lobko, *Sov. J. Quantum Electron.* **8**. 366 (1978).
13. J. Wrobel and M. Vala, *Chem. Phys.* **33**, 93 (1978).
14. G. Millot, B. Lavorel, R. Chaux, R. Saint-Loup, G. Pierre, H. Berger, J. I. Steinfeld and B. Foy, *J. Mol. Spectrosc.* **127**, 156 (1988).
15. R. Chaux, C. Milan, G. Millot, B. Lavorel, R. Saint-Loup and J. Moret-Bailly, *J. Opt. (Paris)* **19**, 3 (1988).
16. M. Rotger, R. Chaux, H. Berger and J. Moret-Bailly, *J. Opt. (Paris)* **21**, 193 (1990).
17. M. Péalat, M. Lefebvre, J. P. Taran and P. L. Kelley, *Phys. Rev. A* **38**, 1948 (1988).
18. R. P. Lucht and R. L. Farrow, *J. Opt. Soc. Am.* **B5**, 1243 (1988).
19. H. Moosmüller, C. Y. She and W. M. Huo, *Phys. Rev. A* **40**, 6983 (1989).
20. G. O. Sitz and R. L. Farrow, *J. Chem. Phys.* **93**, 7883 (1990).
21. B. Lavorel, G. Millot, R. Saint-Loup, H. Berger, L. Bonamy, J. Bonamy and D. Robert, *J. Chem. Phys.* **93**, 2176 (1990).
22. B. Lavorel, G. Millot, R. Saint-Loup, H. Berger, L. Bonamy, J. Bonamy and D. Robert, *J. Chem. Phys.* **93**, 2185 (1990).
23. R. Saint-Loup, B. Lavorel, G. Millot, C. Wenger and H. Berger, *J. Raman Spectrosc.* **21**, 77 (1990).
24. L. S. Rothman, L. D. G. Young, *J. Quant. Spectrosc. Radiat. Transfer* **25**, 505 (1981).

JOURNAL OF MOLECULAR SPECTROSCOPY **192,** 294–308 (1998)
ARTICLE NO. MS987695

Ab Initio Calculations and High-Resolution Spectroscopy of the Bending Pentad of SiH_2D_2 in the 10–16 μm Region

M. Rotger,* V. Boudon,* B. Lavorel,* S. Sommer,† H. Bürger,† J. Breidung,‡
W. Thiel,‡ M. Bétrencourt,§ and J.-C. Deroche§

*Laboratoire de Physique de l'Université de Bourgogne, B.P. 400, F-21011 Dijon Cedex, France; †Anorganische Chemie, Universität-Gesamthochschule, D-42097 Wuppertal, Germany; ‡Universität Zürich, Organisch-Chemisches Institut, Winterthurerstrasse 190, CH-8057 Zürich, Switzerland; and §L.P.M.A., Université Paris-Sud, Bât. 350, F-91405 Orsay, France

Received May 5, 1998; in revised form August 1, 1998

The SiH_2D_2 asymmetric top has nine vibrational modes, five of them forming a pentad strongly perturbed by Coriolis interactions. High-level *ab initio* calculations of SiH_2D_2 have been performed which yield numerous spectroscopic parameters related to the harmonic and anharmonic force fields. The bending pentad comprising $\nu_4(A_1)$, $\nu_7(B_1)$, $\nu_5(A_2)$, $\nu_9(B_2)$, and $\nu_3(A_1)$ has been studied by high-resolution Fourier transform spectroscopy; the region 600–1050 cm^{-1} has been investigated with a resolution of ca. 4×10^{-3} cm^{-1}. Raman BOXCARS spectroscopy has been used for the infrared inactive ν_5 band. The Raman apparatus function was 0.0054 cm^{-1}. Assignments of about 4000 transitions including all bands have been made, mostly employing ground state combination differences techniques, and a global fit has been performed. The fundamentals ν_4 (681.624 cm^{-1}), ν_7 (742.640 cm^{-1}), ν_5 (842.381 cm^{-1}), ν_9 (859.750 cm^{-1}), and ν_3 (942.741 cm^{-1}) are strongly coupled by *A*-, *B*-, and *C*-type Coriolis interactions, and *ab initio* predictions of these interaction parameters were used to set up a network of interactions that was refined by the experimental data. The global standard deviation for the entire body of data is 7.1×10^{-4} cm^{-1}. Satisfactory synthetic spectra which are very sensitive to relative signs of dipole moment derivatives and Coriolis interaction constants were obtained with the guidance of *ab initio* calculations. Finally, fair to good agreement of experimental and *ab initio* calculated molecular parameters was obtained. For the first time, a complete analysis of the pentad of SiH_2D_2 in the 10–16 μm region has been carried out. A full set of rovibrational parameters is given for these five interacting levels, including first and second order Coriolis interaction constants.

1. INTRODUCTION

High-resolution spectra of the heavy homologues of methane such as SiH_4, GeH_4, and SnH_4 have been studied to great extent in the recent decades (*1*). Among these species, the SiH_4 spherical top has been intensively investigated, in both its ground and excited states (*2*), with the aim of understanding processes that are important for industrial applications based on the use of silicon. Moreover, the symmetric top species H_3SiD and $HSiD_3$ have been the targets of numerous investigations with regard to highly excited vibrational states (*3–7*). SiH_2D_2 is the only deuterated variety of silane which is an asymmetric top, and its rovibrational spectrum was until now almost unknown. We can only find in the literature ground state parameters for this molecule, although they are very precise. These have been calculated by merging the numerous data derived from the infrared (*8*) and pure rotational spectra (*9, 10*). Moreover, low-resolution infrared data have been reported (*11*).

In this paper, we report for the first time the analysis of the five lowest excited vibrational states, namely $\nu_4(A_1$, 681 $cm^{-1})$, $\nu_7(B_1$, 742 $cm^{-1})$, $\nu_5(A_2$, 842 $cm^{-1})$, $\nu_9(B_2$, 859 $cm^{-1})$, and $\nu_3(A_1$, 942 $cm^{-1})$. This group of five bending levels forms a pentad which is well separated from the other vibrational modes such as $\nu_2(A_1$, 1582 $cm^{-1})$, $\nu_8(B_2$, 1600 $cm^{-1})$, or $\nu_1(A_1$, 2189 $cm^{-1})$.

In the experimental part, we report the first rovibrational spectra of the ν_5 band obtained thanks to high-resolution Coherent Anti-Stokes Raman Spectroscopy (CARS), this band being infrared inactive. The other bands of the bending pentad have been recorded using high-resolution Fourier transform infrared spectroscopy (FTIR), and the assignments have already been used for the determination of the ground state parameters (*8*). Then, we present results of theoretical calculations which are used for the first detailed rovibrational analysis of the pentad, in which both infrared and Raman data are combined. This leads to a complete set of parameters including first and second order Coriolis interaction constants. Synthetic spectra obtained from these molecular parameters are presented which confirm the agreement of experimental observations and *ab initio* predictions, in particular with regard to interaction constants and dipole moment derivatives.

0022-2852/98 $25.00

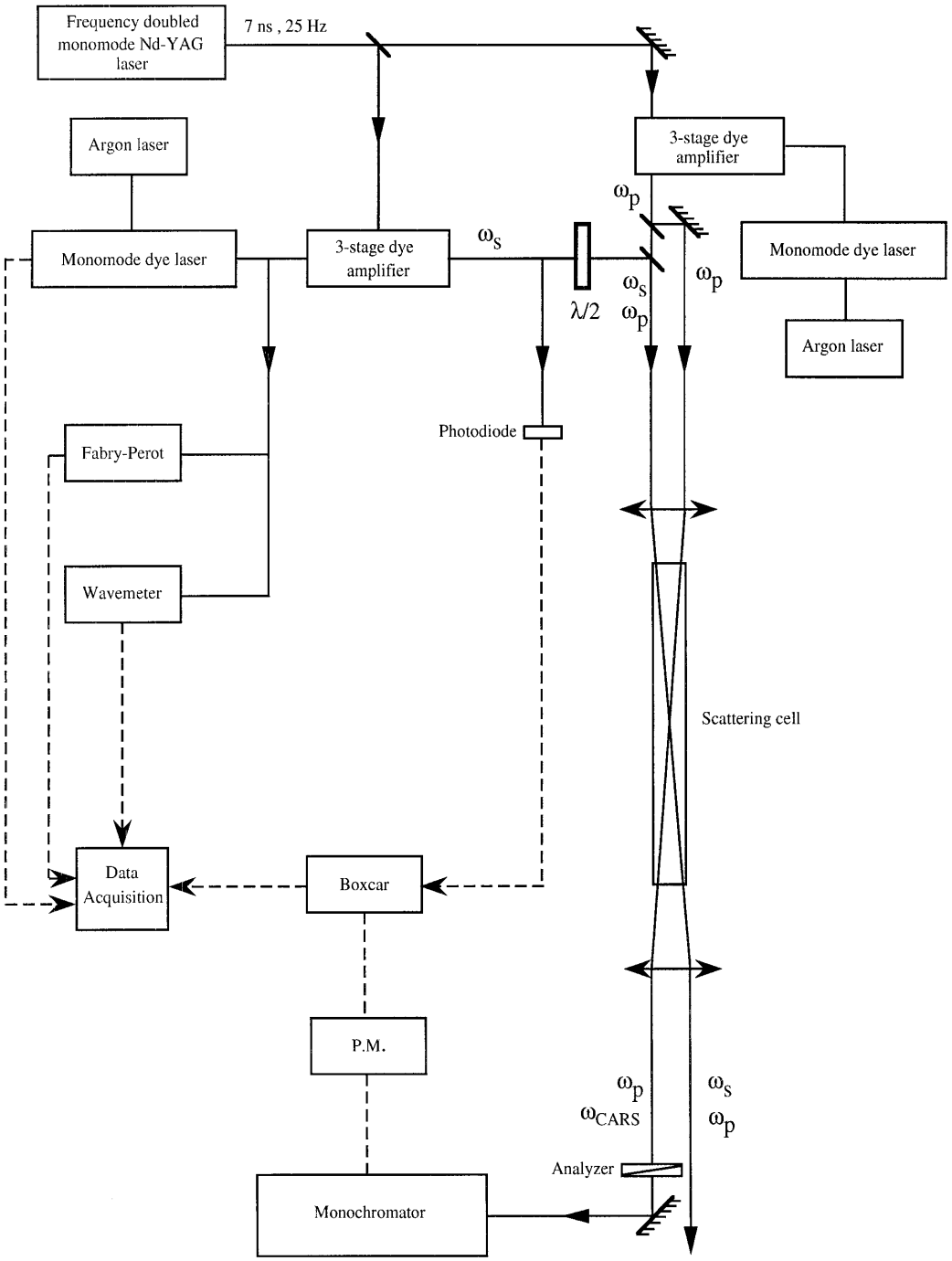

FIG. 1. BOXCARS experimental set-up. P.M. is a photomultiplier; ω_p, ω_s, and ω_{CARS} represent the pump, Stokes, and CARS signal beams, respectively.

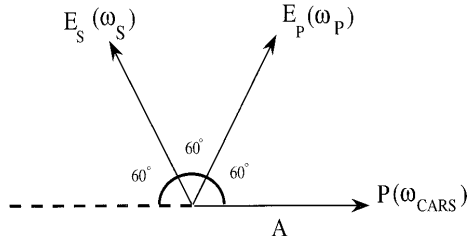

FIG. 2. Polarization directions for the pump beam (P), the Stokes beam (S), and the CARS signal (A is the analyzer's direction) in the BOXCARS experiment.

2. EXPERIMENTAL SECTION

The SiH_2D_2 sample was prepared by reduction of SiH_2Cl_2 with $LiAlD_4$ as described in Ref. (*12*).

2.1 FTIR Spectra

High-resolution infrared spectra have been obtained at Giessen (Germany) with a Bruker 120 HR interferometer (*13*) equipped with a globar source, a KBr beamsplitter, and a Cu:Ge detector for the $\nu_4/\nu_7/\nu_9$ bands and a MCT800 detector for the ν_3 band. The instrumental bandwidth (1/maximum optical path difference) was about 4×10^{-3} cm^{-1}. Cells (18.5 cm long) with KBr windows were used. The ν_3 band has been recorded with a gas pressure of 4 mbar. For the $\nu_4/\nu_7/\nu_9$ region, this pressure was 2 mbar. Calibration was done with N_2O and OCS lines in the 590- and 850-cm^{-1} region, respectively (*14*). Wavenumber precision is estimated to be $0.1–0.2 \times 10^{-3}$ cm^{-1}.

2.2 BOXCARS Spectra

This part of the work is based on high-resolution polarization BOXCARS technique (*15, 16*). We used a BOXCARS spectrometer, which is derived from the stimulated Raman spectrometer in Dijon (*17, 18*). In such a spectrometer, there are two pulsed laser beams: the pump beam at a fixed frequency ω_p and the Stokes beam at a variable frequency ω_s. In our case, this type of spectroscopy was performed using two pulsed amplified c.w. dye lasers. Power values were 160 and 230 kW for pump and Stokes beams, respectively.

Here, the instrumental bandwidth was about 0.0054 cm^{-1}. The accuracy of the CARS wavenumber calibration was about 0.0015 cm^{-1} in the best cases (*19*). This calibration was

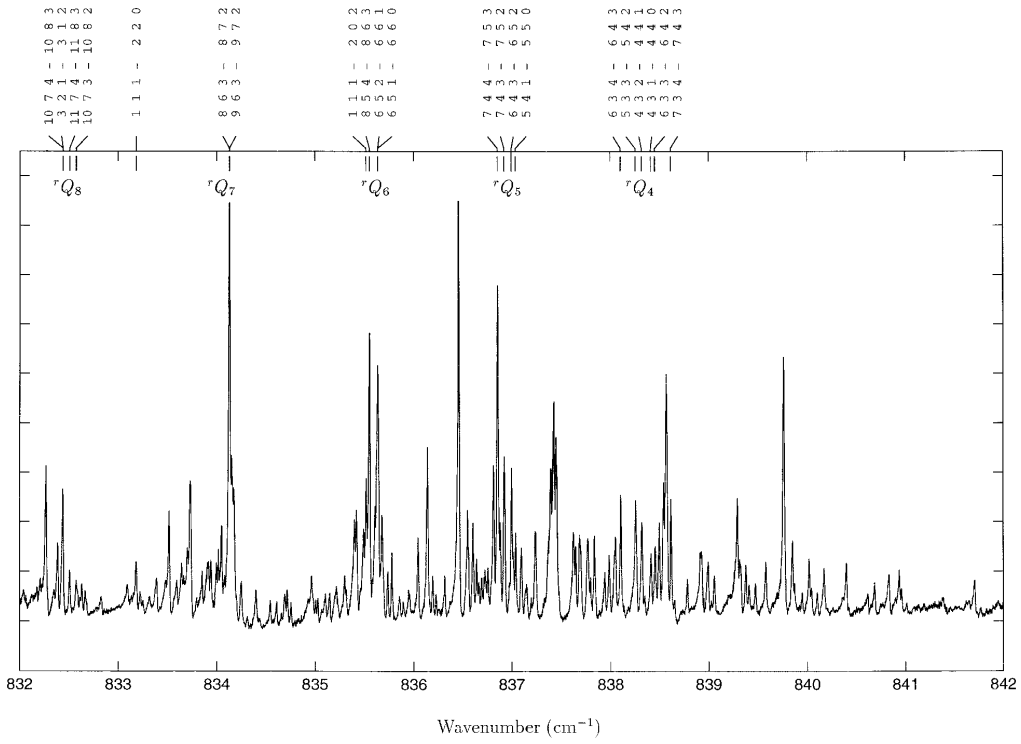

FIG. 3. SiH_2D_2 CARS spectrum in the $\nu_5(A_2)$ region with some $J'K'_aK'_c - J''K''_aK''_c$ assignments at room temperature and a gas pressure of 50 Torrs.

TABLE 1

Equilibrium Bond Length r_e (Å), Equilibrium (A_e, B_e, C_e) and Ground State (A_0, B_0, C_0) Rotational Constants (cm^{-1}), Quartic Centrifugal Distortion Constants (Δ_J, Δ_{JK}, Δ_K, δ_J, δ_K) (10^{-4} cm^{-1}), and Fundamental Vibrational Wavenumbers ν_i (cm^{-1}) of SiH_2D_2

Constant	CCSD(T)/cc-pV(Q,T)Z[a]	Experiment	Ref.[b]
r_e	1.4735	1.4732(2)	Ref. (*1*)
A_e	2.3394	2.3405(7)	(c)
B_e	1.9268	1.9278(6)	(c)
C_e	1.6659	1.6667(5)	(c)
A_0	2.3230	2.3211	Ref. (*8*)
B_0	1.9128	1.9115	Ref. (*8*)
C_0	1.6518	1.6507	Ref. (*8*)
Δ_J	0.155	0.158	Ref. (*8*)
Δ_{JK}	−0.0998	−0.0997	Ref. (*8*)
Δ_K	0.304	0.310	Ref. (*8*)
δ_J	0.0357	0.0368	Ref. (*8*)
δ_K	−0.0602	−0.0615	Ref. (*8*)
A_1 ν_1	2193(2269)	2189	Ref. (*11*)
ν_2	1585(1622)	1587	Ref. (*11*)
ν_3	948(963)	943	This work
ν_4	685(693)	682	This work
A_2 ν_5	846(857)	842	This work
B_1 ν_6	2193(2272)	2183	Ref. (*11*)
ν_7	748(758)	743	This work
B_2 ν_8	1603(1642)	1601	Ref. (*11*)
ν_9	866(879)	860	This work

[a] The ground-state corrections of the rotational constants ($A_e - A_0, \ldots$) and the anharmonic shifts $\omega_i - \nu_i$ of the vibrational wavenumbers have been transferred from MP2/TZ2Pf. Values in parentheses: harmonic wavenumbers ω_i (cm^{-1}).

[b] The experimental ground-state values for the rotational and centrifugal distortion constants and for the fundamental wavenumbers determined in this work are known to more significant digits than quoted (see Tables 6 and 7).

[c] Calculated from the experimental r_e value.

TABLE 2

Computed[a] Coriolis Coupling Constants ζ_{ij} (Dimensionless) and ξ_{ij} (cm^{-1}) Compared with ξ_{ij} (cm^{-1}) and η_{ij} (cm^{-1}) Values Obtained from the Fit for the Pentad of SiH_2D_2

Coriolis Type	ν_i	ν_j	ζ_{ij}	ξ_{ij}	ξ_{ij}	η_{ij}
			Ab initio	*Ab initio*	Experiment	Experiment
A	ν_7	ν_4	−0.6196	−2.9017	−2.698(2)	−0.0248(2)
A	ν_9	ν_5	−0.1940	−0.9075	−0.797(2)	−0.0060(2)
A	ν_3	ν_7	−0.0647	−0.3048	0.40(3)	0.0016(3)
B	ν_9	ν_7	−0.4700	−1.8160	−1.740(7)	0.0315(5)
B	ν_3	ν_5	+0.4587	1.7707	1.48(2)	−0.0235(2)
B	ν_5	ν_4	−0.3808	−1.4757	−0.63(2)	−0.0020(4)
C	ν_5	ν_7	+0.4213	1.4065	1.693(6)	0.0458(2)
C	ν_3	ν_9	−0.7459	−2.4878	−2.752(4)	0.0019(4)
C	ν_9	ν_4	−0.0045	−0.0152	0.832(74)	0.0114(4)

Note. The standard deviations in the unit of the last digits are given in parentheses.

[a] CCSD(T)/cc-pV(Q,T)Z. For sign conventions of the normal coordinates see text.

obtained from wavenumber measurements of the c.w. dye laser provided by a Michelson interferometer (*19, 20*) and from transmission fringes of an étalon.

Since the $\nu_5(A_2)$ region lies at rather low frequency, the BOXCARS (*16*) geometry was used in order to enable a spatial separation of the different frequencies (ω_p, ω_s, and ω_{CARS}) as indicated in Fig. 1. Moreover, it leads to a reduction of the nonresonant background signal produced in the cell windows. Due to the low intensity of this band, we also used crossed polarizations as shown in Fig. 2. This configuration gives maximum CARS signal as explained in Ref. (*21*) and decreases the nonresonant signal in the gas itself. The weak $\nu_5(A_2)$ lines of SiH_2D_2 were recorded several times at room temperature and a gas pressure of 50 Torr in a 50-cm^{-1} range. The main part of the spectrum is shown on Fig. 3.

TABLE 3

Computed[a] Dipole Moment Derivatives (D. $Å^{-1}$. $amu^{-1/2}$) and Infrared Band Intensities A_k (km/mol)[b] of SiH_2D_2

Component i	Mode k	$(\partial\mu_i/\partial Q_k)_0$	A_k
b	A_1 1	+1.1479	55.6
b	2	+0.8480	30.4
b	3	+1.2105	61.9
b	4	+0.9988	42.1
a, b, c	A_2 5	0.0	0.0
c	B_1 6	+1.6066	109.0
c	7	+1.4546	89.3
a	B_2 8	+1.2245	63.3
a	9	+1.6742	118.3

[a] CCSD(T)/cc-pV(Q,T)Z. For sign conventions of the normal coordinates see text.

[b] Double harmonic approximation.

TABLE 4
Computed[a] and Experimental Vibration–Rotation Interaction Constants (10^{-2} cm^{-1}) of SiH_2D_2

Constant	*Ab initio* value	Experimental value	Effective (starred) values
α_1^A	1.396		
α_2^A	0.422		
α_3^A	1.341	-0.1	
α_4^A	10.635	11.1	-2.075 (b)
α_5^A	3.323		-0.284 (c)
α_6^A	1.031		
α_7^A	-11.940	-11.5	0.770 (b)
α_8^A	1.142		
α_9^A	-4.075	-3.75	-0.469 (c)
α_1^B	0.819		
α_2^B	1.095		
α_3^B	-3.029	-2.30	-0.130 (d)
α_4^B	0.709	0.29	-0.589 (e)
α_5^B	1.818		-1.081 (d), 3.116 (e), 0.217 (f)
α_6^B	0.607		
α_7^B	2.837	2.54	0.176 (g)
α_8^B	0.659		
α_9^B	-2.708	-2.88	-0.047 (g)
α_1^C	0.225		
α_2^C	1.180		
α_3^C	-7.757	-8.76	-0.529 (h)
α_4^C	1.024	0.51	
α_5^C	-2.183		-0.224 (i)
α_6^C	0.396		
α_7^C	1.571	2.99	-0.389 (i)
α_8^C	0.785		
α_9^C	7.583	8.76	0.355 (h)

[a] MP2/TZ2Pf. Corresponding equilibrium bond length: 1.4741 Å.
[b] Without contributions from the Coriolis interaction specified by $\zeta_{74}^A = -0.6196$ ($\omega_4 - \omega_7 = -66.2$ cm^{-1}).
[c] Without contributions from the Coriolis interaction specified by $\zeta_{95}^A = -0.1940$ ($\omega_5 - \omega_9 = -22.8$ cm^{-1}).
[d] Without contributions from the Coriolis interaction specified by $\zeta_{35}^B = +0.4593$ ($\omega_3 - \omega_5 = +108.3$ cm^{-1}).
[e] Without contributions from the Coriolis interaction specified by $\zeta_{54}^B = -0.3802$ ($\omega_4 - \omega_5 = -167.0$ cm^{-1}).
[f] Without contributions from the Coriolis interaction specified by ζ_{35}^B and ζ_{54}^B (see footnotes d and e).
[g] Without contributions from the Coriolis interaction specified by $\zeta_{97}^B = -0.4698$ ($\omega_7 - \omega_9 = -123.7$ cm^{-1}).
[h] Without contributions from the Coriolis interaction specified by $\zeta_{39}^C = -0.7458$ ($\omega_3 - \omega_9 = +85.5$ cm^{-1}).
[i] Without contributions from the Coriolis interaction specified by $\zeta_{57}^C = +0.4214$ ($\omega_5 - \omega_7 = +100.8$ cm^{-1}).

3. *AB INITIO* CALCULATIONS

The equilibrium geometry and the harmonic force field of silane (point group T_d) were calculated at the level of coupled cluster theory with single and double excitations (*22*) augmented by a perturbational treatment of connected triple excitations (CCSD(T)) (*23*). Three different basis sets were employed: two of them, labeled TZ2Pf and cc-pV(Q,T)Z, respectively, have been described in previous work (*24*). The third one, denoted as aug-cc-pV(Q,T)Z, is derived from cc-pV(Q,T)Z by the addition of a single diffuse function of each angular momentum to the cc-pVQZ (Si) and cc-pVTZ (H) sets

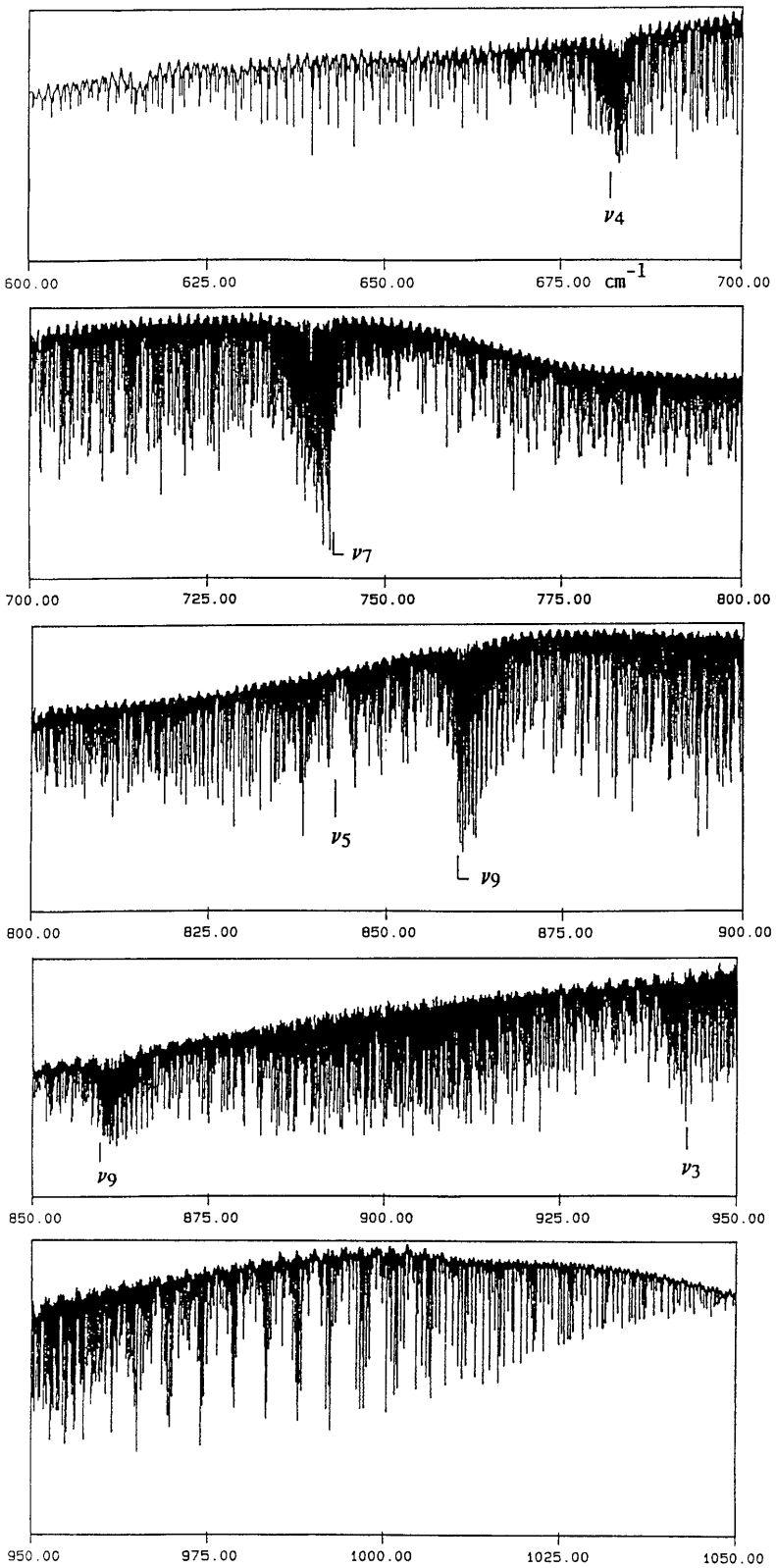

FIG. 4. Overview of the FTIR spectrum of SiH_2D_2 in the 600–1050 cm^{-1} region (room temperature, sample pressure around 3 mbar, and 18.5 cm cell length).

(*25, 26*). The quartic normal coordinate force field of SiH_2D_2 was computed at the level of second-order Møller–Plesset perturbation theory (MP2) (*27*) employing the TZ2Pf basis. Spherical harmonics were used throughout, and all electrons were correlated.

The CCSD(T) and MP2 quantum chemical computations were carried out using a local version of the ACESII (*28*) and the GAUSSIAN94 program (*29*), respectively, with analytic evaluation of the harmonic force fields (*30, 31*).

The MP2/TZ2Pf cubic and quartic normal coordinate force constants were determined with the use of a finite difference procedure (*32*) involving displacements along reduced normal coordinates (stepsize $\Delta q = 0.03$) and the calculation of analytic second derivatives (relative precision $\epsilon < 10^{-7}$) at these displaced geometries. At the MP2/TZ2Pf stationary point of silane, the Cartesian gradient components did not exceed 10^{-8} au. The anharmonic spectroscopic constants were derived from the theoretical normal coordinate force fields applying standard formulas based on second-order rovibrational perturbation theory (*33, 34*).

Both the Coriolis coupling constants and the dipole moment derivatives depend on the signs of the normal coordinates of SiH_2D_2. We have adopted the following sign convention: in the A_1, B_1, and B_2 modes the Si atom moves in the direction of the b, c, and a principal axis of inertia; if the central atom moves in the positive direction of the relevant axis, the associated normal coordinate is positive. In the case of the A_2 mode (ν_5) the normal coordinate was defined to be positive if the H atom with positive b and c coordinates moves in the direction of the positive a axis.

For the sake of brevity, only the CCSD(T)/cc-pV(Q,T)Z results are listed in Tables 1–3 since they are considered to be most reliable. Comparison with CCSD(T)/TZ2Pf and CCSD(T)/aug-cc-pV(Q,T)Z shows that the CCSD(T) results change only slightly with such basis set variations (see below).

TABLE 5
Statistical Information about the Assigned Lines in FTIR and CARS Spectra

Mode	Type	ΔK_c	Number of lines	J'_{max}, $(K'_a)_{max}$
$\nu_4(A_1)$	b	±1, ±3	1148	26, 11(16†)
$\nu_7(B_1)$	c	±0, ±2	1145	24, 9(15†)
$\nu_5(A_2)$	IR	0, ±2, ±4	274	19, 18
	CARS	±1	68	14, 13
$\nu_9(B_2)$	a	±1	392	13, 10(13†)
$\nu_3(A_1)$	b	±1, ±3	980	26, 8(26†)

† First lines ($J' = K'_a$, $K'_c = 0$ or 1) only.

TABLE 6
Rovibrational Parameters for the Ground State of SiH_2D_2 (in cm^{-1}) Taken from Ref. (*8*)

Parameter	$v = 0$
A_0	2.32111957(1)
B_0	1.91149908(9)
C_0	1.65072354(9)
$\Delta_J^0 \times 10^4$	0.158203(5)
$\Delta_{JK}^0 \times 10^4$	−0.099687(16)
$\Delta_K^0 \times 10^4$	0.31008(2)
$\delta_J^0 \times 10^4$	0.036750(2)
$\delta_K^0 \times 10^4$	−0.061483(18)
$\Phi_J^0 \times 10^8$	0.04362(10)
$\Phi_{JK}^0 \times 10^8$	−0.1755(12)
$\Phi_{KJ}^0 \times 10^8$	0.428(4)
$\Phi_K^0 \times 10^8$	−0.144(3)
$\phi_J^0 \times 10^8$	0.01807(5)
$\phi_{JK}^0 \times 10^8$	−0.0683(6)
$\phi_K^0 \times 10^8$	0.050(3)

Note. The standard deviations in the unit of the last digits are given in parentheses.

Table 1 contains the theoretical data for the equilibrium bond distance, the equilibrium and ground state rotational constants, the quartic centrifugal distortion constants (A-reduction), and the vibrational wavenumbers of the SiH_2D_2 isotopomer. Except for the harmonic vibrational wavenumbers, all these quantities can be compared with their experimental counterparts (see Table 1).

Excellent agreement between theory and experiment is found for the equilibrium bond length in silane: the difference is 0.0003 Å, only slightly above the experimental error bar (*1*). Consequently, the computed rotational constants of SiH_2D_2 are very close to the experimental values (within

TABLE 7
Band Centers and Effective Rotational Parameters for the Pentad of SiH_2D_2 (in cm^{-1})

Parameter	$v_4 = 1$	$v_7 = 1$	$v_5 = 1$	$v_9 = 1$	$v_3 = 1$
ν_v	681.62394(3)	742.64029(3)	842.38121(9)	859.750104(4)	942.74106(4)
A_v	2.3233(2)	2.3297(2)	2.3170(2)	2.3286(2)	2.3049(1)
B_v	1.9061(2)	1.9086(2)	1.9139(4)	1.9148(2)	1.9213(4)
C_v	1.64432(7)	1.6640(2)	1.6445(2)	1.6599(2)	1.6405(3)
$\Delta_J^v \times 10^4$	0.15755(4)	0.1408(2)	0.1512(4)	0.1641(2)	0.1868(3)
$\Delta_{JK}^v \times 10^4$	−0.334(5)	−0.072(9)	−0.1042(4)	−0.002(2)	−0.058(3)
$\Delta_K^v \times 10^4$	0.418(6)	0.45(1)	0.257(4)	0.296(2)	0.236(3)
$\delta_J^v \times 10^4$	0.03776(2)	0.03907(9)	0.0304(2)	0.04625(8)	0.0394(2)
$\delta_K^v \times 10^4$	−0.017(3)	0.016(4)	−0.147(3)	−0.061(2)	−0.084(2)
3944 assigned lines, $J_{max} = 27$, $(K_a)_{max} = 23$, $(K_c)_{max} = 27$, $\sigma = 0.71 \times 10^{-3}$ cm^{-1}					

Note. J_{max} is the maximum J value assigned (idem for $(K_a)_{max}$ and $(K_c)_{max}$), and σ is the root mean square of the residuals. The standard deviations in the unit of the last digits are given in parentheses. See also Table 2 for the Coriolis parameters.

0.08%). The theoretical equilibrium quartic centrifugal distortion constants of SiH_2D_2 reproduce the associated experimental ground state data (*8*) to within 3%. The calculated fundamental vibrational wavenumbers of SiH_2D_2 differ from the observed fundamentals (present work and Ref. (*11*)) by at most 10 cm^{-1} (usually slightly too large); except for the antisymmetric SiH_2 stretch (ν_6) (measured only at low resolution, Ref. (*11*)), the deviations do not exceed 6 cm^{-1}. These comparisons between theory and experiment demonstrate the overall accuracy of the CCSD(T)/cc-pV(Q,T)Z harmonic force field of SiH_2D_2.

Table 2 lists the Coriolis coupling constants ζ_{ij} and ξ_{ij} as predicted by the CCSD(T)/cc-pV(Q,T)Z harmonic force field. Only those constants are shown which are relevant for the analysis of the $\nu_4/\nu_7/\nu_5/\nu_9/\nu_3$ pentad in SiH_2D_2. Previous experience suggests that the ζ_{ij} constants should be accurate to 0.01 at the chosen level of theory. The conversion from ζ_{ij} to ξ_{ij} requires harmonic wavenumbers and equilibrium rotational constants which are computed with errors of less than 1% (pentad region) and 0.1%, respectively (see Table 1). Combining these error estimates, the theoretical ξ_{ij} constants in the pentad region are expected to be accurate to about 3–7% (excluding the very small constants ζ_{37}^A and ζ_{94}^C, see Table 2, where relative errors should not be quoted).

Table 3 shows the electric dipole moment derivatives with respect to the normal coordinates of SiH_2D_2 as obtained at the CCSD(T)/cc-pV(Q,T)Z level. There is a modest basis set dependence: employing the smaller TZ2Pf basis causes the calculated dipole derivatives to decrease by 1.7–3.9% compared to the values in Table 3, whereas the dipole derivatives from the larger aug-cc-pV(Q,T)Z basis differ by at most 1.3%. Even at the lower MP2/TZ2Pf level, the results deviate by only up to 3% from those in Table 3. Based on the consistency of the theoretical dipole moment derivatives for different levels and basis sets, it seems likely that the actual errors will be below 10% (possibly even below 5%).

Table 4 reports the MP2/TZ2Pf vibration–rotation interaction constants of SiH_2D_2. In the perturbational expressions of these constants (*33, 34*) the Coriolis contributions may diverge if there is a strong Coriolis resonance. It is then necessary to define effective (starred) constants where the contributions of the corresponding Coriolis resonance are excluded according to Eq. 13 of Ref. (*34*). Such effective constants are also given in Table 4 when appropriate (see footnotes for details). Errors in MP2/TZ2Pf vibration–rotation coupling constants are normally in the range up to 20%, but larger errors cannot be excluded, especially in the case of strong Coriolis resonances (where comparisons may be problematic due to the effective nature of the empirical constants). The deviations between the theoretical and experimental data in Table 4 are consistent

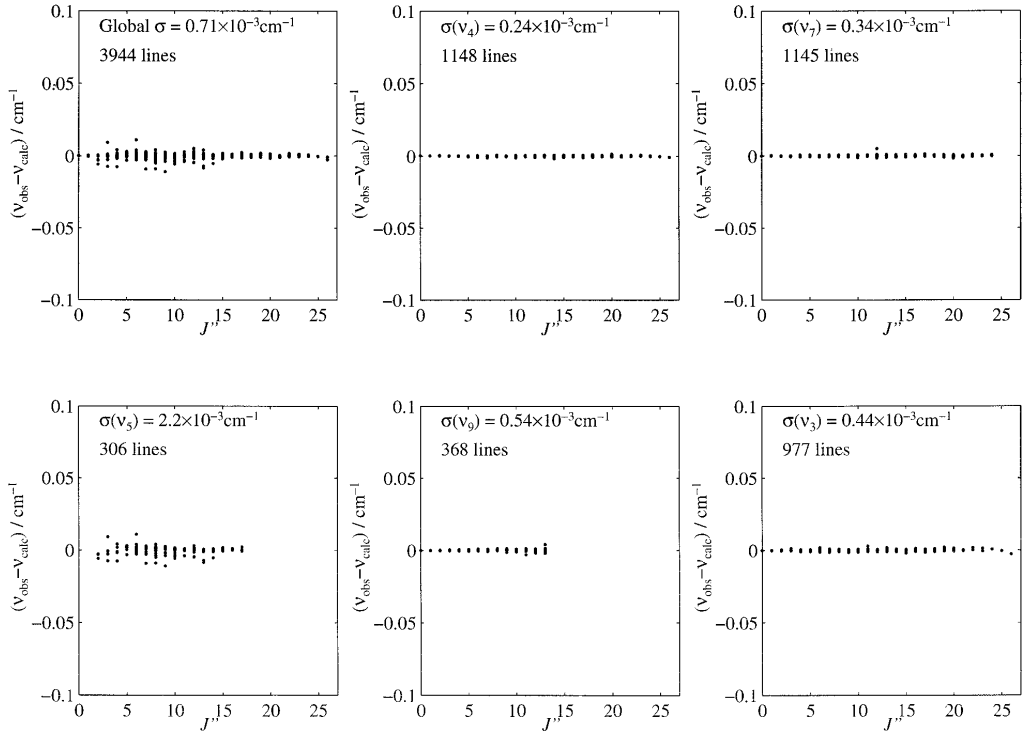

FIG. 5. Diagrams showing the observed-calculated linepositions for each individual band in the pentad. The numbers of lines indicated represent lines retained in the fit.

with these expectations, particularly for the larger coupling constants.

4. DESCRIPTION AND ASSIGNMENT OF THE SPECTRUM

4.1 Infrared Spectrum

The infrared spectrum extends from ca. 600 to ca. 1050 cm^{-1}. The four infrared-active bending fundamentals can be easily located by means of their pronounced Q branches. The overview spectrum is illustrated in Fig. 4. While the Q branches of the a-type and c-type bands ν_9 and ν_7 reveal fairly sharp edges and are degraded to the high and low wavenumbers, respectively, Q branches of the b-type bands ν_3 and ν_4 are broad and less prominent.

In general the spectrum is not very dense, except for the Q branches, although nearly all K_a levels are split, and $\Delta K_c = \pm 2$ and ± 3 transitions can be observed in addition to the stronger ones with $\Delta K_c = 0$ and ± 1. Although SiH_2D_2 is a prolate asymmetric top, it behaves at high J like an oblate rotor, levels with different K_a but the same K_c values coinciding as J increases. Owing to the size of the rotational constants, only rotational levels with $J \leq 25$ are significantly populated.

Assignments could not be made with ease because consecutive lines of J, K_a, or K_c series are far apart. Therefore they had to rely on ground state combination differences (GSCD). These were initially based on the reported ground state constants (*9, 10*) and later, when the number of assignments grew, on GSCD of the present study and Ref. (*8*). Quite generally more than two transitions sharing an upper state were observed. Table 5 gives relevant statistical information on the observations.

The ν_4, ν_7, and ν_3 bands have been assigned rather completely. Rotational levels of these vibrational states are above all globally perturbed. To the contrary, ν_9 and the infrared inactive ν_5 fundamental, besides Coriolis-induced global interactions, reveal numerous local resonances. The Coriolis interaction transfers intensity from ν_9 to infrared inactive ν_5 transitions. Since the strength of this perturbation increases with J, observations for small J and large K_c are rather scarce. The Coriolis resonance between ν_5 and ν_9 is of A type, thus E^+ interacts with E^- and O^+ with O^- levels. Interactions both with $\Delta K_c = -1$

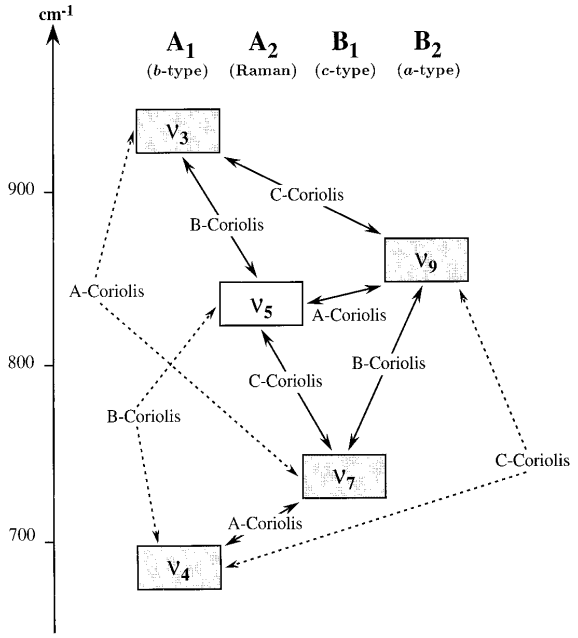

FIG. 6. Coriolis coupling scheme in the pentad of SiH_2D_2. Dashed lines represent "second-neighbor" couplings (see text).

and −3 are predicted from the upper state energy level pattern and indeed were detected in the spectra. However, the ν_5/ν_9 interactions cannot be treated in a satisfactory manner without considering the global perturbations by ν_3, ν_4, and ν_7.

4.2 CARS Spectrum

The CARS spectrum has a rather low intensity. Thus, we have observed only the strongest lines belonging mainly to Q branches of the ν_5 band in the ca. 830 to ca. 860 cm^{-1} region. These lines were also assigned thanks to the GSCD method.

5. THEORETICAL MODEL FOR THE ζ FIT

The theory for asymmetric top molecules is well known (*35*), and we simply recall here the most useful relations. According to perturbation theory, the rovibrational Hamiltonian H can be developed as a series of increasing order terms. Two successive contact transformations can be applied to H in such a way that the first vibrationally nondiagonal term in the development is of order six.

We have adopted the I^r representation (*35*), where the a, b, and c principal inertia axes are attached to the z, x, and y axes of the molecular-fixed frame, respectively (see figure of the molecule in Ref. (*8*)). So, using the asymmetric top reduction (A-reduction), we have the following nonzero pure rotational matrix elements:

$$\begin{aligned}\langle J, k|H^{(A)}_{\text{rot}}|J, k\rangle &= \frac{1}{2}[B^{(A)}_x + B^{(A)}_y]J(J+1) + \left[B^{(A)}_z - \frac{1}{2}(B^{(A)}_x + B^{(A)}_y)\right]k^2 \\ &\quad - \Delta_J J^2(J+1)^2 - \Delta_{JK}J(J+1)k^2 - \Delta_K k^4 \\ &\quad + \Phi_J J^3(J+1)^3 + \Phi_{JK}J^2(J+1)^2k^2 \\ &\quad + \Phi_{KJ}J(J+1)k^4 + \Phi_K k^6, \end{aligned} \quad [1]$$

and

$$\begin{aligned}\langle J, k \pm 2|H^{(A)}_{\text{rot}}|J, k\rangle &= \left\{\frac{1}{4}[B^{(A)}_x - B^{(A)}_y] - \delta_J J(J+1) - \frac{\delta_k}{2}[(k\pm 2)^2 + k^2]\right. \\ &\quad + \phi_J J^2(J+1)^2 + \frac{1}{2}\phi_{JK}J(J+1)[(k\pm 2)^2 + k^2] \\ &\quad \left. + \frac{1}{2}\phi_K[(k\pm 2)^4 + k^4]\right\} \\ &\quad \times \sqrt{[J(J+1) - k(k\pm 1)][J(J+1) - (k\pm 1)(k\pm 2)]}, \end{aligned} \quad [2]$$

k being the projection quantum number on the molecule-fixed z axis.

The Coriolis part of the transformed Hamiltonian,

$$W^{\alpha}_{vv'} = i\xi^{\alpha}_{vv'}J_{\alpha} + \eta^{\beta\gamma}_{vv'}(J_{\beta}J_{\gamma} + J_{\gamma}J_{\beta}), \quad [3]$$

(α, β, and γ being x, y, or z) has the following nonvanishing matrix elements:

$$\langle J, k|W^{z}_{vv'}|J, k\rangle = i\xi^{z}_{vv'} \times k, \quad [4]$$

$$\begin{aligned}\langle J, k|W^{z}_{vv'}|J, k\pm 2\rangle &= \mp\frac{i}{2}\eta^{xy}_{vv'}\sqrt{J(J+1) - k(k\pm 1)} \\ &\quad \times \sqrt{J(J+1) - (k\pm 1)(k\pm 2)}, \end{aligned} \quad [5]$$

$$\begin{aligned}\langle J, k|W^{x}_{vv'}|J, k\pm 1\rangle &= \frac{i}{2}[\xi^{x}_{vv'} \mp \eta^{yz}_{vv'}(2k\pm 1)]\sqrt{J(J+1) - k(k\pm 1)}, \end{aligned} \quad [6]$$

$$\begin{aligned}\langle J, k|W^{y}_{vv'}|J, k\pm 1\rangle &= \frac{1}{2}[\pm\xi^{y}_{vv'} + \eta^{zx}_{vv'}(2k\pm 1)]\sqrt{J(J+1) - k(k\pm 1)}. \end{aligned} \quad [7]$$

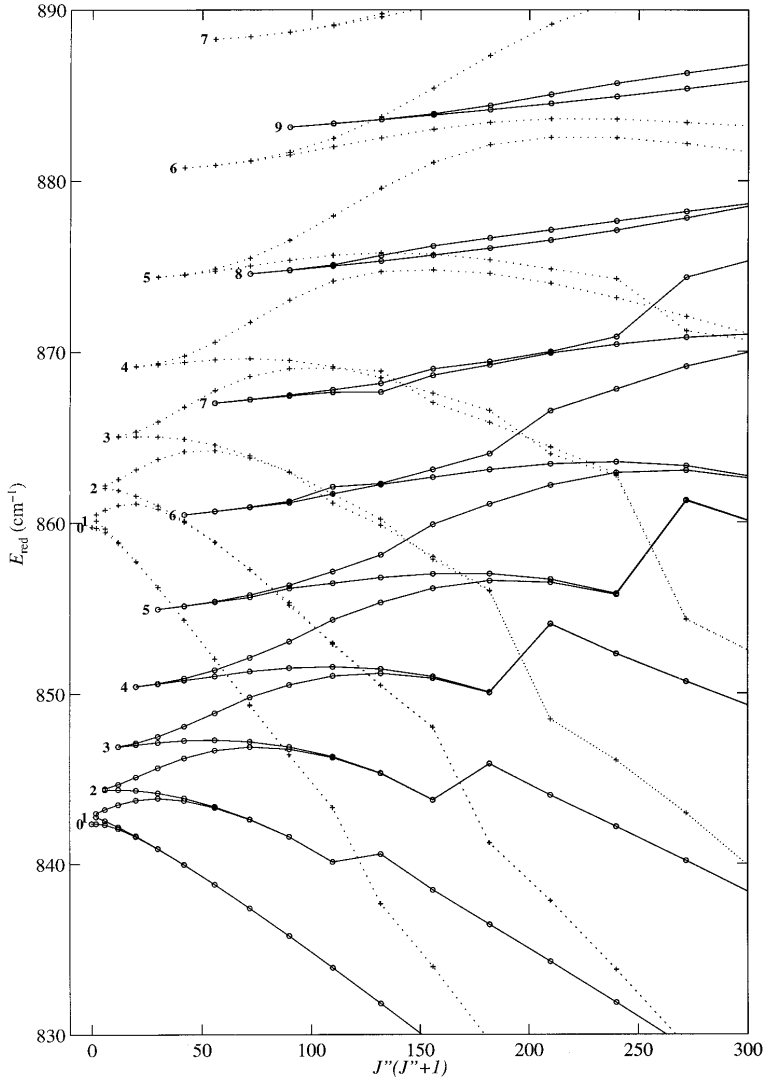

FIG. 7. Calculated reduced energy levels ($\nu - (B_0 + C_0)J(J+1)/2$) in the ν_5/ν_9 region. Continuous lines represent ν_5 levels and dashed lines represent ν_9 levels. Numbers in bold are K''_a values.

Figure 6 shows the allowed Coriolis couplings in the case of the pentad of SiH_2D_2.

To compute the eigenvalues of this Hamiltonian, we can use the well-known Wang transformation (*35*)

$$|J, K^{\pm}, M\rangle = \frac{1}{\sqrt{2}}(|J, K, M\rangle \pm |J, -K, M\rangle), \qquad [8]$$

with $K = |k|$ and M being the projection quantum number on the laboratory-fixed Z axis. This enables us to reduce the problem into four blocks corresponding to the irreducible representations of the C_{2v} symmetry group.

Equations [1], [2], and [4]–[7] will be used in the following to determine the rovibrational parameters.

6. ANALYSIS OF THE SPECTRA

The theory recalled above has been used for the analysis of the spectra. Practically, we have used two programs made available by H. M. Pickett, Jet Propulsion Laboratory, USA (*36*): SPFIT, to perform the data fits employing a least-

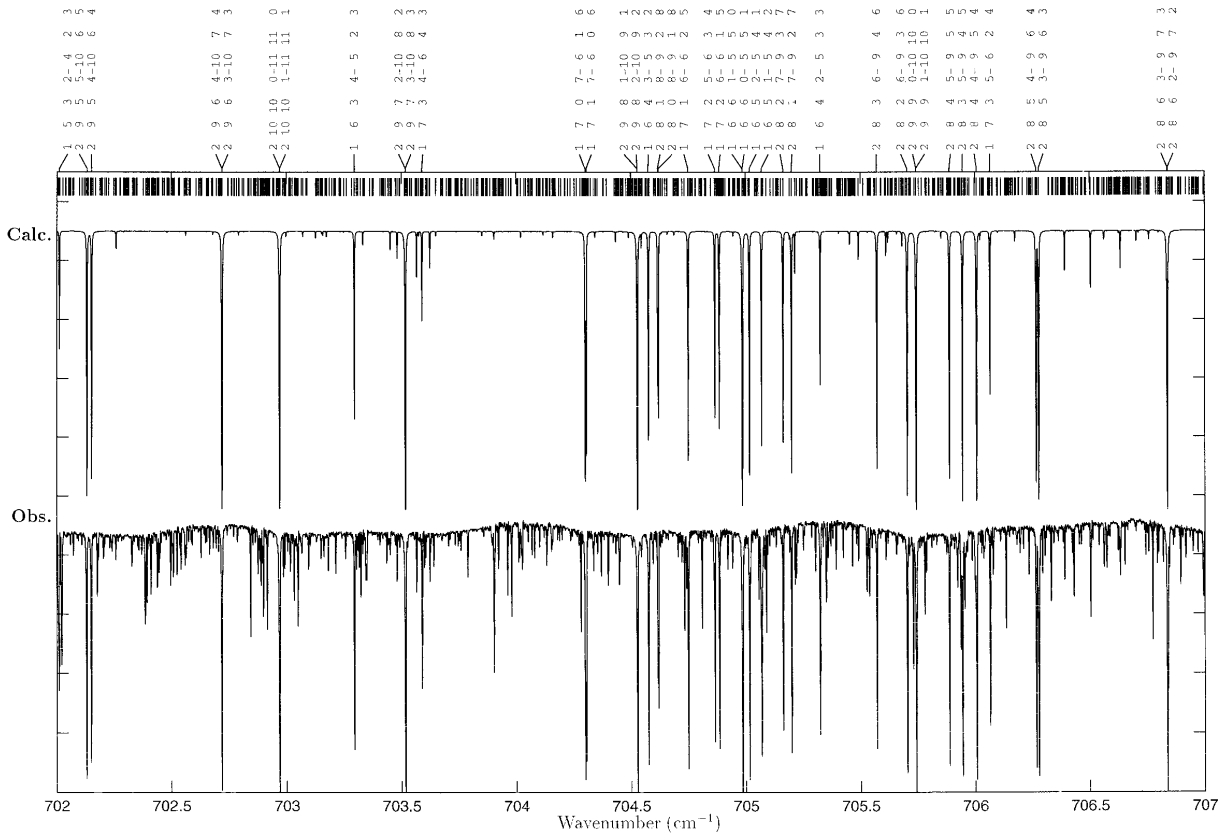

FIG. 8. Simulated spectrum of a part of the ν_4/ν_7 region of SiH_2D_2 calculated with the parameters given in Tables 2, 3, 6, and 7. Some $i\ J'K'_aK'_c - J''K''_aK''_c$ assignments are indicated at the top of the figure, i being the mode number ($1 = \nu_4$, $2 = \nu_7$, $3 = \nu_5$, $4 = \nu_9$, $5 = \nu_3$).

squares fit procedure, and SPCAT, to calculate the simulated spectrum using the fitted parameters.

We have used both sets of data (Fourier transform and polarized CARS spectra) described in Section 2. A better accuracy for the linepositions in the CARS spectra has been reached by averaging data from four different scans. Assignments (IR and CARS spectra) have been realized using the GSCD method, as explained in Section 4. Data for the ν_5 band include CARS lines and also transitions induced by coupling that were observed in the infrared spectrum. All ground state parameters have been fixed to the values taken from the literature (*8*) and listed in Table 6. The sextic rotational parameters for the five fundamentals have been fixed to the ground state values. So 63 parameters were in fact fitted. Many attempts were necessary, because convergence (and stability) of such a fit is somewhat difficult to reach. One important leading criterion was that the rotational parameters should not differ too much from their ground state values.

The results of the fit are given in Tables 2 and 7. We obtained a very good global root mean squares value (σ), of 0.71×10^{-3} cm^{-1}, that is better than the experimental error on linepositions. Among the 4007 assigned transitions, 63 were rejected during the fit, essentially in the $\nu_5/\nu_9/\nu_3$ region. Figure 5 shows in detail the (observed − calculated) linepositions for individual bands as a function of J''. The worst result is for ν_5, but the σ value in this case (2.2×10^{-3} cm^{-1}) is still acceptable in view of the small number of data obtained for this band and their lower precision. Table 2 also gives a comparison between the empirical first-order Coriolis constants and the *ab initio* values. The agreement is not too good for the three "second-neighbor" interactions (dashed lines on Fig. 6), but these constants appear to be difficult to fit with the present data set, so the values obtained here are probably not really significant. Nevertheless, one should notice that their introduction in the fit gave a real improvement. Moreover, the experimental and *ab initio* α values (see Table 4) are in rather satisfactory agreement. The experimental α values have been obtained by subtracting the fitted values of the rotational constants

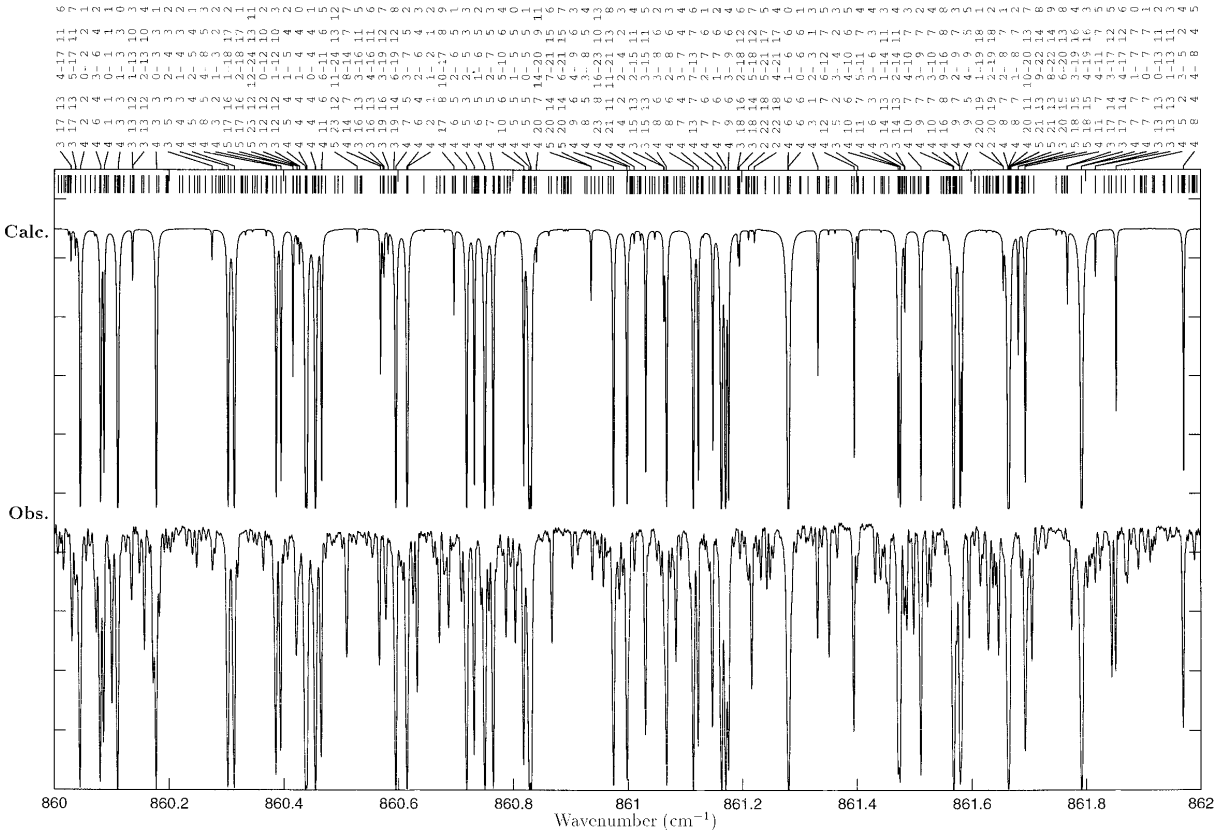

FIG. 9. Simulated spectrum of a part of the ν_9 Q branch of SiH_2D_2 calculated with the parameters given in Tables 2, 3, 6, and 7. Same notations as for Figure 8.

(Table 7) and the effective rotational constants of S. Sommer (*8*) (obtained from an isolated band analysis).

Figure 7 displays some of the reduced energies for the vibrational levels in the ν_5/ν_9 region, as a function of $J''(J''+1)$. The complex mixings occurring between these two vibrational states are clearly seen, especially the intensity transfer from one band to the other near local resonances due to the Coriolis interaction. Figures 8–10 show examples where experimental and calculated spectra are compared. The simulations were computed only for infrared active bands. The vibrational temperature was fixed to 293 K and the Doppler linewidth (FWHM) to 0.002 cm^{-1}. We used *ab initio* values (CCSD(T)/cc-pV(Q,T)Z) for the dipole moment derivatives (see above and Table 3).

7. CONCLUSION

We have recorded in Dijon the first high-resolution Raman spectrum of the ν_5 band of SiH_2D_2 using polarization CARS spectroscopy. We have merged the data on ν_4, ν_7, ν_5, ν_9, and ν_3 obtained by Fourier transform infrared and CARS techniques, which have proved to be complementary. The first technique provides spectra mostly of the four infrared active bands of the pentad and the second furnishes information on the infrared-forbidden ν_5 band.

We were able to fit the data to a complete set of parameters despite the fact that we treat five interacting levels with only a restricted number of assignments in the ν_5/ν_9 region. Nevertheless, these parameters are quite precisely determined. No perturbations other than the Coriolis couplings between these five modes seem to occur here, since no overtone or combination band lies in this region. *Ab initio* calculations have proved to be of great help for performing such a complex analysis.

As a next step, some higher energy levels such as ν_1, ν_2, ν_6, and ν_8 will be studied by Fourier transform spectroscopy. Their analysis will benefit significantly from the present study owing to the expected interactions between overtone and combination levels involving the bending levels. One such interaction be-

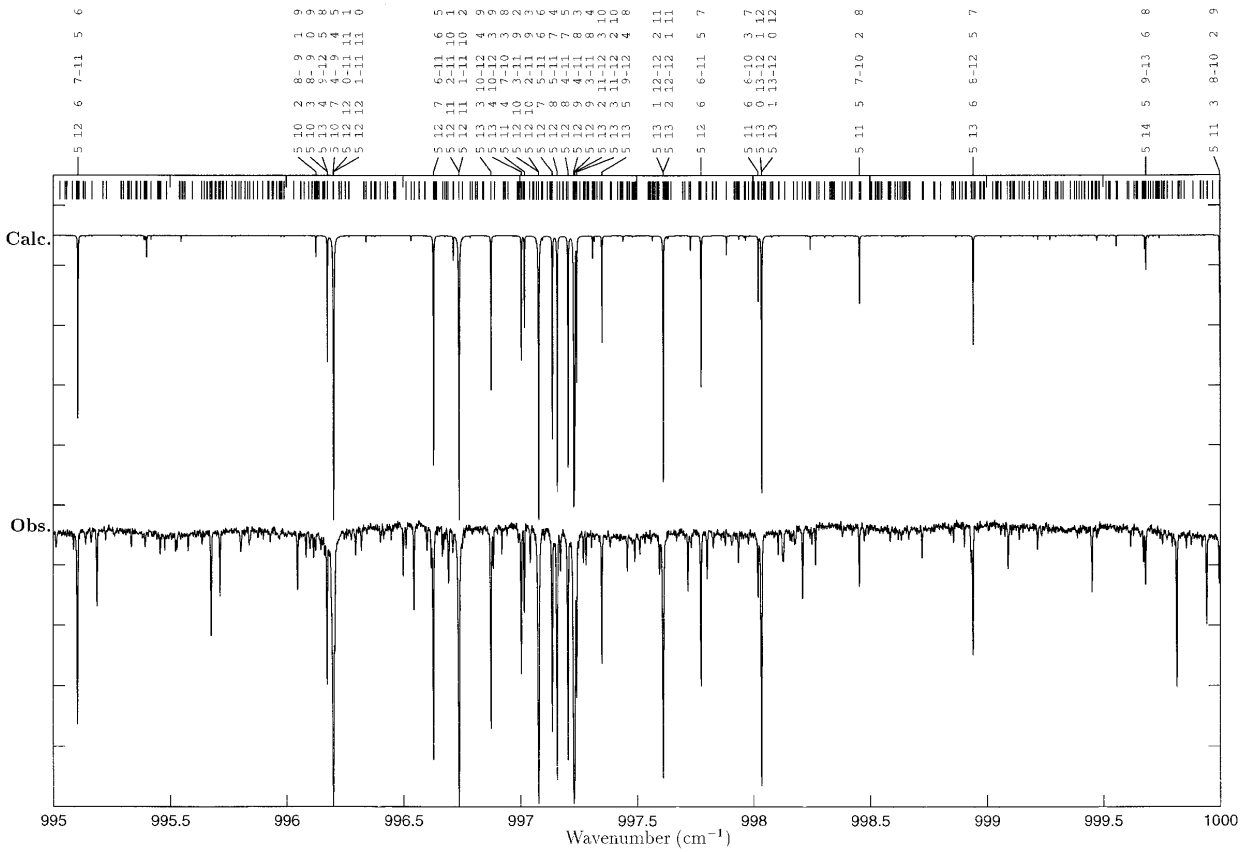

FIG. 10. Simulated spectrum of a part of the ν_3 region of SiH_2D_2 calculated with the parameters given in Tables 2, 3, 6, and 7. Same notations as for Figure 8.

tween ν_8 (B_2) and $\nu_7 + \nu_9$ (A_2) has already been established by a study of the respective CARS spectra (*37*).

ACKNOWLEDGMENTS

We are very grateful to Dr. H. M. Pickett from JPL (USA) who provided his programs (SPCAT and SPFIT) and gave a lot of advice. Dr. D. Luckhaus from ETH Zürich (Switzerland) and Dr. F. Hegelund, Aarhus University (Denmark), are also thanked for useful discussions. K. Lattner, Giessen (Germany), is thanked for recording the infrared spectra. This work was partly supported by the Schweizerischer Nationalfonds. The authors thank Profs. J. Gauss (Mainz) and J. F. Stanton (Austin) for providing a copy of ACESII with CCSD(T) analytic second derivatives.

REFERENCES

1. H. Bürger and A. Rahner, *in* "Vibrational Spectra and Structure," (J. R. Durig, Ed.), vol. 18, p. 217–370, Elsevier, Amsterdam, 1990.
2. G. Pierre, A. Valentin, and L. Henry, *Can. J. Phys.* **62,** 254–259 (1984).
3. L. Fusina, E. Cané, R. Escribano, and H. Bürger, *J. Mol. Spectrosc.* **184,** 385–394 (1997) and references cited therein.
4. C. Frommer, R. W. Lovejoy, R. L. Sams, and W. B. Olson, *J. Mol. Spectrosc.* **89,** 261–267 (1981).
5. K. Ohno, H. Matsuura, and H. Murata, *Chem. Lett.* 27–30 (1982).
6. D. R. J. Boyd, *J. Chem. Phys.* **23,** 922–926 (1955).
7. R. A. Bernheim, F. W. Lampe, J. F. O'Keefe, and J. B. Qualey III, *J. Mol. Spectrosc.* **104,** 194–198 (1984).
8. M. Bétrencourt, J.-C. Deroche, H. Bürger, and S. Sommer, *J. Mol. Spectrosc.* **142,** 220–226 (1990).
9. K. Ohno, H. Matsuura, Y. Endo, and E. Hirota, *J. Mol. Spectrosc.* **118,** 1–17 (1986).
10. K. Ohno, H. Matsuura, Y. Endo, and E. Hirota, *J. Mol. Spectrosc.* **111,** 73–82 (1985).
11. J. H. Meal and M. K. Wilson, *J. Chem. Phys.* **24,** 385–390 (1956).
12. E. G. Rochow, "Comprehensive Inorganic Chemistry," vol. 2, Pergamon, Oxford, UK, 1973.
13. M. Birk, M. Winnewisser, and E. A. Cohen, *J. Mol. Spectrosc.* **136,** 402–445 (1989).
14. G. Guelachvili and K. N. Rao, "Handbook of Infrared Standards," Academic Press, New York, 1986.
15. J. W. Nibler and G. A. Pubanz, *in* "Advances in Spectroscopy," (R. J. H. Clark and R. E. Hester, Eds.), vol. 15, Wiley, New York, 1988.
16. R. Brakel and F. W. Schneider, *in* "Advances in Spectroscopy," (R. J. H. Clark and R. E. Hester, Eds.), vol. 15, Wiley, New York, 1988.
17. G. Millot, B. Lavorel, R. Chaux, R. Saint-Loup, G. Pierre, H. Berger, J. I. Steinfeld, and B. Foy, *J. Mol. Spectrosc.* **127,** 156–177 (1988).

18. B. Lavorel, G. Millot, R. Saint-Loup, H. Berger, L. Bonamy, J. Bonamy, and D. Robert, *J. Chem. Phys.* **93,** 2176–2184 (1990).
19. R. Chaux, C. Milan, G. Millot, B. Lavorel, R. Saint-Loup, and J. Moret-Bailly, *J. Optics* **19,** 3–14 (1988).
20. C. Milan, M. Pullicino, G. Roussel, and J. Moret-Bailly, *J. Optics* **15,** 31–41 (1984).
21. N. Papineau and M. Péalat, *J. Chem. Phys.* **79**(12), 5758–5768 (1983).
22. G. D. Purvis III and R. J. Bartlett, *J. Chem. Phys.* **76,** 1910–1918 (1982).
23. K. Raghavachari, G. W. Trucks, J. A. Pople, and M. Head-Gordon, *Chem. Phys. Lett.* **157,** 479–483 (1989).
24. S. Bailleux, M. Bogey, J. Demaison, H. Bürger, M. Senzlober, J. Breidung, W. Thiel, R. Fajgar, and J. Pola, *J. Chem. Phys.* **106,** 10016–10026 (1997).
25. R. A. Kendall, T. H. Dunning, Jr., and R. J. Harrison, *J. Chem. Phys.* **96,** 6796–6806 (1992).
26. D. E. Woon and T. H. Dunning, Jr., *J. Chem. Phys.* **98,** 1358–1371 (1993).
27. C. Møller and M. S. Plesset, *Phys. Rev.* **46,** 618–622 (1934).
28. J. F. Stanton, J. Gauss, J. D. Watts, W. J. Lauderdale, and R. J. Bartlett, *Int. J. Quantum Chem. Symp.* **26,** 879–894 (1992).
29. M. J. Frisch, G. W. Trucks, H. B. Schlegel, P. M. W. Gill, B. G. Johnson, M. A. Robb, J. R. Cheeseman, T. A. Keith, G. A. Petersson, J. A. Montgomery, K. Raghavachari, M. A. Al-Laham, V. G. Zakrzewski, J. V. Ortiz, J. B. Foresman, J. Cioslowski, B. B. Stefanov, A. Nanayakkara, M. Challacombe, C. Y. Peng, P. Y. Ayala, W. Chen, M. W. Wong, J. L. Andres, E. S. Replogle, R. Gomperts, R. L. Martin, D. J. Fox, J. S. Binkley, D. J. Defrees, J. Baker, J. P. Stewart, M. Head-Gordon, C. Gonzalez, and J. A. Pople, "GAUSSIAN 94," Revision D.2 and E.2, Gaussian, Pittsburgh, PA, 1995.
30. J. Gauss and J. F. Stanton, *Chem. Phys. Lett.* **276,** 70–77 (1997).
31. M. Head-Gordon and T. Head-Gordon, *Chem. Phys. Lett.* **220,** 122–128 (1994).
32. W. Schneider and W. Thiel, *Chem. Phys. Lett.* **157,** 367–373 (1989).
33. I. M. Mills, *in* "Molecular Spectroscopy: Modern Research," (K. N. Rao and C. W. Mathews, Eds.), pp. 115–140, Academic, New York, 1972.
34. D. A. Clabo, Jr., W. D. Allen, R. B. Remington, Y. Yamaguchi, and H. F. Schaefer III, *Chem. Phys.* **123,** 187–239 (1988).
35. D. Papoušek and M. R. Aliev, "Molecular Vibrational–Rotational Spectra," Elsevier, Amsterdam, 1982.
36. H. M. Pickett, *J. Mol. Spectrosc.* **148,** 371–377 (1991).
37. M. Bétrencourt, J.-C. Deroche, B. Lavorel, and M. Rotger, *in* "12th International Conference on High-Resolution Infrared and Microwave Spectroscopy," Dobřříš, 1992.

Troisième partie

Chapitre

2

Spectroscopie Expérimentale des Hexafluorures Colorés

Publications P6, P7, P9, P10, P12, P18
Article de revue P23

2.1 Introduction

Avec V. Boudon s'est établie une collaboration dynamique et enrichissante qui a débuté en 1993 par la spectroscopie expérimentale des hexafluorures colorés et plus particulièrement par celle de l'hexafluorure d'Iridium (IrF_6). En effet, au cours de sa thèse V. Boudon, a mis en place un modèle pour l'analyse des spectres rovibroniques de telles molécules. Cependant, peu de spectres étaient alors disponibles dans la littérature aussi bien à basse qu'à haute résolution.

Les hexafluorures colorés constituent un groupe de molécules à sous-couche électronique incomplète et de ce fait, présentent des états électroniques de base et excités dégénérés. Il se produit dans ce cas des phénomènes de couplages vibroniques (effet Jahn-Teller, ...). Par conséquent, les spectres de ces molécules sont très denses et aucun spectre haute résolution n'avait été encore enregistré à ce jour.

2.2 Résultats

Les publications données ci-après donnent un bon aperçu des spectres enregistrés pour ce type de molécules : des spectres basse résolution de l'ultraviolet à l'infrarouge en passant par le visible ainsi que des spectres Raman mais aussi des spectres à haute résolution dans l'infrarouge. Notre premier travail a consisté à mettre en place des collaborations avec des collègues chimistes (notamment le Professeur D. Avignant de l'université de Clermont-Ferrand et le Professeur H. Selig de l'université de Jérusalem) capables de nous synthétiser des hexafluorures colorés et d'en remplir de petites cuves en quartz avec des fenêtres fixées par adhésion moléculaire. Cette étape franchie, nous pouvions alors en effectuer la spectroscopie à basse résolution sur différents spectromètres commerciaux à Dijon et à Lille. Nous avons ainsi obtenu toute une série de spectres que nous avons interprétés à l'aide d'un modèle simple.

Ces molécules étant lourdes, il s'avérait indispensable de les refroidir thermodynamiquement afin d'avoir des bandes vibrationnelles de modes fondamentaux dépourvues de bandes chaudes et de pouvoir résoudre la structure rovibronique. Du point de vue expérimental, cela est possible en utilisant un jet supersonique avec le spectromètre considéré. Ce type d'expérience a été mise en place à l'ETH de Zürich dans le groupe du Pr. Quack. La complication majeure réside dans le fait que ces substances sont extrêmement corrosives donc très difficiles à manipuler. Il est nécessaire d'utiliser des pompes équipées avec des huiles peu réactives de type Fomblin. Le jet et les pompes ont été installées à la fois sur le spectromètre à Transformée de Fourier et sur le spectromètre à diodes laser de Zürich. Des spectres haute résolution de la bande ν_3 de la molécule ReF_6 ont été enregistrés pour la première fois.

2.3 Perspectives

Cette première expérience zürichoise m'a permis par la suite de mettre en place à Dijon un spectromètre à diode laser et d'enregistrer des portions du spectre de la bande ν_8 de SF_5Cl. Dans l'avenir, nous allons ajouter au spectromètre un jet fente du même type que celui de Zürich.

Les projets expérimentaux seront détaillés dans le chapitre suivant.

D'autres expériences sur les hexafluorures colorés (ReF_6, IrF_6, ...) sont difficiles à mener et ne sont pas envisagées pour le moment. De nouveaux essais seraient éventuellement possibles sur la nouvelle TF plus résolvante de Zürich, le problème principal restant celui de l'obtention de grandes quantités de ces molécules.

2.4 Articles-clés

Sont reproduits ici les trois articles les plus représentatifs de mon activité expérimentale sur les hexafluorures colorés faite en collaboration avec V. Boudon.

- [**P7 :** *J. Raman Spectrosc.*, **27**, 145–148 (1996)] porte sur l'enregistrement du spectre Raman spontanné de la molécule IrF_6.
- [**P10 :** *Spectrochim. Acta A*, **53**, 991–994 (1997)] présente les transitions électroniques situées dans le visible de la molécule OsF_6.
- [**P18 :** *J. Chem. Phys.*, **117-7**, 3196–3206 (2002)] porte sur l'enregistrement et l'analyse de la bande ν_3 des molécules WF_6 et ReF_6.

JOURNAL OF RAMAN SPECTROSCOPY, VOL. 27, 145–148 (1996)

Spontaneous Raman Scattering Spectrum of Gaseous IrF_6 in the Ground Electronic State

M. Rotger* and V. Boudon
Laboratoire de Physique de l'Université de Bourgogne (Unité associée au CNRS No. 1796), Université de Bourgogne, B.P. 138, 21004 Dijon, France

A. T. Nguyen
Instruments SA, Division Jobin Yvon, 16–18 rue du Canal, 91165 Longjumeau Cedex, France

D. Avignant
Laboratoire de Chimie des Solides (Unité associée au CNRS No. 444), Université Blaise Pascal, Clermont-Ferrand, Complexe Scientifique des Cézeaux, 24 avenue des Landais, 63177 Aubière Cedex, France

The Raman spectrum of IrF_6 in the 100–730 cm^{-1} region was observed in the gas phase using argon laser excitation. New values for the $\nu_1(A_{1g})$, $\nu_2(E_g)$, $\nu_5(F_{2g})$ and probably $2\nu_4(F_{1u})$ band centres are given. The *O*, *Q* and *S* branch contours of the $\nu_2(E_g)$ band are described for the first time. The ground vibrational state population analysis allowed confirmation of the Ir—F bond length found in the literature. No evidence for a Jahn–Teller effect in the $X(G_g')$ electronic state was observed.

INTRODUCTION

The transition metal hexafluorides form a very interesting group of molecules, since they are the only compounds of these heavy elements with substantial vapour pressures at room temperature. this implies several industrial applications, such as isotope separation processes (especially with UF_6, NpF_6 and PuF_6) and chemical vapour deposition of thin metal layers on a substrate (WF_6, MoF_6 for integrated circuits;[1] ReF_6, IrF_6 for anti-corrosion layers[2]). In the latter case, it is usual to perform *in situ* Raman or CARS[3] measurements during the deposition reaction in order to analyse the species involved. Hence it is necessary to know the Raman spectrum of the implied hexafluoride well.

We consider here the case of IrF_6, because this molecule is also of considerable theoretical interest owing to the presence of three non-bonding electrons, implying a half-integer total angular momentum. The existence of degenerate electronic states (including the ground state) leads to complex (ro)vibronic couplings. These problems have been treated by Boudon and co-workers.[4,5] Goodman and co-workers[6,7] compared the Raman spectra of several hexafluorides about 30 years ago. The data concerning IrF_6 were recorded in the liquid phase. In 1969, Claassen and Selig[8] presented the Raman spectrum of gaseous IrF_6 at a pressure of 2 atm. The absence of highly sensitive detectors with low dark current such as the CCD (charge coupled device) prevented them from recording this spectrum at ambient temperature (250 Torr) because of an insufficient Raman signal.

In this paper, we present the spontaneous Raman scattering spectrum of gaseous IrF_6 at 300 K in the $X(G_g')$ ground electronic state, corresponding to the 100–730 cm^{-1} region. In the next section, we discuss briefly the methods for IrF_6 synthesis and purification, along with the spectroscopic set-up used. The subsequent section presents the analysis of the data obtained and especially the band profile of the fundamental $\nu_2(E_g)$.

* Author to whom correspondence should be addressed.

CCC 0377-0486/96/020145-04

EXPERIMENTAL

Gas synthesis and purification

Holloway *et al.*[9] improved the IrF_6 synthesis process by use of a dynamic flow system. One of us (D.A.) achieved the synthesis of gas using this method, as follows. Natural iridium powder (*ca.* 0.5 g) was placed in a nickel reactor and first activated using hydrogen. The fluorination reaction (600 °C for 15 min) was complete. Great attention was paid to careful drying of the apparatus, because of the hygroscopic nature of IrF_6. Before being filled into a dry Pyrex container, the gas was passed through three cold traps in order to achieve a first removal of traces of HF.

With the aim of performing spectroscopic studies, the gas needs to be purified once again before filling the quartz spectroscopic cell. This was pumped and heated at 500 °C for 3 days. The IrF_6 vapour was then transferred into it after three successive distillations using solid carbon dioxide (−79 °C).

Spontaneous Raman scattering

This type of spectroscopy was performed by one of us (A.T.N.) using a commercial T64000 Raman system manufactured by Instruments SA, Division Jobin Yvon. It consists of an argon ion cw laser (power *ca* 1 W) used with the green line at 514.5 nm, a triple monochromator and a CCD matrix detector.

Received 4 September 1995
Accepted 26 October 1995

The resolution was between 0.5 and 1 cm^{-1}. The scattered light was collected at 90° from the incident beam. The sample conditions in the quartz cell were temperature 300 K and gas pressure 250 Torr (1 Torr = 133.3 Pa)[10].

RESULTS

Spectrum analysis

Figure 1 shows the spectrum obtained for the 100–730 cm^{-1} region. This is characteristic of an octahedral molecule,[7] with three fundamental bands, namely the very intense $\nu_1(A_{1g})$ stretching mode, near the $\nu_2(E_g)$ mode, and the $\nu_5(F_{2g})$ bending mode at lower energy. Claassen and Selig[8] observed a small peak at 542 cm^{-1} which was assigned to $2\nu_4(F_{1u})$. We noted the possible presence of this transition, but it had a very weak intensity similar to the noise level.

The $\nu_2(E_g)$ band profile is shown in more detail in Fig. 2. We observe *O*, *Q* and *S* branches contours, similar to those of other hexafluorides such as SF_6[11] and WF_6.[8] These branches were not described in Ref. 8. Below we analyse this band aspect by considering the B_0 rotational constant value. In Table 1, we compare our peak positions with those of Claassen and Selig.[8] The agreement is fairly good.

The $\nu_2(E_g)$ band branch structure analysis

Let us consider the most simplified model, in which rotational transitions of this band are given by [see Eqn (49) in Ref. 5, with $D = 0$]:

$$\tilde{\nu}(J) = \tilde{\nu}_2 + B_0 J'(J' + 1) - B_0 J(J + 1) \quad (1)$$

where J and J' are the rotational quantum numbers in the ground and $v_2 = 1$ vibrational states, respectively. The *O* ($J' = J - 2$) and *S* ($J' = J + 2$) branch wavenumbers are then

$$\tilde{\nu}_O(J) = \tilde{\nu}_2 + B_0(2 - 4J); \quad \tilde{\nu}_S(J) = \tilde{\nu}_2 + B_0(6 + 4J) \quad (2)$$

The B_0 rotational constant can be estimated using the Ir—F bond length determined by electron diffraction measurements on solid IrF_6, as given in Ref. 12, that is, $a = 1.830$ Å. We obtain

$$B_0 = \frac{\hbar^2}{8hcm_F a^2} \approx 0.0662 \text{ cm}^{-1} \quad (3)$$

where m_F is the fluorine atomic mass. The J rotational levels population percentage $\mathscr{P}(J)$ in the ground vibra-

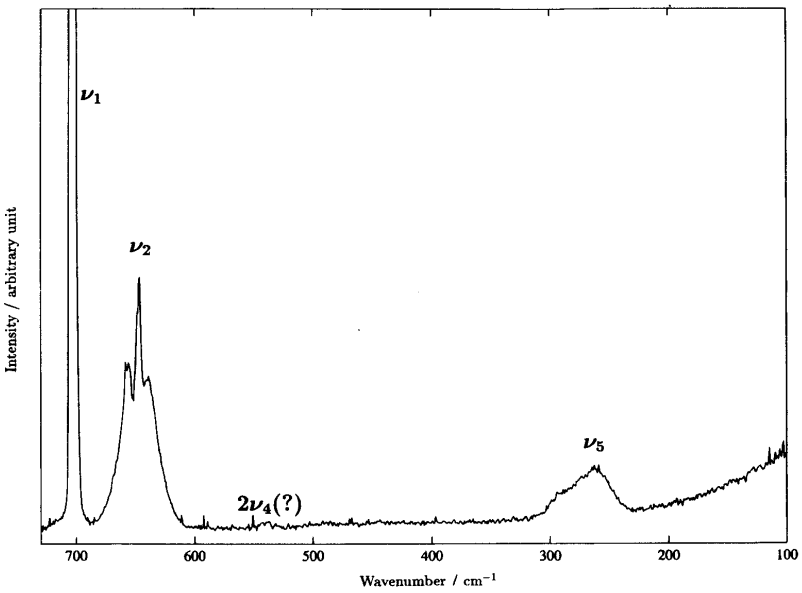

Figure 1. Spontaneous Raman spectrum of IrF_6 in the 100–730 cm^{-1} region.

Table 1. Raman band centers for IrF_6[a]

Assignment	$\tilde{\nu}_5(F_{2g})$/cm⁻¹	$2\tilde{\nu}_4(F_{1u})$/cm⁻¹	$\tilde{\nu}_2(E_g)$/cm⁻¹ *O*	*Q*	*S*	$\tilde{\nu}_1(A_{1g})$/cm⁻¹
This work	265.2	~540.0	639.7	647.3	656.7	701.1
Claassen and Selig[8]	267	542		645		701.7

[a] For the ν_2 band, the *O*, *Q* and *S* peak positions (branch maxima) are given. Note that the *Q* peak position is not its Q_0 origin.

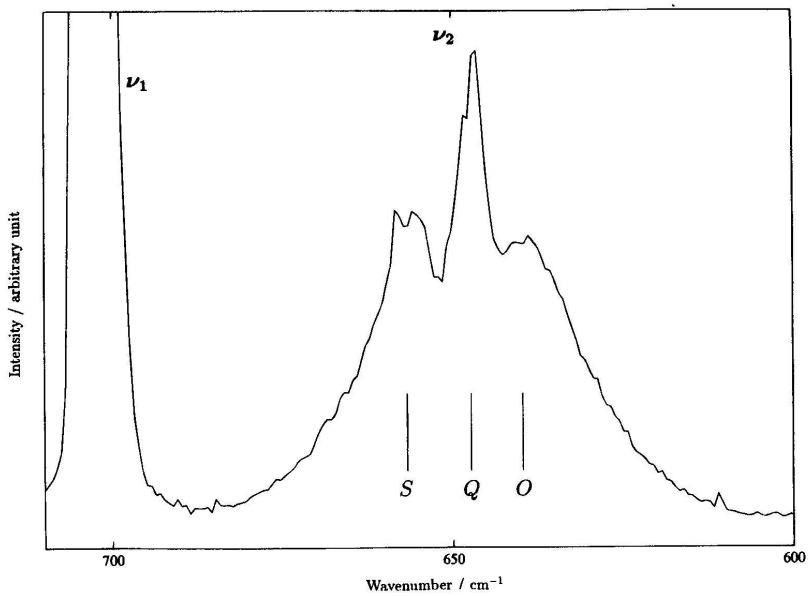

Figure 2. $\nu_2(E_g)$ *O*, *Q* and *S* branch contours with their peak positions.

tional state is given by

$$\mathscr{P}(J) = 100\,\frac{(2J+1)e^{-hcB_0J(J+1)/kT}}{\sum_{J'}(2J'+1)e^{-hcB_0J'(J'+1)/kT}} \qquad (4)$$

The curve obtained for $T = 300$ K (Fig. 3) presents a maximum for $J \approx 39$. As a consequence, the *O* and *S* branch peaks (maximum intensity) should lie around $J = 39$. Owing to the probable presence of hot bands and because we use natural iridium, which contains two isotopes, it is impossible to locate the Q_0 line at this resolution. Thus, the $\tilde{\nu}_2$ value is estimated here as follows. Equation (2) leads to

$$\tilde{\nu}_2 = \frac{\tilde{\nu}_O(J) + \tilde{\nu}_S(J)}{2} - 4B_0 \qquad (5)$$

If we take for $\tilde{\nu}_O$ and $\tilde{\nu}_S$ the experimental *O* and *S* peak positions (see Table 1), we obtain $\tilde{\nu}_2 = 647.9$ cm^{-1}. Then, we obtain

$$\tilde{\nu}_O(39) \approx 637.7 \text{ cm}^{-1}; \quad \tilde{\nu}_S(39) \approx 658.6 \text{ cm}^{-1} \qquad (6)$$

These values are in fairly good agreement with those in Table 1, if we take into account the simplicity of the model and the resolution of the apparatus.

Thus, the wavenumber separation between two *O*(*J*) or *S*(*J*) successive rotational lines should be approximately $4B_0 \approx 0.26$ cm^{-1}. This implies that an apparatus resolution of at least 0.1 cm^{-1} is necessary to observe the rotational fine structure of the $\nu_2(E_g)$ band of IrF_6.

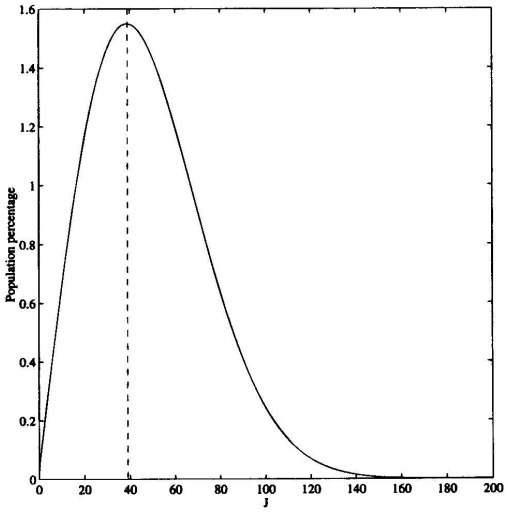

Figure 3. Population percentage of rotational levels in the ground state for $B_0 = 0.0662$ cm^{-1}.

DISCUSSION

We must note that these data (and especially the 'normal' branch aspect of the $\nu_2(E_g)$ band) do not confirm the possible existence of a small Jahn–Teller effect in the $X(G_g')$ state, as mentioned by Bernstein and Webb[13] for solid IrF_6. In such a fourfold degenerate electronic state, the linear Jahn–Teller coupling should split each of the $\nu_2(E_g)$ and $\nu_5(F_{2g})$ fundamentals into two distinct vibronic bands. As noted in Ref. 5, the degeneracy of the $X(G_g')$ state being mainly of spin nature (total electronic spin $S = 3/2$), it cannot be removed by electrostatic forces, such as the Jahn–Teller type. Hence these should be almost negligible. This is not the case for molecules such as TcF_6 or ReF_6, which are known to show strong vibronic couplings,[6,7] just

Table 2. Some spectroscopic parameters for IrF_6

Parameter	Value	Parameter	Value
$\tilde{\nu}_1(A_{1g})$	701.1 cm^{-1}	$\tilde{\nu}_5(F_{2g})$	265.2 cm^{-1}
$\tilde{\nu}_2(E_g)$	647.9 cm^{-1}	B_0	0.06–0.07 cm^{-1}
$\tilde{\nu}_4(F_{1u})$	~270.0 cm^{-1}	a (Ref. 12)	1.830 Å

like the $a(G_g')$ and $e(G_g')$ excited electronic states of IrF_6.[14]

Finally, it should be noted that in our case the signal-to-noise ratio was too poor in the $\nu_5(F_{2g})$ region to enable us to conclude anything about the rotational structure of this band. Table 2 summarizes the spectroscopic parameter values for IrF_6.

CONCLUSION

We have presented the spontaneous Raman scattering spectrum of IrF_6 vapour at ambient temperature. The $\nu_1(A_{1g})$, $\nu_2(E_g)$, $\nu_5(F_{2g})$ and probably $2\nu_4(F_{1u})$ bands have been observed. The *O*, *Q* and *S* branch contours of the $\nu_2(E_g)$ band were described. The positions of the *O* and *S* band maxima are in good agreement with the Ir—F bond length published by Kimura *et al.*[12] and consistent with a value of approximately 0.06–0.07 cm^{-1} for the B_0 rotational constant in the $X(G_g')$ ground electronic state.

This work could be completed by two new steps. The first would be the recording of the spontaneous Raman spectrum over a wider wavelength range of heated IrF_6 in order to observe harmonic and combination bands. The second step would be the CARS or resonance Raman spectroscopy of the $\nu_2(E_g)$ band, since this is the best chance of resolving the rovibronic structure of such a heavy molecule. This possibility is justified by the fact that the B_0 value for IrF_6 is of the same order as that of SF_6, whose $\nu_2(E_g)$ band was resolved by Berger and coworkers[11,15] at ambient temperature (gas pressure *ca* 500 Torr), using a high-resolution (0.03 cm^{-1}) spontaneous Raman spectrometer.

Acknowledgements

We thank Professor H. Selig (Department of Inorganic and Analytical Chemistry, Hebrew University of Jerusalem, Israel) and Professor J. H. Holloway (Department of Chemistry, University of Leicester, UK) for their advice concerning the synthesis and purification of IrF_6. We are very grateful to R. Saint-Loup and P. Michaux (Laboratoire de Physique de l'Université de Bourgogne, Dijon, France) for their technical support.

REFERENCES

1. C. Bernard, R. Madar and Y. Pauleau, *Solid State Technol.* **2**, 79 (1989).
2. B. A. Macklin and J. C. Withers, in *Conference on Chemical Vapor Deposition of Refractory Metals, Alloys and Compounds*, September 1967, Gatlinburg, TN, p. 161 (1967).
3. M. Pons, A. Benezech, P. Huguet, R. Gaufres, P. Diez and J. Lafforet, *J. Chem. Vapor. Depos.* **2**, 135 (1993).
4. V. Boudon and F. Michelot, *J. Mol. Spectrosc.* **165**, 554 (1994).
5. V. Boudon, F. Michelot and J. Moret-Bailly, *J. Mol. Spectrosc.* **166**, 449 (1994).
6. B. Weinstock and G. L. Goodman, *Adv. Chem. Phys.* **9**, 169 (1965).
7. H.H. Claassen, G. L. Goodman, J. H. Holloway and H. Selig, *J. Chem. Phys.* **53**, 341 (1970).
8. H. H. Claassen and H. Selig, *Isr. J. Chem.* **7**, 499 (1969).
9. J. H. Holloway, E. G. Hope, G. Stanger and D. A. Boyd, *J. Fluorine Chem.* **56**, 77 (1992).
10. G. H. Cady and B. Hargreaves, *J. Chem. Soc.* 1563 (1929).
11. H. Berger, A. Aboumajd and R. Saint-Loup, *J. Phys. Lett.* **38**, L-373 (1977).
12. M. Kimura, V. Schomaker, D. W. Smith and B. Weinstock, *J. Chem. Phys.* **48**, 4001 (1968).
13. E. R. Bernstein and J. D. Webb, *Mol. Phys.* **37**, 203 (1979).
14. J. C. D. Brand, G. L. Goodman and B. Weinstock, *J. Mol. Spectrosc.* **37**, 464 (1971).
15. A. Aboumajd, H. Berger and R. Saint-Loup, *J. Mol. Spectrosc.* **78**, 486 (1979).

ELSEVIER

Spectrochimica Acta Part A 53 (1997) 991–994

SPECTROCHIMICA ACTA PART A

Absorption spectrum of the $f(A_{1g}) \leftarrow X(E_g)$, $a(F_{2g})$ electronic transition of OsF_6

M. Rotger [a,*], V. Boudon [a], H. Selig [b]

[a] *Laboratoire de Physique de l'Université de Bourgogne, (Unité associée au CNRS), BP 400-21011 Dijon, Cedex, France*
[b] *Department of Inorganic and Analytical Chemistry, The Hebrew University of Jerusalem, Jerusalem 91904, Israel*

Received 22 November 1996; accepted 30 December 1996

Abstract

The absorption spectrum of the visible band of OsF_6 has been recorded using a commercial spectrophotometer. The first vibronic assignments for this band have been realized using the analogy with the $d \leftarrow X$ transition of IrF_6. Some vibronic parameter values are derived. © 1997 Elsevier Science B.V.

Keywords: Osmium hexafluoride; Absorption spectroscopy; Vibronic transitions

In a previous paper [1], we have analyzed in detail the vibronic bands of IrF_6. We present here a preliminary study of another third-row transition-metal hexafluoride, namely OsF_6. There are only a very few studies on the near-infrared and visible absorption spectroscopy of this molecule. Moffit et al. [2], and more recently Holloway et al. [3] have recorded low-resolution spectra, but without giving any assignment of the vibronic bands. Michalopoulos and Bernstein [4] have performed a more detailed study, but only concerning the solid phase. Osmium hexafluoride possesses a very complex vibronic absorption band system in the 3700–18 600 cm^{-1} region, with accidental near degeneracies of some of the seven low-lying electronic states. Moreover, five of these electronic states are strongly perturbed by Jahn–Teller couplings [5,6]. Thus, up to now, no vibronic assignment has been performed for this molecule. In this paper, we present a detailed analysis and parameter values concerning the visible band of OsF_6, since this is the most simple one to study because it corresponds to a transition to the totally symmetric f electronic state, which is well isolated from the others.

Osmium hexafluoride is a pale-yellow gas, with a vapour pressure of 266 torr at 300 K [7]. One of us, H. Selig, has filled a 2 cm length quartz cell with this substance, using a method similar to that described in Ref. [1].

The lower part of Fig. 1 shows the absorption spectrum of the $f(A_{1g}) \leftarrow X(E_g)$, $a(F_{2g})$ transition, recorded using a Cary 5E (Varian) commercial spectrophotometer. The apparatus resolution was a few wavenumbers in this region. This is the first detailed spectrum of this band. The upper part of Fig. 1 recalls the spectrum of the $d(E'_{2g}) \leftarrow X(G'_g)$

* Corresponding author. Tel.: + 33 380395967; fax: + 33 380395971; e-mail: rotger@jupiter.u-bourgogne.fr

PII S0584-8539(97)00016-0

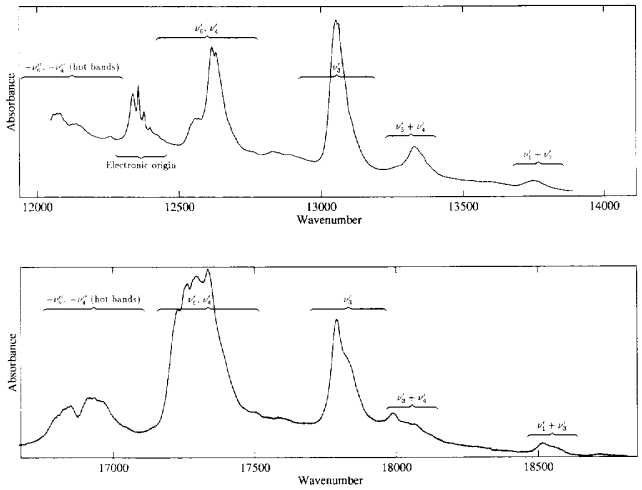

Fig. 1. Comparison between the absorption spectra of the $d(E'_{2g}) \leftarrow X(G'_g)$ transition of IrF_6 and the $f(A_{1g}) \leftarrow X(E_g)$, $a(F_{2g})$ transition of OsF_6 (wavenumber in cm^{-1}).

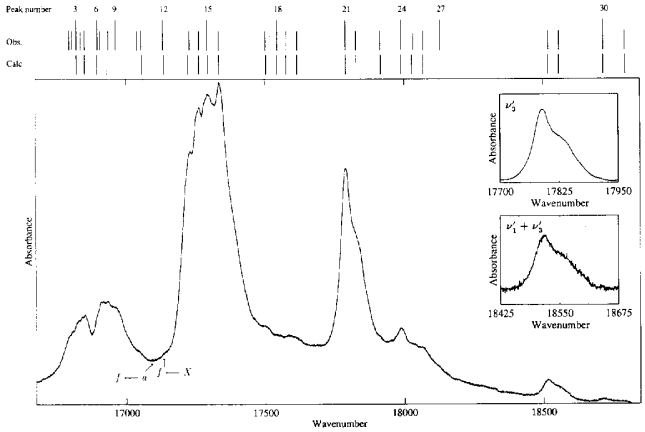

Fig. 2. Absorption spectrum of the $f(A_{1g}) \leftarrow X(E_g)$, $a(F_{2g})$ transition (wavenumber in cm^{-1}), with observed and calculated peak positions. The ν'_3 and $\nu'_1 + \nu'_3$ band profiles are displayed on the right.

transition of IrF_6 obtained using the same apparatus (see Ref. [1]). Since the $f(A_{1g})$ state of OsF_6 and the $d(E'_{2g})$ one of IrF_6 are unperturbed by complex vibronic couplings (due to their symmetry) both spectra should be very similar. So, we have used the IrF_6 spectrum to make a rough assignment of the OsF_6 one. We have identified here three main features that are the hot band region, the ν'_6, ν'_4 region and the ν'_3 one. The $\nu'_1 + \nu'_3$ region is also easily identified thanks to its band profile which is identical to that of ν'_3 (see Fig. 2). Then, more detailed assignments have been obtained using the following simple hypotheses:

Table 1
Assignments and fit for the $f(A_{1g}) \leftarrow X(E_g)$, $a(F_{2g})$ transition

Peak no.	ν_{obs} (cm^{-1})	Assignment	ν_{calc} (cm^{-1})	$\nu_{obs} - \nu_0^X$ (cm^{-1})	$\nu_{obs} - \nu_0^a$ (cm^{-1})
1	16 796.8	?	—		
2	16 806.3	?	—		
3	16 822.2	$f \leftarrow a + \nu_4''^a$	16 822.2		−274.8
4	16 837.0	?	—		
5	16 851.7	$f \leftarrow X + \nu_4''^X$	16 851.7	−284.7	
6	16 898.2	$f \leftarrow a + \nu_6''^a$	16 896.9		−199.0
7	16 907.7	?	—		
8	16 936.2	$f \leftarrow X + \nu_6''^X$	16 932.4	−200.2	
9	16 963.7	?	—		
10	17 040.8	?	—		
11	17 055.5	$f + \nu_6' \leftarrow X + \nu_6''^X$	17 059.3	−80.9	
12	17 132.7	$f \leftarrow X$	17 136.4	−3.7	
13	17 228.8	$f + \nu_6' \leftarrow a$	17 224.1		131.6
14	17 263.7	$f + \nu_6' \leftarrow X$	17 263.3	127.3	
15	17 293.2	$f + \nu_4' \leftarrow a$	17 296.7		196.0
16	17 334.2	$f + \nu_4' \leftarrow X$	17 335.9	197.8	
17	17 502.3	$f + \nu_5' + \nu_6' \leftarrow a$	17 503.5		405.1
18	17 544.0	$f + \nu_5' + \nu_6' \leftarrow X$	17 542.8	407.6	
19	17 577.7	$f + \nu_4' + \nu_5' \leftarrow a$	17 576.2		480.5
20	17 616.4	$f + \nu_4' + \nu_5' \leftarrow X$	17 615.4	480.0	
21	17 789.7	$f + \nu_3' \leftarrow a$	17 790.3		692.5
22	17 827.7	$f + \nu_3' \leftarrow X$	17 829.6	691.3	
23	17 915.2	$f + \nu_3' + \nu_4' + \nu_6' \leftarrow a + \nu_6''^a$	17 916.5		818.0
24	17 990.0	$f + \nu_3' + \nu_4' \leftarrow a$	17 989.9		892.8
25	18 033.1	$f + \nu_3' + \nu_4' \leftarrow X$	18 029.1	896.7	
26	18 069.5	$f + \nu_3' + \nu_5' \leftarrow a$	18 069.8		972.3
27	18 128.6	?	—		
28	18 519.3	$f + \nu_1' + \nu_3' \leftarrow a$	18 517.5		1422.1
29	18 557.4	$f + \nu_1' + \nu_3' \leftarrow X$	18 556.8	1421.0	
30	18 716.9	$f + \nu_1' + \nu_3' + \nu_4' \leftarrow a$	18 717.1		1619.7
31	18 794.8	$f + \nu_1' + \nu_3' + \nu_5' \leftarrow a$	18 797.0		1697.6

ν_i', $\nu_i''^X$ and $\nu_i''^a$ are the vibrational frequencies of mode i in the $f(A_{1g})$, $X(E_g)$ and $a(F_{2g})$ electronic states, respectively. ν_0^X and ν_0^a are the wavenumbers for the $f(A_{1g}) \leftarrow X(E_g)$ and $f(A_{1g}) \leftarrow a(F_{2g})$ origins. Peak numbers are the same as in Fig. 2.

- The $a(F_{2g})$ electronic state of OsF_6 lies at very low energy and is therefore thermally populated at room temperature. Thus, transitions arise from both the $X(E_g)$ and $a(F_{2g})$ states, i.e. they should appear two times.
- The origins of the electronic transitions $f(A_{1g}) \leftarrow X(E_g)$ and $f(A_{1g}) \leftarrow a(F_{2g})$ must be extremely weak, since they correspond to symmetry forbidden transitions.
- Hot band assignments have been realized using the ground electronic state vibrational frequencies given in Ref. [8] and assuming that these frequencies do not differ too much for the $a(F_{2g})$ electronic state.

In Table 1, we give the observed frequencies and the result of the fit that we have realized using a least-squares method. The corresponding peak positions (observed and calculated) are displayed at the top of Fig. 2. As we mentioned before, the origins of the electronic transitions are extremely weak ($f(A_{1g}) \leftarrow a(F_{2g})$ being even invisible). Generally speaking, the whole band has a rather low intensity. Table 2 gives the values of the vibronic parameters obtained from the data of Table 1. The standard deviations are given in parenthesis in the units of the last two figures of the parameters. We find that the first electronic state $a(F_{2g})$ lies at only ~ 40 cm^{-1}. Thus, around

Table 2
Vibronic parameters for OsF_6 (in cm^{-1})

Electronic state	ν_0	$\nu_1(A_{1g})$	$\nu_3(F_{1u})$	$\nu_4(F_{1u})$	$\nu_5(F_{2g})$	$\nu_6(F_{2u})$
$X(E_g)$	0	—	—	284.7 (3.4)	—	204.0 (2.6)
	—	733	720[a]	272[a]	276[a]	205[a]
$a(F_{2g})$	39.2 (1.5)	—	—	275.0 (3.5)	—	200.3 (2.5)
$f(A_{1g})$	17136.4 (1.6)	727.2 (2.1)	693.1 (1.6)	199.5 (1.5)	279.4 (1.6)	126.9 (1.7)

The column ν_0 gives the energies of the electronic states.
[a] From Ref. [8].

56% of the molecules are in this state at 300 K. The values of the vibrational wavenumbers (ν_4 and ν_6) that we deduce for the $X(E_g)$, $a(F_{2g})$ ground electronic state doublet are consistent with those found in the literature [8]. Seven unattributed bands are also listed in Table 1.

This preliminary study will now be used as a starting point for the global analysis of the five electronic bands of OsF_6. In particular, the Jahn–Teller parameters in the $b(F_{1g})$, $d(F_{2g})$ and $e(E_g)$ states are still to be determined. Furthermore, the structure of the $X(E_g)$, $a(F_{2g})$ ground electronic state doublet should be examined using Raman or infrared spectroscopy.

References

[1] V. Boudon, M. Rotger and D. Avignant, J. Mol. Spectrosc., 175 (1996) 327.
[2] W. Moffit, G.L. Goodman, M. Fred and B. Weinstock, Mol. Phys., 2 (1959) 109.
[3] J.H. Holloway, E.G. Hope, G. Stanger and D.A. Boyd, J. Fluor. Chem., 56 (1992) 77.
[4] D.L. Michalopoulos and E.R. Bernstein, Mol. Phys., 47(1) (1982) 1.
[5] V. Boudon and F. Michelot, J. Mol. Spectrosc., 165 (1994) 554.
[6] V. Boudon, F. Michelot and J. Moret-Bailly, J. Mol. Spectrosc., 166 (1994) 449.
[7] G.H. Cady and B. Hargreaves, J. Chem. Soc., (1961) 1563.
[8] B. Weinstock and G.L. Goodman, Adv. Chem. Phys., 9 (1964) 169.

JOURNAL OF CHEMICAL PHYSICS VOLUME 117, NUMBER 7 15 AUGUST 2002

High-resolution spectroscopy of the ν_3 band of WF_6 and ReF_6 in a supersonic jet

V. Boudon and M. Rotger
Laboratoire de Physique de l'Université de Bourgogne (UMR CNRS 5027), 9 av. A. Savary, B.P. 47870, F-21078 Dijon, France

Y. He, H. Hollenstein, M. Quack,[a] and U. Schmitt[b]
Physical Chemistry, ETH Zürich, CH-8093 Zürich, Switzerland

(Received 17 October 2000; accepted 13 March 2002)

We have recorded the Fourier-transform infrared (FTIR) spectrum of the ν_3 fundamental band of WF_6 in a continuous supersonic jet expansion with an instrumental bandwidth of 0.0024 cm^{-1} (FWHM, full width at half maximum, unapodized), using a Bomem DA.002 spectrometer. Some parts of this band have also been recorded with 0.0007 cm^{-1} bandwidth using a diode laser spectrometer combined with a pulsed slit jet expansion. A multiple-pass arrangement has been used for the slit jet to observe low-intensity lines. In each case, we have used a WF_6:He mixture with a seeding ratio 1:3 leading to a rotational temperature of ca. 50 K. This work extends the previous investigation of Takami and Kuze [J. Chem. Phys. **80**, 5994 (1984)] to much higher J transitions. In both P and R branches, rotational lines have been recorded for J up to 46–48. We have used a tensorial Hamiltonian adapted to the group chain $O(3) \supset O_h$ and developed to the third order for the analysis of the spectra. A least-squares fit for each of the four main isotopic species: $^{182}WF_6$, $^{183}WF_6$, $^{184}WF_6$, and $^{186}WF_6$ results in band centers (in this order) 714.538 19, 714.214 06, 713.895 44, and 713.266 21 cm^{-1}. We report furthermore first results on the high-resolution spectra of ν_3 of ReF_6, which exhibits a fourfold degenerate electronic ground state of G_g' species in the O_h^S group. Supersonic jet-FTIR spectra show a moderately structured relatively broad band, whereas the diode laser spectroscopy of the seeded jet in the range 708–733 cm^{-1} results in line resolved spectra of high complexity. A preliminary analysis is discussed, while a complete analysis still represents an appreciable challenge. © *2002 American Institute of Physics.* [DOI: 10.1063/1.1475754]

I. INTRODUCTION

The present paper aims at contributing to a systematic understanding of the ν_3 fundamental rovibronic structure of transition metal hexafluorides in general and WF_6 and ReF_6 in particular. These constitute the interesting first two members of this group of molecules arising from the third row elements and provide a striking contrast to each other. While WF_6 shows a relatively simple band structure of the degenerate $\nu_3(F_{1u})$ fundamental in the infrared spectrum, which has been the subject of several previous investigations also at high-resolution,[1–4] ReF_6 is an open-shell molecule, which exhibits a fourfold degenerate electronic ground state resulting in the prediction that ν_3 should consist of four transitions to four vibronic sublevels.[5] The observed spectra previously revealed only broad structures.[5–8]

In the present work we first provide an extended high-resolution analysis for ν_3 of WF_6 and then proceed to a first attempt at the high-resolution rovibronic spectroscopy of ReF_6. Tungsten hexafluoride is the first member of the third-row transition-metal hexafluoride series. It has a high vapor pressure (more than one atmosphere at room temperature[9]) and this leads to interesting opportunities for applications. First of all, this material is currently used to deposit tungsten thin films in microelectronics by chemical vapor deposition techniques.[10,11] WF_6 could also be a good candidate for laser isotope separation of tungsten. But this requires an accurate knowledge of the spectroscopic constants.[12] Furthermore, tungsten isotopes are of interest in isotope geology and dating.[13–15] The spectroscopy of W compounds as part of the group 6 elements has also gained further recent interest because of the proof that the transuranium element 106 Seaborgium (Sg) falls in this group,[16,17] and a corresponding conclusion holds presumably true for element 107 (Nielsbohrium, Ns or Bohrium, Bh) in relation to Re. The low resolution infrared[1,5] and Raman[18,19] spectra of this molecule have been known for a long time. But no rotational structure has been resolved in these early papers. Indeed, for such heavy transition-metal hexafluorides, high-resolution spectroscopy is not a simple task, since room temperature spectra are completely congested by hot bands due to the presence of low energy vibrational modes.[20,21] For WF_6, the ν_6 mode lies at 127 cm^{-1} (Ref. 20) and the ground vibrational state has a population of only 1.3% at 300 K. The thermal congestion is illustrated in the survey spectrum of Fig. 1, showing the FTIR spectrum of the ν_3 stretching fundamental region (around 14 μm). At room temperature, the structure is dominated by hot bands, even if some faint structures can be

[a]Author to whom correspondence should be addressed. Electronic mail: martin@quack.ch
[b]Present address: Institut für Physikalische Chemie der Universität Göttingen, Tammannstrasse 6, D-37077 Göttingen, Germany.

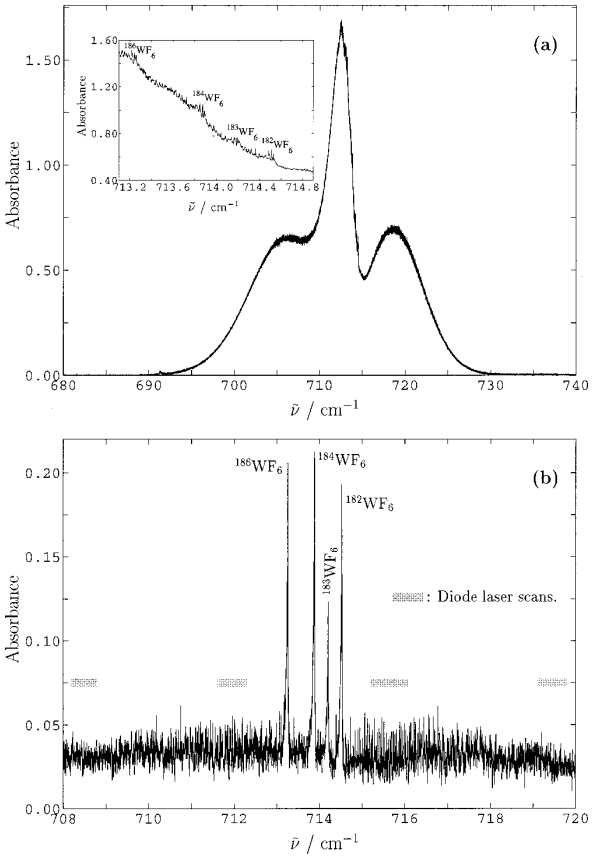

FIG. 1. (a) Overview FTIR spectrum of the ν_3 band of WF_6 at room temperature (0.3 mbar WF_6 in a 18 cm length glass cell with KBr windows), with an instrumental bandwidth of 0.0024 cm^{-1} (FWHM, unapodized). A detail is shown near the band center region, with the ν_3 Q branches of the four isotopomers. (b) Overview FTIR spectrum of the same region using a WF_6:He supersonic jet with a seeding ratio 1:3. The rotational temperature is estimated to 50 K. The gray sticks show the regions covered by the jet + diode laser experiment.

resolved, such as the ν_3 Q branches of the four isotopomers of natural abundance WF_6, and some very high J structures on top of the P and R wings. At low temperature in the supersonic jet expansion, the Q-branch structures of the four isotopomers emerge prominently.

Several authors have used a supersonic free jet of WF_6 in the past in order to achieve low temperature (vibrational and rotational) spectra and thus to resolve the rotational structure.[2–4] The most complete previous work was that of Takami and Kuze[4] who determined rotational constants for the four main isotopic species. They obtained a rotational temperature of 30 K. Under these conditions, rotational lines could be seen only up to $J=29$. In this paper we report a reinvestigation of the supersonic jet expansion spectroscopy of WF_6 with a higher rotational temperature (50 K) in which we were able to observe and identify rotational lines up to $J=48$. This enables us to give some refined values for the parameters.

Rhenium hexafluoride is the second member of the third-row transition series. Its vapor pressure is lower than that of WF_6 but still relatively high (590 torr at 300 K[9]). This molecule is used for the chemical vapor deposition of rhenium anticorrosion layers and in microelectronics in association with WF_6 (deposition of tungsten–rhenium alloys[10,22–24]). However, a particular interest of this molecule is its electronic structure having an unpaired d electron.[25–29] As explained, for example, in Ref. 29, this leads to a fourfold degenerate electronic ground state of G_g' species in the group O_h^S (symmetry group of the octahedron with its spinorial representations, see Ref. 30) as well as to the presence of half-integer angular momenta. ReF_6 pertains to a family of molecules often called "colored hexafluorides" since these open-shell systems (ReF_6,OsF_6,IrF_6,PtF_6,...) possess some low-lying electronic states leading to the absorption of visible or near infrared light. For instance, the first excited electronic state of ReF_6 lies at 5000 cm^{-1}.[29] The degeneracy of the electronic ground state implies complex rovibronic couplings. The unusual band profile observed at low resolution for the ν_3 fundamental[5,7,8] led McDowell and Asprey[5] to suspect that a quadratic vibronic coupling could be responsible for a splitting of the $v_3=1$ vibrational level (F_{1u} symmetry) into four vibronic sublevels (since $G_g'\otimes F_{1u}=E_{1u}'\oplus E_{2u}'\oplus 2G_u'$ in O_h^S), but this theoretical suggestion has never been supported by experiment through a high-resolution study which necessitates the use of a supersonic jet expansion, for the same reasons as explained above for WF_6. Moreover, the extremely aggressive nature of ReF_6 makes such a study difficult.

We report here the first supersonic jet expansion spectroscopy of rhenium hexafluoride. We present FTIR-jet and diode laser spectra of a seeded jet in the range 708–733 cm^{-1} which are to our knowledge the first resolved rovibronic spectra of an open-shell transition-metal hexafluoride ever recorded. The spectra show very complex and extensive line structures. An approximate model enables us to obtain a first estimate of the order of magnitude of the vibronic coupling parameters. A preliminary account of the present work has been presented in Ref. 31.

II. EXPERIMENT

Natural abundance tungsten hexafluoride (<0.2% $^{180}WF_6$, 26.4% $^{182}WF_6$, 14.4% $^{183}WF_6$, 30.6% $^{184}WF_6$, and 28.4% $^{186}WF_6$) and rhenium hexafluoride (37.40% $^{185}ReF_6$, 62.60% $^{187}ReF_6$) were furnished by the COMURHEX company in Pierrelatte (France). The BF_3 calibration gas was purchased from Elf Atochem (France). All substances were used without any further purification. The identity of the compounds was obvious from the spectra and the precise purity is not relevant for the present investigation, not attempting the measurement of quantitative band strengths.

A. WF_6 spectra

We have recorded the spectra in two different ways: (i) A Fourier-transform infrared spectrum is obtained for WF_6 in a continuous supersonic jet expansion setup described in Refs. 32 and 33 with an instrumental bandwidth of 0.0024 cm^{-1} (FWHM, unapodized), using a Bomem DA.002 spectrom-

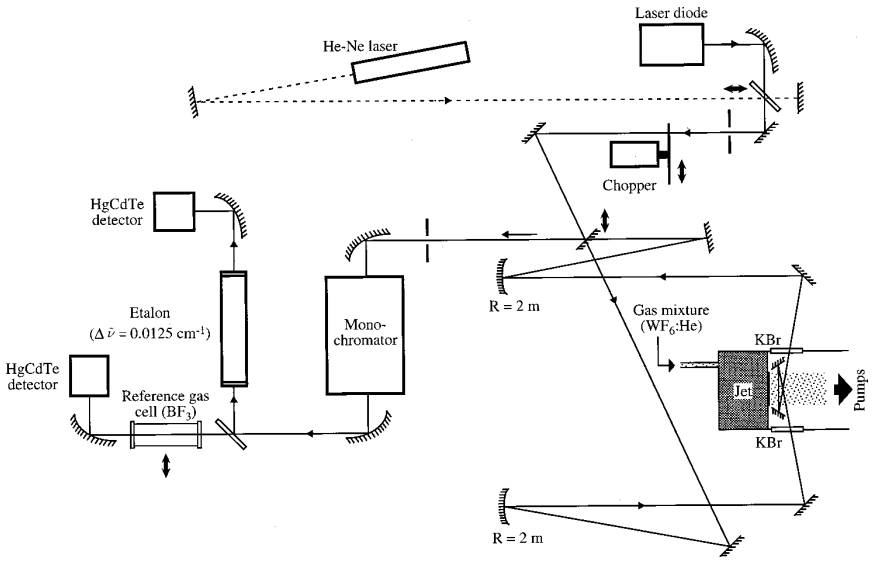

FIG. 2. Schematic drawing of the jet +diode laser experimental setup. $\Delta\tilde{\nu}$ is the free spectral range of the étalon.

eter. (ii) Diode laser spectra are taken with an instrumental bandwidth of 0.0007 cm^{-1} using a pulsed slit jet apparatus described in Ref. 34. The Doppler widths for WF_6 and ReF_6 fall in the range 0.0002 to 0.0005 cm^{-1} between 50 and 300 K (a range also expected to be relevant for the jet expansion) and thus the effective resolution in our experiments is largely determined by the instrumental bandwidths. For the present investigation, various parts of the jet system have been improved and exchanged to guarantee resistance to chemically very aggressive substances. The pumping system consisted of a 2000 m^3/h roots pump (WKP 2000, Balzers/Pfeiffer), which was backed by a 63 m^3/h rotary pump (Alcatel 2063CP). The pump oil was FOMBLIN® for both.

We have used a mixture of tungsten hexafluoride with helium, to achieve a better vibrational cooling. The WF_6:He seeding ratio was 1:3. Under these conditions, the rotational temperature was approximately T_{rot}=50 K. No hot band lines were observed. The vibrational ground state population should be about 95% at 50 K vibrational temperature.[21]

Figure 2 describes schematically the "jet+diode laser" experiment. The slit was 0.5×35 mm in dimension and operated below 0.5 Hz with an opening time of 2.5 ms. The diode laser frequency was scanned by modulating its current with a triangle signal.[34] The backing pressure was 350 mbar. A monochromator was used to select only one emission mode of the multimode diode laser output at a time. Using two small mirrors placed on both sides of the slit, we were able to perform up to nine passes in the jet. This was necessary for observing the high-J transitions (below 709 cm^{-1} and above 719 cm^{-1}) where the absorption was very weak. Figure 1(b) shows the wavenumber ranges where diode laser scans were carried out for WF_6.

The frequency calibration of the diode laser absorption spectra was realized as follows (see Fig. 3). First, the absorption spectrum was recorded simultaneously with the transmission fringes of a 40 cm long Fabry–Perot étalon. Then the spectrum of a reference gas (BF_3) in the cell was recorded, again together with étalon fringes. Etalon fringes were used to linearize the frequency scale, while the BF_3 lines from a FTIR spectrum gave the absolute calibration. We have chosen BF_3 as a reference gas, since it has a dense spectrum in the whole 660–740 cm^{-1} region.[35] For this purpose, we have recorded a FTIR spectrum of natural BF_3 (20% $^{10}BF_3$, 80% $^{11}BF_3$) at room temperature at the highest resolution (see above). This spectrum is displayed in Fig. 4. The BF_3 FTIR spectrum was itself calibrated against CO_2 and H_2O lines with an accuracy of about 0.0005 cm^{-1} in the 720 cm^{-1} region.[36]

B. ReF_6 spectra

For ReF_6, we have used the same experimental setup as described above. Diode laser spectra were calibrated in the same way, using BF_3 lines. We have used various seeding ratios with helium and argon to optimize the conditions. Figure 5 shows the survey FTIR spectra and the regions where diode laser scans were carried out. ReF_6 experiments are

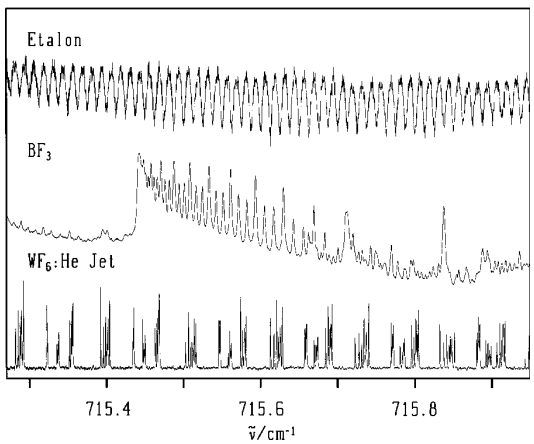

FIG. 3. Typical raw experimental data, showing transmission fringes of the étalon, reference gas peaks (10 mbar of BF_3 in a 18 cm long glass cell with KBr windows) and jet spectrum of the WF_6:He mixture.

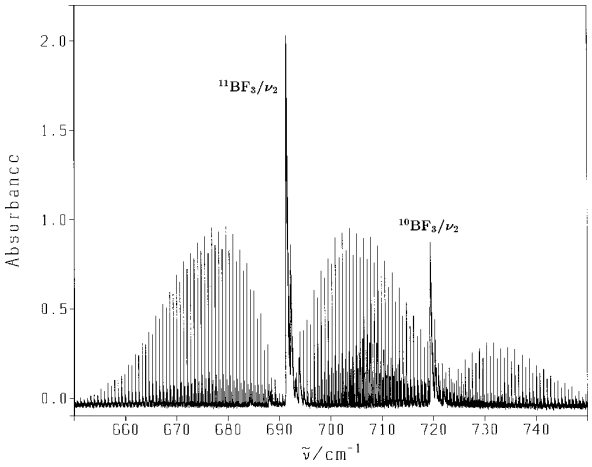

FIG. 4. FTIR spectrum of the ν_2 band of BF_3 at room temperature (0.5 mbar of BF_3 in a 18 cm long glass cell with KBr windows).

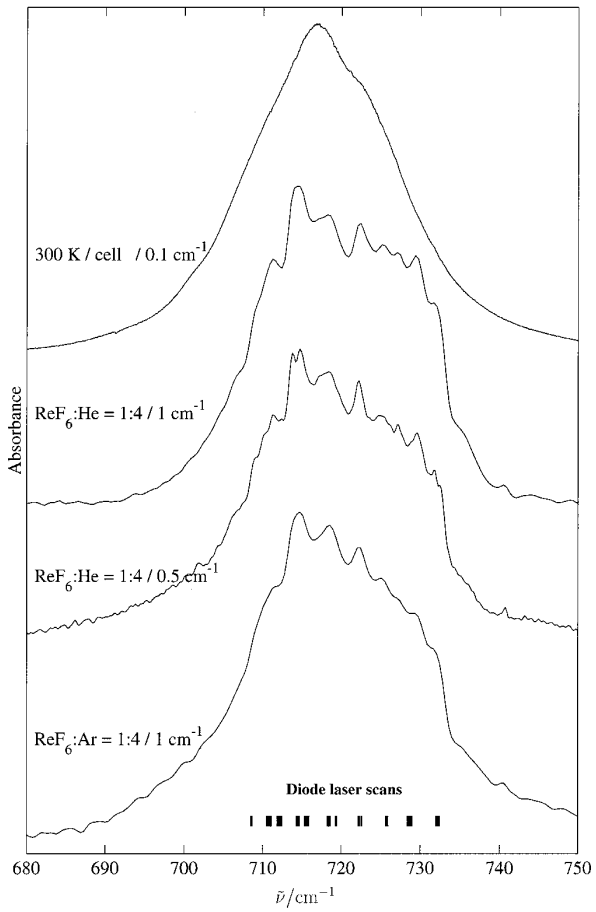

FIG. 5. Overview low-resolution FTIR spectra of the ν_3 band of ReF_6 at room temperature (0.3 mbar ReF_6 in a 18 cm length glass cell with KBr windows) and in a supersonic jet at different mixtures and instrumental bandwidths conditions.

more difficult to realize due to the chemical reactivity which is much greater for this species than for WF_6. As can be seen from Fig. 5, jet-cooled spectra of the ν_3 band show a band which is about as broad as that at room temperature. This is due to the rovibronic interactions which spread the quantum levels over a large energy range and thus the cooling effect does not result in the same band narrowing as for WF_6 (see Fig. 1). A consequence of this is that the effective absorption of ν_3 of ReF_6 is rather low since the absorption strength is distributed over a very large number of lines in a rather large wave number range. This low intensity prevented us to record high-resolution jet-FTIR spectra. However, it was possible to record diode laser spectra of the ReF_6:He supersonic expansion jet as will be described in Sec. IV B, using up to nine passes in the jet, corresponding to an effective optical pathlength up to 315 mm.

III. THEORY

A. The WF_6 closed-shell molecule and general aspects

The theory used here is based on the model developed by Champion, Loëte, and Pierre[37] for the analysis of spherical-top spectra. Since we consider here the ν_3 band as isolated, we can use the completely transformed Hamiltonian,

$$\tilde{H}=\tilde{H}_{\{0\}}+\tilde{H}_{\{\nu_3\}}+\cdots. \tag{1}$$

Here, $\tilde{H}_{\{0\}}$ is the purely rotational contribution which can be written as

$$\tilde{H}_{\{0\}}=\sum_{\Omega_r,K_r} t_0^{\Omega_r(K_r)}\beta^0_{\Omega_r,K_r}R^{\Omega_r(K_r,A_1)}, \tag{2}$$

the $R^{\Omega_r(K_r,A_1)}$ operators being defined as usual.[37,38] Here, $t_0^{\Omega_r(K_r)}$ is a parameter and $\beta^0_{\Omega_r,K_r}$ is a coefficient used to match the traditional spectroscopic notations[39] for the scalar terms [see below, Eq. (4)]. The ν_3 contribution is then

$$\tilde{H}_{\{\nu_3\}}=\sum_{K_v,\Omega_r,K_r,K} t_{3,3}^{2\Omega_r((K_vK_r)K)} \times\beta^2_{\Omega_r,K_r}[{}^{\varepsilon}V_{3,3}^{2(K_v)}\otimes R^{\Omega_r(K_r)}]^{(K,A_1)}, \tag{3}$$

where we realize the coupling of the vibrational (${}^{\varepsilon}V_{3,3}^{2(K_v)}$) and rotational operators in the $O(3)$ group. This is not the usual method,[40] but we choose it for consistency with the coupling scheme we use for molecules with a degenerate electronic ground state, like ReF_6 (see next paragraph). The $t_{3,3}^{2\Omega_r((K_vK_r)K)}$ are again parameters, and the $\beta^{\Omega_v}_{\Omega_r,K_r}$ factors are defined as

$$\beta^{\Omega_v}_{\Omega_r,K_r}=\begin{cases}\left(-\dfrac{\sqrt{3}}{4}\right)^{\Omega_r/2}(\sqrt{3})^{\Omega_v/2} & \text{if } K_r=0,\\ 1 & \text{if } K_r\neq 0.\end{cases} \tag{4}$$

Four vibrational operators are involved in Eq. (3), which are

$${}^{+}V_{3,3}^{0(0)}=\mathbb{I}\ \text{(identity operator)}, \tag{5}$$

$$ {}^{+}V_{3,3}^{2(0)} = -[a_3^{+(1)} \otimes a_3^{(1)}]^{(0)} = \frac{1}{\sqrt{3}} N_3^{(0)}, \tag{6} $$

$$ {}^{-}V_{3,3}^{2(1)} = -\frac{1}{\sqrt{3}} [a_3^{+(1)} \otimes a_3^{(1)}]^{(1)} = -\frac{1}{\sqrt{6}} l_3^{(1)}, \tag{7} $$

$$ {}^{+}V_{3,3}^{2(2)} = -\frac{1}{\sqrt{5}} [a_3^{+(1)} \otimes a_3^{(1)}]^{(2)}. \tag{8} $$

$N_3^{(0)}$ is the usual "number" operator and $l_3^{(1)}$ is the vibrational angular momentum. The upper left index $\epsilon = \pm$ gives the parity (even/odd) in the conjugate momenta $p_\sigma^{(F_{1u})}$ ($\sigma = x$, y, or z). Note that the parity index g or u has been omitted here for simplicity, since it is u for $a_3^{(1)}$ and $a_3^{+(1)}$ and g everywhere else. Overall parity could be defined as well by using the nonrigid molecule group S_6^*,[41,42] but this is not needed for the present analysis, which assumes a semirigid molecular framework, although it might be of interest at high energy or for reactive processes.[42]

Effective Hamiltonians for the ground and $v_3 = 1$ vibrational states are obtained simply by projecting the completely reduced Hamiltonian [Eq. (1)] on the subspaces spanned by the vibrational functions of these states, that is

$$ \mathbf{H}^{\langle 0 \rangle} = P^{\langle 0 \rangle} \tilde{H} P^{\langle 0 \rangle} = \mathbf{H}_{\{0\}}^{\langle 0 \rangle}, \tag{9} $$

$$ \mathbf{H}^{\langle \nu_3 \rangle} = P^{\langle \nu_3 \rangle} \tilde{H} P^{\langle \nu_3 \rangle} = \mathbf{H}_{\{0\}}^{\langle \nu_3 \rangle} + \mathbf{H}_{\{\nu_3\}}^{\langle \nu_3 \rangle}. \tag{10} $$

Practically, we use a coupled rovibrational basis of the type

$$ |\Psi_{\mathrm{rv}}\rangle = |v_3, (J, l_3) R, n C \sigma\rangle, \tag{11} $$

by setting $\mathbf{R} = \mathbf{J} - l_3$, $\mathbf{J}$ being the total and $\mathbf{R}$ the rotational angular momentum, where

$$ |R - l_3| \leqslant J \leqslant R + l_3 \tag{12} $$

and l_3 and thus R and C have u parity. It should be noted here, that g and u "parity" do not refer to the total parity. For a more detailed discussion of this point and the role of total (positive or negative) parity, we refer to Ref. 43, in conjunction with a more detailed analysis of the ReF_6 spectrum. C is the rovibrational symmetry in the O_h point group and σ its component. The matrix elements for $\mathbf{H}_{\{0\}}$ and $\mathbf{H}_{\{\nu_3\}}$ are then given by

$$ \langle v_3 = 0, (J, l_3 = 0) J n'' C \sigma | \mathbf{H}_{\{0\}} | v_3 = 0, (J, l_3 = 0) J n' C \sigma \rangle = \sum_{\Omega_r, K_r} (-1)^J \beta_{\Omega_r, K_r}^0 F_{A_1}^{(K_r \; J \; J)} {}_{n' C \sigma \; n'' C \sigma} \langle J \| R^{\Omega_r(K_r)} \| J \rangle t_0^{\Omega_r(K_r)}, \tag{13} $$

and

$$ \begin{aligned} &\langle \nu_3 = 1, (J, l_3 = 1) R'' n'' C \sigma | \mathbf{H}_{\{\nu_3\}} | v_3 = 1, (J, l_3 = 1) R' n' C \sigma \rangle \\ &= \sum_{\Omega_v, K_v, \Omega_r, K_r, K} (-1)^{R''} \beta_{\Omega_r, K_r}^{\Omega_v} F_{A_1}^{(K \; R' \; R'')} {}_{n' C \sigma \; n'' C \sigma} \sqrt{[R'][R''][K]} \begin{Bmatrix} K_r & J & J \\ K_v & 1 & 1 \\ K & R' & R'' \end{Bmatrix} \langle J \| R^{\Omega_r(K_r)} \| J \rangle \\ &\quad \times \langle 1,1 \| V_{3,3}^{\Omega_v(K_v)} \| 1,1 \rangle t_{3,3}^{\Omega_v \Omega_r((K_v K_r) K)}. \end{aligned} \tag{14} $$

The F are oriented coupling coefficients in the group chain $O(3) \supset O_h$.[44] The necessary reduced matrix elements can be expressed as follows:

$$ \langle J \| R^{\Omega_r(K_r)} \| J \rangle = \left(-\frac{4J(J+1)}{\sqrt{3}} \right)^{(\Omega_r - K_r)/2} \times \left(\frac{2^{K_r} (K_r!)^2 (2J + K_r + 1)!}{(2K_r)! (2J - K_r)!} \right)^{1/2}, \tag{15} $$

$$ \langle 1,1 \| V_{3,3}^{\Omega_v(K_v)} \| 1,1 \rangle = 1, \quad \Omega_v \neq 0, \tag{16} $$

$$ \langle 1,1 \| V_{3,3}^{0(0)} \| 1,1 \rangle = \sqrt{3}. \tag{17} $$

As we only study here an isolated fundamental band, the dipole moment operator necessary for transition moment calculations was simply developed to order zero and the corresponding parameter was set to 1 (as we do not consider absolute intensities). Relative line intensities were computed using the Boltzmann rotational partition function and the nuclear spin statistical weights for XY_6 molecules having Y ligands with a 1/2 spin.[45,46]

To conclude this paragraph, let us mention that in their work, Takami and Kuze[4] used Hamiltonians for the ground and $v_3 = 1$ states using the Amat–Nielsen ordering scheme[39] and expressed as

$$ H_{\{0\}} = B_0 J(J+1) - D_0 J^2 (J+1)^2 - D_{044} T_{044}, \tag{18} $$

$$ \begin{aligned} H_{\{\nu_3\}} = {} & \nu_3 + B_3 J(J+1) - D_3 J^2 (J+1)^2 \\ & + [-2B\zeta_3 + F_{110} J(J+1)] T_{110} \\ & + \alpha_{220} T_{220} - D_{044} T_{044} + \alpha_{224} T_{224} + F_{134} T_{134}. \end{aligned} \tag{19} $$

This formulation is not so different from ours since the T_{ijk}'s and F_{ijk}'s are also spherical tensor operators and the matrix elements of these two Hamiltonians can be calculated through formulas very similar to (13) and (14). However, our formulation has some important advantages: First, it is more

TABLE I. Effective parameters for the ν_3 band of WF_6 (in cm^{-1}). J_{max} is the maximum J value observed in the P or R branch, and σ is the root mean square of the residuals.

Level	Order	Parameter	$^{182}WF_6$ (26.4%)	$^{183}WF_6$ (14.4%)	$^{184}WF_6$ (30.6%)	$^{186}WF_6$ (28.4%)	Notation of Ref. 39
$v_3=0$	0	$t_0^{2(0)}$ [a]	0.066 1000	0.066 1000	0.066 1000	0.066 1000	B_0
$v_3=1$	0	$t_{3,3}^{20((00)0)}$	714.557 65(22)	714.233 387(21)	713.914 60(21)	713.285 14(19)	ν_3
	1	$t_{3,3}^{21((11)0)}$	−0.041 253(27)	−0.040 994(27)	−0.040 634(17)	−0.040 149(27)	$-3\sqrt{2}B\zeta_3$
	2	$t_{3,3}^{22((00)0)}$	$-4.558(41)\times10^{-5}$	$-4.574(37)\times10^{-5}$	$-4.989(52)\times10^{-5}$	$-4.809(40)\times10^{-5}$	$\Delta B=B_3-B_0$
		$t_{3,3}^{22((22)0)}$	$-2.496(65)\times10^{-5}$	$-1.156(96)\times10^{-5}$	$-0.831(91)\times10^{-5}$	$-0.622(73)\times10^{-5}$	$-\frac{5}{4}\alpha_{220}$
		$t_{3,3}^{22((22)4)}$	$-9.169(54)\times10^{-5}$	$-9.141(64)\times10^{-5}$	$-9.301(60)\times10^{-5}$	$-9.259(56)\times10^{-5}$	$-\frac{30}{\sqrt{6}}\alpha_{224}$
	3	$t_{3,3}^{23((11)0)}$	$-0.64(14)\times10^{-7}$	$-1.36(13)\times10^{-7}$	$0.28(14)\times10^{-7}$	$-0.31(15)\times10^{-7}$	$-\frac{3\sqrt{6}}{8}F_{110}$
		$t_{3,3}^{23((13)4)}$ [b]	0.0	0.0	0.0	0.0	$\frac{3\sqrt{5}}{2}F_{134}$
	$\tilde{\nu}_0$ [c]		714.538 19	714.214 06	713.895 44	713.266 21	
	$J_{max}(P/R)$		46	47	48	43	
	Assigned transitions		260	201	232	253	
	$\sigma/10^{-3}$ cm^{-1}		1.2	1.3	1.3	1.2	

[a]Fixed to the value of electron diffraction measurement of Ref. 48.
[b]Fixed to zero (see text).
[c]Band center (see text, the uncertainty is of the same order as in line 2 of the table). The full list of wave numbers of measured and calculated line positions is available through EPAPS (Ref. 70).

general as it enables the systematic expansion of the rovibrational Hamiltonian with a straightforward extension to any vibrational level or polyad. Second, it uses the so-called "vibrational extrapolation" [37] in which the Hamiltonian for a given polyad (here ν_3) contains the parameters of all the lower polyads (here the ground state). The correspondence between our parameters and those of Ref. 4 is easy to establish and is given in the last column of Table I.

B. The ReF_6 open-shell molecule

It has been shown in Ref. 47 that the vibronic Hamiltonian for the $\nu_3(F_{1u})$ mode in a G_g' electronic state can be written as

$$H=\hbar\omega_3(N_3^{(0)}+\tfrac{3}{2})+H_{JTQ}^{(0,A_1)}+H_{JTQ}^{(4,A_1)}, \quad (20)$$

where $\omega_3/2\pi$ is the harmonic oscillator frequency, $N_3^{(0)}=a_3^{+(1)}\cdot a_3^{(1)}$ is the number operator and the two quadratic vibronic terms are

$$H_{JTQ}^{(0,A_1)}=2\sqrt{6}\hbar\omega_3 Q_0[[q_3^{(1)}\otimes q_3^{(1)}]^{(2)}\otimes T^{(2)}]^{(0,A_1)}, \quad (21)$$

$$H_{JTQ}^{(4,A_1)}=2\sqrt{6}\hbar\omega_3 Q_4[[q_3^{(1)}\otimes q_3^{(1)}]^{(2)}\otimes T^{(2)}]^{(4,A_1)}, \quad (22)$$

where $q_3^{(1)}=(a_3^{(1)}+a_3^{+(1)})/\sqrt{2}$, $T^{(2)}$ is an electronic operator,[47] $\omega_3/2\pi$ is the harmonic oscillator frequency and Q_0, Q_4 are the quadratic vibronic parameters. Formulæ for the calculation of the matrix elements of this Hamiltonian in a coupled vibronic basis

$$|\Psi_{ev}\rangle=|[\Psi_{v3}^{(l_3)}\otimes\Phi^{(3/2)}]_{\sigma_0}^{(J_3,n_0C_0)}\rangle \quad (23)$$

are given in Ref. 47. Here,

$$|l_3-\tfrac{3}{2}|\leq J_3\leq l_3+\tfrac{3}{2}, \quad (24)$$

$\mathbf{J}_3$ being the vibronic angular momentum. As this Hamiltonian matrix is of infinite dimension, we can calculate the energy levels in practice by truncating v_3 at some high value (say, $v_3=20$). Figure 6 shows the four resulting eigenvalues for $v_3=1$ (as a function of Q_0 and Q_4) that correspond to the four vibronic sublevels expected for the ν_3 band.

As the complete treatment of the rovibronic interactions

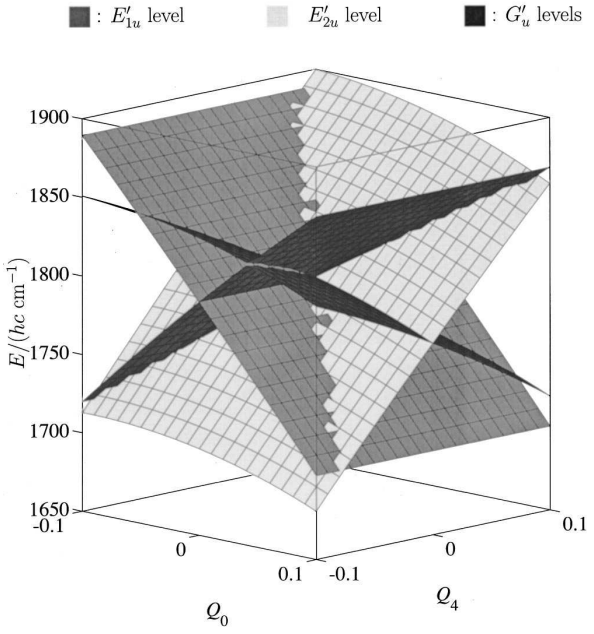

FIG. 6. Eigenvalues of the vibronic Hamiltonian for $v_3=1$ plotted as a function of Q_0 and Q_4 for $\tilde{\nu}_3=719.5\ cm^{-1}$ of ReF_6 (including the zero point energy for ν_3 only). The four sublevels E_{1u}', E_{2u}' and $2G_u'$ are shown with avoided crossings for the latter.

TABLE II. Effective parameters for the ν_3 band of WF_6 (in cm^{-1}) from Ref. 4.

Level	Order	Parameter	$^{182}WF_6$	$^{183}WF_6$	$^{184}WF_6$	$^{186}WF_6$
$\upsilon_3=1$	0	$t_{3,3}^{20((00)0)}$	714.557 67(12)	714.234 30(14)	713.915 20(13)	713.286 31(13)
	1	$t_{3,3}^{21((11)0)}$	−0.041 027(20)	−0.040 763(27)	−0.040 528(20)	−0.039 983(14)
	2	$t_{3,3}^{22((00)0)}$ [a]	-4.312×10^{-5}	-4.393×10^{-5}	-4.616×10^{-5}	-5.010×10^{-5}
		$t_{3,3}^{22((22)0)}$	-1.68×10^{-5} [b]	-1.68×10^{-5} [b]	-1.68×10^{-5} [b]	$-1.68(8)\times10^{-5}$
		$t_{3,3}^{22((22)4)}$	$-9.23(8)\times10^{-5}$	$-9.06(16)\times10^{-5}$	$-9.06(12)\times10^{-5}$	$-9.044(65)\times10^{-5}$
	3	$t_{3,3}^{20((11)0)}$	$-1.3(3)\times10^{-7}$	$-1.1(3)\times10^{-7}$	$-1.5(2)\times10^{-7}$	$-2.1(2)\times10^{-7}$
		$\tilde{\nu}_0$ [c]	714.538 32	714.215 08	713.896 09	713.267 46

[a]Calculated from the B_3 value through $t_{3,3}^{22((00)0)}=\Delta B=B_3-B_0$.
[b]Fixed to the value determined for $^{186}WF_6$ (see Ref. 4).
[c]Band center (see text).

(i.e., including rotation) remains a very difficult problem, we will only use a very crude model in this paper in order to get a preliminary qualitative interpretation of the spectra. We can apply the following simple effective Hamiltonian:

$$\tilde{H}=H_{\mathrm{JTQ}}^{(0_g,A_{1g})}+H_{\mathrm{JTQ}}^{(4_g,A_{1g})}+\tilde{H}_{\{0\}}+\tilde{H}_{\{\nu_3\}}+\cdots \tag{25}$$

with

$$\tilde{H}_{\{0\}}=B_0\mathbf{J}^2-2B_0\zeta_0\mathbf{J}\cdot\mathbf{J}_3+\cdots, \tag{26}$$

$$\tilde{H}_{\{\nu_3\}}=\Delta B\mathbf{J}^2-2\Delta(B\zeta)\mathbf{J}\cdot\mathbf{J}_3+\cdots, \tag{27}$$

where B_0 is the ground state rotational constant and the ζ are "Coriolis-type" coupling constants. ΔB and $\Delta(B\zeta)$ are the differences between the $\upsilon_3=1$ and ground state values, i.e., $\Delta B=B_3-B_0$ and $\Delta(B\zeta)=B_3\zeta_3-B_0\zeta_0$. If we set

$$\Delta E_{\mathrm{JT}}^{J_3}(\nu_3,Q_0,Q_4)=E_{\mathrm{JT}}^{1,J_3}(\nu_3,Q_0,Q_4)-E_{JT}^{0,3/2}(\nu_3,Q_0,Q_4), \tag{28}$$

where $E_{\mathrm{JT}}^{0,3/2}$ and E_{JT}^{1,J_3} are the eigenvalues of the vibronic Hamiltonian (20) for $\upsilon_3=0$ and $\upsilon_3=1$, respectively, the transition energies are (with $\mathbf{R}=\mathbf{J}-\mathbf{J}_3$):

$$\Delta E=\Delta E_{\mathrm{JT}}^{J_3}(\nu_3,Q_0,Q_4)+B_3(1-\zeta_3)J'(J'+1)-B_0(1-\zeta_0)J''(J''+1)+\Delta(B\zeta)R(R+1)+\cdots. \tag{29}$$

It seems reasonable to assume that the main term responsible of the octahedral splitting of the R levels is the same as that for "normal" molecules (A_{1g} electronic state), i.e., we can add the term

$$H_{\mathrm{oct}}=-\frac{\sqrt{2}}{5\sqrt{35}}g[[a^{+(1)}\otimes a^{(1)}]^{(2)}\otimes R^{2(2)}] \tag{30}$$

(this is the lowest order anisotropic vibration–rotation interaction term), where g is the octahedral-splitting parameter. The matrix elements of this operator can be calculated in the same way as in Eq. (14).

IV. ANALYSIS OF THE SPECTRA

A. WF_6

We have developed the effective Hamiltonian $\mathbf{H}_{\{\nu_3\}}^{\langle\nu_3\rangle}$ defined in the preceding section up to the third order ($\Omega_v+\Omega_r-2\leqslant3$). $\mathbf{H}_{\{0\}}^{\langle0\rangle}$ ($\equiv\mathbf{H}_{\{0\}}^{\langle\nu_3\rangle}$) has been developed to the zeroth order only, as in Refs. 4 and 40. The value of $t_0^{0(0)}=B_0$ has been fixed to 0.0661 cm^{-1} obtained from the electron diffraction.[48] A least-squares-fit program has then been used to determine the effective parameters for each of the four isotopic species. Preliminary assignments have been realized using the parameters of Takami and Kuze.[4] These have been refined in the high-J regions after several fits. We have used both sets of data (Fourier transform and diode laser spectra) described in Sec. II. All the observed lines in the diode laser spectra could be assigned. The parameter $t_{3,3}^{23((13)4)}$ has been fixed to zero, since all attempts to determine it led to a value lower than the uncertainty in terms of one standard deviation. Attempts to determine fourth order parameters were also unsuccessful. Thus, six parameters could be determined for each isotopomer.

The results are summarized in Table I. When we use the parameters from Ref. 4 (Table II) the simulation shows severe discrepancies when compared to our measurements (more than 0.02 cm^{-1}) in the high-J regions ($J\geqslant30$) which were not observed previously.[4] With our new sets of parameters, the agreement of experiment and simulation is good over the whole range observed.

Figures 7–9 show examples of comparisons between experimental and calculated spectra. The simulations were computed for a rotational temperature $T_{\mathrm{rot}}=50$ K and a Gaussian linewidth (FWHM) of 0.0007 cm^{-1} (diode laser spectra) or 0.004 cm^{-1} (FTIR spectra, apodized).

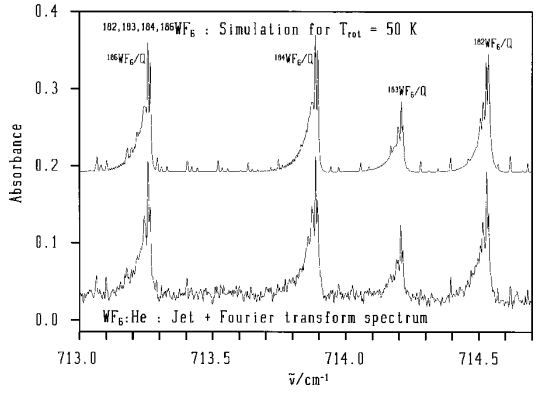

FIG. 7. WF_6 jet-FTIR spectrum and simulation of the ν_3 Q branch region.

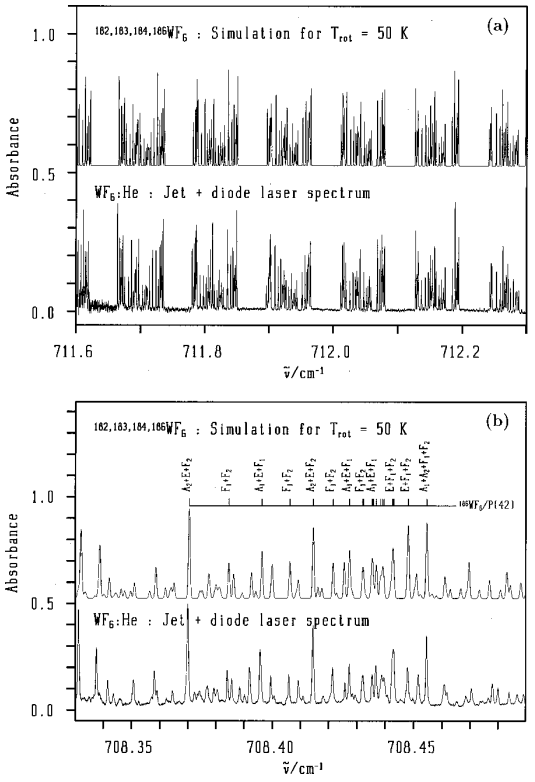

FIG. 8. (a) WF_6 jet+diode laser spectrum and simulation: part of the ν_3 P branch region. (b) WF_6 jet+diode laser spectrum and simulation in the region of the $^{186}WF_6$ $P(42)$ lines of the ν_3 band. Symmetry species (group O) are given for some of these lines.

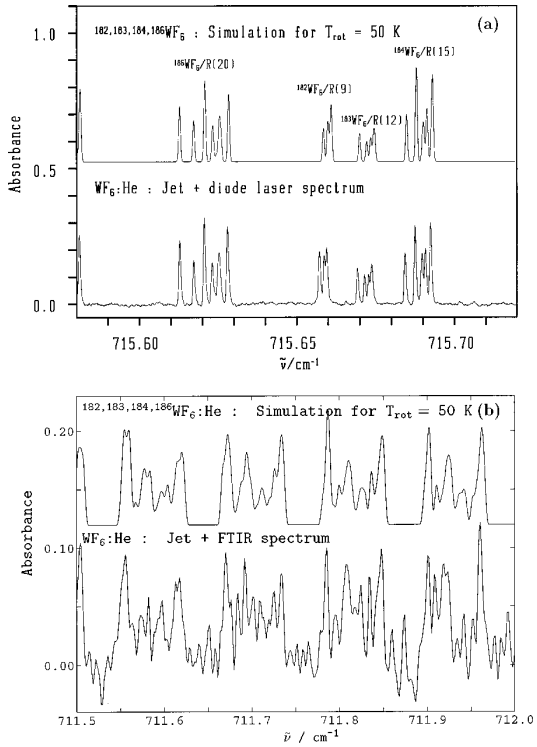

FIG. 9. (a) WF_6 jet+diode laser spectrum and simulation: detail in the ν_3 R branch region. (b) WF_6 jet-FTIR spectrum and simulation: detail in the ν_3 P branch region.

The cluster structure[49] is very well developed for high-J values as it can be seen in the case of the $P(42)$ lines of $^{186}WF_6$ [Fig. 8(b)]. As Harter and Patterson have shown,[49–51] for high-J values, the levels tend to group into sixfold and eightfold degenerate clusters. In a semiclassical interpretation, these clusters correspond to an angular momentum $\mathbf{J}$ precessing around a C_4 or a C_3 symmetry axis, respectively. In Fig. 8(b), the C_4 clusters of the $P(42)$ lines are seen on the left (A_2+E+F_2,F_1+F_2,A_1+E+F_1,...) and the C_3 clusters appear on the right ($A_1+A_2+F_1+F_2$,$E+F_1+F_2$,...). In other words, this means that the corresponding rotational energy surface $E(J_x,J_y,J_z)$ obtained by calculating the energy for continuous "classical" values of the angular momentum vector components J_x, J_y, J_z, has minima on C_4 axes and maxima on C_3 axes. We do not detail this point any further here, since the structure of rovibrational clusters of a degenerate vibrational level from the semiclassical point of view has already been discussed by Harter and co-workers in the case of tetrahedral molecules[52–54] (including the treatment of the Coriolis interaction[53]). More recently, the case of the ν_6 band of $Mo(CO)_6$ (Ref. 55) and of various bands of P_4 (Ref. 56) have been investigated, from both semiclassical and fully classical point of views. The cluster ordering observed here is consistent with the positive value of α_{224} (see Table I) just as in the case of GeF_4,[57] for instance.

Figure 10 displays the reduced energies for the $v_3=1$ vibrational level of $^{182}WF_6$. In the upper part of this figure, the distribution among the different J values of the rotational levels that we observed is shown.

The band center ν_0 can be calculated through[58]

$$\nu_0=\nu_3-2B\zeta_3-\frac{\alpha_{220}}{2}+\cdots$$

$$=t_{3,3}^{20((00)0)}+\frac{\sqrt{2}}{3}t_{3,3}^{21((11)0)}+\frac{2}{5}t_{3,3}^{22((22)0)}+\cdots. \quad (31)$$

This gives the following values:

$$\tilde{\nu}_0(^{182}WF_6)=714.538\,19\ \mathrm{cm}^{-1}, \quad (32)$$

$$\tilde{\nu}_0(^{183}WF_6)=714.214\,06\ \mathrm{cm}^{-1}, \quad (33)$$

$$\tilde{\nu}_0(^{184}WF_6)=713.895\,44\ \mathrm{cm}^{-1}, \quad (34)$$

$$\tilde{\nu}_0(^{186}WF_6)=713.266\,21\ \mathrm{cm}^{-1}. \quad (35)$$

Thus, the isotopic shift for WF_6 can be estimated to be

$$\Delta\tilde{\nu}_0/\Delta m=-0.3176\ \mathrm{cm}^{-1}u^{-1}. \quad (36)$$

This can also be read approximately directly from the Q branches from Fig. 1(b) and is consistent with Ref. 4. The band center of the remaining isotopomer $^{180}WF_6$ would be roughly

$$\tilde{\nu}_0(^{180}WF_6)\simeq 715.170\ \mathrm{cm}^{-1}, \quad (37)$$

but its very low natural abundance (0.135%) prevents it from being identified under our experimental conditions. The apparent higher precision of $t_{3,3}^{20((00)0)}$ for $v_3=1$ in line 2 of Table I for the isotope $^{183}WF_6$ results from a combination of correlation effects and accidental statistics of the lines. Thus, while numerically significant, it has no physical meaning.

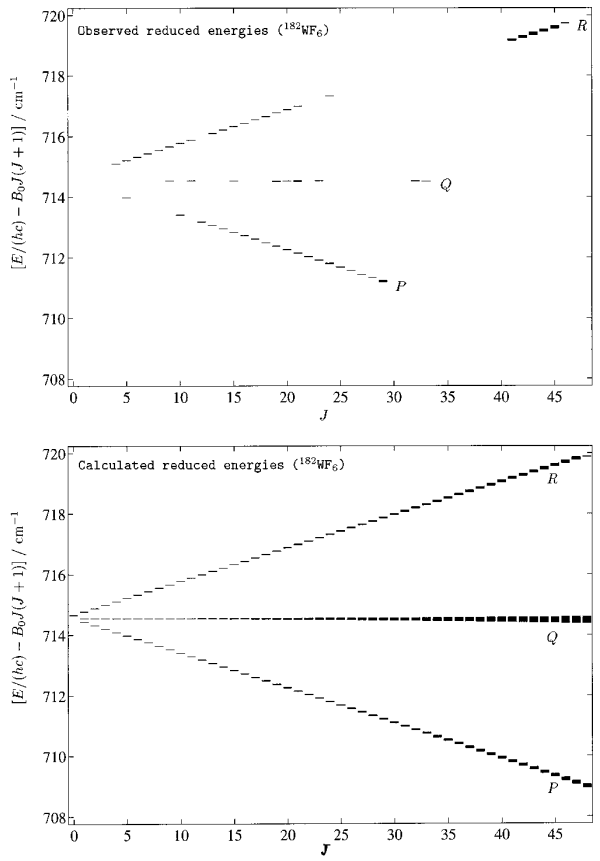

FIG. 10. Observed (upper) and calculated (lower part) reduced energy levels for the $\nu_3=1$ vibrational level of $^{182}WF_6$.

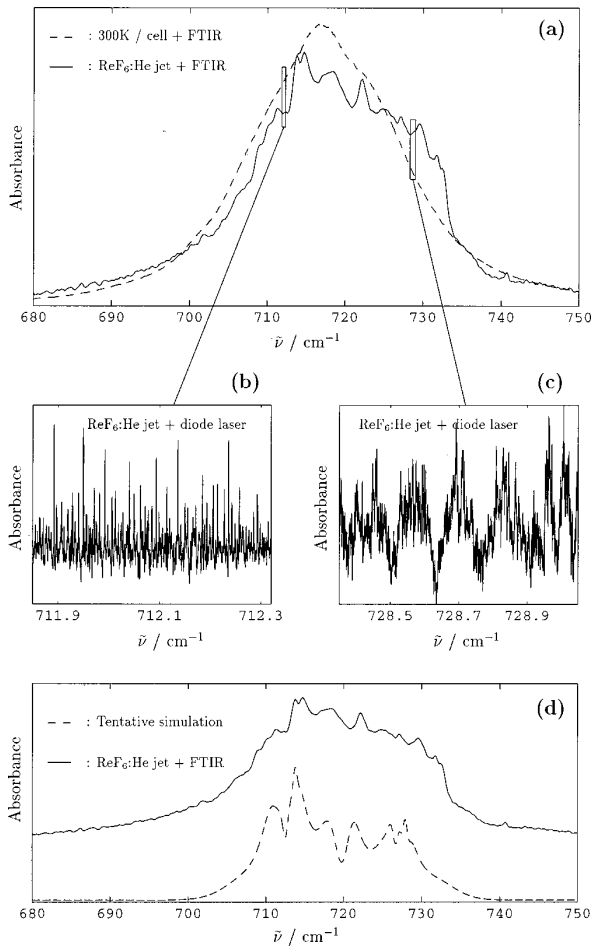

FIG. 11. (a) Overview low-resolution FTIR spectra of the ν_3 band of ReF_6 at room temperature and in a ReF_6:He jet (the instrumental bandwidth is 0.1 and 0.5 cm^{-1}, respectively). (b), (c) Jet+diode laser spectra of a ReF_6:He jet in the ν_3 band region. (d) Low-resolution (instrumental bandwidth of 0.5 cm^{-1}) jet-FTIR spectrum of the ν_3 band of ReF_6 compared to our tentative simulation (see text).

B. ReF_6

Figures 5, 11, and 12 show surveys and examples of low and high-resolution spectra for ν_3 of ReF_6. The differences to the surveys of ν_3 in WF_6 shown in Fig. 1 are most striking. Even in the FTIR supersonic jet spectra of ReF_6 shown in Figs. 11(a) and 11(d) the fine structure is just about becoming visible in form of some humps superimposed on a broad background. However, this "broad background" at high resolution can be resolved into a rich substructure of numerous lines that are well separated, with spacings that are of the order of frequently 0.01 cm^{-1} or less. This can be seen particularly in the diode laser spectra shown in Fig. 12, where the reproducibility of the traces demonstrates that all the stronger lines are clearly real line structure, well above the noise level. The total number of unambiguously assigned lines just in the regions covered by our diode laser scans indicated in Fig. 5 exceeds 700. The linewidths are frequently 0.001 cm^{-1} and less, although some lines are broader, which may indicate blending of several lines. At present, a full analysis of this extremely rich and dense fine structure is not possible. However, the line density is of the expected order of magnitude in agreement with our simulations and agrees with theoretical expectations of the complexity of these spectra.

The coarse superstructure appearing in the FTIR-jet spectra is amenable to at least a very preliminary analysis. In order to compute a "tentative simulation" using the simple rovibronic model described in Sec. III B, we have used the following parameters for both isotopomers of ReF_6: (i) $\tilde{\nu}_3=720.13$ cm^{-1} for $^{185}ReF_6$ and $\tilde{\nu}_3=719.50$ cm^{-1} for $^{187}ReF_6$, (ii) $B_0=0.066\,23$ cm^{-1}, value from electron diffraction measurements,[48] (iii) $\Delta B=B_3-B_0=-5\times10^{-5}$ cm^{-1}, $g=-0.97\times10^{-5}$ cm^{-1} and $\zeta_3=0.14$ (WF_6 values), (iv) $\zeta_0=-0.80$ a tentative value, (v) $Q_0=0.008$ and $Q_4=-0.006$ a "reasonable" order of magnitude, considering the general aspect of the band at 300 K. Much smaller or much larger values would lead to a band profile incompatible with what is observed. The resulting simulation [Fig. 11(d)] at a resolution of 0.5 cm^{-1} seems quite reasonable compared to the jet-FTIR spectrum and taking into account the crudeness of the model employed. This seems to confirm at least the order of magnitude of the quadratic vibronic coupling parameters given above. Table III summarizes the vibrational fundamentals for ReF_6 as far as known today, including the

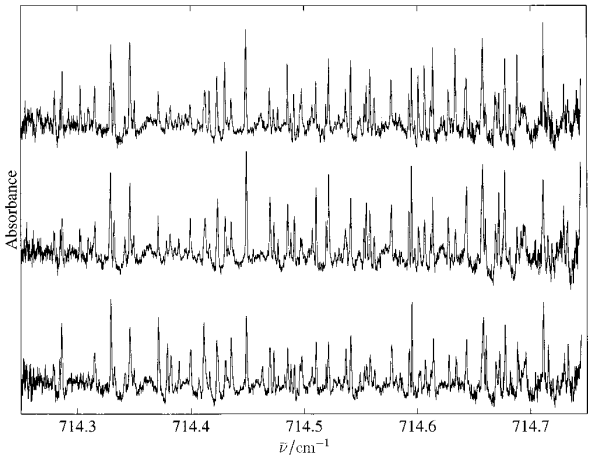

FIG. 12. Three jet+diode laser scans of a ReF_6:He=1:4 mixture (backing pressure of about 750 mbar) in the 714.5 cm^{-1} region.

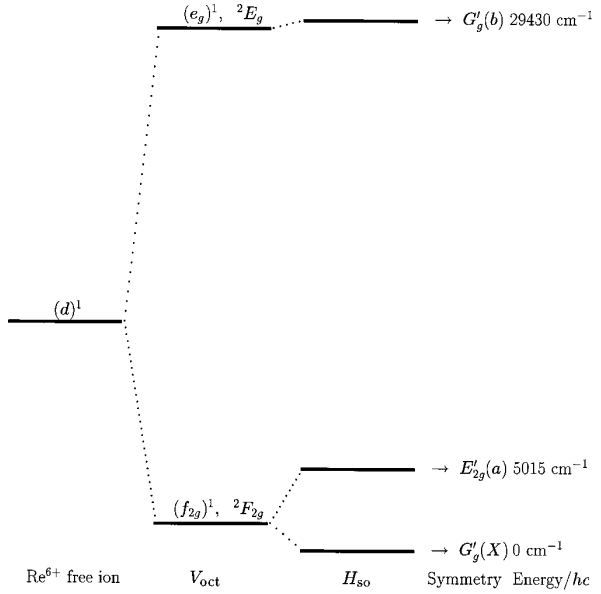

FIG. 13. The electronic levels of ReF_6. V_{oct} is the ligand field potential and H_{SO} is the spin–orbit coupling operator.

preliminary band center estimates of ν_3 from the present work. It is clear that much remains to be done on the vibronic level structure in this molecule.

V. CONCLUSIONS AND OUTLOOK

The high resolution FTIR and diode laser spectra obtained and analyzed in the present work confirm the theoretical expectation of completely different spectral structure for these two prototypes for a closed shell hexafluoride molecule with a nondegenerate ground state on the one hand and for an open shell molecule with a degenerate electronic ground state on the other. The rovibrational spectra of the ν_3 stretching fundamental of WF_6 show a simple structure under conditions of supersonic jet cooling, allowing for a straightforward analysis. Our results extend significantly the previous work[4] but agree with it, where there is overlap. There are no obvious interactions of ν_3 with other vibrational levels even at high J, the closest vibrational level expected in this region being far away [$\nu_2+\nu_5$ at 810 cm^{-1} (Ref. 5)]. Our analysis could be extended to other levels such as the ν_4 fundamental at 258 cm^{-1} (Ref. 5) or combination and overtones with some technical difficulties but no fundamental obstacles to be expected. Besides an improved understanding of the rovibrational level structure our results on WF_6 are potentially useful for two frequency laser isotope separation of W isotopes with selective preexcitation around 700 cm^{-1}, using, for instance, coincidences with the lines of the Raman shifted CO_2 laser or other high power lasers.[12,59,60]

The ν_3 fundamental of ReF_6 stands in stark contrast to the relatively simple structures observed for WF_6. Even under conditions of supersonic jet cooling the overall structure in the FTIR spectrum remains unresolved, with some broad features but no prominent Q-branch structures being visible. At the highest resolutions achieved in the diode laser spectra, this structure is, however, largely resolved into an extremely large number of closely spaced lines. While the broader features of the overall structure was amenable to a preliminary analysis with a simple model Hamiltonian, providing a first estimate of some of the ν_3 band parameters, the understanding of the detailed fine structure is at present not available, and remains a task to be handled in the future once the theory is further developed.[43,61] The complexity of this spectrum is indeed expected because of the complex electronic structure with a $G'_g(X)$ electronic ground state leading to complex rovibronic effects. The overall electronic structure of ReF_6 is summarized in Fig. 13. It indicates that beyond the complexities arising in the range of fundamental vibrations, the near infrared overtone spectrum might be of considerable interest because of potential vibronic interactions with the E'_{2g} electronic state near 5000 cm^{-1}. Such high vibrational levels might become accessible via recent high

TABLE III. The vibrational fundamentals of ReF_6 in its ground electronic state (in cm^{-1}).

Vibration	Symmetry	Activity	$^{185}ReF_6$	$^{187}ReF_6$	Reference
$\tilde{\nu}_1$	A_{1g}	Raman	753.7		66
$\tilde{\nu}_2$	E_g	Raman	575.0 (593[a])		29, 66
$\tilde{\nu}_3$	F_{1u}	Infrared	720.13 (715[a])	719.50 (715[a])	This work (7)
$\tilde{\nu}_4$	F_{1u}	Infrared	269.3 (257[a])		29, 7
$\tilde{\nu}_5$	F_{2g}	Raman	286.3 (246[a])		29, 66
$\tilde{\nu}_6$	F_{2u}	Inactive	166.0 (193[a])		29, 7

[a]First value reported in the literature [7, 66].

sensitivity techniques such as cw diode laser supersonic jet cavity ring down spectroscopy.[62,63] Of course also the higher electronic states have some interest in their own right.[27,64,65]

While the high resolution infrared spectroscopy of ReF_6 is still in its infancy, it offers some interesting opportunities for the future. Besides laser isotope separation, which might be more difficult because of the complex spectra, the very dense ultrahigh resolution spectra of open shell compounds of this type might reveal effects from parity mixing under the weak nuclear force which will be less efficient than in chiral molecules, but potentially much more efficient than in light atom closed shell molecules,[67,68] both in the absence or the presence of level crossings in magnetic fields.[69] Full understanding of the high resolution spectra which are the first ever recorded for such a case might open the route towards such investigations.

ACKNOWLEDGMENTS

We are very grateful to Alex Jourdan from COMURHEX company (Pierrelatte, France) for giving us substantial samples of WF_6 and ReF_6. Our work is supported financially by the Schweizerischer National Fonds (including a postdoctoral fellowship extended to V.B. during his stay at ETH Zürich) and by ETH Zürich (including the AGS, C^4 and CSCS projects). This work has also profited from stimulus and discussions with Jacques Moret-Bailly and Françoise Michelot.

[1] J. Gaunt, Trans. Faraday Soc. **49**, 1122 (1953).
[2] D. Travis, J. McGurk, D. McKeown, and R. Denning, Chem. Phys. Lett. **45**, 287 (1977).
[3] G. Baronov, A. Britov, S. Karavaev, A. Karachevskii, S. Kulikov, A. Merzlyakov, S. Sivachenko, and Y. I. Shcherbina, Sov. J. Quantum Electron. **11**, 947 (1981).
[4] M. Takami and H. Kuze, J. Chem. Phys. **80**, 5994 (1984); see also Y. Mitzugai, H. Kuze, H. Jones, and M. Takami, Appl. Phys. B: Photophys. Laser Chem. **32**, 43 (1983).
[5] R. McDowell and L. Asprey, J. Mol. Spectrosc. **45**, 491 (1973).
[6] J. Gaunt, Trans. Faraday Soc. **50**, 209 (1954).
[7] H. Claassen, J. Malm, and H. Selig, J. Chem. Phys. **36**, 2890 (1962).
[8] I. Levin, S. Abramowitz, and A. Müller, J. Mol. Spectrosc. **41**, 415 (1972).
[9] G. Cady and B. Hargreaves, J. Chem. Soc. **1961**, 1563.
[10] C. Bernard, R. Madar, and Y. Pauleau, Solid State Technol. **2**, 79 (1989).
[11] N. Desatnik and B. Thompson, J. Electrochem. Soc. **141**, 3532 (1994).
[12] M. Quack, Infrared Phys. **29**, 441 (1989); J. Chem. Phys. **69**, 1282 (1978).
[13] A. N. Halliday, Contemp. Phys. **38**, 103 (1997).
[14] D. C. Lee and A. N. Halliday, Nature (London) **378**, 771 (1995).
[15] D. C. Lee and A. N. Halliday, Science **274**, 1876 (1996).
[16] M. Schädel, W. Brüchle, R. Dressler *et al.*, Nature (London) **388**, 55 (1997).
[17] C. Nash and B. Bursten, J. Am. Chem. Soc. **121**, 10830 (1999).
[18] K. Tanner and A. Duncan, J. Am. Chem. Soc. **73**, 1164 (1951).
[19] H. Claassen and H. Selig, Isr. J. Chem. **7**, 499 (1969).
[20] H. Claassen, G. Goodman, J. Holloway, and H. Selig, J. Chem. Phys. **53**, 341 (1970).
[21] D. Jackson, Informal report LA-6025-MS, Los Alamos National Laboratory.
[22] L. Roberts, The properties of C.V.D. deposits of W and W–Re alloys, High temperature materials, 6th Plansee seminar, June 1968, Reutte, Austria, 1969.
[23] Y. Lakhotkin and A. Krasovskiy, Russ. Metall. **1**, 21 (1983).
[24] M. Pons, A. Benezech, P. Huguet, R. Gaufres, P. Diez, and J. Lafforet, J. Chem. Vap. Deposition **2**, 135 (1993).
[25] W. Moffit, G. Goodman, M. Fred, and B. Weinstock, Mol. Phys. **2**, 109 (1959).
[26] J. Brand, G. Goodman, and B. Weinstock, J. Mol. Spectrosc. **37**, 161 (1971).
[27] R. McDiarmid, J. Mol. Spectrosc. **38**, 495 (1971).
[28] J. Holloway, G. Stanger, E. Hope, W. Levason, and J. Ogden, J. Chem. Educ. **1988**, 1341.
[29] M. Rotger, V. Boudon, and H. Selig, Spectrochim. Acta, Part A **55**, 1575, 734 (1999).
[30] V. Boudon and F. Michelot, J. Mol. Spectrosc. **165**, 554 (1994).
[31] V. Boudon, Y. He, U. Schmitt, M. Quack, and M. Rotger, in *15th Colloquium on High Resolution Molecular Spectroscopy* (Glasgow, United Kingdom, 1997); V. Boudon, M. Rotger, Y. He, U. Schmitt, and M. Quack, in *16th Colloquium on High Resolution Molecular Spectroscopy* (Dijon, France, 1999).
[32] A. Amrein, M. Quack, and U. Schmitt, J. Phys. Chem. **92**, 5455 (1988).
[33] M. Quack, Annu. Rev. Phys. Chem. **41**, 839 (1990).
[34] H. Hollenstein, M. Quack, and E. Richard, Chem. Phys. Lett. **222**, 176 (1994).
[35] S. Yamamoto, R. Kuwabara, M. Takami, and K. Kuchitsu, J. Mol. Spectrosc. **115**, 333 (1986).
[36] G. Guelachvili and K. N. Rao, *Handbook of Infrared Standards* (Academic, Orlando, FL, 1986).
[37] J.-P. Champion, M. Loëte, and G. Pierre, in *Spectroscopy of the Earth's Atmosphere and Interstellar Medium*, edited by K. N. Rao and A. Weber (Academic, San Diego, CA, 1992), pp. 339–422.
[38] J. Moret-Bailly, Can. J. Phys. **15**, 237 (1961).
[39] A. Robiette, D. Gray, and F. Briss, Mol. Phys. **32**, 1591 (1976).
[40] M. Terki-Hassaine, G. Pierre, H. Bürger, and H. Willner, J. Mol. Spectrosc. **185**, 93 (1997).
[41] H. C. Longuet-Higgins, Mol. Phys. **6**, 445 (1963).
[42] M. Quack, Mol. Phys. **34**, 477 (1977).
[43] V. Boudon, M. Rey, M. Rotger, M. Loëte, H. Hollenstein, and M. Quack (unpublished).
[44] J. Champion, G. Pierre, F. Michelot, and J. Moret-Bailly, Can. J. Phys. **55**, 512 (1977).
[45] C. Cantrell and H. Galbraith, J. Mol. Spectrosc. **58**, 158 (1975).
[46] H. Berger, J. Phys. (France) **38**, 1371 (1977).
[47] V. Boudon, F. Michelot, and J. Moret-Bailly, J. Mol. Spectrosc. **166**, 449 (1994).
[48] M. Kimura, V. Schomaker, D. Smith, and B. Weinstock, J. Chem. Phys. **48**, 4001 (1968).
[49] W. Harter and C. Patterson, J. Chem. Phys. **66**, 4872 (1977).
[50] W. Harter and C. Patterson, J. Chem. Phys. **66**, 4886 (1977).
[51] W. Harter, Comput. Phys. Rep. **8**, 319 (1988).
[52] W. G. Harter, H. W. Galbraith, and C. W. Patterson, J. Chem. Phys. **69**, 4888 (1978).
[53] W. G. Harter, C. W. Patterson, and H. W. Galbraith, J. Chem. Phys. **69**, 4896 (1978).
[54] C. W. Patterson, H. W. Galbraith, B. J. Krohn, and W. G. Harter, J. Mol. Spectrosc. **77**, 457 (1979).
[55] G. Dhont, D. Sadovskiĭ, B. Zhilinskiĭ, and V. Boudon, J. Mol. Spectrosc. **201**, 95 (2001).
[56] Ch. Van-Hecke, D. Sadovskiĭ, B. Zhilinskiĭ, and V. Boudon, Eur. Phys. J. D **17**, 13 (2001).
[57] V. Boudon, H. Bürger, and E. B. Mkadmi, J. Mol. Spectrosc. **206**, 172 (2001).
[58] B. Bobin and K. Fox, J. Phys. (Paris) **34**, 571 (1973).
[59] D. Lupo and M. Quack, Chem. Rev. **1987**, 87.
[60] M. Quack, Infrared Phys. Technol. **36**, 365 (1995).
[61] M. Rey, V. Boudon, M. Loëte, and F. Michelot, J. Mol. Spectrosc. **204**, 106 (2000).
[62] M. Hippler and M. Quack. J. Chem. Phys. **116**, 6045 (2002).
[63] M. Hippler and M. Quack, Chem. Phys. Lett. **314**, 273 (1999).
[64] J. C. D. Brand, G. L. Goodman, and B. Weinstock, J. Mol. Spectrosc. **38**, 445 (1971).
[65] G. R. Meredith, J. D. Webb, and E. R. Bernstein, Mol. Phys. **34**, 995 (1977).
[66] H. H. Claassen and H. Selig, Isr. J. Chem. **7**, 499 (1969); H. H. Claassen, G. L. Goodman, J. H. Holloway, and H. Selig, J. Chem. Phys. **53**, 341 (1970).

[67] A. Bakasov, T.-K. Ha, and M. Quack, J. Chem. Phys. **109**, 7263 (1998).
[68] R. Berger and M. Quack, J. Chem. Phys. **112**, 3148 (2000).
[69] M. J. M. Pepper, I. Shavitt, P. Von Ragué Schleyer, M. N. Glukhovtsev, R. Janoschek, and M. Quack, J. Comput. Chem. **16**, 207 (1995).
[70] See EPAPS Document No. E-JCPSA6-116-005222 for four tables containing the observed and calculated transition wave numbers for WF_6 (Table I: $^{182}WF_6$, Table II: $^{183}WF_6$, Table III: $^{184}WF_6$, Table IV: $^{186}WF_6$). This document may be retrieved via the EPAPS homepage (http://www.aip.org/pubservs/epaps.html) or from ftp.aip.org in the directory /epaps/. See the EPAPS homepage for more information.

Quatrième partie

Spectroscopie des Toupies Quasi-sphériques

QUATRIÈME PARTIE

Chapitre

1

Spectroscopie des Toupies Sphériques et Quasi-Sphériques

Publications P13, P14, P15, P16, P19, P20, P21, P22, P24
Article de revue P23

1.1 Introduction

Depuis longtemps le laboratoire de Dijon est spécialisé dans l'étude des toupies sphériques (XY_4 (T_d), XY_6 (O_h)) telles que le méthane, le silane, l'hexafluorure de soufre ... Peu d'études spectroscopiques réalisées au sein de notre groupe étaient jusqu'à présent sorties de ce cadre (à l'exception de la thèse de Ch. Roche sur CH_3D et des travaux récents de A. Nikitin et J.-P. Champion sur quelques molécules de symétrie C_{3v}, comme CH_3Cl). Cependant, certaines molécules dites quasi-sphériques (c'est-à-dire avec un paramètre de sphéricité $\gamma = \frac{2(C-B)}{C+B}$ proche de zéro) peuvent être vues comme dérivant de toupies sphériques. De ce fait, nous pouvons envisager le développement de nouveaux modèles dérivés des modèles toupies sphériques. Nous avons réalisé cette extension jusqu'à présent pour deux molécules SF_5Cl et SO_2F_2. Par rapport aux modèles dits "classiques" existants, le modèle dijonnais présente un certain nombre d'avantages :

- En spectroscopie, il y a deux notions importantes : l'opérateur (Hamiltonien, Moment de Transition, ...) et la base. La base dérivée de la base sphérique semble ici mieux appropriée que les bases des modèles classiques (base de Wang, par exemple).
- Le modèle dijonnais est un modèle global capable de tenir compte de tous les types d'interaction possibles entre bandes. Il permet une génération systématique de tous les opérateurs d'interaction et les autres sous forme de développement limité jusqu'à un ordre donné.
- C'est l'unique modèle basé sur l'extrapolation des paramètres. Il est construit un peu comme les "poupées russes" (par emboitement des polyades) et permet donc de prédire de façon relativement fiable le spectre d'une polyade supérieure en utilisant tous les paramètres des polyades inférieures.

A la fin de ce chapitre, un article présente également l'analyse d'une bande d'une toupie sphérique ($^{80}SeF_6$) à l'aide du formalisme dijonnais (programmes HTDS).

1.2 Eléments de théorie

Il s'agit d'étudier des molécules dont le groupe de symétrie dérive des groupes tétraédrique, T_d et octaédrique O_h. Par exemple, la molécule SF_5Cl (groupe de symétrie C_{4v}) dérive de la molécule SF_6 (groupe de symétrie O_h) et la molécule SO_2F_2 dérive de l'ion tétraédrique SO_4^{2-}.

Par conséquent, du point de vue théorique, il s'agit de réorienter tous les éléments (tenseurs et bases) développés dans les groupes "toupies sphériques" vers les groupes de symétrie des molécules considérées (SF_5Cl, SO_2F_2, ...).

Cette ré-orientation se fait mathématiquement grâce à la matrice $\widetilde{G}$ définie par :

$$\left|j,nC,\widetilde{C}\widetilde{\sigma}\right\rangle = \sum_{\sigma} {}^{(C)}\widetilde{G}^{\sigma}_{\widetilde{C}\widetilde{\sigma}} \left|j,nC\sigma\right\rangle . \tag{IV.1.1}$$

Cette matrice est déterminée par une méthode de projection. C est une représentation irréductible de T_d ou O_h, σ une de ses composantes, $\widetilde{C}$ est une représentation irréductible du sous-groupe C_{2v} ou C_{4v}.

Les détails techniques concernant cette approche sont donnés dans les articles reproduits à la fin de ce chapitre.

1.3 Résultats récents concernant SO_2F_2

Pour valider ces modèles, il est important de les confronter à des données expérimentales. Ainsi, le niveau de base ou des bandes fondamentales ont été analysées ainsi que des polyades (diade de SF_5Cl et triade de SO_2F_2). Ces bandes ont été enregistrées par H. Bürger de Wuppertal. Ces analyses semblent meilleures que celles réalisées avec le formalisme classique.

Pour l'analyse du niveau de base de SO_2F_2, le rms (ou déviation standard) est légèrement plus faible (voir table 1.1).

TAB. 1.1 – *Résultats sur l'analyse du niveau de base de SO_2F_2*

	Reduction S^a	Reduction 6^a	$t_9 = 0^b$	t_9 "Optimisé"
RMS (kHz)	102.85	79.27	72.85	69.87
σ (kHz)	26	21	23.47	23.29

[a]: K. Sarka *et al.*, Journal of Molecular Spectroscopy, **200**, 55–64, (2000). [b]: $t_9 = 0$ est l'analyse de la réduction S dans notre modèle.

Pour la triade $\nu_3/\nu_7/\nu_9$ (qui dérive de la bande ν_4 de la toupie sphérique SO_4^{2-}), moins de paramètres sont ajustés, par contre de nouveaux paramètres entrent en jeu par rapport à l'analyse classique (voir table 1.2). L'analyse de la triade n'est pas totalement terminée (voir figure 1.1). Des attributions principalement dans la bande ν_3 sont à effectuer. L'analyse de la diade très serrée ν_4/ν_5 qui dérive de la bande ν_2 de la toupie sphérique SO_4^{2-} pourrait s'avérer encore plus prometteuse, car dans ce cas l'approche usuelle utilisant l'hamiltonien de Watson pose de graves problèmes de convergence.

TAB. 1.2 – *Résultats sur l'analyse de la triade de SO_2F_2*

	Modèle Classique[a]	Modèle Tensoriel (en cours)
Nombre de paramètres	79 (3 pour les interactions)	42 (10 pour les interactions)
Degré du Développement	8	6
J_{Max}	86	79
Nombre d'attributions IR	4806	2331
Nombre d'attributions MW	499	384
RMS_{IR} / 10^{-3} cm^{-1}	0.553	1.244
RMS_{MW} / 10^{-6} cm^{-1}	5.2	3.895

[a] H. Bürger *et al.*, Journal of Molecular Structure, **612**, 133–141, (2002).

Finalement, pour la molécule SO_2F_2, nous avons établit les formules de correspondance entre les deux jeux de paramètres jusqu'au degré 6. Il est en effet important de pouvoir faire le lien entre ce

que nous avons développé et l'approche usuelle de Watson. Ainsi, nous avons :

$$\left\{\begin{array}{rcl}
B_{002} &=& -\sqrt{2}t_3 - \frac{20\sqrt{14}}{7}t_9 - \frac{816b\sqrt{55}}{11}t_{18} - \frac{816a\sqrt{55}}{11}t_{19} + \cdots \\
B_{020} &=& 2\sqrt{6}t_2 + \frac{10\sqrt{30}}{3}t_7 - \frac{50\sqrt{42}}{21}t_8 - \frac{56\sqrt{462}}{11}t_{16} + \frac{392\sqrt{66}}{11}t_{17} + \cdots \\
B_{200} &=& t_1 - \frac{2\sqrt{6}}{3}t_2 - \frac{4}{5}t_7 + \frac{4\sqrt{42}}{7}t_8 + \frac{80\sqrt{462}}{77}t_{16} - \frac{80\sqrt{66}}{11}t_{17} + \cdots \\
T_{400} &=& t_4 + \frac{8\sqrt{2}}{3}t_5 + \frac{2\sqrt{30}}{5}t_7 - \frac{2\sqrt{42}}{7}t_8 + \frac{16\sqrt{10}}{5}t_{13} - \frac{16\sqrt{14}}{7}t_{14} - \frac{160\sqrt{462}}{231}t_{16} + \frac{160\sqrt{66}}{33}t_{17} + \cdots \\
T_{220} &=& -8\sqrt{2}t_5 - 4\sqrt{30}t_7 + \frac{20\sqrt{42}}{7}t_8 - \frac{40\sqrt{10}}{3}t_{13} + \frac{200\sqrt{14}}{21}t_{14} + \frac{100\sqrt{462}}{11}t_{16} - \frac{700\sqrt{66}}{11}t_{17} + \cdots \\
T_{040} &=& \frac{14\sqrt{30}}{3}t_7 - \frac{10\sqrt{42}}{3}t_8 - \frac{140\sqrt{462}}{11}t_{16} + \frac{980\sqrt{66}}{11}t_{17} + \cdots \\
T_{202} &=& \frac{4\sqrt{6}}{3}t_6 + \frac{4\sqrt{14}}{7}t_9 - \frac{80\sqrt{42}}{21}t_{15} - \frac{80b\sqrt{55}}{11}t_{18} - \frac{80a\sqrt{55}}{11}t_{19} + \cdots \\
T_{004} &=& -\frac{\sqrt{30}}{3}t_7 - \frac{\sqrt{42}}{3}t_8 + \frac{76\sqrt{462}}{11}t_{16} + \frac{76\sqrt{66}}{11}t_{17} + \cdots \\
T_{022} &=& -4\sqrt{14}t_9 + \frac{984b\sqrt{55}}{11}t_{18} + \frac{984a\sqrt{55}}{11}t_{19} + \cdots \\
\Phi_{600} &=& t_{10} - \frac{32\sqrt{6}}{9}t_{11} - \frac{8\sqrt{10}}{5}t_{13} + \frac{8\sqrt{14}}{7}t_{14} + \frac{20\sqrt{462}}{231}t_{16} - \frac{20\sqrt{66}}{33}t_{17} + \cdots \\
\Phi_{420} &=& \frac{32\sqrt{6}}{3}t_{11} + 16\sqrt{10}t_{13} - \frac{80\sqrt{14}}{7}t_{14} - \frac{20\sqrt{462}}{11}t_{16} + \frac{140\sqrt{66}}{11}t_{17} + \cdots \\
\Phi_{240} &=& -\frac{56\sqrt{10}}{3}t_{13} + \frac{40\sqrt{14}}{3}t_{14} + \frac{60\sqrt{462}}{11}t_{16} - \frac{420\sqrt{66}}{11}t_{17} + \cdots \\
\Phi_{240} &=& -4\sqrt{462}t_{16} + 28\sqrt{66}t_{17} + \cdots \\
\Phi_{402} &=& -\frac{16\sqrt{2}}{3}t_{12} - \frac{16\sqrt{42}}{21}t_{15} - \frac{8b\sqrt{55}}{11}t_{18} - \frac{8a\sqrt{55}}{11}t_{19} + \cdots \\
\Phi_{222} &=& \frac{16\sqrt{42}}{3}t_{15} + \frac{144b\sqrt{55}}{11}t_{18} + \frac{144a\sqrt{55}}{11}t_{19} + \cdots \\
\Phi_{042} &=& -24b\sqrt{55}t_{18} - 24a\sqrt{55}t_{19} + \cdots \\
\Phi_{204} &=& \frac{4\sqrt{10}}{3}t_{13} + \frac{4\sqrt{14}}{3}t_{14} + \frac{2\sqrt{462}}{11}t_{16} + \frac{2\sqrt{66}}{11}t_{17} + \cdots \\
\Phi_{024} &=& -2\sqrt{462}t_{16} - 2\sqrt{66}t_{17} + \cdots \\
\Phi_{006} &=& 8at_{18} - 8bt_{19} + \cdots
\end{array}\right.$$

où nous avons défini les quantités suivantes :

$$\left\{\begin{array}{rcl}
a &=& \frac{3\sqrt{55}}{4\sqrt{1684 + 79\sqrt{421}}} \\
b &=& -\frac{79 + 4\sqrt{421}}{4\sqrt{1684 + 79\sqrt{421}}}
\end{array}\right.$$

Ces formules peuvent bien évidemment être inversées. Notons toutefois qu'il s'agit de développements. Ceci est du à l'emploi, dans notre cas, de la construction de Moret-Bailly pour les opérateurs rotationnels, qui est différente de celle de Watson.

1.4 Perspectives

Pour aller encore plus loin, il me semble important de faire une analyse globale des niveaux rovibrationnels de SO_2F_2. Il s'agit d'ajuster simultanément le niveau de base, la diade et la triade de SO_2F_2. Pour cela, il reste cependant à finir l'analyse de la triade et à analyser la diade.

En matière d'analogie entre formalisme classique et formalisme tensoriel, il m'apparaît important d'aller encore plus loin dans ce domaine, notamment en faisant l'analogie des étiquettes des niveaux.

Ce type de modèle peut être appliqué à l'analyse des bandes d'autres toupies quasi-sphériques telles que celles de la molécule IOF_5, ...

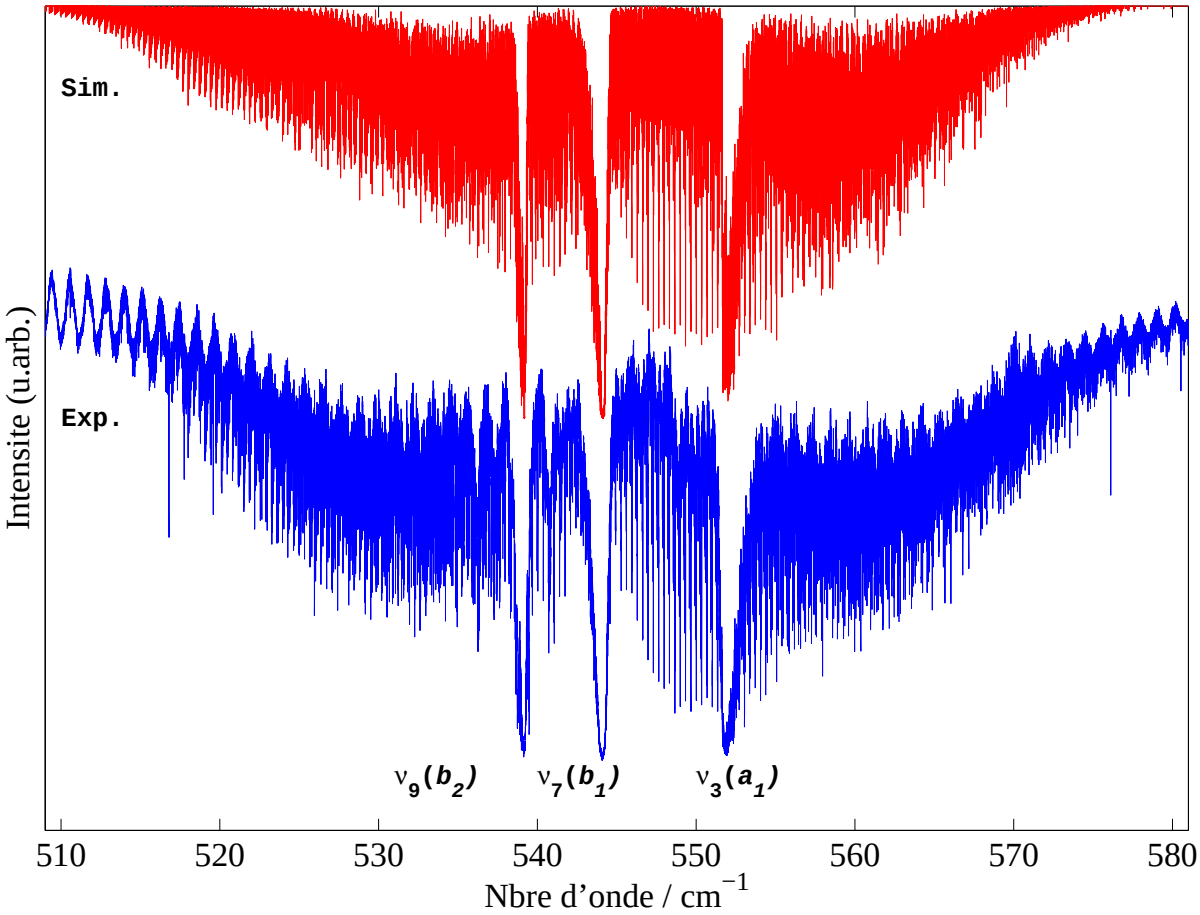

FIG. 1.1 – *La triade de SO_2F_2*

Du point de vue expérimental, certaines toupies quasi-sphériques ayant des spectres très denses, il s'avère indispensable de les enregistrer avec un jet supersonique. C'est le cas de la bande ν_8 de SF_5Cl. Nous comptons enregistrer des portions de cette bande à Dijon (spectromètre à diode laser + jet) et la vue d'ensemble sera enregistrée dans le groupe du Pr. M. Quack à Zürich. Le jet qui va être mis en place à Dijon est du même type que celui de Zürich. C'est un jet fente pulsé qui consomme de ce fait assez peu de substance et qui est mobile. Nous pourrions envisager de l'utiliser sur d'autres expériences du laboratoire.

1.5 Articles-clés

Sont reproduits ici les articles de base sur l'analyse de la toupie sphérique $^{80}SeF_6$ avec le modèle dijonnais (HTDS) et les modèles dérivés pour les toupies symétriques (SF_5Cl) et asymétriques (SO_2F_2). A titre d'exemple, deux analyses sont données et ont ainsi permis de tester nos formules ainsi que nos chaînes de programmes.

- [**P15 :** *Chem. Phys. Lett.*, **339**, 83–88 (2001)] présente l'analyse de la bande ν_4 de la molécule sphérique $^{80}SeF_6$.
- [**P13 :** *J. Mol. Spectrosc.*, **200**, 123–130 (2000)] nous donne les outils tensoriels pour une chaîne de groupes dérivant du groupe octaédrique O_h.
- [**P14 :** *J. Mol. Spectrosc.*, **200**, 131–137 (2000)] nous explicite les opérateurs hamiltonien et moments de transition pour une chaîne de groupes dérivant du groupe octaédrique O_h.

– [**P16 :** *J. Mol. Spectrosc.*, **208**, 169–179 (2001)] présente l'analyse de la diade ν_1/ν_8 de SF_5Cl dérivant de SF_6 à l'aide du modèle précédement développé.
– [**P19 :** *J. Mol. Spectrosc.*, **216**, 297–307 (2002)] donne les outils tensoriels et les opérateurs pour une chaîne de groupes dérivant du groupe tétraèdrique T_d.
– [**P21 :** *J. Mol. Spectrosc.*, **222**, 172–179 (2003)] présente l'analyse du niveau vibrationnel de base de SO_2F_2, moécule dérivant de l'ion sulfate SO_4^{2-}.

ELSEVIER

4 May 2001

Chemical Physics Letters 339 (2001) 83–88

CHEMICAL PHYSICS LETTERS

www.elsevier.nl/locate/cplett

High-resolution spectroscopy and analysis of the ν_4 band of $^{80}SeF_6$

M. Rotger [a,*], V. Boudon [a], H. Bürger [b], H. Willner [c]

[a] *Laboratoire de Physique de l'Université de Bourgogne, UMR CNRS 5027, 9, Avenue Alain Savary, B.P. 47 870, F-21078 Dijon Cedex, France*

[b] *Anorganische Chemie, Universität-GH, D-42097 Wuppertal, Germany*

[c] *Anorganische Chemie, FB 6, Gerhard-Mercator-Universität, D-47048 Duisburg, Germany*

Received 19 October 2000

Abstract

The Fourier-transform spectrum of the ν_4 bending region of $^{80}SeF_6$ around 435 cm^{-1} has been recorded at a temperature of 217 K with a resolution of 2.3×10^{-3} cm^{-1}. This fundamental has been analyzed using the set of programs called highly spherical top data system (HTDS). Altogether 958 transitions were assigned and fitted with an rms of 0.0003 cm^{-1}. The effective Hamiltonian was developed up to the fourth order. Parameters and simulations are presented. The ν_4 band center is located at 435.099 cm^{-1}. © 2001 Elsevier Science B.V. All rights reserved.

1. Introduction

The spectroscopy of the SeF_6 molecule is relatively unexplored in spite of significant interest in this molecule. A major case for high resolution studies of SeF_6 is to supply reliable spectroscopic data for laser isotope separation of Se by infrared multiphoton dissociation. For instance, ^{76}Br, which is a useful radioactive tracer for brain diagnostics, is produced by proton bombardment of ^{76}Se. Thus it is challenging to isolate this isotope. A successful experiment on isotope selective infrared multiphoton dissociation performed in the ν_3 region has been reported by Tiee and Wittig [1,2]. Moreover, this molecule, which belongs to the O_h point group, is a rather heavy spherical top and is an interesting target for the study of fundamental problems related to molecular physics and symmetry [3–5]. This molecule is the second member of group 16 (chalcogen) hexafluorides which also comprise SF_6 [6,7], TeF_6 [8,9] and radioactive PoF_6 [10]. These are stable and chemically inert molecules, contrary to the transition metal hexafluorides like WF_6, ReF_6, IrF_6 UF_6, which are highly reactive.

Apart from the strong stretching fundamental ν_3 [11,12], no other high-resolution study has been performed up to now. The Raman spectra of the $\nu_1(A_{1g})$, $\nu_2(E_g)$ and $\nu_5(F_{2g})$ bands have been recorded at low resolution [13]. However, high-resolution studies are still scarce because of severe hot band problems: at room temperature most of the molecules are in one of the many low-lying vibrational states. Even in SeF_6, which is the second lightest of the hexafluorides, population in the ground vibrational state is only 13% at 300 K.

* Corresponding author. Fax: +33-3-80-39-59-71.
E-mail address: maud.rotger@u-bourgogne.fr (M. Rotger).

0009-2614/01/$ - see front matter
PII: S0009-2614(01)00299-8

Another important problem concerning SeF_6 is the high number of isotopes with significant abundance for natural selenium: ^{74}Se (0.9%), ^{76}Se (9.0%), ^{77}Se (7.6%), ^{78}Se (23.5%), ^{80}Se (49.6%) and ^{82}Se (9.4%). Therefore, to circumvent this isotopic effect, we have chosen a monoisotopic $^{80}SeF_6$ sample. Further spectroscopic studies should investigate other isotopomers.

In this Letter, we present the high-resolution spectrum of the second strong band active in the infrared, namely the ν_4 bending mode. The experimental details are given in Section 2. The theoretical background is recalled in Section 3 and the results of the analysis are given and discussed in the last two Sections.

2. Experimental

Monoisotopic $^{80}SeF_6$ was prepared by burning ^{80}Se powder in an excess of fluorine and purified by successive cold traps. The spectrum was recorded using a Bruker 120 HR spectrometer equipped with a globar source, a 3.5 μm mylar beamsplitter, and a BSi bolometer. The resolution (1/maximum optical path difference) was 2.3×10^{-3} cm^{-1}. A double jacketed stainless steel cell of 24 cm length, equipped with CsBr windows and cooled to −56°C, was employed. The gas pressure was 0.4 mbar and 219 scans were collected. Calibration was done using lines of the ν_2 band of CO_2 [14]. Wavenumber precision was about 2×10^{-4} cm^{-1}.

3. Theory

The theoretical model described below to develop the Hamiltonian operator is based on the tensorial formalism and vibrational extrapolation methods used in Dijon. These methods have already been explained for example in [15]. We only recall here the basic principles and their application to the case of XY_6 molecules belonging to the O_h group [16].

If we consider an XY_6 molecule for which the vibrational levels are grouped in a series of polyads designed by P_k ($k = 0, \ldots, n$), P_0 being the ground state (GS), the Hamiltonian operator can be put in the following form (after performing some contact transformations):

$$\mathscr{H} = \mathscr{H}_{\{P_0 \equiv GS\}} + \mathscr{H}_{\{P_1\}} + \cdots + \mathscr{H}_{\{P_k\}} + \cdots + \mathscr{H}_{\{P_{n-1}\}} + \mathscr{H}_{\{P_n\}}. \quad (1)$$

Terms like $\mathscr{H}_{\{P_k\}}$ contain rovibrational operators which have no matrix elements within the $P_{k'>k}$ basis sets. The effective Hamiltonian for polyad P_n

Table 1
Effective parameters of the Hamiltonian for the ν_4 band of $^{80}SeF_6$

Level	Order	Parameter $t^{\Omega(K,n\Gamma)\Gamma_v\Gamma'_v}_{\{s\}\{s'\}}$			$^{80}SeF_6$ (Value/cm)[a]	'Usual' notation and comments
		$\Omega(K,n\Gamma)$	$\{s\}\ \Gamma_v$	$\{s'\}\ \Gamma'_v$		
GS	0	$2(0,0A_{1g})$	$000000A_{1g}$	$000000A_{1g}$	$7.8130718020 \times 10^{-2}$ [b]	B_0
$\nu_4 = 1$	0	$0(0,0A_{1g})$	$001000F_{1u}$	$001000F_{1u}$	435.128461 (65)	ν_4
	1	$1(1,0F_{1g})$	$001000F_{1u}$	$001000F_{1u}$	$0.627798\ (25) \times 10^{-1}$	$3\sqrt{2}B\zeta_{54}$ [c]
	2	$2(0,0A_{1g})$	$001000F_{1u}$	$001000F_{1u}$	$0.12649\ (44) \times 10^{-4}$	$B_4 - B_0$
	2	$2(2,0E_g)$	$001000F_{1u}$	$001000F_{1u}$	$-0.22346\ (25) \times 10^{-4}$	$-(1/2)\alpha_{220} - 6\alpha_{224}$
	2	$2(2,0F_{2g})$	$001000F_{1u}$	$001000F_{1u}$	-0.6×10^{-4} [d]	$-(3/4)\alpha_{220} + 6\alpha_{224}$
	3	$3(1,0F_{1g})$	$001000F_{1u}$	$001000F_{1u}$	$-0.4647\ (23) \times 10^{-7}$	$-(3\sqrt{3}/4\sqrt{2})F_{110}$
	3	$3(3,0F_{1g})$	$001000F_{1u}$	$001000F_{1u}$	$0.1306\ (12) \times 10^{-7}$	$(3/\sqrt{5}/2)F_{134}$
	4	$4(0,0A_{1g})$	$001000F_{1u}$	$001000F_{1u}$	$-0.157\ (65) \times 10^{-10}$	$-(D_4 - D_0)$

958 assigned lines, $J_{max} = 95, \sigma = 0.3 \times 10^{-3}$ cm^{-1} (rms)

[a] One S.D. in parentheses.
[b] Fixed.
[c] ν_4 Coriolis interaction.
[d] Fixed, see text.

is obtained by projecting $\mathscr{H}$ in the P_n Hilbert subspace, i.e.,

$$H^{\langle P_n\rangle} = P^{\langle P_n\rangle}\mathscr{H}P^{\langle P_n\rangle} = H^{\langle P_n\rangle}_{\{\mathrm{GS}\}} + H^{\langle P_n\rangle}_{\{P_1\}} + \cdots + H^{\langle P_n\rangle}_{\{P_k\}} + \cdots + H^{\langle P_n\rangle}_{\{P_{n-1}\}} + H^{\langle P_n\rangle}_{\{P_n\}}. \quad (2)$$

The different terms are written in the form

$$\mathscr{H}_{\{P_k\}} = \sum_{\text{all indexes}} t^{\Omega(K,n\Gamma)\Gamma_v\Gamma'_v}_{\{s\}\{s'\}} \left[R^{\Omega(K,n\Gamma)} \otimes {}^{\varepsilon}V^{\Omega_v(\Gamma_v\Gamma'_v)\Gamma}_{\{s\}\{s'\}}\right]^{(A_{1g})}. \quad (3)$$

In this equation, the $t^{\Omega(K,n\Gamma)\Gamma_v\Gamma'_v}_{\{s\}\{s'\}}$ terms are the parameters to be determined, $R^{\Omega(K,n\Gamma)}$ and ${}^{\varepsilon}V^{\Omega_v(\Gamma_v\Gamma'_v)\Gamma}_{\{s\}\{s'\}}$ are rotational and vibrational operators of respective degree Ω and Ω_v. Their construction is described in [15]. Again, the vibrational operators only have matrix elements within the $P_{k'\leqslant k}$ basis sets. The order of each individual term is $\Omega + \Omega_v - 2$.

Such a Hamiltonian development scheme enables the treatment of any polyad system. In this work, we will use only the two following effective Hamiltonians:

- The ground state effective Hamiltonian,

$$H^{\langle \mathrm{GS}\rangle} = H^{\langle \mathrm{GS}\rangle}_{\{\mathrm{GS}\}}. \quad (4)$$

- The ν_4 stretching fundamental effective Hamiltonian,

$$H^{\langle \nu_4\rangle} = H^{\langle \nu_4\rangle}_{\{\mathrm{GS}\}} + H^{\langle \nu_4\rangle}_{\{\nu_4\}}. \quad (5)$$

In order to calculate transition intensities, we developed the dipole moment operator through the zeroth order using the same methods [16].

We use a coupled vibrational basis taking into account the six vibrational modes of XY_6 molecules (of respective symmetry $A_{1g}, E_g, F_{1u}, F_{1u}, F_{2g}$ and F_{2u}). The Hamiltonian and dipole moment matrix elements are calculated in the coupled rovibrational basis

$$\left|\left[\Psi^{(J,nC)}_r \otimes \Psi^{(C_v)}_v\right]^{(\Gamma)}\right\rangle, \quad (6)$$

as described in [16]. In this last equation, the $\Psi^{(J,nC)}_r$s and $\Psi^{(C_v)}_v$s are rotational and harmonic oscillator wave functions, respectively.

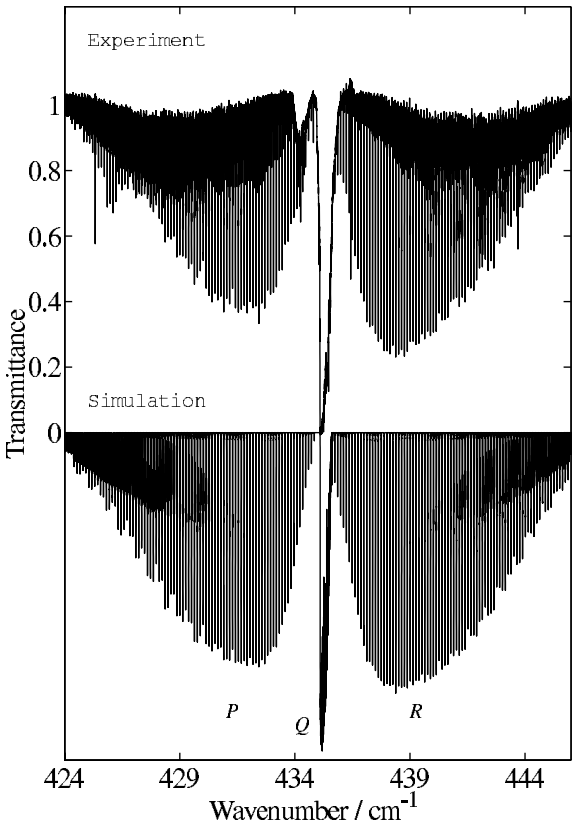

Fig. 1. The ν_4 rovibrational band: experiment and simulation.

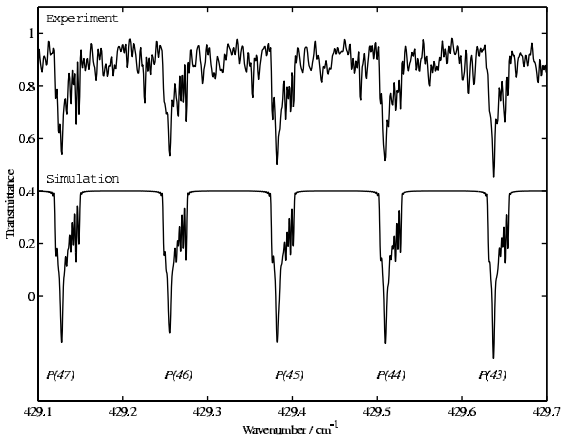

Fig. 2. The P branches for high J values: experiment and simulation.

4. Analysis of the ν_4 spectrum

In the following, $\mathscr{H}_{\{GS\}}$ is developed to the zeroth order and $\mathscr{H}_{\{\nu_4\}}$ is developed to the fourth order. The simulations and fits were realized using the HTDS (highly spherical top data system) software developed in Dijon for XY_6 molecules [17].

The assignments of the ν_4 band were made as follows. Preliminary simulations were calculated using the model briefly described above, with some parameters of the ν_3 band taken from the literature [12]. The only ground-state parameter $t^{2(0,0A_{1g})A_{1g}A_{1g}}_{\{0\}\{0\}} = B_0$ (rotational constant) has been fixed to the value given in [12]. The parameter relative to the band center has been roughly evaluated from the experimental spectrum. In a first attempt, we have manually adjusted the $t^{1(1,F_{1g})F_{1u}F_{1u}}_{\{4\}\{4\}}$ (Coriolis) and the $t^{2(0,0A_{1g})F_{1u}F_{1u}}_{\{4\}\{4\}}$ (ΔB) parameters with the aim of obtaining good agreement between theory and experiment. As it is usual for heavy molecules, the Q-branch is not sufficiently resolved to allow assignments of Q lines. In this case, the parameters $t^{2(2,0E_g)F_{1u}F_{1u}}_{\{4\}\{4\}}$ and $t^{2(2,0F_{2g})F_{1u}F_{1u}}_{\{4\}\{4\}}$ cannot be determined simultaneously. Therefore, we decided to vary $t^{2(2,0F_{2g})F_{1u}F_{1u}}_{\{4\}\{4\}}$ manually until the Q-branch profile was correct, and then we fixed the parameter in all further fits to the value obtained in this way,

$$t^{2(2,0F_{2g})F_{1u}F_{1u}}_{\{4\}\{4\}} = -0.6 \times 10^{-4}\ \mathrm{cm}^{-1}.$$

Then, assignments were made and fits were performed using a least-squares procedure described elsewhere [18,17]. J values have been increased step by step up to $J = 95$. The concomitantly performed simulations enabled many new assignments. The results are given in Table 1. Altogether, 958 assigned lines were used in the fit and the rms was 0.0003 cm^{-1}.

5. Discussion

As can be seen in the overview shown in Fig. 1 and the detailed spectra of Figs. 2 and 3, the simulation is very satisfactory. But we notice the presence of hot bands, especially the $\nu_4 + \nu_6 - \nu_6$ band [7], which could not yet be analyzed. This is mainly due to the lack of information on the inactive ν_6 fundamental. Fig. 4 shows the observed and calculated reduced energy levels obtained by subtracting the scalar term, i.e.,

$$E_{\mathrm{red}} = E - \sum_{\Omega} t^{\Omega(0,0A_{1g})A_{1g}A_{1g}}_{\{0\}\{0\}} (J(J+1))^{\Omega/2}$$
$$= E - B_0 J(J+1). \qquad (7)$$

The ν_4 band center m_4 can be calculated from [19]

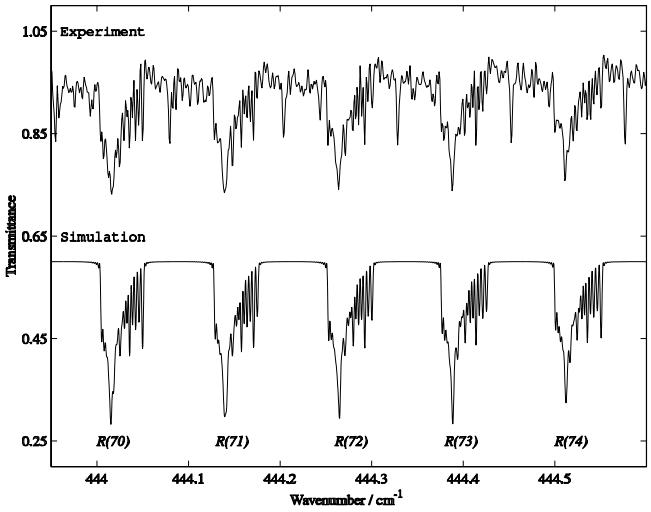

Fig. 3. The R branches for high J values: experiment and simulation.

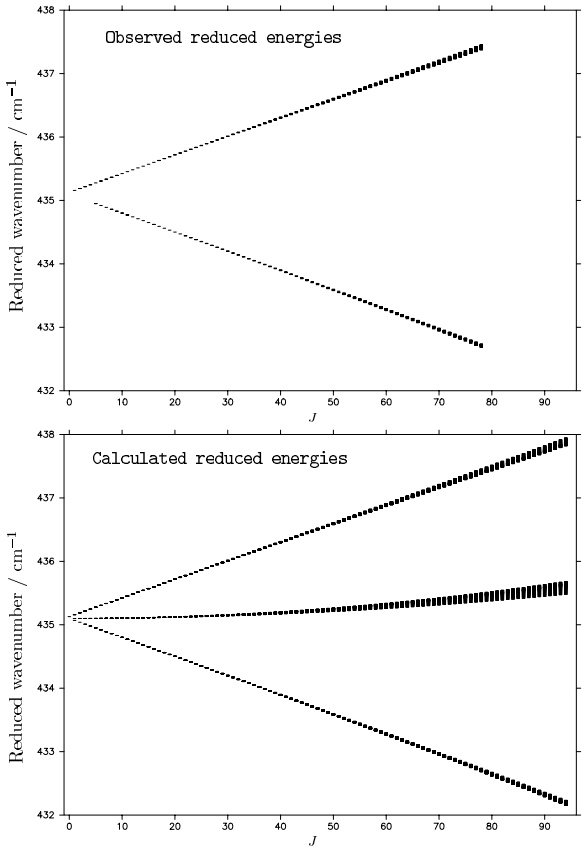

Fig. 4. Reduced energy levels of the ν_4 band of $^{80}SeF_6$.

$$m_4 = t^{0(0,0A_{1g})F_{1u}F_{1u}}_{\{4\}\{4\}} - \frac{\sqrt{2}}{3} t^{1(1,0F_{1g})F_{1u}F_{1u}}_{\{4\}\{4\}} + \frac{2}{5}\left(t^{2(2,0E_g)F_{1u}F_{1u}}_{\{4\}\{4\}} + t^{2(2,0F_{2g})F_{1u}F_{1u}}_{\{4\}\{4\}}\right) + \cdots \quad (8)$$

which leads to

$$m_4 \simeq 435.0988 \text{ cm}^{-1}. \quad (9)$$

If we evaluate the Coriolis factors using

$$t^{1(1,0F_{1g})F_{1u}F_{1u}}_{\{i\}\{i\}} = 3\sqrt{2}B\zeta_i \simeq 3\sqrt{2}B_0\zeta_i \quad (10)$$

with $i = 3$ or 4 and taking

$$t^{1(1,0F_{1g})F_{1u}F_{1u}}_{\{3\}\{3\}} = 0.0999145(7) \text{ cm}^{-1} \quad (11)$$

from [12] we obtain

$$\zeta_3 + \zeta_4 \simeq 0.491,$$

which is close to the value 1/2 predicted from the zeta sum rule [20].

6. Conclusion

We have measured and performed a rotational analysis of the fundamental ν_4 band of $^{80}SeF_6$. The results enable us to simulate this band with good agreement to the experimental spectrum.

The hot band lines visible in our spectrum could be analyzed if we had more information on the levels involved, which are essentially ν_6 and $\nu_4 + \nu_6$. So, future developments of the present study could include the direct observation of the Raman active ν_2 fundamental band of $^{80}SeF_6$ by means of stimulated Raman spectroscopy. We also plan to try to record the FTIR spectrum of the $\nu_2 + \nu_6$ combination band at low temperature or even in a supersonic jet.

The set of programs called HTDS can be accessed through ftp (user anonymous) at jupiter.u-bourgogne.fr or on the web at the URL: http://www.u-bourgogne.fr/LPUB/shTDS.html

Acknowledgements

Support from the Région Bourgogne for the computer equipment of the Laboratoire de Physique de l'Université de Bourgogne is gratefully acknowledged. H.B. thanks the Deutsche Forschungsgemeinschaft for support.

References

[1] J.J. Tiee, C. Wittig, Appl. Phys. Lett. 32 (4) (1978) 236.
[2] J.J. Tiee, C. Wittig, J. Chem. Phys. 69 (11) (1978) 4756.
[3] W.G. Harter, C.W. Patterson, J. Chem. Phys. 66 (1977) 4872.
[4] W.G. Harter, C.W. Patterson, J. Chem. Phys. 66 (1977) 4886.
[5] R.S. McDowell, C.W. Patterson, W.G. Harter, Los Alamos Science – Los Alamos Laboratory, 3 (1, Winter/Spring) (1982) 38.
[6] K. Kim, W. Person, D. Seitz, B. Krohn, J. Mol. Spectrosc. 76 (1979) 322.
[7] V. Boudon, G. Pierre, H. Bürger, J. Mol. Spectrosc. 205 (2001) 304.

[8] R.S. McDowell, R.F. Holland, W.H. McCulla, G.K. Anderson, M.J. Reisfeld, J. Mol. Struct. 145 (1986) 243.
[9] Y. Matsumoto, M. Takami, J. Chem. Phys. 85 (7) (1986) 3785.
[10] B. Weinstock, C.L. Chernick, J. Am. Chem. Soc. 82 (1960) 4116.
[11] M. Takami, J. Chem. Phys. 84 (1) (1986) 73.
[12] M. Terki-Hassaine, G. Pierre, H. Bürger, H. Willner, J. Mol. Spectrosc. 185 (1997) 93.
[13] H.H. Claassen, G.L. Goodman, J.H. Holloway, H. Selig, J. Chem. Phys. 53 (1970) 341.
[14] G. Guelachvili, K.N. Rao, Handbook of Infrared Standards, Academic Press, Orlando, 1986.
[15] J.P. Champion, M. Loëte, G. Pierre, in: K.N. Rao, A. Weber (Eds.), Spectroscopy of the Earth's Atmosphere and Interstellar Medium, Academic Press, San Diego, 1992, p. 339.
[16] N. Cheblal, M. Loëte, V. Boudon, J. Mol. Spectrosc. 197 (1999) 222.
[17] Ch. Wenger, V. Boudon, J.P. Champion, G. Pierre, J. Quant. Spectrosc. Radiat. Transfer 66 (2000) 1.
[18] Ch. Wenger, J.P. Champion, J. Quant. Spectrosc. Radiat. Transfer 59 (1998) 471.
[19] B. Bobin, K. Fox, J. Phys. (Paris) 34 (1973) 571.
[20] R.S. McDowell, J. Chem. Phys. 43 (1965) 319.

Journal of Molecular Spectroscopy **200,** 123–130 (2000)
doi:10.1006/jmsp.1999.8034, available online at http://www.idealibrary.com on IDEAL®

Spectroscopy of XY_5Z (C_{4v}) Molecules: A Tensorial Formalism Adapted to the $O(3) \supset O_h \supset C_{4v}$ Chain

M. Rotger, V. Boudon, and M. Loëte

Laboratoire de Physique de l'Université de Bourgogne, UMR CNRS 5027, 9 Avenue Alain Savary, B.P. 47 870, F-21078 Dijon Cedex, France

E-mail: rotger@jupiter.u-bourgogne.fr

Received September 28, 1999; in revised form November 10, 1999

A tensorial formalism adapted to the case of XY_5Z symmetric tops has been developed as an extension of the usual one for the octahedral molecules. We use the $O(3) \supset O_h \supset C_{4v}$ group chain. All the coupling coefficients and formulas for the computation of matrix elements are given for this chain. Such relations are also deduced in the C_{4v} group itself.

Key Words: tensorial formalism; XY_5Z symmetric tops.

1. INTRODUCTION

High-resolution rovibrational spectroscopy of XY_5Z molecules with C_{4v} symmetry is not well known both in infrared absorption and in Raman scattering (*1*). However, some pure rotational spectra have been recorded which can supply us with accurate ground state constants (*2*). Moreover, these molecules are good candidates for photochemical reactions such as photodissociation. For example, one could investigate quantitative kinetic analysis by means of controlled IR laser excitation (*3*), which can lead to the simple bond fission

$$XY_5Z \xrightarrow{nh\nu} XY_5 + Z, \qquad [1]$$

just as it has already been studied for CF_3I or C_6F_5I molecules (*4*).

In this aim, a better knowledge of the rovibrational energy levels is needed.

Therefore, we propose a new tensorial formalism adapted to the case of C_{4v} symmetric tops such as SF_5Cl, SF_5Br, SeF_5Cl, SeF_5Br, WF_5Cl, IOF_5, ... It is an extension of the usual formalism already developed in Dijon for octahedral XY_6 molecules in the $O(3) \supset O_h$ group chain (*5, 6*).

We work in the $O(3) \supset O_h \supset C_{4v}$ chain because most of these symmetric tops result from the substitution of one ligand of the corresponding spherical tops and thus are relatively close to octahedral symmetry. For example, SF_5Cl has a vibrational level scheme quite similar to that of the SF_6 molecule (*7*).

In the first part of this article, we briefly recall the basic principles used for the XY_6 molecules and developed in Dijon thanks to the tensorial formalism.

Then, we extend these principles to the $O(3) \supset O_h \supset C_{4v}$ chain. Coupling coefficients and formulas for the computation of matrix elements of tensor operators are derived for this chain.

In the last part, coupling coefficients are calculated for the C_{4v} group itself and some coefficient values are given in the appendixes. We intend to use these formulas for calculating the reduced matrix elements of particular operators such as the Hamiltonian and transition moment operators (dipole moment and polarizability). Such calculations will be described in a subsequent paper. All this should enable us to analyze and simulate the rovibrational spectrum of the $^{32}SF_5\,^{35}Cl$ molecule.

2. ORIENTATION IN THE $O(3) \supset O_h$ CHAIN

Let us first recall quickly the basic principles of the orientation in the chain $O(3) \supset O_h$ that is used for XY_6 octahedral molecules (like SF_6, WF_6, UF_6, $\cdots$).

This has been explained in detail in Refs. (*5, 8*) so we will only point out here the essential features of the method.

The $O(3)$ standard basis, say $|j, m\rangle$, is oriented into the O_h subgroup so that we obtain a new oriented basis through

$$|j, nC\sigma\rangle = \sum_m {}^{(j)}G^m_{nC\sigma}|j, m\rangle. \qquad [2]$$

There are several possible methods to find a G matrix that realizes this orientation. The one that has been retained in preceding works (*8*) is based on the fact that the Hamiltonian is constructed as a linear combination of spherical tensors that are invariant in O_h:

0022-2852/00 $35.00

TABLE 1
Characters for the Irreducible Representations of C_{4v}

C_{4v}	I	$2C_4$	C_2	$2\sigma_v$	$2\sigma_d$
a_1	1	1	1	1	1
a_2	1	1	1	-1	-1
b_1	1	-1	1	1	-1
b_2	1	-1	1	-1	1
e	2	0	-2	0	0

TABLE 2
Multiplication Table for the Irreducible Representations of C_{4v}

	a_1	a_2	b_1	b_2	e
a_1	a_1	a_2	b_1	b_2	e
a_2	a_2	a_1	b_2	b_1	e
b_1	b_1	b_2	a_1	a_2	e
b_2	b_2	b_1	a_2	a_1	e
e	e	e	e	e	$a_1 + \{a_2\}^* + b_1 + b_2$

* { ... } is the antisymmetric part.

$$H^{(A_{1g})} = \sum_k C_k H^{(k_g, A_{1g})}. \qquad [3]$$

In the following, we omit the parity indices for simplicity, except in a few cases where it is useful to understand selection rules. The G matrix can be obtained by diagonalizing one of these operators. For reasons explained elsewhere (*9, 10*), an operator of the type $H^{(4,A_1)}$ (rank four in $O(3)$) is chosen. If we write the matrix elements

$$\langle j, nC\sigma|H^{(4,A_1)}|j, nC\sigma\rangle = \sum_{m,m',q} {}^{(j)}G^{nC\sigma(4)}_{m} G^{q}_{A_1} {}^{(j)}G^{m'}_{nC\sigma} \langle j, m|H^{(4)}_q|j, m'\rangle \qquad [4]$$

and if we apply the Wigner–Eckart theorem on both sides (that is, in O_h and in $O(3)$, respectively), and then simplify by the reduced matrix element $\langle j\|H^{(4)}\|j\rangle$, we can see that the equation above is equivalent to diagonalize the matrix

$$A(j)^{m'}_{m} = (-1)^{j-m} \sum_q {}^{(4)}G^{q}_{A_1} \bar{V}\begin{pmatrix} 4 & j & j \\ q & -m & m' \end{pmatrix}, \qquad [5]$$

(the $\bar{V}$ are Wigner coefficients). The eigenvectors of this matrix lead to the G matrix, provided that appropriate phase choices are made, as explained in Refs. (*8, 10*).

This $|j, nC\sigma\rangle$-oriented basis is the starting point of our work since we will now realize a second reorientation in the C_{4v} subgroup.

In view of further applications to molecules, we follow Refs. (*11, 12*) to set the variances of irreducible tensors and kets. In the molecule-fixed frame, we take tensorial sets of type $|\cdots\rangle$ considered as contravariant: $\Psi^{m}_{(j)}$, and tensorial sets of type $\langle\cdots|$ considered as covariant: $\Psi^{(j)}_{m}$. The inverse convention is taken in the laboratory-fixed frame.

3. ORIENTATION IN THE $O(3) \supset O_h \supset C_{4v}$ CHAIN

The C_{4v} point group has eight symmetry elements. Its character and multiplication tables are recalled in Tables 1 and 2, respectively.

Table 3 shows the decomposition of O_h irreducible representations (irreps) into C_{4v} irreps.

We also define here our notations: all tilded symbols ($\tilde{C}$, $\tilde{F}$, $\cdots$) represent C_{4v} symbols (irreps, coupling coefficients, $\cdots$) and primed symbols (F', K', $\cdots$) represent oriented coupling coefficients in $O_h \supset C_{4v}$. We also denote the C_{4v} irreps by lowercase letters (a_1, a_2, $\cdots$) to avoid any confusion with O_h irreps. In the following, $[\tilde{C}]$ is the dimension of irrep $\tilde{C}$.

We can introduce a new $O(3) \supset O_h \supset C_{4v}$ oriented basis thanks to the following expression:

$$|j, nC\sigma, \tilde{C}\tilde{\sigma}\rangle = \sum_{\sigma} {}^{(C)}G'^{\sigma}_{\tilde{C}\tilde{\sigma}}|j, nC\sigma\rangle. \qquad [6]$$

If we call G' the matrix that realizes the orientation of the ($O(3) \supset$) O_h basis into the C_{4v} subgroup, we have for every element R of C_{4v} (which also pertains to O_h),

$$[\tilde{D}^{(\tilde{C})}(R)]^{\tilde{\sigma}'}_{\tilde{\sigma}}\delta_{\tilde{C}',\tilde{C}} = \sum_{\sigma,\sigma'} {}^{(C)}G'^{\tilde{C}'\tilde{\sigma}'}_{\sigma'} [D^{(C)}(R)]^{\sigma'(C)}_{\sigma} G'^{\sigma}_{\tilde{C}\tilde{\sigma}}, \qquad [7]$$

where $\tilde{C}'$ labels an irreducible representation of C_{4v} and $\tilde{\sigma}$ its component. D and $\tilde{D}$ are the matrices of R in O_h and C_{4v}, respectively.

To calculate the matrix G' we use the projection method as follows. We apply to the $|C, \sigma\rangle$ basis functions of O_h the projector

TABLE 3
$O_h \supset C_{4v}$ Correlation Table

C	$\widetilde{C}$
A_{1g}	a_1
A_{2g}	b_1
E_g	$a_1 + b_1$
F_{1g}	$a_2 + e$
F_{2g}	$b_2 + e$
A_{1u}	a_2
A_{2u}	b_2
E_u	$a_2 + b_2$
F_{1u}	$a_1 + e$
F_{2u}	$b_1 + e$

$$P_{\tilde{\sigma}}^{(\tilde{C})} = \frac{[\tilde{C}]}{[C_{4v}]} \sum_{R \in C_{4v}} ([\tilde{D}^{(\tilde{C})}(R)]_{\tilde{\sigma}}^{\tilde{\sigma}})^* P_R,$$

where $[C_{4v}] = 8$ (number of elements in C_{4v}) and with

$$P_R|C, \sigma\rangle = \sum_{\sigma'} [D^{(C)}(R)]_{\sigma}^{\sigma'}|C, \sigma'\rangle,$$

that defines the action of the symmetry element R on $|C, \sigma\rangle$. We have thus

$$|C, \tilde{C}, \tilde{\sigma}\rangle = P_{\sigma}^{(\tilde{C})}|C, \sigma\rangle. \qquad [8]$$

For the two-dimensional C_{4v} representation e the component $|C, e, 1\rangle$ is found as above, and the second one $|C, e, 2\rangle$ is obtained by applying P_R on both members of Eq. [8] using

$$P_R|\tilde{C}, \tilde{\sigma}\rangle = \sum_{\sigma'} [\tilde{D}^{(\tilde{C})}(R)]_{\tilde{\sigma}}^{\tilde{\sigma}'}|\tilde{C}, \tilde{\sigma}'\rangle, \qquad [9]$$

for applying P_R in C_{4v}. Here we choose $R = C_4$ since its matrix is

$$C_4 = \begin{pmatrix} 0 & 1 \\ -1 & 0 \end{pmatrix},$$

i.e., it simply exchanges components 1 and 2. For example, we obtain

$$|F_{1g}, e, 1\rangle = |F_{1g}, y\rangle,$$

and then $P_{C_4}|F_{1g}, e, 1\rangle = -|F_{1g}, e, 2\rangle = P_{C_4}|F_{1g}, y\rangle = |F_{1g}, x\rangle$, implying $|F_{1g}, e, 2\rangle = -|F_{1g}, x\rangle$, with a suitable choice for R in order to ensure consistent phases.

We are now able to calculate each G' value as it is given in Appendix A. We can therefore build the oriented basis $|j, nC\sigma, \tilde{C}\tilde{\sigma}\rangle$.

In the following, we will put particular attention on the different phase choices to be made, since these are essential to obtain consistent phases for all the coupling coefficients and formulas developed hereafter.

In a general way, the contracovariant change is made using the metric tensor (*11*):

$$T_{\tilde{C}\tilde{\sigma}}^{(C)} = \epsilon_C \begin{pmatrix} C \\ \tilde{C}\tilde{\sigma}\tilde{C}'\tilde{\sigma}' \end{pmatrix} T_{(C)}^{\tilde{C}'\tilde{\sigma}'},$$

$$T_{(C)}^{\tilde{C}\tilde{\sigma}} = \epsilon'_C \begin{pmatrix} \tilde{C}'\tilde{\sigma}'\tilde{C}\tilde{\sigma} \\ C \end{pmatrix} T_{\tilde{C}'\tilde{\sigma}'}^{(C)}. \qquad [10]$$

We adopt here Einstein's summation convention. ϵ_C and ϵ'_C are phase factors to be chosen. We choose here a real metric tensor; thus we have $\epsilon_C = \epsilon'_C$ and $\epsilon_C^2 = 1$. To match what has been done for the $O(3) \supset O_h$ chain, we define our F'-oriented coupling coefficients in terms of the F ones of O_h (*8*) by

$$F' \begin{matrix} (C_{1\tau} & C_{2\nu} & C_{3\chi}) \\ \tilde{C}_1\tilde{\sigma}_1 & \tilde{C}_2\tilde{\sigma}_2 & \tilde{C}_3\tilde{\sigma}_3 \end{matrix} = \sum_{\sigma_1,\sigma_2,\sigma_3} {}^{(C_{1\tau})}G'^{\,\sigma_1}_{\tilde{C}_1\tilde{\sigma}_1}\, {}^{(C_{2\nu})}G'^{\,\sigma_2}_{\tilde{C}_2\tilde{\sigma}_2}\, {}^{(C_{3\chi})}G'^{\,\sigma_3}_{\tilde{C}_3\tilde{\sigma}_3}\, F \begin{matrix} (C_{1\tau} & C_{2\nu} & C_{3\chi}) \\ \sigma_1 & \sigma_2 & \sigma_3 \end{matrix}, \qquad [11]$$

where τ, ν, and χ are parity indexes (g or u).

As explained in Ref. (*11*), the various coupling coefficients for two irreducible tensors can be related by the following general relations

$$F' \begin{matrix} \tilde{C}_1\tilde{\sigma}_1 & \tilde{C}_2\tilde{\sigma}_2 & (C_3) \\ (C_1 & C_2) & \tilde{C}_3\tilde{\sigma}_3 \end{matrix} = K(C_1C_2C_3) \begin{pmatrix} C_3 \\ \tilde{C}_3\tilde{\sigma}_3\, \tilde{C}'_3\tilde{\sigma}'_3 \end{pmatrix} \begin{pmatrix} \tilde{C}'_1\tilde{\sigma}'_1\, \tilde{C}_1\tilde{\sigma}_1 \\ C_1 \end{pmatrix} \begin{pmatrix} \tilde{C}'_2\tilde{\sigma}'_2\, \tilde{C}_2\tilde{\sigma}_2 \\ C_2 \end{pmatrix} \times F' \begin{matrix} (C_1 & C_2) & \tilde{C}'_3\tilde{\sigma}'_3 \\ \tilde{C}'_1\tilde{\sigma}'_1 & \tilde{C}'_2\tilde{\sigma}'_2 & (C_3) \end{matrix}, \qquad [12]$$

$$F' \begin{matrix} \tilde{C}_1\tilde{\sigma}_1 & \tilde{C}_2\tilde{\sigma}_2 & \tilde{C}_3\tilde{\sigma}_3 \\ (C_1 & C_2 & C_3) \end{matrix} = K'(C_1C_2C_3) \begin{pmatrix} \tilde{C}'_1\tilde{\sigma}'_1\, \tilde{C}_1\tilde{\sigma}_1 \\ C_1 \end{pmatrix} \begin{pmatrix} \tilde{C}'_2\tilde{\sigma}'_2\, \tilde{C}_2\tilde{\sigma}_2 \\ C_2 \end{pmatrix} \begin{pmatrix} \tilde{C}'_3\tilde{\sigma}'_3\, \tilde{C}_3\tilde{\sigma}_3 \\ C_3 \end{pmatrix} \times F' \begin{matrix} (C_1 & C_2 & C_3) \\ \tilde{C}'_1\tilde{\sigma}'_1 & \tilde{C}'_2\tilde{\sigma}'_2 & \tilde{C}'_3\tilde{\sigma}'_3 \end{matrix}, \qquad [13]$$

$$F' \begin{matrix} (C_1 & C_2) & \tilde{C}_3\tilde{\sigma}_3 \\ \tilde{C}_1\tilde{\sigma}_1 & \tilde{C}_2\tilde{\sigma}_2 & (C_3) \end{matrix} = \epsilon_{C_3} e^{i\phi(C_1C_2C_3)} [C_3]^{1/2} \begin{pmatrix} \tilde{C}'_3\tilde{\sigma}'_3\, \tilde{C}_3\tilde{\sigma}_3 \\ C_3 \end{pmatrix} \times F' \begin{matrix} (C_1 & C_2 & C_3) \\ \tilde{C}_1\tilde{\sigma}_1 & \tilde{C}_2\tilde{\sigma}_2 & \tilde{C}_3\tilde{\sigma}_3 \end{matrix}, \qquad [14]$$

$$F' \begin{matrix} \tilde{C}_1\tilde{\sigma}_1 & \tilde{C}_2\tilde{\sigma}_2 & (C_3) \\ (C_1 & C_2) & \tilde{C}_3\tilde{\sigma}_3 \end{matrix} = \epsilon'_{C_3} e^{i\psi(C_1C_2C_3)} [C_3]^{1/2} \begin{pmatrix} C_3 \\ \tilde{C}_3\tilde{\sigma}_3\, \tilde{C}'_3\tilde{\sigma}'_3 \end{pmatrix} \times F' \begin{matrix} \tilde{C}_1\tilde{\sigma}_1 & \tilde{C}_2\tilde{\sigma}_2 & \tilde{C}'_3\tilde{\sigma}'_3 \\ (C_1 & C_2 & C_3) \end{matrix}, \qquad [15]$$

where $[C_3]$ is the dimension of the C_3 representation of O_h.

For a consistent symmetry adaptation in $O_h \supset C_{4v}$, the phase factors $K(C_1C_2C_3)$, $K'(C_1C_2C_3)$, $e^{i\phi(C_1C_2C_3)}$, $e^{i\psi(C_1C_2C_3)}$ must be carefully chosen. We make here similar choices as in Ref. (*10*) in order to be consistent with the works on the $O(3) \supset O_h$ chain, that is,

$$\epsilon_{C_3} = \epsilon'_{C_3} = 1, \tag{16}$$

$$K(C_1C_2C_3) = (-1)^{2C_3}, \quad K'(C_1C_2C_3) = 1, \tag{17}$$

$$e^{i\phi(C_1C_2C_3)} = (-1)^{2C_1}, \tag{18}$$

$$e^{i\psi(C_1C_2C_3)} = (-1)^{2C_2}. \tag{19}$$

Then, the preceding equations [12]–[15] reduce to relations similar to those between the Clebsch–Gordan and $3C$–$C\sigma$ Wigner's symbols for $O(3) \supset O_h$. We have then

$$\begin{pmatrix} \tilde{C}\tilde{\sigma} & \tilde{C}'\tilde{\sigma}' \\ C & C \end{pmatrix} \equiv \begin{pmatrix} C \\ \tilde{C}\tilde{\sigma}\ \tilde{C}'\tilde{\sigma}' \end{pmatrix} = (-1)^{2C} \begin{pmatrix} C \\ \tilde{C}'\tilde{\sigma}'\tilde{C}\tilde{\sigma} \end{pmatrix} = [C]^{1/2} \begin{pmatrix} C & 0 & C \\ \tilde{C}\tilde{\sigma} & 0 & \tilde{C}'\tilde{\sigma}' \end{pmatrix} = \delta_{\tilde{C},\tilde{C}'}\delta_{\tilde{\sigma},\tilde{\sigma}'}, \tag{20}$$

and all the F' coefficients are real.

Within our $O(3) \supset O_h \supset C_{4v}$ chain the Wigner–Eckart theorem, for covariant quantities, can be written

$$\langle \Psi^{(C\tau)}_{\tilde{C}'\tilde{\sigma}'} | T^{(\Gamma_\mu)}_{\tilde{\Gamma}\tilde{\gamma}} | \Psi^{(C\tau)}_{\tilde{C}\tilde{\sigma}} \rangle = F' \begin{pmatrix} \Gamma_\mu & C_\tau & C'_{\tau'} \\ \tilde{\Gamma}\tilde{\gamma} & \tilde{C}\tilde{\sigma} & \tilde{C}'\tilde{\sigma}' \end{pmatrix} \langle C'_{\tau'} \| T^{(\Gamma_\mu)} \| C_\tau \rangle. \tag{21}$$

with the choice $e^{i\Phi_E} = 1$ (*10*) as in preceding works.

4. TENSORIAL ALGEBRA IN THE C_{4v} GROUP

4.1. $3\tilde{C}$–$\tilde{\sigma}$ Coefficients and the Wigner–Eckart Theorem in C_{4v}

We are now able to deduce $3\tilde{C}$–$\tilde{\sigma}$ coupling coefficients for the C_{4v} group itself. We follow a method given by Lulek in Refs. (*13, 14*) and used in (*10*). This method is based on the use of Racah's factorization lemma, which can be written here as

$$F' \begin{pmatrix} C_{1\tau} & C_{2v} & C_{3\chi} \\ \tilde{C}_1\tilde{\sigma}_1 & \tilde{C}_2\tilde{\sigma}_2 & \tilde{C}_3\tilde{\sigma}_3 \end{pmatrix} = K' \begin{pmatrix} C_{1\tau} & C_{2v} & C_{3\chi} \\ \tilde{C}_1 & \tilde{C}_2 & \tilde{C}_3 \end{pmatrix} \tilde{F} \begin{pmatrix} \tilde{C}_1 & \tilde{C}_2 & \tilde{C}_3 \\ \tilde{\sigma}_1 & \tilde{\sigma}_2 & \tilde{\sigma}_3 \end{pmatrix}, \tag{22}$$

where F' is our $O_h \supset C_{4v}$ oriented $3C$ coefficient, $\tilde{F}$ is a $3\tilde{C}$–$\tilde{\sigma}$ coefficient for C_{4v} and K' is an $O_h \supset C_{4v}$ isoscalar factor.

The $3\tilde{C}$–$\tilde{\sigma}$ matrix being unitary, we can define

$$N(C_{1\tau}\tilde{C}_1, C_{2v}\tilde{C}_2, C_{3\chi}\tilde{C}_3) = \left| K' \begin{pmatrix} C_{1\tau} & C_{2v} & C_{3\chi} \\ \tilde{C}_1 & \tilde{C}_2 & \tilde{C}_3 \end{pmatrix} \right|^2 = \sum_{\tilde{\sigma}_1,\tilde{\sigma}_2,\tilde{\sigma}_3} \left| F' \begin{pmatrix} C_{1\tau} & C_{2v} & C_{3\chi} \\ \tilde{C}_1\tilde{\sigma}_1 & \tilde{C}_2\tilde{\sigma}_2 & \tilde{C}_3\tilde{\sigma}_3 \end{pmatrix} \right|^2. \tag{23}$$

The solution of the system of Eq. [22] with the preceding condition on N, leads to the desired $3\tilde{C}$–$\tilde{\sigma}$ coefficients

$$\tilde{F} \begin{pmatrix} \tilde{C}_1 & \tilde{C}_2 & \tilde{C}_3 \\ \tilde{\sigma}_1 & \tilde{\sigma}_2 & \tilde{\sigma}_3 \end{pmatrix} = \epsilon_{\tilde{C}_1\tilde{C}_2\tilde{C}_3} \frac{1}{\sqrt{N(C_{1\tau}\tilde{C}_1, C_{2v}\tilde{C}_2, C_{3\chi}\tilde{C}_3)}} \times F' \begin{pmatrix} C_{1\tau} & C_{2v} & C_{3\chi} \\ \tilde{C}_1\tilde{\sigma}_1 & \tilde{C}_2\tilde{\sigma}_2 & \tilde{C}_3\tilde{\sigma}_3 \end{pmatrix}, \tag{24}$$

where $\epsilon_{C_1C_2C_3}$ is a phase factor that has been fixed to 1 in reference to what has been chosen in O_h or T_d.

We impose that our $3\tilde{C}$–$\tilde{\sigma}$ coefficients are left unchanged by any even permutation of their columns and that for an odd permutation they are multiplied by the factor

$$(-1)^{\tilde{C}_1+\tilde{C}_2+\tilde{C}_3}. \tag{25}$$

We note here that this is an equivalent rule to the one used in $O(3)$ or O_h or T_d (*8, 10*). This also implies that the K' coefficients are left unchanged by any even permutation of their columns and that for an odd permutation they are multiplied by the factor

$$(-1)^{C_1+C_2+C_3+\tilde{C}_1+\tilde{C}_2+\tilde{C}_3}. \tag{26}$$

The $(-1)^{\tilde{C}}$ phases are obtained in multiplying each C_{4v} representation by itself. In the result, the symmetric part is associated to $(-1)^{\tilde{C}} = 1$ and the antisymmetric one to $(-1)^{\tilde{C}} = -1$, so that we obtain

$$(-1)^{a_1} = (-1)^{b_1} = (-1)^{b_2} = (-1)^{e} = 1, \tag{27}$$

$$(-1)^{a_2} = -1 \tag{28}$$

(since $(-1)^e$ is undetermined we chose to set it equal to 1).

For completeness we must now also define a metric tensor; in the same way as in Eq. [10] we have for C_{4v}

$$T^{(\tilde{C})}_{\tilde{\sigma}} = \epsilon_{\tilde{C}} \begin{pmatrix} \tilde{C} \\ \tilde{\sigma}\tilde{\sigma}' \end{pmatrix} T^{\tilde{\sigma}'}_{(\tilde{C})}, \tag{29}$$

$$T^{\tilde{\sigma}}_{(\tilde{C})} = \epsilon'_{\tilde{C}} \begin{pmatrix} \tilde{\sigma}'\tilde{\sigma} \\ \tilde{C} \end{pmatrix} T^{(\tilde{C})}_{\tilde{\sigma}'}. \tag{30}$$

Likewise, the Clebsch–Gordan coefficients can be determined through relations similar to Eqs. [12]–[15] and with the same phase factors choice as in the preceding section:

$$\tilde{F}\begin{matrix}\tilde{\sigma}_1 & \tilde{\sigma}_2 & (\tilde{C}_3)\\ (\tilde{C}_1 & \tilde{C}_2) & \tilde{\sigma}_3\end{matrix} = \tilde{F}\begin{matrix}(\tilde{C}_1 & \tilde{C}_2) & \tilde{\sigma}_3\\ \tilde{\sigma}_1 & \tilde{\sigma}_2 & (\tilde{C}_3)\end{matrix}, \quad [31]$$

$$\tilde{F}\begin{matrix}\tilde{\sigma}_1 & \tilde{\sigma}_2 & \tilde{\sigma}_3\\ (\tilde{C}_1 & \tilde{C}_2 & \tilde{C}_3)\end{matrix} = \tilde{F}\begin{matrix}(\tilde{C}_1 & \tilde{C}_2 & \tilde{C}_3)\\ \tilde{\sigma}_1 & \tilde{\sigma}_2 & \tilde{\sigma}_3\end{matrix}, \quad [32]$$

$$\tilde{F}\begin{matrix}(\tilde{C}_1 & \tilde{C}_2) & \tilde{\sigma}_3\\ \tilde{\sigma}_1 & \tilde{\sigma}_2 & (\tilde{C}_3)\end{matrix} = \sqrt{[\tilde{C}_3]}\,\tilde{F}\begin{matrix}(\tilde{C}_1 & \tilde{C}_2 & \tilde{C}_3)\\ \tilde{\sigma}_1 & \tilde{\sigma}_2 & \tilde{\sigma}_3\end{matrix}, \quad [33]$$

$$\tilde{F}\begin{matrix}\tilde{\sigma}_1 & \tilde{\sigma}_2 & (\tilde{C}_3)\\ (\tilde{C}_1 & \tilde{C}_2) & \tilde{\sigma}_3\end{matrix} = \sqrt{[\tilde{C}_3]}\,\tilde{F}\begin{matrix}\tilde{\sigma}_1 & \tilde{\sigma}_2 & \tilde{\sigma}_3\\ (\tilde{C}_1 & \tilde{C}_2 & \tilde{C}_3)\end{matrix}. \quad [34]$$

Equations [33] and [34] lead to

$$\begin{pmatrix}\tilde{C}\\ \tilde{\sigma}\tilde{\sigma}'\end{pmatrix} = \delta_{\sigma,\sigma'}, \quad [35]$$

and the $\tilde{F}$ coefficients are real. The values of our $3\tilde{C}$–$\tilde{\sigma}$ symbols are given in Appendix B.

We can also introduce the two orthogonality relations which will be useful for the calculations of the $6\tilde{C}$ factors (see next paragraph)

$$\sum_{\tilde{C}_1,\tilde{\sigma}_1,\tilde{C}_2,\tilde{\sigma}_2} F'\begin{matrix}(C_1 & C_2 & C_3)\\ \tilde{C}_1\tilde{\sigma}_1 & \tilde{C}_2\tilde{\sigma}_2 & \tilde{C}_3\tilde{\sigma}_3\end{matrix} F'\begin{matrix}\tilde{C}_1\tilde{\sigma}_1 & \tilde{C}_2\tilde{\sigma}_2 & \tilde{C}'_3\tilde{\sigma}'_3\\ (C_1 & C_2 & C'_3)\end{matrix} = \frac{1}{[C_3]}\,\delta_{C_3,C_3}\delta_{\tilde{C}_3\tilde{\sigma}_3,\tilde{C}_3\tilde{\sigma}_3}, \quad [36]$$

$$\sum_{\tilde{C}_1,\tilde{\sigma}_1,\tilde{C}_2,\tilde{\sigma}_2} [C_3]\,F'\begin{matrix}(C_1 & C_2 & C_3)\\ \tilde{C}_1\tilde{\sigma}_1 & \tilde{C}_2\tilde{\sigma}_2 & \tilde{C}_3\tilde{\sigma}_3\end{matrix} \times F'\begin{matrix}\tilde{C}'_1\tilde{\sigma}'_1 & \tilde{C}'_2\tilde{\sigma}'_2 & \tilde{C}_3\tilde{\sigma}_3\\ (C_1 & C_2 & C_3)\end{matrix} = \delta_{\tilde{C}'_1\tilde{\sigma}'_1,\tilde{C}_1\tilde{\sigma}_1}\delta_{\tilde{C}'_2\tilde{\sigma}'_2,\tilde{C}_2\tilde{\sigma}_2}. \quad [37]$$

The Wigner–Eckart theorem in C_{4v} can be expressed (for covariants sets) by

$$\langle \Psi^{(\tilde{C}')}_{\tilde{\sigma}'} | T^{(\tilde{C}_0)}_{\tilde{\sigma}_0} | \Psi^{(\tilde{C})}_{\tilde{\sigma}} \rangle = \tilde{F}\begin{matrix}(\tilde{C}_0 & \tilde{C} & \tilde{C}')\\ \tilde{\sigma}_0 & \tilde{\sigma} & \tilde{\sigma}'\end{matrix} \langle \tilde{C}' \| T^{(\tilde{C}_0)} \| \tilde{C} \rangle, \quad [38]$$

again with $e^{i\Phi_E} = 1$ (*10*).

We can also note a useful formula which relates the reduced matrix elements in C_{4v} of a symmetry adapted tensor to those in O_h

$$\langle C'\tilde{C}' \| T^{(C_0,\tilde{C}_0)} \| C\tilde{C} \rangle = K'\begin{pmatrix}C_0 & C & C'\\ \tilde{C}_0 & \tilde{C} & \tilde{C}'\end{pmatrix} \langle C' \| T^{(C_0)} \| C \rangle, \quad [39]$$

as well as the formula relating reduced matrix elements in $O(3)$ or C_{4v} for an $O(3) \supset O_h \supset C_{4v}$ oriented tensor:

$$\langle j'n'C'\tilde{C}' \| T^{(j_0,n_0C_0,\tilde{C}_0)} \| jnC\tilde{C} \rangle = (-1)^{j'} K'\begin{pmatrix}j_0 & j & j'\\ n_0C_0 & nC & n'C'\end{pmatrix} \times K'\begin{pmatrix}C_0 & C & C'\\ \tilde{C}_0 & \tilde{C} & \tilde{C}'\end{pmatrix} \langle j' \| T^{(j_0)} \| j \rangle. \quad [40]$$

4.2. *Recoupling Coefficients for C_{4v}*

We will now consider briefly the recoupling coefficients for C_{4v}. By analogy with what has been done by Fano and Racah (*15*) for $O(3)$ and in Refs. (*8, 10*) for $O(3) \supset O_h$, we can define $6\tilde{C}$ coefficients from the recoupling matrix for three irreducible representations by the relation:

$$\begin{aligned}&|||\tilde{C}_1\rangle \times |\tilde{C}_2\rangle;\ \tilde{C}_{12}\rangle \times |\tilde{C}_3\rangle;\ \tilde{C},\ \tilde{\sigma}\rangle\\ &\quad = [\tilde{C}_{12}]^{1/2} \times \sum_{\tilde{C}_{23}} [\tilde{C}_{23}]^{1/2} \begin{Bmatrix}\tilde{C}_1 & \tilde{C}_2 & \tilde{C}_{12}\\ \tilde{C}_3 & \tilde{C} & \tilde{C}_{23}\end{Bmatrix}\\ &\qquad \times \|\tilde{C}_1\rangle \times \|\tilde{C}_2\rangle \times |\tilde{C}_3\rangle;\ \tilde{C}_{23}\rangle;\ \tilde{C},\ \tilde{\sigma}\rangle.\end{aligned} \quad [41]$$

Expanding the two members of expression [41] and taking our conventions as well as [36] and [37] into account, we obtain

$$\begin{Bmatrix}\tilde{C}_1 & \tilde{C}_2 & \tilde{C}_{12}\\ \tilde{C}_3 & \tilde{C} & \tilde{C}_{23}\end{Bmatrix} = \frac{(-1)^{\tilde{C}_1+\tilde{C}_2+\tilde{C}-\tilde{C}_3}}{\tilde{F}\begin{matrix}(\tilde{C}_1 & \tilde{C}_2 & \tilde{C}_{12})\\ \tilde{\sigma}_1 & \tilde{\sigma}_2 & \tilde{\sigma}_{12}\end{matrix}} \times \sum_{\tilde{\sigma}_3\tilde{\sigma}\tilde{\sigma}_{23}} \tilde{F}\begin{matrix}(\tilde{C}_1 & \tilde{C}_{23} & \tilde{C})\\ \tilde{\sigma}_1 & \tilde{\sigma}_{23} & \tilde{\sigma}\end{matrix} \tilde{F}\begin{matrix}(\tilde{C}_2 & \tilde{C}_3 & \tilde{C}_{23})\\ \tilde{\sigma}_2 & \tilde{\sigma}_3 & \tilde{\sigma}_{23}\end{matrix} \times \tilde{F}\begin{matrix}(\tilde{C}_{12} & \tilde{C}_3 & \tilde{C})\\ \tilde{\sigma}_{12} & \tilde{\sigma}_3 & \tilde{\sigma}\end{matrix}. \quad [42]$$

The nonvanishing of a $6\tilde{C}$ implies four triangular conditions:

$$\tilde{C}_1 \otimes \tilde{C}_{23} \supset \tilde{C}, \quad [43]$$

$$\tilde{C}_2 \otimes \tilde{C}_3 \supset \tilde{C}_{23}, \quad [44]$$

$$\tilde{C}_{12} \otimes \tilde{C}_3 \supset \tilde{C}, \quad [45]$$

$$\tilde{C}_1 \otimes \tilde{C}_2 \supset \tilde{C}_{12}. \quad [46]$$

The $6\tilde{C}$ are unchanged by any even permutation of their columns but must be multiplied by

$$(-1)^{\tilde{C}_1+\tilde{C}_2+\tilde{C}_{12}+\tilde{C}_3+\tilde{C}+\tilde{C}_{23}}$$

for any odd permutation.

Let us finally note the three following symmetries:

$$\begin{Bmatrix} \tilde{C}_1 & \tilde{\Gamma}_2 & \tilde{\Gamma}_3 \\ \tilde{\Gamma}_1 & \tilde{C}_2 & \tilde{C}_3 \end{Bmatrix} = \begin{Bmatrix} \tilde{C}_1 & \tilde{C}_2 & \tilde{C}_3 \\ \tilde{\Gamma}_1 & \tilde{\Gamma}_2 & \tilde{\Gamma}_3 \end{Bmatrix}, \quad [47]$$

$$\begin{Bmatrix} \tilde{\Gamma}_1 & \tilde{\Gamma}_2 & \tilde{C}_3 \\ \tilde{C}_1 & \tilde{C}_2 & \tilde{\Gamma}_3 \end{Bmatrix} = \begin{Bmatrix} \tilde{C}_1 & \tilde{C}_2 & \tilde{C}_3 \\ \tilde{\Gamma}_1 & \tilde{\Gamma}_2 & \tilde{\Gamma}_3 \end{Bmatrix}, \quad [48]$$

$$\begin{Bmatrix} \tilde{\Gamma}_1 & \tilde{C}_2 & \tilde{\Gamma}_3 \\ \tilde{C}_1 & \tilde{\Gamma}_2 & \tilde{C}_3 \end{Bmatrix} = \begin{Bmatrix} \tilde{C}_1 & \tilde{C}_2 & \tilde{C}_3 \\ \tilde{\Gamma}_1 & \tilde{\Gamma}_2 & \tilde{\Gamma}_3 \end{Bmatrix}. \quad [49]$$

It is then possible to show the following very useful formula, which gives the reduced matrix elements of two coupled tensor operators of C_{4v} acting on the same space:

$$\begin{aligned} \langle \tilde{C}' \| [T^{(\tilde{C}_1)} \times T^{(\tilde{C}_2)}]^{(\tilde{C}_0)} \| \tilde{C} \rangle &= (-1)^{\tilde{C}_1+\tilde{C}_2+\tilde{C}+\tilde{C}'} \sum_{\tilde{C}''} [\tilde{C}_0]^{1/2} \begin{Bmatrix} \tilde{C}_1 & \tilde{C}_2 & \tilde{C}_0 \\ \tilde{C} & \tilde{C}' & \tilde{C}'' \end{Bmatrix} \\ &\times \langle \tilde{C}' \| T^{(\tilde{C}_1)} \| \tilde{C}'' \rangle \langle \tilde{C}'' \| T^{(\tilde{C}_2)} \| \tilde{C} \rangle. \end{aligned} \quad [50]$$

In the same way, we can define the $9\tilde{C}$ symbols by

$$\begin{aligned} &\langle\langle\langle \tilde{C}_1 \rangle \times |\tilde{C}_2\rangle; \tilde{C}_{12}\rangle \times \|\tilde{C}_3\rangle \times |\tilde{C}_4\rangle; \tilde{C}_{34}\rangle; \tilde{C}, \tilde{\sigma}\rangle \\ &= ([\tilde{C}_{12}][\tilde{C}_{34}][\tilde{C}_{13}][\tilde{C}_{24}])^{1/2} \begin{Bmatrix} \tilde{C}_1 & \tilde{C}_2 & \tilde{C}_{12} \\ \tilde{C}_3 & \tilde{C}_4 & \tilde{C}_{34} \\ \tilde{C}_{13} & \tilde{C}_{24} & \tilde{C} \end{Bmatrix} \\ &\times \langle\langle\langle \tilde{C}_1 \rangle \times |\tilde{C}_3\rangle; \tilde{C}_{13}\rangle \times \|\tilde{C}_2\rangle \times |\tilde{C}_4\rangle; \tilde{C}_{24}\rangle; \tilde{C}, \tilde{\sigma}\rangle. \end{aligned} \quad [51]$$

We merely say that these $9\tilde{C}$ symbols can be calculated from the $6\tilde{C}$ symbols through the relation

$$\begin{aligned} \begin{Bmatrix} \tilde{C}_1 & \tilde{C}_2 & \tilde{C}_{12} \\ \tilde{C}_3 & \tilde{C}_4 & \tilde{C}_{34} \\ \tilde{C}_{13} & \tilde{C}_{24} & \tilde{C} \end{Bmatrix} &= \sum_{\tilde{C}''} [\tilde{C}''] \begin{Bmatrix} \tilde{C}_1 & \tilde{C}_3 & \tilde{C}_{13} \\ \tilde{C}_{24} & \tilde{C} & \tilde{C}'' \end{Bmatrix} \\ &\times \begin{Bmatrix} \tilde{C}_2 & \tilde{C}_4 & \tilde{C}_{24} \\ \tilde{C}_3 & \tilde{C}'' & \tilde{C}_{34} \end{Bmatrix} \begin{Bmatrix} \tilde{C}_{12} & \tilde{C}_{34} & \tilde{C} \\ \tilde{C}'' & \tilde{C}_1 & \tilde{C}_2 \end{Bmatrix}, \end{aligned} \quad [52]$$

and that the nonvanishing of a $9\tilde{C}$ symbol implies the six following triangular conditions:

$$\tilde{C}_1 \otimes \tilde{C}_2 \supset \tilde{C}_{12}, \quad [53]$$

$$\tilde{C}_3 \otimes \tilde{C}_4 \supset \tilde{C}_{34}, \quad [54]$$

$$\tilde{C}_{13} \otimes \tilde{C}_4 \supset \tilde{C}, \quad [55]$$

$$\tilde{C}_1 \otimes \tilde{C}_3 \supset \tilde{C}_{13}, \quad [56]$$

$$\tilde{C}_2 \otimes \tilde{C}_4 \supset \tilde{C}_{24}, \quad [57]$$

$$\tilde{C}_{12} \otimes \tilde{C}_{34} \supset \tilde{C}. \quad [58]$$

This enables us to express the reduced matrix elements of two coupled tensor operators acting on two different spaces:

$$\begin{aligned} &\langle \tilde{C}'_1 \tilde{C}'_2, \tilde{C}' \| [T^{(\tilde{\Gamma}_1)} \times U^{(\tilde{\Gamma}_2)}]^{(\tilde{\Gamma}_0)} \| \tilde{C}_1 \tilde{C}_2, \tilde{C} \rangle \\ &= ([\tilde{C}][\tilde{C}'][\tilde{\Gamma}_0])^{1/2} \begin{Bmatrix} \tilde{\Gamma}_1 & \tilde{C}_1 & \tilde{C}'_1 \\ \tilde{\Gamma}_2 & \tilde{C}_2 & \tilde{C}'_2 \\ \tilde{\Gamma}_0 & \tilde{C} & \tilde{C}' \end{Bmatrix} \\ &\times \langle \tilde{C}'_1 \| T^{(\tilde{\Gamma}_1)} \| \tilde{C}_1 \rangle \langle \tilde{C}'_2 \| U^{(\tilde{\Gamma}_2)} \| \tilde{C}_2 \rangle. \end{aligned} \quad [59]$$

We can also introduce the $12\tilde{C}$ coefficients given in terms of $9\tilde{C}$ and $6\tilde{C}$ symbols (*16*):

$$\begin{aligned} &\begin{Bmatrix} \tilde{C}_1 & \tilde{C}_2 & \tilde{C}_3 & \tilde{C}_4 \\ \tilde{C}_5 & \tilde{C}_6 & \tilde{C}_7 & \tilde{C}_8 \\ \tilde{C}_9 & \tilde{C}_{10} & \tilde{C}_{11} & \tilde{C}_{12} \end{Bmatrix} \\ &= (-1)^{\tilde{C}_3+\tilde{C}_7+\tilde{C}_9+\tilde{C}_{10}} \sum_{\tilde{x}} [\tilde{x}] \begin{Bmatrix} \tilde{C}_1 & \tilde{C}_2 & \tilde{C}_3 \\ \tilde{C}_5 & \tilde{C}_6 & \tilde{C}_7 \\ \tilde{C}_9 & \tilde{C}_{10} & \tilde{x} \end{Bmatrix} \\ &\times \begin{Bmatrix} \tilde{C}_{11} & \tilde{C}_3 & \tilde{C}_4 \\ \tilde{C}_7 & \tilde{C}_{12} & \tilde{x} \end{Bmatrix} \begin{Bmatrix} \tilde{C}_{11} & \tilde{C}_9 & \tilde{C}_8 \\ \tilde{C}_{10} & \tilde{C}_{12} & \tilde{x} \end{Bmatrix}. \end{aligned} \quad [60]$$

5. CONCLUSION

To study C_{4v} XY_5Z molecules, we have developed a tensorial formalism adapted to the chain $O(3) \supset O_h \supset C_{4v}$ as an extension of what has already been done in Dijon in the case of $O(3) \supset O_h$. We have determined coupling and recoupling coefficients in this chain but also in the C_{4v} group itself. The Wigner–Eckart theorem with useful formulas for the computation of reduced matrix elements of tensor operators have been given. Special attention has been given to the various phase choices. We intend to apply this formalism to the spectroscopy

of monoisotopic $^{32}SF_5$ ^{35}Cl in a preliminary step, but, first, we will give in a subsequent paper some expressions for calculating the matrix elements of different operators such as the Hamiltonian and the transition moment operators (dipole moment and polarizability).

APPENDIX A

Numeric Values of All the G′ Coefficients

We give in the following table numeric values of G'-matrix elements calculated as indicated in Section 3. Finally, we should mention that the programs for the computation of numerical values of G' coefficients, $3\tilde{C}$–$\tilde{\sigma}$, $6\tilde{C}$, $9\tilde{C}$, and $12\tilde{C}$ symbols and K' isoscalar factors are available upon request.

TABLE A1
Numeric Values of all the G' Coefficients

C_τ	σ	$\tilde{C}$	$\tilde{\sigma}$	G'
A_{1g}	1	a_1	1	1
A_{2g}	1	b_1	1	1
A_{1u}	1	a_2	1	1
A_{2u}	1	b_2	1	1
E_g	1	a_1	1	1
E_u	1	a_2	1	1
E_g	2	b_1	1	1
E_u	2	b_2	1	1
F_{1g}	z	a_2	1	1
F_{1u}	z	a_1	1	1
F_{1g}	y	e_1	1	-1
F_{1g}	x	e_2	1	1
F_{1u}	x	e_1	1	1
F_{1u}	y	e_2	1	1
F_{2g}	z	b_2	1	1
F_{2g}	y	e_1	1	1
F_{2g}	x	e_2	1	1
F_{2u}	z	b_1	1	1
F_{2u}	x	e_1	1	1
F_{2u}	y	e_2	1	-1

APPENDIX B

Numeric Values of the 3C̃–σ̃ (F̃) Coefficients

We also give here numeric values for the $3\tilde{C}$–$\tilde{\sigma}$ coefficients.

TABLE B2
Numeric Values of the $3\tilde{C}$–$\tilde{\sigma}$ ($\tilde{F}$) Coefficients

$\tilde{C}_1$	$\tilde{\sigma}_1$	$\tilde{C}_2$	$\tilde{\sigma}_2$	$\tilde{C}_3$	$\tilde{\sigma}_3$	$3\tilde{C}$–$\tilde{\sigma}$
a_1	1	a_1	1	a_1	1	1.0
a_1	1	a_2	1	a_2	1	1.0
a_1	1	b_1	1	b_1	1	1.0
a_1	1	b_1	1	b_2	1	1.0
a_1	1	e	1	e	1	$1/\sqrt{2}$
a_1	1	e	2	e	2	$1/\sqrt{2}$
a_2	1	a_1	1	a_2	1	1.0
a_2	1	a_2	1	a_1	1	1.0
a_2	1	b_1	1	b_1	1	1.0
a_2	1	b_1	1	b_1	1	-1.0
a_2	1	e	1	e	2	$-1/\sqrt{2}$
a_2	1	e	2	e	1	$1/\sqrt{2}$
b_1	1	a_1	1	b_1	1	1.0
b_1	1	a_2	1	b_2	1	-1.0
b_1	1	b_1	1	a_1	1	1.0
b_1	1	b_2	1	a_2	1	1.0
b_1	1	e	1	e	1	$-1/\sqrt{2}$
b_1	1	e	2	e	2	$1/\sqrt{2}$
b_2	1	a_1	1	b_2	1	1.0
b_2	1	a_2	1	b_1	1	1.0
b_2	1	b_1	1	a_2	1	-1.0
b_2	1	b_2	1	a_1	1	1.0
b_2	1	e	1	e	2	$1/\sqrt{2}$
b_2	1	e	2	e	1	$1/\sqrt{2}$
e	1	a_1	1	e	1	$1/\sqrt{2}$
e	2	a_1	1	e	2	$1/\sqrt{2}$
e	1	a_2	1	e	2	$1/\sqrt{2}$
e	2	a_2	1	e	1	$-1/\sqrt{2}$
e	1	b_1	1	e	1	$-1/\sqrt{2}$
e	2	b_1	1	e	2	$1/\sqrt{2}$
e	1	b_2	1	e	2	$1/\sqrt{2}$
e	2	b_2	1	e	1	$1/\sqrt{2}$
e	1	e	1	a_1	1	$1/\sqrt{2}$
e	2	e	2	a_1	1	$1/\sqrt{2}$
e	1	e	2	a_2	1	$-1/\sqrt{2}$
e	2	e	1	a_2	1	$1/\sqrt{2}$
e	1	e	1	b_1	1	$-1/\sqrt{2}$
e	2	e	2	b_1	1	$1/\sqrt{2}$
e	1	e	2	b_2	1	$1/\sqrt{2}$
e	2	e	1	b_2	1	$1/\sqrt{2}$

ACKNOWLEDGMENTS

Support from the Région Bourgogne for the computer equipment of the Laboratoire de Physique de l'Université de Bourgogne is gratefully acknowledged.

REFERENCES

1. J. E. Griffiths, *Spectrochim. Acta, Part A* **23,** 2145–2157 (1967).
2. J. Bellet, R. Jurek, and J. Chanussot, *J. Mol. Spectrosc.* **78,** 16–30 (1979).
3. M. Quack, *Infrared Phys. Technol.* **36,** 365–380 (1995).
4. Y. He, J. Pochert, M. Quack, R. Ranz, and G. Seyfang, *Faraday Discuss.* **102** (1995).
5. J.-P. Champion, M. Loëte, and G. Pierre, *in* "Spectroscopy of the Earth's Atmosphere and Interstellar Medium" (K. N. Rao and A. Weber, Eds.), pp. 339–422, Academic Press, San Diego, 1992.
6. N. Cheblal, M. Loëte, and V. Boudon, *J. Mol. Spectrosc.,* in press.
7. R. Jurek, A. Poinsot, and P. Goulet, *J. Phys.* **47,** 645–648 (1986).
8. J. P. Champion, G. Pierre, F. Michelot, and J. Moret-Bailly, *Can. J. Phys.* **55**(6), 512–520 (1977).
9. B. I. Zhilinskii, V. L. Perevalov, and Vl. G. Tyuterev, "Méthode des opérateurs tensoriels irréductibles et théorie des spectres des molécules," 1986. [translated from Russian]
10. V. Boudon and F. Michelot, *J. Mol. Spectrosc.* **165,** 554–579 (1994).
11. F. Michelot, Thèse d'état, Dijon, 1980.
12. F. Michelot, B. Bobin, and J. Moret-Bailly, *J. Mol. Spectrosc.* **76,** 374–411 (1979).
13. B. Lulek, T. Lulek, and B. Szczepaniak, *Acta Phys. Pol. A* **54**(5), 545–559 (1978).
14. B. Lulek and T. Lulek, *Acta Phys. Pol., A* **54**(5), 561–572 (1978).
15. U. Fano and G. Racah, "Irreducible Tensorial Sets," Academic Press, New York, 1959.
16. M. Rotenberg, N. Metropolis, R. Bivins, and J. K. Wooten, Jr., "The 3-*j* and 6-*j* Symbols," The Technology Press, Cambridge, MA, 1959.

Journal of Molecular Spectroscopy **200,** 131–137 (2000)
doi:10.1006/jmsp.1999.8035, available online at http://www.idealibrary.com on IDEAL®

Spectroscopy of XY_5Z (C_{4v}) Molecules: Development of the Hamiltonian and the Transition Moment Operators Using a Tensorial Formalism

M. Rotger, V. Boudon, and M. Loëte

Laboratoire de Physique de l'Université de Bourgogne, UMR CNRS 5027, 9 Avenue Alain Savary, B.P. 47 870, F-21078 Dijon Cedex, France

E-mail: rotger@jupiter.u-bourgogne.fr

Received September 28, 1999; in revised form November 11, 1999

We present a development of the Hamiltonian, dipole moment, and polarizability operators of XY_5Z (C_{4v}) molecules using a tensorial formalism derived from the one developed previously in Dijon for XY_6 molecules. These operators are involved in the calculation of the energies and intensities of rovibrational transitions and are essential for spectrum simulations. Expressions for the matrix elements are derived for all these operators. © 2000 Academic Press

Key Words: tensorial formalism; XY_5Z symmetric tops; Hamiltonian; dipole moment; polarizability.

1. INTRODUCTION

The theory of the Hamiltonian and transition moments operators (dipole moment and polarizability) is essential for the calculation and prediction of rovibrational spectra in polyatomic molecules. The tensorial formalism developed in Dijon for the expansion of the Hamiltonian operator of spherical top molecules has also been applied to the transition moments operators, as explained in a review paper (*1*). These works deal with the case of tetrahedral molecules (T_d point group) but also more recently with the case of octahedral molecules (O_h point group). As it has also been detailed in Ref. (*2*), octahedral molecules form an important family of spherical top species and XY_5Z (C_{4v}) molecules can be derived from these spherical tops by the substitution of one ligand. Their rovibrational spectroscopy is quite unknown, since one only finds microwave data or low-resolution vibrational studies in the literature (*3, 4*). There are almost no data concerning their transition moments. However, high-resolution spectra could be quite easily recorded for molecules such as SF_5Cl, SF_5Br, SeF_5Cl, SeF_5Br, WF_5Cl, IOF_5, ... Thus, a theoretical model for the interpretation of frequencies and intensities will be necessary. This does not concern only fundamental bands but also combination, harmonic, and hot bands. The experimental study of harmonic bands on these molecules is important because they are good candidates for photodissociation and more generally laser chemistry processes similar to those studied by Quack *et al.* on CF_3I or C_6F_5I (*5*).

Here, we work in the $O(3) \supset O_h \supset C_{4v}$ group chain, for which a tensorial formalism has been developed as detailed in a preceding paper (*6*), hereafter referred to as I. Therefore, we use here the same notations, that is, all tilded symbols ($\tilde{C}$, $\tilde{F}$, ...) represent C_{4v} symbols (irreducible representations, coupling coefficients, ...) and primed symbols (F', K', ...) represent oriented coupling coefficients in $O_h \supset C_{4v}$. We also denote the C_{4v} irreps by lowercase letters (a_1, a_2, ...) to avoid any confusion with O_h irreducible representations (irreps).

The aim of this paper is to provide a tensorial development of the Hamiltonian and transition moments operators (dipole moment and polarizability). The latter enable us to determine the matrix elements which appear in intensity calculations for rovibrational electric dipole and Raman transitions. As we make extensive use of tensorial formalism, the nonexpert reader should refer to Refs. (*1, 2*) and to I, where these notions are explained in detail. Section 2 recalls the basic theory of transformed operators and Section 3 deals more specifically with the case of XY_5Z (C_{4v}) symmetric molecules.

2. BASIC PRINCIPLES

In this section, we recall briefly the basic principles of the expansion of the Hamiltonian and transition moment operators. This is valuable for any polyatomic molecule and can be found in detail, for example, in Ref. (*7*).

2.1. *Transformed Operators*

Successive Van Vleck contact transformations are generally applied to the Hamiltonian and transition moment operators. The aim of these contact transformations is to introduce appropriate basis functions in which the transformed Hamiltonian $\tilde{H}$ has a completely diagonal or block diagonal form with respect to some vibrational subspace. These subspaces of close vibrational levels correspond to the so-called polyads.

0022-2852/00 $35.00

If A represents either H (Hamiltonian), μ (dipole moment), or α (polarizability), the transformed operator $\tilde{A}$ is given by

$$\tilde{A} = TAT^{-1} = A + i[S, A] + \tfrac{1}{2}[S, [S, A]] + \ldots, \quad [1]$$

with $T = e^{iS}$. S is a Hermitian operator and is called the generator of the contact transformation. It has been shown that S is always a sum of rovibrational operators (*1*).

2.2. Dipole Moment

The dipole moment components in the laboratory-fixed frame (LFF) μ_Θ with $\Theta = X$, Y, or Z can be related to the components μ_θ with $\theta = x$, y, or z in the molecule-fixed frame (MFF) by

$$\mu_\Theta = \sum_\theta \lambda_{\Theta,\theta}\mu_\theta, \quad [2]$$

where $\lambda_{\Theta,\theta}$ are the direction cosines.

In the small amplitude motion approximation one can expand each component μ_θ as a power series in the dimensionless normal coordinates $q_{s,\sigma}$ (where s is the oscillator index and the σ's are its components)

$$\mu_\theta = \mu_\theta^e + \sum_{s,\sigma}\left(\frac{\partial\mu_\theta}{\partial q_{s,\sigma}}\right)_e q_{s,\sigma} + \frac{1}{2}\sum_{s,\sigma,s',\sigma'}\left(\frac{\partial^2\mu_\theta}{\partial q_{s,\sigma}\partial q_{s',\sigma'}}\right) q_{s,\sigma}q_{s',\sigma'}, \quad [3]$$

where μ_θ^e is the permanent dipole moment of the molecule if it exists. The other terms are induced by molecular vibrations.

One can show that the LFF components of the transformed dipole moment can be written in the symmetrized form (*1*) as follows:

$$\tilde{\mu}_\Theta = \frac{1}{2}\sum_\theta (\lambda_{\Theta,\theta}\tilde{\mu}_\theta + \tilde{\mu}_\theta\lambda_{\Theta,\theta}). \quad [4]$$

Like the contact transformation generator S, $\tilde{\mu}_\theta$, $\tilde{\mu}_\Theta$ are also sums of rovibrational operators, as implied by Eq. [1].

To establish the expressions of $\tilde{\mu}_\theta$ and $\tilde{\mu}_\Theta$, it is necessary to introduce in a first step the spherical components of the dipole moment operator. The LFF spherical components, denoted $\mu_m^{(1)}$, are related to the MFF ones $\mu_k^{(1)}$ through (*1*),

$$\mu_m^{(1)} = \sum_k \mathcal{D}_{km}^{(1)}\mu_k^{(1)}, \quad [5]$$

where the $\mathcal{D}_{km}^{(1)}$ are Wigner's harmonic functions (*8*) (k, m = -1, 0, or 1). The Cartesian and spherical components in both frames are linked through the relations

$$\mu_\Theta = \sum_m \langle 1; m|\Theta\rangle\mu_m^{(1)}, \quad [6]$$

$$\mu_\theta = \sum_k \langle 1; k|\theta\rangle\mu_k^{(1)}, \quad [7]$$

where the $\langle 1; m|\Theta\rangle$ and $\langle 1; k|\theta\rangle$ are called Stone coefficients (*9*).

2.3. Polarizability

The application of an electric field E to the molecules induces a dipole moment, defined as

$$\mu_{\Theta_1} = \sum_{\Theta_2} \alpha_{\Theta_1\Theta_2}E_{\Theta_2}, \quad [8]$$

where $\alpha_{\Theta_1\Theta_2}$ is a LFF component of the polarizability tensor.

We can relate them to the MFF components $\alpha_{\theta_1\theta_2}$ through

$$\alpha_{\Theta_1\Theta_2} = \sum_{\theta_1,\theta_2} \lambda_{\Theta_1,\theta_1}\lambda_{\Theta_2,\theta_2}\alpha_{\theta_1\theta_2}, \quad [9]$$

where $\lambda_{\Theta_1,\theta_1}$ and $\lambda_{\Theta_2,\theta_2}$ are the direction cosines.

As for the dipole moment, we can develop the $\alpha_{\theta_1\theta_2}$ as a series of dimensionless normal coordinates like

$$\alpha_{\theta_1\theta_2} = \alpha_{\theta_1\theta_2}^e + \sum_{s,\sigma}\left(\frac{\partial\alpha_{\theta_1\theta_2}}{\partial q_{s,\sigma}}\right)_e q_{s,\sigma} + \frac{1}{2}\sum_{s,\sigma,s',\sigma'}\left(\frac{\partial^2\alpha_{\theta_1\theta_2}}{\partial q_{s,\sigma}\partial q_{s',\sigma'}}\right)_e q_{s,\sigma}q_{s',\sigma'} + \ldots, \quad [10]$$

where $\alpha_{\theta_1\theta_2}^e$ is the permanent polarizability, if it exists. The other terms are induced by molecular vibrations.

Just as for the dipole moment, one has to consider the transformed polarizability and in the LFF we have

$$\tilde{\alpha}_{\Theta_1\Theta_2} = \tfrac{1}{2}\sum_\theta (\lambda_{\Theta_1,\theta_1}\lambda_{\Theta_2,\theta_2}\tilde{\alpha}_{\theta_1\theta_2} + \tilde{\alpha}_{\theta_1\theta_2}\lambda_{\Theta_1,\theta_1}\lambda_{\Theta_2,\theta_2}). \quad [11]$$

The spherical components in the LFF ($\alpha_m^{(L)}$) and in the MFF ($\alpha_k^{(L)}$) are linked through

$$\alpha_m^{(L)} = \sum_k \mathcal{D}_{km}^{(L)}\alpha_k^{(L)}, \quad [12]$$

where L takes only the values 0 and 2. For the $\mathcal{D}_{km}^{(L)}$ Wigner's harmonics (*8*) $L = 0$ implies m, $k = 0$ and $L = 2$ implies m, $k = 0, \pm1, \pm2$.

TABLE 1

Symmetry of the Hamiltonian (H), Dipole Moment (μ), and Polarizability (α) Operators Expressed in the Molecular-Fixed Frame (MFF) and Laboratory-Fixed Frame (LFF) for Molecules Belonging to O_h and C_{4v} Symmetry Groups

Operator	O_h		C_{4v}	
	MFF	LFF	MFF	LFF
H	A_{1g}	A_{1g}	a_1	a_1
μ	F_{1u}	A_{1u}	$a_1 \oplus e$	a_2
α	$A_{1g} \oplus E_g \oplus F_{2g}$	A_{1g}	$2a_1 \oplus b_1 \oplus b_2 \oplus e$	a_1

Finally, we have

$$\alpha_{\Theta_1\Theta_2} = \sum_{L,m} \langle L;\, m|\Theta_1\Theta_2\rangle \alpha_m^{(L)}, \qquad [13]$$

$$\alpha_{\theta_1\theta_2} = \sum_{L,k} \langle L;\, k|\theta_1\theta_2\rangle \alpha_k^{(L)}, \qquad [14]$$

where the $\langle L;\, m|\Theta_1\Theta_2\rangle$ and $\langle L;\, k|\theta_1\theta_2\rangle$ are Stone coefficients (*9*).

3. TENSORIAL FORMALISM FOR XY_5Z (C_{4v}) SYMMETRIC MOLECULES

In this section, we will focus on the particularities of the tensorial expressions of the Hamiltonian and transition moments in the C_{4v} group. Table 1 shows the symmetries of the Hamiltonian, dipole moment, and polarizability operators in the LFF and MFF for O_h and C_{4v} symmetry groups. In the following, we omit the parity indexes for simplicity, except in a few cases where it is useful to understand selection rules.

3.1. Expression of the Hamiltonian

The initial (or untransformed) Hamiltonian is expanded as a series of rovibrational operators which are noted $T^{\Omega(K_g,n\Gamma_g,\tilde{\Gamma})\Gamma_{1\mu}\Gamma_{2\mu}\Gamma_{vg}}_{\{n_s\}\{m_s\}}$

$$H = \sum_{\text{all indexes}} t^{\Omega(K_g,n\Gamma_g,\tilde{\Gamma})\Gamma_{1\mu}\Gamma_{2\mu}\Gamma_{vg}}_{\{n_s\}\{m_s\}} T^{\Omega(K_g,n\Gamma_g,\tilde{\Gamma})\Gamma_{1\mu}\Gamma_{2\mu}\Gamma_{vg}}_{\{n_s\}\{m_s\}}, \qquad [15]$$

with the coupled rovibrational operators

$$T^{\Omega(K_g,n\Gamma_g,\tilde{\Gamma})\Gamma_{1\mu}\Gamma_{2\mu}\Gamma_{vg}}_{\{n_s\}\{m_s\}} = (R^{\Omega(K_g,n\Gamma_g,\tilde{\Gamma})} \otimes {}^{\epsilon}V^{\Gamma_{1\mu}\Gamma_{2\mu}(\Gamma_{vg},\tilde{\Gamma})}_{\{n_s\}\{m_s\}})^{(a_1)}, \qquad [16]$$

where $\Omega \leq 2$ and $\mu = g$ or u is the parity index. The $t^{\Omega(K_g,n\Gamma_g,\tilde{\Gamma})\Gamma_{1\mu}\Gamma_{2\mu}\Gamma_{vg}}_{\{n_s\}\{m_s\}}$ are the parameters of the model.

The $R^{\Omega(K_g,n\Gamma_g)}$ (rotational) and ${}^{\epsilon}V^{\Gamma_{1\mu}\Gamma_{2\mu}(\Gamma_{vg})}_{\{n_s\}\{m_s\}}$ (vibrational) operators are constructed exactly in the same way as in O_h (*2*). They are oriented in C_{4v} using

$$A^{(\Gamma_\tau,\tilde{\Gamma})}_{\tilde{\gamma}} = \sum_{\gamma} {}^{(\Gamma_\tau)}G'^{\gamma}_{\tilde{\Gamma}\tilde{\gamma}} A^{(\Gamma_\tau)}_{\gamma}, \qquad [17]$$

($\tau = g$ or u). The expression of the rotational and vibrational operators is detailed in Ref. (*1*). G' coefficients are given in I. To ensure that H is unchanged under time reversal, the parity ϵ of the vibrational operators in the conjugate momenta $p_{s,\sigma}$ is related to the rotational degree Ω through

$$\epsilon = (-1)^{\Omega}. \qquad [18]$$

The order of the development is defined as $\Omega + \Omega_V - 2$, Ω_V being the degree of ${}^{\epsilon}V^{\Gamma_{1\mu}\Gamma_{2\mu}(\Gamma_{vg})}_{\{n_s\}\{m_s\}}$ in the a^+ (creation) and a (annihilation) operators.

The transformed Hamiltonian has the same form as the initial one, that is

$$\tilde{H} = \sum_{\text{all indexes}} \tilde{t}^{\Omega(K_g,n\Gamma_g,\tilde{\Gamma})\Gamma_{1\mu}\Gamma_{2\mu}\Gamma_{vg}}_{\{n_s\}\{m_s\}} T^{\Omega(K_g,n\Gamma_g,\tilde{\Gamma})\Gamma_{1\mu}\Gamma_{2\mu}\Gamma_{vg}}_{\{n_s\}\{m_s\}}, \qquad [19]$$

where the transformed parameter set $\{\tilde{t}^{\Omega(K_g,n\Gamma_g,\tilde{\Gamma})\Gamma_{1\mu}\Gamma_{2\mu}\Gamma_{vg}}_{\{n_s\}\{m_s\}}\}$ depends on both the initial parameter set noted $\{t^{\Omega(K_g,n\Gamma_g,\tilde{\Gamma})\Gamma_{1\mu}\Gamma_{2\mu}\Gamma_{vg}}_{\{n_s\}\{m_s\}}\}$ and on the set of parameters of the contact transformation operator S.

In the following, we use the rovibrational coupled basis

$$|[\Psi_r^{(J,nC_r,\tilde{C}_r)} \otimes \Psi_v^{(C_v,\tilde{C}_v)}]\rangle, \qquad [20]$$

where $\Psi_r^{(J,nC_r,\tilde{C}_r)}$ is the rotational basis and $\Psi_v^{(C_v,\tilde{C}_v)}$ the vibrational one, with

$$|\Psi_v^{(C_v,\tilde{C}_v)}\rangle = |[[[[[\Psi_{v_1}^{(A_{1g})} \otimes \Psi_{v_2}^{(E_g)}]^{(C_{23})} \otimes \Psi_{v_3}^{(l_3,n_3C_3)}]^{(C_{23})} \otimes \Psi_{v_4}^{(l_4,n_4C_4)}]^{(C_{234})} \otimes \Psi_{v_5}^{(l_5,n_5C_5)}]^{(C_{2345})} \otimes \Psi_{v_6}^{(l_6,n_6C_6)}]^{(C_v,\tilde{C}_v)}\rangle, \qquad [21]$$

where $v_1, v_2, \ldots, v_6$ are the harmonic oscillator quantum numbers for the XY_6 "parent" molecule and $\tilde{C}_v$ is the vibrational symmetry in the C_{4v} group as illustrated in Fig. 1 in the case of SF_6 and SF_5Cl.

The Hamiltonian eigenfunctions are linear combinations of the rovibrational functions [20] and we denote them

$$|\Phi_{M\sigma}^{(JC_\tau\tilde{C}\tilde{\alpha})}\rangle, \qquad [22]$$

where $\tilde{\alpha}$ numbers the energy levels in increasing order within a (J, $\tilde{C}$) block.

The general expression of the matrix elements of the Hamiltonian operator is given in the appendix.

In Table 2, we give the correspondence between some of our parameters and the "classical" ones, as used in Ref. (*7*), for the

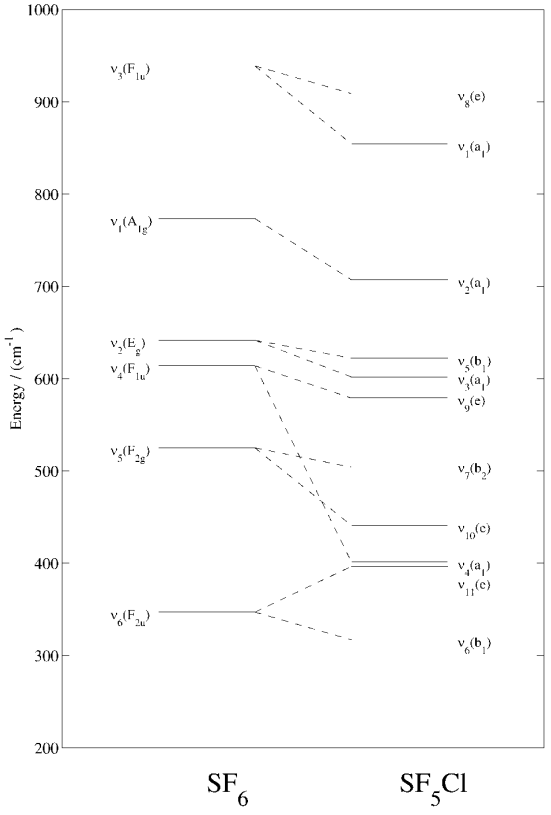

FIG. 1. Vibrational scheme correlation between SF_6 and SF_5Cl molecules.

$\nu_1(a_1)/\nu_8(e)$ dyad arising from the parent fundamental $\nu_3(F_{1u})$.

3.2. Expression of the Dipole Moment

Each component of the initial dipole moment in the MFF is expanded as a series of purely vibrational operators

$$\mu_\theta^{(\tilde{\Gamma})} = \sum_{\text{all indexes}} \mu_{\{n_s\}\{m_s\}}^{\Gamma_{1\mu}\Gamma_{2\mu'}(\Gamma_\tau,\tilde{\Gamma})} + V_{\{n_s\}\{m_s\}}^{\Gamma_{1\mu}\Gamma_{2\mu'}(\Gamma_\tau,\tilde{\Gamma})}, \qquad [23]$$

(μ, μ', and $\tau = g$ or u), where the $\mu_{\{n_s\}\{m_s\}}^{\Gamma_{1\mu}\Gamma_{2\mu'}(\Gamma_\tau,\tilde{\Gamma})}$ are the dipole parameters and $\tilde{\Gamma} = a_1$ or e.

As S is a Hermitian operator and contains rovibrational operators, then, the transformed dipole moment must be expanded as a series of rovibrational operators by

$$\mu_\theta^{(\tilde{\Gamma})} = \sum_{\{i\}} \mu^{\{i\}} M_\theta^{(\{i\},\tilde{\Gamma})}, \qquad [24]$$

with

$$M_\theta^{(\{i\},\tilde{\Gamma})} = (R^{\Omega(K_g,\Gamma_{rg},\tilde{\Gamma}_r)} \otimes {}^{\epsilon}V_{\{n_s\}\{m_s\}}^{\Gamma_{1\mu}\Gamma_{2\mu'}(\Gamma_{v\tau},\tilde{\Gamma}_v)})_\theta^{(\tilde{\Gamma})}, \qquad [25]$$

and $\epsilon = (-1)^\Omega$. The order of the development is $\Omega + \Omega_V - 1$.

The LFF components of the transformed dipole moment are

$$\mu_\Theta^{(a_2)} = \sqrt{3} \sum_m \langle 1; m|\Theta\rangle \sum_{\{i\}} \mu^{\{i\}}[C^{(1g,F_{1g},\tilde{\bar{\Gamma}})} \otimes M^{(\{i\},\tilde{\Gamma})}]^{(a_2)}, \qquad [26]$$

where $\tilde{\bar{\Gamma}} = a_2 \times \tilde{\Gamma}$ and $C^{(1g,F_{1g},\tilde{\bar{\Gamma}})}$ is the direction cosine tensor. Θ is equal to X, Y, or Z.

The square brackets represent the symmetrized tensor product defined as:

$$[A^{(\tilde{\Gamma}_1)} \otimes B^{(\tilde{\Gamma}_2)}]^{(\tilde{\Gamma})} = \tfrac{1}{2}((A^{(\tilde{\Gamma}_1)} \otimes B^{(\tilde{\Gamma}_2)})^{(\tilde{\Gamma})} + (-1)^{\tilde{\Gamma}_1+\tilde{\Gamma}_2+\tilde{\Gamma}}(B^{(\tilde{\Gamma}_2)} \otimes A^{(\tilde{\Gamma}_1)})^{(\tilde{\Gamma})}). \qquad [27]$$

The strength of a transition between the molecular rovibrational states $\tilde{\Phi}_i$ (with energy E_i) and $\tilde{\Phi}_f$ (with energy E_f) is calculated thanks to

TABLE 2
Correspondence between Our Parameters and the Usual Ones

Level	Order	Parameter $t_{\{n_s\}\{m_s\}}^{\Omega(K_g,n\Gamma_g,\tilde{\Gamma})\Gamma_{1\mu}\Gamma_{2\mu}\Gamma_{vg}}$					Notation of
		Ω	$(K_g, n\Gamma_g, \tilde{\Gamma})$	$\{n_s\}\Gamma_{1\mu}$	$\{m_s\}\Gamma_{2\mu}$	Γ_{vg}	Ref. [7]
Ground State	0	2	$(0_g, 0A_{1g}, a_1)$	$000000A_{1g}$	$000000A_{1g}$	A_{1g}	$\frac{2B_0 + C_0}{3}$
	2	2	$(2_g, 0E_g, a_1)$	$000000A_{1g}$	$000000A_{1g}$	A_{1g}	$\frac{C_0 - B_0}{2\sqrt{6}}$
$[\nu_3(XY_6) = 1]$	0	0	$(0_g, 0A_{1g}, a_1)$	$001000F_{1u}$	$001000F_{1u}$	E_g	$\frac{2(\omega_8 - \omega_1)}{3}$
$\equiv \nu_1 + \nu_8 = 1$		0	$(0_g, 0A_{1g}, a_1)$	$001000F_{1u}$	$001000F_{1u}$	A_{1g}	$\frac{2\omega_8 + \omega_1}{3}$
	1	1	$(1_g, 0F_{1g}, a_2)$	$001000F_{1u}$	$001000F_{1u}$	F_{1g}	$-2\sqrt{3}(B\zeta)$ (ν_8 Coriolis)
		1	$(1_g, 0F_{1g}, e)$	$001000F_{1u}$	$001000F_{1u}$	F_{1g}	$-\sqrt{6}(C\zeta)$ (ν_1/ν_8 Coriolis)

TABLE 3
Spin Statistic Weights in C_{4v}

$\tilde{C}$	a_1	a_2	b_1	b_2	e
g_i	0	12	1	6	6

$$S_{if} = K_{if} g_i e^{-(hcE_i/kT)} \sum_{M_i,M_f} |\langle \tilde{\Phi}_i | \tilde{\mu}_Z | \tilde{\Phi}_f \rangle|^2, \qquad [28]$$

where K_{if} is a numerical coefficient and g_i is the spin statistical weight of state $\tilde{\Phi}_i$. The values of spin statistic weights in XY_5Z (C_{4v}) molecules with Y ligands having a $\frac{1}{2}$ spin are listed in Table 3. The sum is realized over the spherical components M_i and M_f of the two states in the LFF. The appendix gives the general expression for the matrix elements of the transformed dipole moment operator.

3.3. Expression of the Polarizability

Each component of the initial polarizability in the MFF is expanded as a series of purely vibrational operators

$$\alpha_\theta^{(\tilde{\Gamma})} = \sum_{\text{all indexes}} \alpha_{\{n_s\}\{m_s\}}^{\Gamma_{1\mu}\Gamma_{2\mu'}(\Gamma_\tau,\tilde{\Gamma})} + V_{\{n_s\}\{m_s\}}^{\Gamma_{1\mu}\Gamma_{2\mu'}(\Gamma_\tau,\tilde{\Gamma})}, \qquad [29]$$

where μ, μ' and $\tau = g$ or u and the $\alpha_{\{n_s\}\{m_s\}}^{\Gamma_{1\mu}\Gamma_{2\mu'}(\Gamma_\tau,\tilde{\Gamma})}$ are the polarizability parameters and θ is a component of the operator $\alpha^{(\tilde{\Gamma})}$.

For the same reasons as before, we can write the transformed polarizability as a series of rovibrational operators by

$$\tilde{\alpha}_\theta^{(\tilde{\Gamma})} = \sum_{\{i\}} \tilde{\alpha}^{(\{i\},\tilde{\Gamma})} P_\theta^{(\{i\},\tilde{\Gamma})}, \qquad [30]$$

with

$$P_\theta^{(\{i\},\tilde{\Gamma})} = (R^{\Omega(K_g,\Gamma_{rg},\tilde{\Gamma}_\nu)} \otimes \epsilon V_{\{n_s\}\{m_s\}}^{\Gamma_{1\mu}\Gamma_{2\mu'}(\Gamma_{\nu\tau},\tilde{\Gamma}_\nu)})_\theta^{(\tilde{\Gamma})}, \qquad [31]$$

and $\epsilon = (-1)^\Omega$. The order of the development is $\Omega + \Omega_V - 1$.

The LFF components of the transformed polarizability are

$$\begin{aligned}\tilde{\alpha}_{\Theta_1\Theta_2}^{(a_1)} = {} & \langle 0;\, 0 | \Theta_1\Theta_2 \rangle \sum_{\{i\}} \tilde{\alpha}^{\{i\}} [C^{(0g,A_{1g},a_1)} \otimes P^{(\{i\},a_1)}]^{(a_1)} \\ & + \sqrt{2} \sum_m \langle 2;\, m | \Theta_1\Theta_2 \rangle \sum_{\{i\}} \tilde{\alpha}^{\{i\}} \\ & \times [C^{(2g,E_g,\tilde{\Gamma}_\nu)} \otimes P^{(\{i\},\tilde{\Gamma}_\nu)}]^{(a_1)} \\ & + \sqrt{3} \sum_m \langle 2;\, m | \Theta_1\Theta_2 \rangle \sum_{\{i\}} \tilde{\alpha}^{\{i\}} \\ & \times [C^{(2g,F_{2g},\tilde{\Gamma}'_\nu)} \otimes P^{(\{i\},\tilde{\Gamma}'_\nu)}]^{(a_1)},\end{aligned} \qquad [32]$$

where $\tilde{\Gamma}_\nu = a_1$ or b_1 and $\tilde{\Gamma}'_\nu = b_2$ or e and Θ_1, $\Theta_2 = X$, Y, or Z. The first term represents the isotropic part of the polarizability and the two others constitute the anisotropic part.

The intensity of Raman transitions is expressed as:

$$I_{if} = R_{ij} g_i e^{-(hcE_i/kT)} \sum_{\Theta,\Theta'} \sum_{M_i,M_f} |\langle \tilde{\Phi}_i | \tilde{\alpha}_{\Theta,\Theta'} | \tilde{\Phi}_f \rangle|^2. \qquad [33]$$

The general expression for the matrix elements of the transformed polarizability operator is given in the appendix.

3.4. Selection Rules

The selection rules come directly from the expressions of the matrix elements given in the appendix. The rules concerning J comes from the nonzero condition of the K isoscalar factors. They are given explicitly in Table 4.

4. CONCLUSION

In this paper, we have proposed a method to expand the Hamiltonian and the transition moments operators for XY_5Z (C_{4v}) symmetric top molecules using a tensorial formalism. We have pointed out the main differences between O_h and C_{4v} groups. The formulas necessary to calculate the matrix elements of these operators have been given as well as the related selection rules. A new version of the STDS software called C4VTDS developed in Dijon for the calculation of XY_4 and XY_6 molecular spectra (*10, 11*) has been recently rewritten for the case of XY_5Z molecules; it uses the formulas derived in the present paper for frequency and intensity calculations. All this should enable us to analyze the ν_1/ν_8 dyad recorded by means of FTIR spectroscopy in Wuppertal (Germany). Later, we intend to analyze hexacarbonyl molecules such as $W(^{12}CO)_5$ ^{13}CO and $Cr(^{12}CO)_5$ ^{13}CO.

TABLE 4
Selection Rules for the Hamiltonian ($\tilde{H}$), Dipole Moment ($\tilde{\mu}$), and Polarizability ($\tilde{\alpha}$) Operators

	$\tilde{H}$	$\tilde{\mu}$	$\tilde{\alpha}^{(0)}$	$\tilde{\alpha}^{(2)}$
ΔJ	0	0, ± 1	0	0, ± 1, ± 2
ΔM	0	0, ± 1	0	0, ± 1, ± 2
$\tilde{C}'$	$\tilde{C}$	$\tilde{C} \otimes a_2$	$\tilde{C}$	$\tilde{C}$

Note. $\tilde{\alpha}^{(0)}$ and $\tilde{\alpha}^{(2)}$ are the isotropic and anisotropic parts of the polarizability, respectively.

APPENDIX

Matrix Elements of the Hamiltonian Operator

$$\langle [\Psi_r^{(J',n'C'_r,\tilde{C}'_r)} \otimes \Psi_{v'}^{(C'_v,\tilde{C}'_v)}]_{\tilde{\sigma}}^{(\tilde{C})} | [R^{\Omega(K_g,n\Gamma_g,\tilde{\Gamma})} \otimes \epsilon V_{\{n_s\}\{m_s\}}^{\Gamma_{1\mu}\Gamma_{2\mu}(\Gamma_{vg},\tilde{\Gamma}')}]^{(a_1)} \times |[\Psi_r^{(J,nC_r,\tilde{C}_r)} \otimes \Psi_v^{(C_v,\tilde{C}_v)}]_{\tilde{\sigma}}^{(\tilde{C})}\rangle = \delta_{J,J'} \frac{(-1)^{J+\tilde{C}_v+\tilde{C}'_r-\tilde{C}-\tilde{\Gamma}}}{\sqrt{[\tilde{\Gamma}]}} \times \begin{Bmatrix} \tilde{C}'_r & \tilde{C} & \tilde{C}_v \\ \tilde{C}'_v & \tilde{\Gamma} & \tilde{C}'_r \end{Bmatrix} K' \begin{pmatrix} \Gamma_r & C_r & C'_r \\ \tilde{\Gamma} & \tilde{C}_r & \tilde{C}'_r \end{pmatrix} \times K \begin{pmatrix} K & J & J \\ n_r\Gamma_r & nC_r & n'C'_r \end{pmatrix} \times \langle \Psi_{v'}^{(C'_v,\tilde{C}'_v)} || \epsilon V_{\{n_s\}\{m_s\}}^{\Gamma_{1\mu}\Gamma_{2\mu}(\Gamma_{vg},\tilde{\Gamma})} || \Psi_v^{(C_v,\tilde{C}_v)} \rangle \langle \Psi_r^{(J)} || R^{\Omega(K)} || \Psi_r^{(J)} \rangle. \quad [A.34]$$

Matrix Elements of the Dipole Moment Operator

$$\langle [\Psi_r^{(J',n'C'_r,\tilde{C}'_r)} \otimes \Psi_{v'}^{(v',J',C'_v,\tilde{C}'_v)}]_{\tilde{\sigma}}^{(\tilde{C})} | [C^{(1g,F_{1g},\tilde{\Gamma})} \otimes M^{([\tilde{s}],\tilde{\Gamma}')}]^{(a_2)} \times |[\Psi_r^{(J,nC_r,\tilde{C}_r)} \otimes \Psi_v^{(v,J,C_v,\tilde{C}_v)}]_{\tilde{\sigma}}^{(\tilde{C})}\rangle = \frac{1}{2}\sqrt{[\tilde{C}][\bar{\tilde{C}}][\tilde{\Gamma}]} \times \tilde{F} \begin{pmatrix} a_2 & \tilde{C} & \bar{\tilde{C}} \\ 1 & \tilde{\sigma} & \bar{\tilde{\sigma}} \end{pmatrix} \langle J' || C^{(1)} || J \rangle \times \langle \Psi_{v'}^{(v',J',C'_v,\tilde{C}'_v)} || \epsilon V_{\{n_s\}\{m_s\}}^{\Gamma_{1\mu}\Gamma_{2\mu'}(\Gamma_{vg},\tilde{\Gamma}')} || \Psi_v^{(v,J,C_v,\tilde{C}_v)} \rangle \times \left\{ (-1)^{J+J'} \langle J || R^{\Omega(K)} || J \rangle \sum_{\tilde{C}''_r} \left[\begin{Bmatrix} \tilde{\Gamma}'_r & \tilde{\Gamma}'_v & \tilde{\Gamma} & a_2 \\ \tilde{C}'_r & \tilde{C}'_v & \tilde{C} & \tilde{C}'_r \\ \tilde{C}''_r & \tilde{C}'_v & \bar{\tilde{\Gamma}} & \bar{\tilde{C}} \end{Bmatrix} \times \sum_{n'',C''_r} K' \begin{pmatrix} C'_r & F_1 & C''_r \\ \tilde{C}'_r & \bar{\tilde{\Gamma}} & \tilde{C}''_r \end{pmatrix} K' \begin{pmatrix} C''_r & \Gamma_r & C_r \\ \tilde{C}''_r & \tilde{\Gamma}_r & \tilde{C}_r \end{pmatrix} \times K \begin{pmatrix} 1 & J & J' \\ 0F_1 & n''C''_r & n'C'_r \end{pmatrix} K \begin{pmatrix} K & J & J \\ n_r\Gamma_r & nC_r & n''C''_r \end{pmatrix} \right] + -(-1)^{\tilde{\Gamma}_r+\tilde{\Gamma}'_v+\bar{\tilde{\Gamma}}+\tilde{C}_r+\tilde{C}'_v+\tilde{C}'_r+\tilde{C}'_v+\tilde{C}+\bar{\tilde{C}}} \langle J' || R^{\Omega(K)} || J' \rangle \times \sum_{\tilde{C}''_r} \left[\begin{Bmatrix} \tilde{\Gamma}'_r & \tilde{\Gamma}'_v & \tilde{\Gamma} & a_2 \\ \tilde{C}'_r & \tilde{C}'_v & \bar{\tilde{C}} & \tilde{C}_r \\ \tilde{C}''_r & \tilde{C}_v & \bar{\tilde{\Gamma}} & \tilde{C} \end{Bmatrix} \times \sum_{n'',C''_r} K' \begin{pmatrix} C''_r & F_1 & C_r \\ \tilde{C}''_r & \bar{\tilde{\Gamma}} & \tilde{C}_r \end{pmatrix} K' \begin{pmatrix} C'_r & \Gamma_r & C''_r \\ \tilde{C}'_r & \tilde{\Gamma}_r & \tilde{C}''_r \end{pmatrix} \times K \begin{pmatrix} 1 & J & J' \\ 0F_1 & nC_r & n''C''_r \end{pmatrix} K \begin{pmatrix} K & J' & J' \\ n_r\Gamma_r & n''C''_r & n'C'_r \end{pmatrix} \right] \right\}. \quad [A.35]$$

Matrix Elements of the Polarizability Operator

$$\langle [\Psi_r^{(J',n'C'_r,\tilde{C}'_r)} \otimes \Psi_{v'}^{(v',J',C'_v,\tilde{C}'_v)}]_{\tilde{\sigma}}^{(\tilde{C})} | [C^{(L_g,\Gamma_g,\tilde{\Gamma})} \otimes P^{([\tilde{s}],\tilde{\Gamma}')}]^{(a_1)} | \times [\Psi_r^{(J,nC_r,\tilde{C}_r)} \otimes \Psi_v^{(v,J,C_v,\tilde{C}_v)}]_{\tilde{\sigma}}^{(\tilde{C})}\rangle = \frac{1}{2}(-1)^{\tilde{C}_r+\tilde{C}_v+\tilde{C}} \langle J' || C^{(L)} || J \rangle \times \langle \Psi_{v'}^{(v',J',C'_v,\tilde{C}'_v)} || \epsilon V_{\{n_s\}\{m_s\}}^{\Gamma_{1\mu}\Gamma_{2\mu'}(\Gamma_{vg},\tilde{\Gamma}')} || \Psi_v^{(v,J,C_v,\tilde{C}_v)} \rangle \left\{ \begin{matrix} \tilde{C}'_v & \tilde{C} & \tilde{C}'_r \\ \tilde{C}'_r & \tilde{\Gamma}_v & \tilde{C}'_v \end{matrix} \right\} \times \left\{ (-1)^{J+J'+\tilde{\Gamma}_r+\tilde{\Gamma}'_v+\tilde{\Gamma}} \langle J || R^{\Omega(K)} || J \rangle \sum_{\tilde{C}''_r} \left[\begin{Bmatrix} \tilde{\Gamma}'_r & \tilde{\Gamma} & \tilde{\Gamma}'_v \\ \tilde{C}'_r & \tilde{C}_r & \tilde{C}''_r \end{Bmatrix} \times \sum_{n'',C''_r} K' \begin{pmatrix} C'_r & \Gamma & C''_r \\ \tilde{C}'_r & \tilde{\Gamma} & \tilde{C}''_r \end{pmatrix} K' \begin{pmatrix} C''_r & \Gamma_r & C_r \\ \tilde{C}''_r & \tilde{\Gamma}_r & \tilde{C}_r \end{pmatrix} \times K \begin{pmatrix} L & J & J' \\ \Gamma & n''C''_r & n'C'_r \end{pmatrix} K \begin{pmatrix} K & J & J \\ n_r\Gamma_r & nC_r & n''C''_r \end{pmatrix} + \langle J' || R^{\Omega(K)} || J' \rangle \sum_{\tilde{C}''_r} \left[\begin{Bmatrix} \tilde{\Gamma}'_r & \tilde{\Gamma} & \tilde{\Gamma}'_v \\ \tilde{C}_r & \tilde{C}'_r & \tilde{C}''_r \end{Bmatrix} \times \sum_{n'',C''_r} K' \begin{pmatrix} C''_r & \Gamma & C_r \\ \tilde{C}''_r & \tilde{\Gamma} & \tilde{C}_r \end{pmatrix} K' \begin{pmatrix} C'_r & \Gamma_r & C''_r \\ \tilde{C}'_r & \tilde{\Gamma}_r & \tilde{C}''_r \end{pmatrix} \times K \begin{pmatrix} L & J & J' \\ \Gamma & nC_r & n''C''_r \end{pmatrix} K \begin{pmatrix} K & J' & J' \\ n_r\Gamma_r & n''C''_r & n'C'_r \end{pmatrix} \right] \right\}. \quad [A.36]$$

The following should be noted. The K's are isoscalar factors for the $O(3) \supset O_h$ group chain (I) and the K''s are isoscalar factors for the $O_h \supset C_{4v}$ group chain. The $\{\ldots\}$ are $6\tilde{C}$ and $12\tilde{C}$ coefficients for the C_{4v} group (see I).

Only nonvanishing matrix elements are considered in the above formula. Here, $[C]$ is the dimension of the irreducible representation C.

In relations [A.34] and [A.35], the $C^{(L_g)}$ reduced matrix elements are given by (I):

$$\langle \Psi_{M'}^{(J')} || C_m^{(L_g)} || \Psi_M^{(J)} \rangle = (-1)^{1+J'-M'} \sqrt{[J][J']} \times \begin{pmatrix} J' & 1 & J \\ -M' & m & M \end{pmatrix}. \quad [A.37]$$

ACKNOWLEDGMENTS

Support from the Région Bourgogne for the computer equipment of the Laboratoire de Physique de l'Université de Bourgogne is gratefully acknowledged.

REFERENCES

1. J.-P. Champion, M. Loëte, and G. Pierre, *in* "Spectroscopy of the Earth's Atmosphere and Interstellar Medium" (K. N. Rao and A. Weber, Eds.), pp. 339–422, Academic Press, San Diego, CA, 1992.

2. N. Cheblal, M. Loëte, and V. Boudon, *J. Mol. Spectrosc.*, in press.
3. J. E. Griffiths, *Spectrochim. Acta, Part A* **23,** 2145–2157 (1967).
4. J. Bellet, R. Jurek, and J. Chanussot, *J. Mol. Spectrosc.* **78,** 16–30 (1979).
5. Y. He, J. Pochert, M. Quack, R. Ranz, and G. Seyfang, *Faraday Discuss.* **102,** (1995).
6. M. Rotger, V. Boudon, and M. Loëte, submitted for publication.
7. D. Papoušek and M. R. Aliev, *in* "Molecular Vibrational–Rotational Spectra," Elsevier, New York, 1982.
8. A. R. Edmonds, *in* "Angular Momentum in Quantum Mechanics," Princeton University Press, Princeton, NJ, 1982.
9. A. J. Stone, *Mol. Phys.* **29,** 1461–1471 (1975).
10. Ch. Wenger and J.-P. Champion, *J. Quant. Spectrosc. Radiat. Transfer* **29,** 471–480 (1998).
11. Ch. Wenger, V. Boudon, J.-P. Champion, and G. Pierre, *J. Quant. Spectrosc. Radiat. Transfer,* in press.

Journal of Molecular Spectroscopy **208,** 169–179 (2001)
doi:10.1006/jmsp.2001.8385, available online at http://www.idealibrary.com on IDEAL®

High-Resolution Spectroscopy and Preliminary Analysis of the ν_1/ν_8 Dyad of $SF_5{}^{35}Cl$

M. Rotger,* A. Decrette,* V. Boudon,* M. Loëte,* S. Sander,† and H. Willner†

*Laboratoire de Physique de l'Université de Bourgogne, UMR CNRS 5027, 9, Avenue Alain Savary, B.P. 47 870, F-21078 Dijon Cedex, France; and †Anorganische Chemie, Fachbereich 6, Gerhard-Mercator-Universität, D-47048 Duisburg, Germany

E-mail: maud.rotger@u-bourgogne.fr

Received January 12, 2001; in revised form April 4, 2001

The Fourier transform infrared spectrum of monoisotopic $SF_5{}^{35}Cl$ has been recorded in the 650- to 960-cm^{-1} region at a temperature of 203 K, a pressure of 0.2 mbar, and an instrumental bandwidth of 0.002 cm^{-1}. The ν_1/ν_8 dyad near 900 cm^{-1} has been analyzed with an effective Hamiltonian developed up to the fourth order and the help of a recently developed set of programs called C_{4v}TDS (C_{4v} Top Data System, http://www.u-bourgogne.fr/LPUB/C4VTDS.html); 1346 transitions for ν_1, 351 transitions for ν_8, and 406 ground state combination differences have been assigned and fitted. A global fit has been obtained with an rms of 0.00082 cm^{-1} for the $\nu_1(a_1)$ band, of 0.0011 cm^{-1} for the $\nu_8(e)$ band, and of 0.00064 cm^{-1} for the ground state.

Key Words: molecular spectroscopy; C_{4v} symmetric top; $SF_5{}^{35}Cl$.

1. INTRODUCTION

XY_5Z molecules are good candidates for photochemical reactions such as photodissociation (*1, 2*):

$$XY_5Z \xrightarrow{nh\nu} XY_5 + Z. \qquad [1]$$

In the case of SF_5Z (Z = Cl, Br, ...), this leads to the SF_5 radical (*3, 4*). This one is a decomposition product of sulfur hexafluoride and is therefore involved in various processes such as plasma processing of semiconductors (*5*). It also appears as a dissociation product of SF_6 when this molecule is employed as an insulator in high-voltage power systems (*6*). Another example is the presence of this radical in chemistry for the synthesis of larger molecules employed in explosives and powders as indicated in Ref. (*7*). The SF_5 group can provide explosives with improved properties (increased density, decreased sensitivity, good thermal stability, and more energy in the detonation). Moreover, a molecule containing this SF_5 group, namely SF_5CF_3, has recently been identified in the atmosphere as a potent greenhouse gas (*8*). In order to better understand and to model photodissociative processes such as those in reaction [1], the knowledge of the infrared spectra of XY_5Z molecules is needed.

However, high-resolution spectroscopy of XY_5Z molecules with C_{4v} symmetry is quite unexplored both in infrared absorption and in Raman scattering. Microwave rotational spectra of SF_5Cl and SF_5Br were obtained several years ago by Jurek and co-workers as reported in detail in Refs. (*9–16*). In the literature, one only finds low-resolution infrared and Raman spectra of species like SF_5Cl (*17–19*), SF_5Br (*20*), SeF_5Cl and TeF_5Cl (*21*), SeF_5Br, WF_5Cl (*22*), IOF_5 (*23*), ...

To achieve the analysis of rovibrational spectra of these molecules, we have proposed a new tensorial formalism (*24, 25*) adapted to the case of C_{4v} symmetric tops. It is an extension of the usual formalism already developed in Dijon for octahedral XY_6 molecules (*26, 27*) in the $O(3) \supset O_h$ group chain. We work in the $O(3) \supset O_h \supset C_{4v}$ chain because XY_5Z symmetric tops result from the substitution of one ligand of the corresponding spherical top and thus are relatively close to octahedral symmetry. For example, SF_5Cl has a vibrational level scheme, as illustrated in Fig. 1, quite similar to that of the SF_6 molecule. The ν_1/ν_8 dyad is correlated to the strong ν_3 fundamental band of SF_6. So, this dyad has been chosen as a first test to validate our theoretical model.

Our main purpose is to test this new theoretical approach for the analysis of symmetric tops (regarding them as quasi-spherical ones) by starting a preliminary analysis in the region of the ν_1/ν_8 dyad.

In order to simplify the dense and complex spectrum we used an isotopically enriched sample. The $SF_5{}^{35}Cl$ monoisotopic species has been synthesized in Duisburg. The Fourier transform spectra in the 650–960 cm^{-1} region have been recorded in Wuppertal. Using the tensorial formalism and the C_{4v}TDS software developed in Dijon for XY_5Z molecules, we were able to perform a preliminary analysis of the ν_1/ν_8 dyad of $SF_5{}^{35}Cl$. We have unambiguously determined several parameters up to the fourth order that enable a satisfactory reproduction of the $\nu_1(a_1)$ parallel band and a quite satisfactory one for the very dense and partially unresolved $\nu_8(e)$ perpendicular band.

0022-2852/01 $35.00

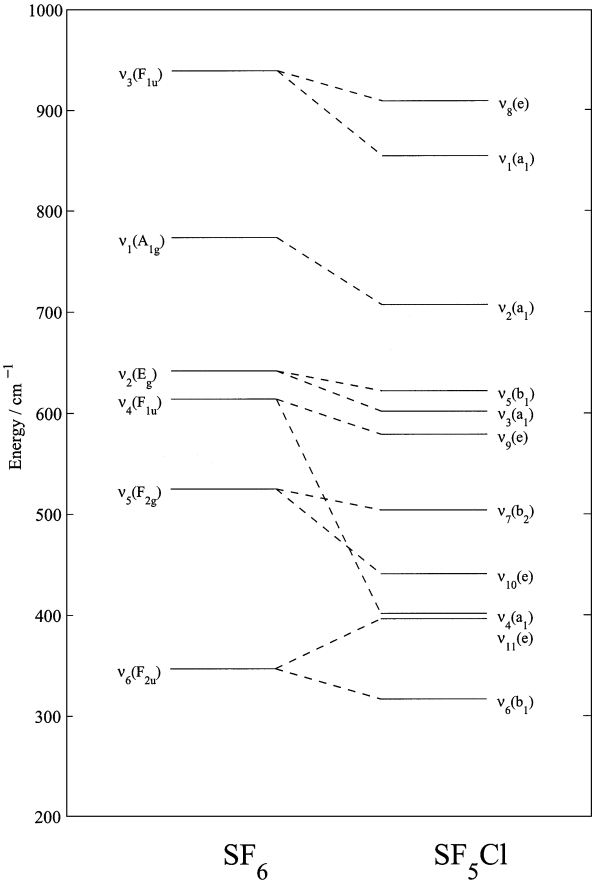

FIG. 1. $SF_6 \rightarrow SF_5Cl$ correlation scheme.

The experimental details concerning the synthesis of the monoisotopic species and the recording of absorption spectra are given in Section 2. The theoretical model based on the tensorial formalism is recalled in Section 3 and the results concerning the ν_1/ν_8 dyad analysis are given in the last Section.

2. EXPERIMENT

$SF_5{}^{35}Cl$ was generated in a two step synthesis. In the first step 48 mg (0.83 mmol) $Na^{35}Cl$ (99.7%, Chemotrade, Düsseldorf) was placed in a 23-mL glass container fitted with a valve with PTFE stem (Young, London). The evacuated reactor was filled with 550 mbar of fluorine (0.52 mmol) and then shaken for 20 min at room temperature. Chlorine was obtained in quantitative yield after the excess of fluorine was pumped off while the reactor was cooled to –196°C:

$$2Na^{35}Cl + F_2 \rightarrow 2NaF + {}^{35}Cl_2. \quad [2]$$

In the second step, a 280 mL glass reactor was filled with 0.20 mmol $^{35}Cl_2$ together with 0.20 mmol S_2F_{10} and heated to 170°C for 2 h:

$$^{35}Cl_2 + S_2F_{10} \rightarrow 2SF_5{}^{35}Cl. \quad [3]$$

A large excess of chlorine would be desirable to increase the yield of SF_5Cl, but here the valuable isotopically enriched chlorine was the limiting factor. The reaction products were separated by low temperature condensation in vacuum in a series of traps held at –95, –110, and –196°C. Less volatile unreacted S_2F_{10} was trapped at –95°C, while highly volatile products like SF_6 and $^{35}Cl_2$ were collected in the liquid nitrogen cold trap. At intermediate temperature $SF_5{}^{35}Cl$ was obtained and further purified in the same manner by trap-to-trap condensation using temperatures of –105, –125, and –196°C, respectively. A yield of 42 mg of pure $SF_5{}^{35}Cl$ (0.26 mmol, 72% yield related on reacted chlorine) was obtained.

The whole spectrum of the dyad was recorded in Wuppertal using a Bruker 120 HR spectrometer equipped with a Globar source, a KBr beamsplitter covered by germanium, and an MCT600 detector. The resolution (1/maximum optical path difference) was about 2.0×10^{-3} cm^{-1}. A double jacketed stainless steel cell of 22 cm length, equipped with CsBr windows and cooled to –70°C, was employed in the aim of suppressing hot bands. The gas pressure was 0.2 mbar and 277 scans were

TABLE 1
Experimental Conditions

Temperature / K	203
Pressure / mbar	0.2
Absorption length / cm	20
Recorded domain / cm^{-1}	650 – 960
Resolution / cm^{-1}	$\simeq 0.002$
Number of scans	277
Calibration	CO_2 lines

TABLE 2
Spin Statistics Weights

$\widetilde{C}$	a_1	a_2	b_1	b_2	e
g_i	12	12	8	8	12

TABLE 3
Effective Hamiltonian Parameters for the ν_2 (a_1) Band

Level	Order	Parameter $t^{\Omega(K_g,n\Gamma_g,\widetilde{\Gamma})\Gamma_{1\mu}\Gamma_{2\mu}\Gamma_{vg}}_{\{n_s\}\{m_s\}}$			
		$\Omega(K_g,n\Gamma_g,\widetilde{\Gamma})$	$\{n_s\}$ $\Gamma_{1\mu}$	$\{m_s\}$ $\Gamma_{2\mu}$	Γ_{vg}
$v=1$	0	$0(0,0A_{1g},a_1)$	001000 F_{1u}	001000 F_{1u}	A_{1g}
	2	$2(0,0A_{1g},a_1)$	001000 F_{1u}	001000 F_{1u}	A_{1g}
	2	$2(2,0E_g,\ a_1)$	001000 F_{1u}	001000 F_{1u}	A_{1g}
	4	$4(0,0A_{1g},a_1)$	001000 F_{1u}	001000 F_{1u}	A_{1g}
	4	$4(2,0E_g,\ a_1)$	001000 F_{1u}	001000 F_{1u}	A_{1g}
	4	$4(4,0A_{1g},a_1)$	001000 F_{1u}	001000 F_{1u}	A_{1g}
	4	$4(4,0E_g,\ a_1)$	001000 F_{1u}	001000 F_{1u}	A_{1g}

collected. Calibration was done using CO_2 lines wavenumbers as reported in Ref. (*28*). All these experimental conditions are collected in Table 1.

3. THEORY

The theoretical model described below to develop the Hamiltonian operator is based on the tensorial formalism and vibrational extrapolation methods used in Dijon. These methods have already been explained, for example, in Refs. (*26, 27, 29, 30*). We only recall here the basic principles and their applications to the case of XY_5Z molecules (*24, 25*) belonging to the C_{4v} group.

The background of the model is based on the idea of considering XY_5Z molecules as deformed XY_6 molecules, by substitution of one ligand. Practically, this means that we start from the $O(3) \supset O_h$ formalism used for octahedral species (*26*) and make a symmetry reduction (or reorientation) into the C_{4v} group. This procedure has been detailed in Ref. (*24*). In the following, all the C_{4v} oriented tensor operators will be denoted in the form

$$T_{\tilde{\sigma}}^{(\ldots,\Gamma,\tilde{\Gamma})},$$

Γ ($=A_{1\tau}, A_{2\tau}, E_\tau, F_{1\tau}, F_{2\tau}, \tau = g$ or u) and $\tilde{\Gamma}$ ($=a_1, a_2, b_1, b_2, e$) denoting O_h and C_{4v} irreducible representations (irreps), respectively. This way of handling XY_5Z molecules has some consequences for the labeling of Hamiltonian and transition moment parameters. The energy level labels are also different from the "usual" ones used in the standard treatment of symmetric tops, as it will be detailed below.

TABLE 4
Effective Hamiltonian Parameters for the Partial Fit of the ν_1 (a_1) Parallel Band Alone

Level	Order	Parameter $t_{\{n_s\}\{m_s\}}^{\Omega(K_g,n\Gamma_g,\tilde{\Gamma})\Gamma_{1\mu}\Gamma_{2\mu}\Gamma_{vg}}$				Value / cm^{-1}†	Constraint
		$\Omega(K_g, n\Gamma_g, \tilde{\Gamma})$	$\{n_s\}$ $\Gamma_{1\mu}$	$\{m_s\}$ $\Gamma_{2\mu}$	Γ_{vg}		
$v=0$	0	$2(0,0A_{1g},a_1)$	000000 A_{1g}	000000 A_{1g}	A_{1g}	$0.706410(10) \times 10^{-1}$	
	0	$2(2,0E_g,a_1)$	000000 A_{1g}	000000 A_{1g}	A_{1g}	0.5989339×10^{-2}	Fixed
	2	$4(0,0A_{1g},a_1)$	000000 A_{1g}	000000 A_{1g}	A_{1g}	$0.724(42) \times 10^{-8}$	
	2	$4(2,0E_g,a_1)$	000000 A_{1g}	000000 A_{1g}	A_{1g}	$-0.305(10) \times 10^{-8}$	
	2	$4(4,0A_{1g},a_1)$	000000 A_{1g}	000000 A_{1g}	A_{1g}	0.0	Fixed
	2	$4(4,0E_g,a_1)$	000000 A_{1g}	000000 A_{1g}	A_{1g}	0.0	Fixed
$v=1$	0	$0(0,0A_{1g},a_1)$	001000 F_{1u}	001000 F_{1u}	E_g	$0.36744781661 \times 10^{2}$	Fixed
⋆	0	$0(0,0A_{1g},a_1)$	001000 F_{1u}	001000 F_{1u}	A_{1g}	$0.892255306(97) \times 10^{3}$	
	1	$1(1,0F_{1g},a_2)$	001000 F_{1u}	001000 F_{1u}	F_{1g}	0.0	Fixed
	1	$1(1,0F_{1g},e)$	001000 F_{1u}	001000 F_{1u}	F_{1g}	0.0	Fixed
⋆	2	$2(0,0A_{1g},a_1)$	001000 F_{1u}	001000 F_{1u}	A_{1g}	$-0.16750(11) \times 10^{-3}$	
	2	$2(0,0A_{1g},a_1)$	001000 F_{1u}	001000 F_{1u}	E_g	0.0	Fixed
⋆	2	$2(2,0E_g,a_1)$	001000 F_{1u}	001000 F_{1u}	A_{1g}	$0.72118(80) \times 10^{-4}$	
	2	$2(2,0E_g,a_1)$	001000 F_{1u}	001000 F_{1u}	E_g	0.0	Fixed
	2	$2(2,0E_g,b_1)$	001000 F_{1u}	001000 F_{1u}	E_g	0.0	Fixed
	2	$2(2,0F_{2g},b_2)$	001000 F_{1u}	001000 F_{1u}	F_{2g}	0.0	Fixed
	2	$2(2,0F_{2g},e)$	001000 F_{1u}	001000 F_{1u}	F_{2g}	0.0	Fixed
	3	$3(1,0F_{1g},a_2)$	001000 F_{1u}	001000 F_{1u}	F_{1g}	0.0	Fixed
	3	$3(1,0F_{1g},e)$	001000 F_{1u}	001000 F_{1u}	F_{1g}	0.0	Fixed
	3	$3(3,0F_{1g},a_2)$	001000 F_{1u}	001000 F_{1u}	F_{1g}	0.0	Fixed
	3	$3(3,0F_{1g},e)$	001000 F_{1u}	001000 F_{1u}	F_{1g}	0.0	Fixed
	3	$3(3,0F_{2g},e)$	001000 F_{1u}	001000 F_{1u}	F_{2g}	0.0	Fixed
⋆	4	$4(0,0A_{1g},a_1)$	001000 F_{1u}	001000 F_{1u}	A_{1g}	$0.40149(22) \times 10^{-7}$	
	4	$4(0,0A_{1g},a_1)$	001000 F_{1u}	001000 F_{1u}	E_g	0.0	Fixed
⋆	4	$4(2,0E_g,a_1)$	001000 F_{1u}	001000 F_{1u}	A_{1g}	$-0.262321(89) \times 10^{-7}$	
	4	$4(2,0E_g,a_1)$	001000 F_{1u}	001000 F_{1u}	E_g	0.0	Fixed
	4	$4(2,0E_g,b_1)$	001000 F_{1u}	001000 F_{1u}	E_g	0.0	Fixed
	4	$4(2,0F_{2g},b_2)$	001000 F_{1u}	001000 F_{1u}	F_{2g}	0.0	Fixed
	4	$4(2,0F_{2g},e)$	001000 F_{1u}	001000 F_{1u}	F_{2g}	0.0	Fixed
⋆	4	$4(4,0A_{1g},a_1)$	001000 F_{1u}	001000 F_{1u}	A_{1g}	$0.79570(65) \times 10^{-8}$	
	4	$4(4,0A_{1g},a_1)$	001000 F_{1u}	001000 F_{1u}	E_g	0.0	Fixed
⋆	4	$4(4,0E_g,a_1)$	001000 F_{1u}	001000 F_{1u}	A_{1g}	$-0.67172(69) \times 10^{-8}$	
	4	$4(4,0E_g,a_1)$	001000 F_{1u}	001000 F_{1u}	E_g	0.0	Fixed
	4	$4(4,0E_g,b_1)$	001000 F_{1u}	001000 F_{1u}	E_g	0.0	Fixed
	4	$4(4,0F_{1g},e)$	001000 F_{1u}	001000 F_{1u}	F_{2g}	0.0	Fixed
	4	$4(4,0F_{2g},b_2)$	001000 F_{1u}	001000 F_{1u}	F_{2g}	0.0	Fixed
	4	$4(4,0F_{2g},e)$	001000 F_{1u}	001000 F_{1u}	F_{2g}	0.0	Fixed

ν_1 : 1347 assigned lines, J_{max}=79, $\sigma^{\ddagger}$=0.74 × 10^{-3} cm^{-1}

⋆ "ν_1" parameters.
† One standard deviation in parentheses.
‡ Root mean square.

If we consider an XY_5Z molecule for which the vibrational levels are grouped in a series of polyads designed by P_k ($k = 0, \ldots, n$), P_0 being the ground state (GS), the Hamiltonian operator can be put in the following form (after performing some contact transformations):

$$\mathcal{H} = \mathcal{H}_{\{P_0 \equiv \mathrm{GS}\}} + \mathcal{H}_{\{P_1\}} + \cdots + \mathcal{H}_{\{P_k\}} + \cdots + \mathcal{H}_{\{P_{n-1}\}} + \mathcal{H}_{\{P_n\}}. \quad [4]$$

Terms like $\mathcal{H}_{\{P_k\}}$ contain rovibrational operators which have no matrix elements within the $P_{k'<k}$ basis sets. The effective Hamiltonian for polyad P_n is obtained by projecting $\mathcal{H}$ in the P_n Hilbert subspace; i.e.,

$$H^{\langle P_n\rangle} = P^{\langle P_n\rangle}\mathcal{H}P^{\langle P_n\rangle} = H^{\langle P_n\rangle}_{\{\mathrm{GS}\}} + H^{\langle P_n\rangle}_{\{P_1\}} + \cdots + H^{\langle P_n\rangle}_{\{P_k\}} + \cdots + H^{\langle P_n\rangle}_{\{P_{n-1}\}} + H^{\langle P_n\rangle}_{\{P_n\}}. \quad [5]$$

The different terms are written in the form

$$\mathcal{H}_{\{P_k\}} = \sum_{\text{all indices}} t^{\Omega(K_g, n\Gamma_g, \tilde{\Gamma})\Gamma_{1\mu}\Gamma_{2\mu}\Gamma_{vg}}_{\{n_s\}\{m_s\}} \times \beta\left(R^{\Omega(K_g, n\Gamma_g, \tilde{\Gamma})} \otimes {}^{\epsilon} V^{\Gamma_{1\mu}\Gamma_{2\mu}(\Gamma_{vg}, \tilde{\Gamma})}_{\{n_s\}\{m_s\}}\right)^{(a_1)}. \quad [6]$$

TABLE 5

Effective Hamiltonian Parameters for the Partial Fit of the ν_8 (e) Perpendicular Band Alone

Level	Order	Parameter $t^{\Omega(K_g,n\Gamma_g,\tilde{\Gamma})\Gamma_{1\mu}\Gamma_{2\mu}\Gamma_{vg}}_{\{n_s\}\{m_s\}}$ $\Omega(K_g, n\Gamma_g, \tilde{\Gamma})$	$\{n_s\}$ $\Gamma_{1\mu}$	$\{m_s\}$ $\Gamma_{2\mu}$	Γ_{vg}	Value / cm^{-1}†	Constraint
$v=0$	0	$2(0,0A_{1g},a_1)$	000000 A_{1g}	000000 A_{1g}	A_{1g}	$0.70641047500 \times 10^{-1}$	Fixed
	0	$2(2,0E_g,a_1)$	000000 A_{1g}	000000 A_{1g}	A_{1g}	$0.59893390000 \times 10^{-2}$	Fixed
	2	$4(0,0A_{1g},a_1)$	000000 A_{1g}	000000 A_{1g}	A_{1g}	$0.72422073329 \times 10^{-8}$	Fixed
	2	$4(2,0E_g,a_1)$	000000 A_{1g}	000000 A_{1g}	A_{1g}	$-0.30519427531 \times 10^{-8}$	Fixed
	2	$4(4,0A_{1g},a_1)$	000000 A_{1g}	000000 A_{1g}	A_{1g}	$0.575(24) \times 10^{-9}$	
	2	$4(4,0E_g,a_1)$	000000 A_{1g}	000000 A_{1g}	A_{1g}	0.0	Fixed
$v=1$	0	$0(0,0A_{1g},a_1)$	001000 F_{1u}	001000 F_{1u}	E_g	$0.3688315(48) \times 10^{2}$	
⋆	0	$0(0,0A_{1g},a_1)$	001000 F_{1u}	001000 F_{1u}	A_{1g}	$0.89225530618 \times 10^{3}$	Fixed
	1	$1(1,0F_{1g},a_2)$	001000 F_{1u}	001000 F_{1u}	F_{1g}	0.146847(20)	
	1	$1(1,0F_{1g},e)$	001000 F_{1u}	001000 F_{1u}	F_{1g}	−0.17430(32)	
⋆	2	$2(0,0A_{1g},a_1)$	001000 F_{1u}	001000 F_{1u}	A_{1g}	$-0.16749865122 \times 10^{-3}$	Fixed
	2	$2(0,0A_{1g},a_1)$	001000 F_{1u}	001000 F_{1u}	E_g	$0.1080(42) \times 10^{-4}$	
⋆	2	$2(2,0E_g,a_1)$	001000 F_{1u}	001000 F_{1u}	A_{1g}	$0.72118140770 \times 10^{-4}$	Fixed
	2	$2(2,0E_g,a_1)$	001000 F_{1u}	001000 F_{1u}	E_g	$-0.38521(24) \times 10^{-3}$	
	2	$2(2,0E_g,b_1)$	001000 F_{1u}	001000 F_{1u}	E_g	$-0.7499(40) \times 10^{-4}$	
	2	$2(2,0F_{2g},b_2)$	001000 F_{1u}	001000 F_{1u}	F_{2g}	0.0	Fixed
	2	$2(2,0F_{2g},e)$	001000 F_{1u}	001000 F_{1u}	F_{2g}	$-0.96(30) \times 10^{-5}$	
	3	$3(1,0F_{1g},a_2)$	001000 F_{1u}	001000 F_{1u}	F_{1g}	$-0.43(34) \times 10^{-8}$	
	3	$3(1,0F_{1g},e)$	001000 F_{1u}	001000 F_{1u}	F_{1g}	0.0	Fixed
	3	$3(3,0F_{1g},a_2)$	001000 F_{1u}	001000 F_{1u}	F_{1g}	0.0	Fixed
	3	$3(3,0F_{1g},e)$	001000 F_{1u}	001000 F_{1u}	F_{1g}	0.0	Fixed
	3	$3(3,0F_{2g},e)$	001000 F_{1u}	001000 F_{1u}	F_{2g}	0.0	Fixed
⋆	4	$4(0,0A_{1g},a_1)$	001000 F_{1u}	001000 F_{1u}	A_{1g}	$0.40148807034 \times 10^{-7}$	Fixed
	4	$4(0,0A_{1g},a_1)$	001000 F_{1u}	001000 F_{1u}	E_g	0.0	Fixed
⋆	4	$4(2,0E_g,a_1)$	001000 F_{1u}	001000 F_{1u}	A_{1g}	$-0.26232060022 \times 10^{-7}$	Fixed
	4	$4(2,0E_g,a_1)$	001000 F_{1u}	001000 F_{1u}	E_g	0.0	Fixed
	4	$4(2,0E_g,b_1)$	001000 F_{1u}	001000 F_{1u}	E_g	0.0	Fixed
	4	$4(2,0F_{2g},b_2)$	001000 F_{1u}	001000 F_{1u}	F_{2g}	0.0	Fixed
	4	$4(2,0F_{2g},e)$	001000 F_{1u}	001000 F_{1u}	F_{2g}	0.0	Fixed
⋆	4	$4(4,0A_{1g},a_1)$	001000 F_{1u}	001000 F_{1u}	A_{1g}	$0.79570213033 \times 10^{-8}$	Fixed
	4	$4(4,0A_{1g},a_1)$	001000 F_{1u}	001000 F_{1u}	E_g	0.0	Fixed
⋆	4	$4(4,0E_g,a_1)$	001000 F_{1u}	001000 F_{1u}	A_{1g}	$-0.67171864616 \times 10^{-8}$	Fixed
	4	$4(4,0E_g,a_1)$	001000 F_{1u}	001000 F_{1u}	E_g	0.0	Fixed
	4	$4(4,0E_g,b_1)$	001000 F_{1u}	001000 F_{1u}	E_g	0.0	Fixed
	4	$4(4,0F_{1g},e)$	001000 F_{1u}	001000 F_{1u}	F_{2g}	0.0	Fixed
	4	$4(4,0F_{2g},b_2)$	001000 F_{1u}	001000 F_{1u}	F_{2g}	0.0	Fixed
	4	$4(4,0F_{2g},e)$	001000 F_{1u}	001000 F_{1u}	F_{2g}	0.0	Fixed

ν_8 : 270 assigned lines, $J_{\max}$=79, $\sigma^{\ddagger}$=1.25 × 10^{-3} cm^{-1}

⋆ "ν_1" parameters.

† One standard deviation in parentheses.

‡ Root mean square.

In this equation, the $t^{\Omega(K_g,n\Gamma_g,\widetilde{\Gamma})\Gamma_{1\mu}\Gamma_{2\mu}\Gamma_{vg}}_{\{n_s\}\{m_s\}}$ are the parameters to be determined. $R^{\Omega(K_g,n\Gamma_g,\widetilde{\Gamma})}$ and $\in V^{\Gamma_{1\mu}\Gamma_{2\mu}(\Gamma_{vg},\widetilde{\Gamma})}_{\{n_s\}\{m_s\}}$ are rotational and vibrational operators of respective degree Ω (maximum degree in the rotational angular momentum components J_x, J_y, and J_z) and Ω_v (degree in creation and anihilation operators). Their construction is described in Ref. (*29*). The order of each individual term is $\Omega+\Omega_v-2$. β is a numerical factor equal to $\sqrt{[\Gamma_1]}$ $(-\sqrt{3}/4)^{\Omega/2}$ if $(K_g, n\Gamma_g)=(0, 0A_{1g})$ and equal to 1 otherwise.

Such an Hamiltonian development scheme enables the treatment of any polyad system. In this work, we will use only the two following effective Hamiltonians:

- The ground state effective Hamiltonian

$$H^{\langle GS\rangle} = H^{\langle GS\rangle}_{\{GS\}}. \quad [7]$$

- The ν_2 effective Hamiltonian

$$H^{\langle \nu_2\rangle} = H^{\langle \nu_2\rangle}_{\{GS\}} + H^{\langle \nu_2\rangle}_{\{\nu_2\}}. \quad [8]$$

- The ν_1/ν_8 stretching dyad effective Hamiltonian

$$H^{\langle \nu_1/\nu_8\rangle} = H^{\langle \nu_1/\nu_8\rangle}_{\{GS\}} + H^{\langle \nu_1/\nu_8\rangle}_{\{\nu_1/\nu_8\}}. \quad [9]$$

Recall that the ν_1/ν_8 dyad comes from the splitting of the ν_3

TABLE 6
Effective Hamiltonian Parameters for the Global Fit of the ν_1/ν_8 Dyad

Level	Order	Parameter $t^{\Omega(K_g,n\Gamma_g,\widetilde{\Gamma})\Gamma_{1\mu}\Gamma_{2\mu}\Gamma_{vg}}_{\{n_s\}\{m_s\}}$				Value / cm^{-1}†	Notation
		$\Omega(K_g,n\Gamma_g,\widetilde{\Gamma})$	$\{n_s\}$ $\Gamma_{1\mu}$	$\{m_s\}$ $\Gamma_{2\mu}$	Γ_{vg}		of Papoušek [31]
$v=0$	0	$2(0,0A_{1g},a_1)$	000000 A_{1g}	000000 A_{1g}	A_{1g}	$0.707411(12)\times10^{-1}$	$\simeq \frac{C_0+2B_0}{3}$
	0	$2(2,0E_g,\ a_1)$	000000 A_{1g}	000000 A_{1g}	A_{1g}	$0.605408(55)\times10^{-2}$	$\simeq \frac{C_0-B_0}{2\sqrt{6}}$
	2	$4(0,0A_{1g},a_1)$	000000 A_{1g}	000000 A_{1g}	A_{1g}	$0.1608(28)\times10^{-7}$	
	2	$4(2,0E_g,\ a_1)$	000000 A_{1g}	000000 A_{1g}	A_{1g}	$-0.5695(94)\times10^{-8}$	
	2	$4(4,0A_{1g},a_1)$	000000 A_{1g}	000000 A_{1g}	A_{1g}	$0.701(66)\times10^{-9}$	
	2	$4(4,0E_g,\ a_1)$	000000 A_{1g}	000000 A_{1g}	A_{1g}	0.0 ‡	
$v=1$	0	$0(0,0A_{1g},a_1)$	001000 F_{1u}	001000 F_{1u}	E_g	$0.3678841(18)\times10^{\ 2}$	$\simeq \frac{2(\nu_8-\nu_1)}{3}$
⋆	0	$0(0,0A_{1g},a_1)$	001000 F_{1u}	001000 F_{1u}	A_{1g}	$0.89229944(17)\times10^{\ 3}$	$\simeq \frac{\nu_1+2\nu_8}{3}$
	1	$1(1,0F_{1g},a_2)$	001000 F_{1u}	001000 F_{1u}	F_{1g}	0.148416(18)	ν_8 Coriolis
	1	$1(1,0F_{1g},\ e)$	001000 F_{1u}	001000 F_{1u}	F_{1g}	−0.18170(67)	(ν_1,ν_8) Coriolis
⋆	2	$2(0,0A_{1g},a_1)$	001000 F_{1u}	001000 F_{1u}	A_{1g}	$-0.11848(29)\times10^{-3}$	
	2	$2(0,0A_{1g},a_1)$	001000 F_{1u}	001000 F_{1u}	E_g	$-0.830(10)\times10^{-4}$	
⋆	2	$2(2,0E_g,\ a_1)$	001000 F_{1u}	001000 F_{1u}	A_{1g}	$-0.7800(18)\times10^{-4}$	
	2	$2(2,0E_g,\ a_1)$	001000 F_{1u}	001000 F_{1u}	E_g	$-0.7953(46)\times10^{-4}$	
	2	$2(2,0E_g,\ b_1)$	001000 F_{1u}	001000 F_{1u}	E_g	$-0.829(11)\times10^{-4}$	
	2	$2(2,0F_{2g},b_2)$	001000 F_{1u}	001000 F_{1u}	F_{2g}	0.0 ‡	
	2	$2(2,0F_{2g},\ e)$	001000 F_{1u}	001000 F_{1u}	F_{2g}	$-0.414(63)\times10^{-4}$	
	3	$3(1,0F_{1g},a_2)$	001000 F_{1u}	001000 F_{1u}	F_{1g}	$0.2802(97)\times10^{-6}$	
	3	$3(1,0F_{1g},\ e)$	001000 F_{1u}	001000 F_{1u}	F_{1g}	0.0 ‡	
	3	$3(3,0F_{1g},a_2)$	001000 F_{1u}	001000 F_{1u}	F_{1g}	0.0 ‡	
	3	$3(3,0F_{1g},\ e)$	001000 F_{1u}	001000 F_{1u}	F_{1g}	$-0.478(45)\times10^{-6}$	
	3	$3(3,0F_{2g},\ e)$	001000 F_{1u}	001000 F_{1u}	F_{2g}	$0.1253(99)\times10^{-5}$	
⋆	4	$4(0,0A_{1g},a_1)$	001000 F_{1u}	001000 F_{1u}	A_{1g}	$0.3827(12)\times10^{-7}$	
	4	$4(0,0A_{1g},a_1)$	001000 F_{1u}	001000 F_{1u}	E_g	$-0.231(10)\times10^{-8}$	
⋆	4	$4(2,0E_g,\ a_1)$	001000 F_{1u}	001000 F_{1u}	A_{1g}	$-0.27003(56)\times10^{-7}$	
	4	$4(2,0E_g,\ a_1)$	001000 F_{1u}	001000 F_{1u}	E_g	0.0 ‡	
	4	$4(2,0E_g,\ b_1)$	001000 F_{1u}	001000 F_{1u}	E_g	0.0 ‡	
	4	$4(2,0F_{2g},b_2)$	001000 F_{1u}	001000 F_{1u}	F_{2g}	0.0 ‡	
	4	$4(2,0F_{2g},\ e)$	001000 F_{1u}	001000 F_{1u}	F_{2g}	0.0 ‡	
⋆	4	$4(4,0A_{1g},a_1)$	001000 F_{1u}	001000 F_{1u}	A_{1g}	$0.8461(48)\times10^{-8}$	
	4	$4(4,0A_{1g},a_1)$	001000 F_{1u}	001000 F_{1u}	E_g	0.0 ‡	
⋆	4	$4(4,0E_g,\ a_1)$	001000 F_{1u}	001000 F_{1u}	A_{1g}	$-0.7281(46)\times10^{-8}$	
	4	$4(4,0E_g,\ a_1)$	001000 F_{1u}	001000 F_{1u}	E_g	$-0.220(10)\times10^{-8}$	
	4	$4(4,0E_g,\ b_1)$	001000 F_{1u}	001000 F_{1u}	E_g	0.0 ‡	
	4	$4(4,0F_{1g},\ e)$	001000 F_{1u}	001000 F_{1u}	F_{2g}	0.0 ‡	
	4	$4(4,0F_{2g},b_2)$	001000 F_{1u}	001000 F_{1u}	F_{2g}	0.0 ‡	
	4	$4(4,0F_{2g},\ e)$	001000 F_{1u}	001000 F_{1u}	F_{2g}	0.0 ‡	

GSCD : 406 assigned lines, J_{max}=79, σ¶=0.64 × 10^{-3} cm^{-1}
ν_1 : 1346 assigned lines, J_{max}=79, σ¶=0.82 × 10^{-3} cm^{-1}
ν_8 : 351 assigned lines, J_{max}=79, σ¶=1.10 × 10^{-3} cm^{-1}

⋆ "ν_1" parameters.
† One standard deviation in parentheses.
‡ Fixed.
¶ Root mean square.

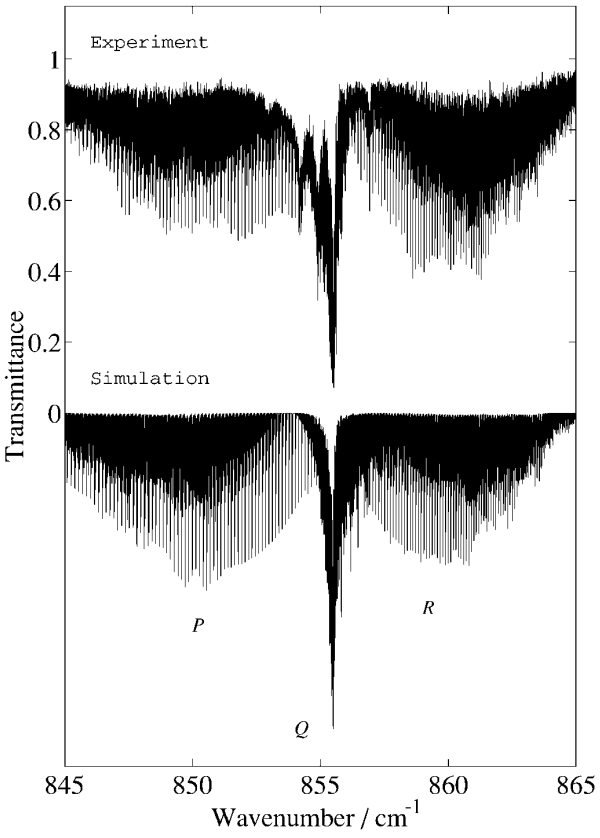

FIG. 2. The ν_1 parallel band: experiment and simulation.

band of the XY_6 "parent" molecule; thus $\mathcal{H}_{\{\nu_1/\nu_8\}}$ is constructed using ${}^{\epsilon}V^{\Gamma_{1\mu}\Gamma_{2\mu}(\Gamma_{\nu g},\tilde{\Gamma}')}_{\{3\}\{3\}}$ vibrational operators which involve $a_3^{+(F_{1u})}$ and $a_3^{(F_{1u})}$ creation and anihilation operators.

The matrix elements are calculated in the coupled basis

$$\left|\left[\Psi_r^{(J,nC_r,\tilde{C}_r)} \otimes \Psi_v^{(C_v,\tilde{C}_v)}\right]_{\tilde{\sigma}}^{(\tilde{C})}\right\rangle, \qquad [10]$$

with

$$\begin{aligned}\left|\Psi_v^{(C_v,\tilde{C}_v)}\right\rangle = \Big|&\Big[\Big[\Big[\Big[\Psi_{v_1}^{(A_{1g})} \otimes \Psi_{v_2}^{(l_2,C_2)} \otimes \Psi_{v_3}^{(l_3,n_3C_3)}\Big]^{(C_{23})} \\ &\otimes \Psi_{v_4}^{(l_4,n_4C_4)}\Big]^{(C_{234})} \otimes \Psi_{v_5}^{(l_5,n_5C_5)}\Big]^{(C_{2345})} \\ &\otimes \Psi_{v_6}^{(l_6,n_6C_6)}\Big]^{(C_v,\tilde{C}_v)}\Big\rangle. \qquad [11]\end{aligned}$$

$v_1, \ldots, v_6$ are vibration quantum numbers for the XY_6 "parent" molecule. $\tilde{C}_v$ is the vibrational symmetry in C_{4v}:

$$D^{(C_v)} \supset \tilde{D}^{(\tilde{C}_v)}. \qquad [12]$$

Expressions of the matrix elements are given in Ref. (25). All the rovibrational levels are described by $(J, \tilde{\alpha}, \tilde{C})$ labels where $\tilde{\alpha}$ is a numbering index for levels that have the same C_{4v} symmetry within a J block. This labeling is related to our group chain choice which considers XY_5Z molecules like near-spherical tops. In this way, the usual K quantum number is hidden and related to the $\tilde{C}$ symmetry. So, the K values do not appear explicitely in our labels, and the ΔK nomenclature does not occur in our transition labels.

The strength of a transition between the molecular rovibrational states $\tilde{\Phi}_i$ (with energy E_i) and $\tilde{\Phi}_f$ (with energy E_f) is calculated using

$$S_{if} = K_{if} g_i e^{-\frac{hcE_i}{kT}} \sum_{M_i,M_f} |\langle\tilde{\Phi}_i|\tilde{\mu}_Z|\tilde{\Phi}_f\rangle|^2, \qquad [13]$$

where K_{if} is a numerical coefficient and g_i is the spin statistical weight of state $\tilde{\Phi}_i$. The values of spin statistical weights in XY_5Z (C_{4v}) molecules, with Y ligands having spin $\frac{1}{2}$, are listed in Table 2. The sum is realized over the spherical components M_i

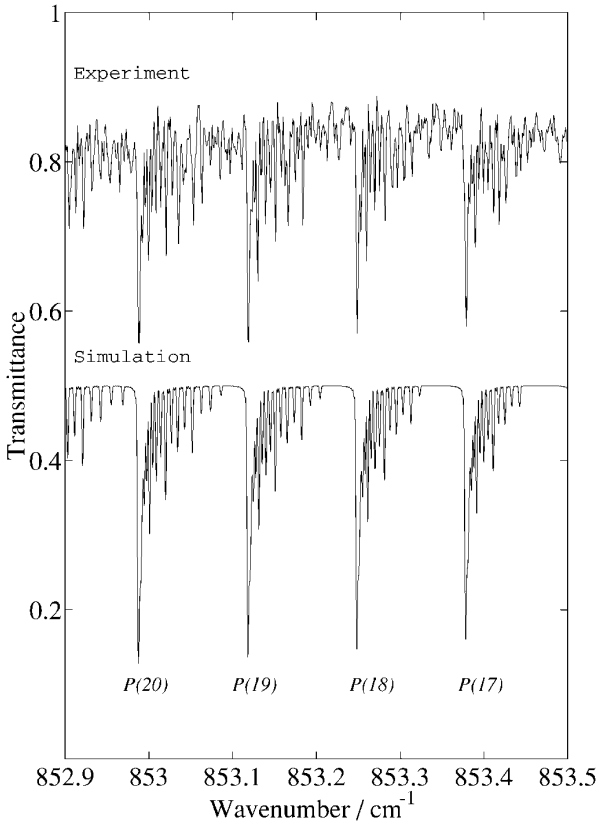

FIG. 3. Part of the ν_1 P branch: experiment and simulation.

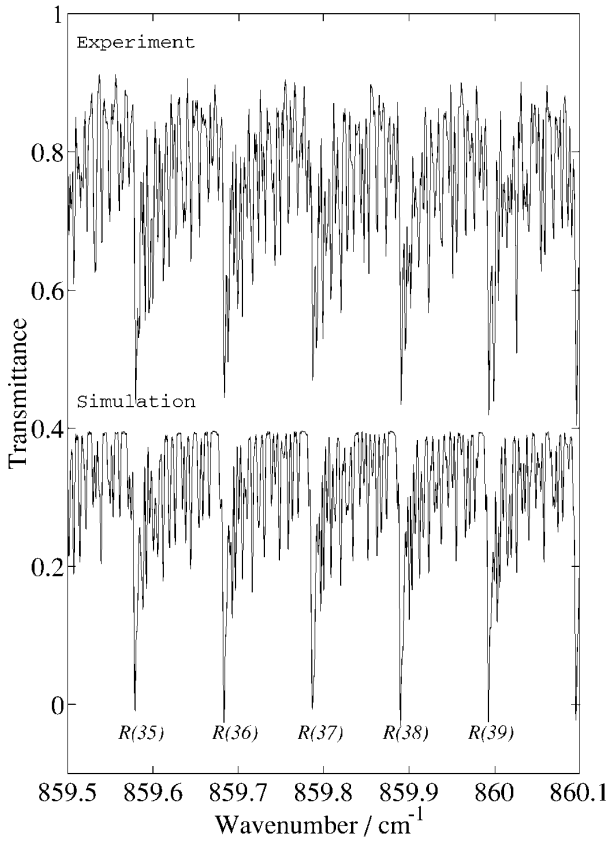

FIG. 4. Part of the ν_1 R branch: experiment and simulation.

and M_f of the two states in the laboratory-fixed frame (LFF). In order to calculate transition intensities, we developed the dipole moment operator through the zeroth order only using the methods explained in Ref. (*25*). The two parameters (one for the "ν_1" parallel band and the other for the "ν_8" perpendicular band) have been set to 1.0 to calculate relative intensities.

4. ANALYSIS AND DISCUSSION

We have performed a step by step analysis. As explained above, we use a dyad model in which the ν_1 and ν_8 bands are strongly linked to each other. As a first step, we have tried to interpret the ν_1 region (840–870 cm^{-1}) by fitting a subset of effective rovibrational parameters (see below). Second, we have fixed this set and fitted some of the remaining parameters to interpret the ν_8 region (900–920 cm^{-1}). Finally, after these two preliminary steps, we could make a global fit of the dyad and of the ground state. For this, $\mathcal{H}_{\{GS\}}$ has been developed to the second order and $\mathcal{H}_{\{\nu_1/\nu_8\}}$ to the fourth order.

The $\nu_1(a_1)$ vibration gives rise to a parallel band. In order to find which parameters could be fitted with only the ν_1 region data, we consider the $\nu_2(a_1)$ parallel band (see Fig. 1). It comes from the $\nu_1(A_{1g})$ band of the "parent" XY_6 molecule. Table 3 lists the corresponding effective Hamiltonian parameters in isolated band scheme up to the fourth order of the development. The parameter labels are the same for any isolated parallel band, in particular for the ν_1 band of interest in the present work. Hereafter, they will be mentioned as "ν_1" parameters and marked by a star ($\star$) in Tables 4, 5, and 6. The other $v = 1$ parameters will be considered as "ν_8" parameters. The correspondence between some of our parameters and the "usual" ones is given in Ref. (*25*).

Preliminary simulations of the ν_1 region were obtained using the model described above and we started from the rotational ground state parameters of Jurek *et al.* (*9–16*). We fixed the "ν_8" parameters to zero, with just one exception. The value of $t_{\{3\}\{3\}}^{0(0,0A_{1g},a_1)F_{1u}F_{1u}E_g} \simeq 2(\omega_8 - \omega_1)/3$ (see below and Ref. (*25*)) has been fixed in this first step around 36.74 cm^{-1}. This number is approximated from the Q branch positions in the experimental FTIR spectrum.

The assignments of this region were realized as follows. We first changed the "ν_1" parameters manually with the aim of obtaining good agreement between the simulated spectrum and the experimental one. After several trials, we could make 1347 assignments up to $J_{max} = 79$. However, for medium and high J values, assignments become more and more difficult to perform because of the problem of overlapping structure between successive J clusters. Nevertheless, it was possible to fit ten "ν_1" parameters as well as three ground state parameters (see Table 4) with a satisfactory global standard deviation of 0.74×10^{-3} cm^{-1}. The successive fits were realized using a new set of programs called C_{4v}TDS derived from HTDS (*27*) and STDS (*30*) software.

In a second step, we tried to analyze the ν_8 region. The ν_8 perpendicular band spectrum is much denser than that of the ν_1 band. It shows no obvious J cluster structure as it was the case for the preceding band. The most characteristic region is the Q-branch central part and it has been the starting point for this preliminary analysis.

For this analysis, all the "ν_1" parameters have been fixed to their values listed in Table 4 except $t_{\{0\}\{0\}A_{1g}A_{1g}A_{1g}}^{4(4,0A_{1g},a_1)}$, as it was the only parameter of the ground state which could be released in this second partial fit. The spectrum being very dense and not well resolved, assignments were very difficult to realize and less certain. So, compared to the ν_1 band, only a few assignments (270) have been performed. But we have been able to determine nine parameters with a global standard deviation of 1.25×10^{-3} cm^{-1}. Among these parameters, two are Coriolis ones ($t_{\{1\}\{1\}F_{1u}F_{1u}F_{1g}}^{1(1,0F_{1g},a_2)}$ and $t_{\{1\}\{1\}F_{1u}F_{1u}F_{1g}}^{1(1,0F_{1g},e)}$ in Table 5) and are important for the Q branch structure of the ν_8 band. All the results of this fit are summarized in Table 5.

Finally, we were able to analyze both bands simultaneously. We added a third set of assignments consisting of 406 ground state combination differences (GSCD) calculated using the ν_1 assignments. All these data can be fitted simultaneously thanks to the vibrational extrapolation which is recalled in Eq. [9].

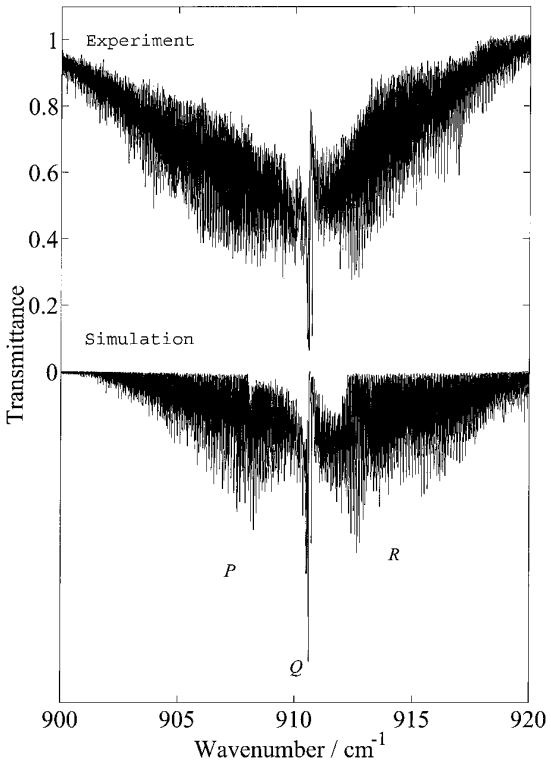

FIG. 5. The ν_8 perpendicular band : experiment and simulation.

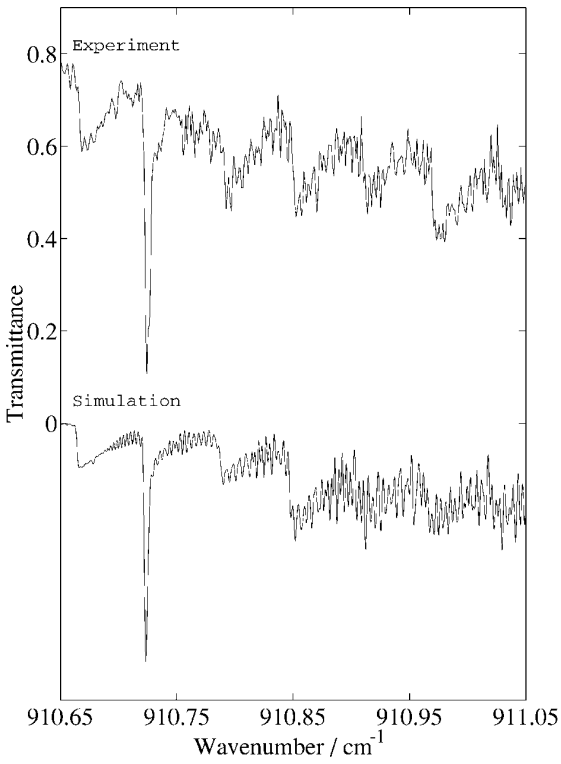

FIG. 7. Part of the ν_8 Q branch: experiment and simulation.

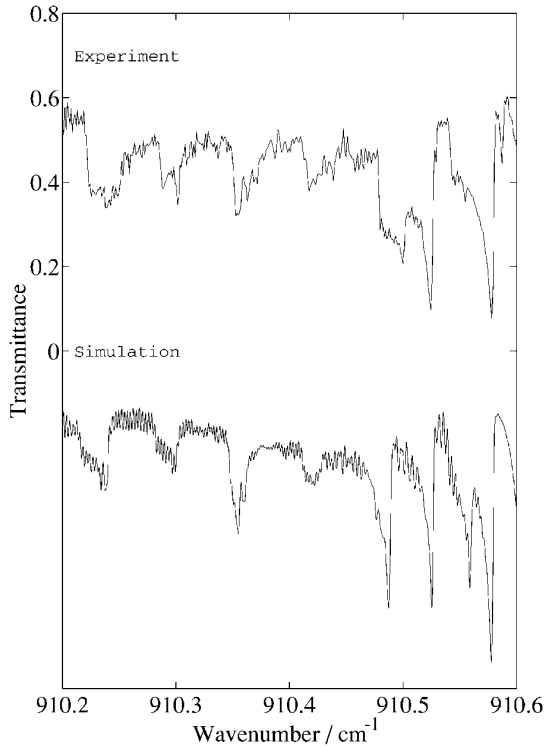

FIG. 6. Part of the ν_8 Q branch: experiment and simulation.

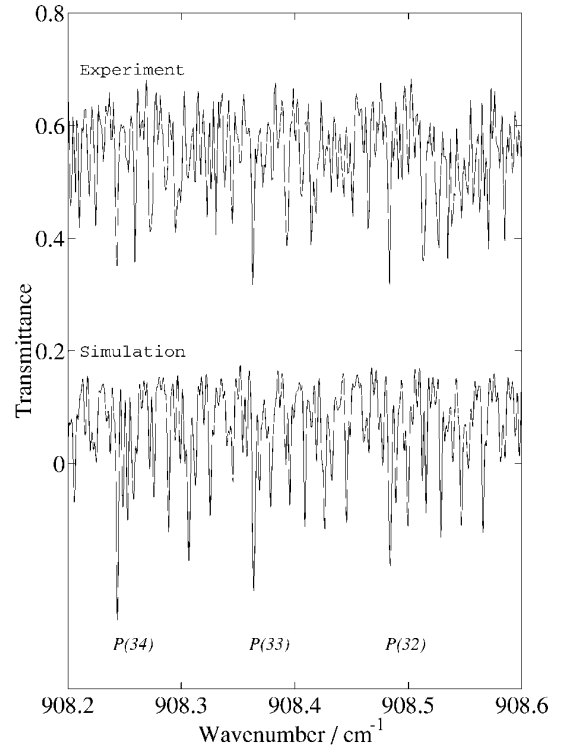

FIG. 8. Part of the ν_8 P branch: experiment and simulation.

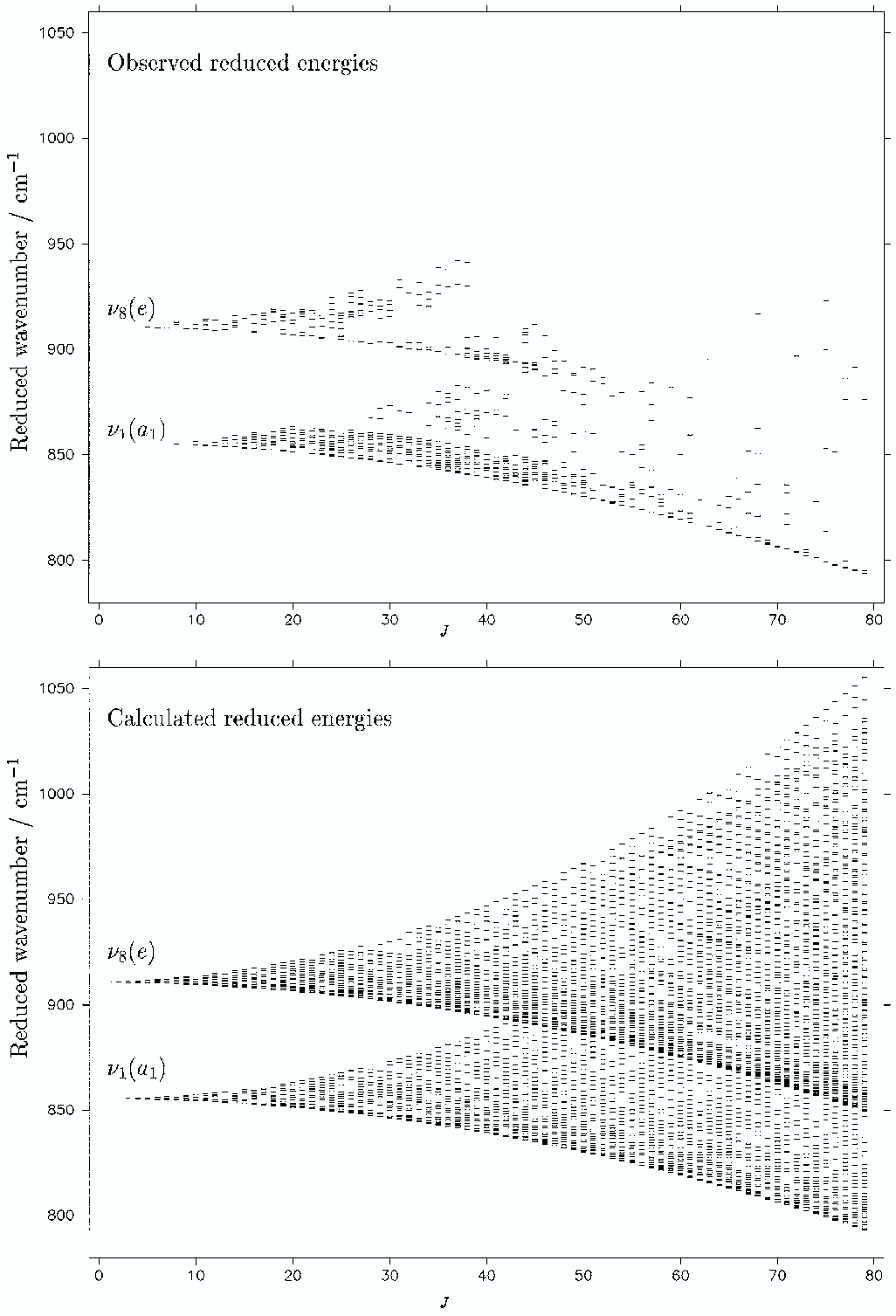

FIG. 9. Reduced observed and calculated energy levels of the ν_1/ν_8 dyad of $SF_5{}^{35}Cl$.

TABLE 7
Effective Harmonic Wavenumbers in cm^{-1}

	Ref. [18]	This work†
ν_1	854.6(2)	855.51103(1)
ν_8	909.0(2)	910.69364(26)

† One standard deviation in parentheses.

All parameters that were determined with physical significance have been freed step by step. It has even been possible, by including more and more assignments, to fit the first two ground state parameters, which are related to the B_0 and C_0 constants as indicated in Table 6 . No more assignments have been realized in the ν_1 region but 81 ones were added for the ν_8 band. In this way, both the ground state and the dyad were fitted simultanously. So 24 parameters were adjusted together and the root mean square for the ground state is equal to 0.64×10^{-3} cm^{-1}. We obtained a standard deviation of 0.82×10^{-3} cm^{-1} for the ν_1 parallel band and of 1.10×10^{-3} cm^{-1} for the ν_8 perpendicular band. In this way, some assigned lines are not purely ν_1 or ν_8 lines but a mixing of both. The resulting parameters are listed in Table 6.

Figures 2 to 8 show synthetic spectra calculated with the parameters of the final fit (see Table 6).

Figure 2 shows the experimental and calculated overview spectra of the $\nu_1(a_1)$ band. It exhibits a clear *P–Q–R* structure. We can notice the presence of other *Q* branches due to hot bands, which should be, $\nu_1 + \nu_6 - \nu_6$, $\nu_1 + \nu_{11} - \nu_{11}$, $\nu_1 + \nu_4 - \nu_4$ or $\nu_1 + \nu_{10} - \nu_{10}$. Having no data on the levels involved in these bands, they have neither been analyzed nor simulated. Figures 3 and 4 show parts of the *P* and *R* branches of the $\nu_1(a_1)$ band, showing good agreement between experiment and theory.

As we can notice in Fig. 3, for low *J* values, the different *J* clusters of the ν_1 band are well separated from each other.

But in Fig. 4, for medium ($\simeq$30) *J* values, we can notice the beginning of overlap between successive structures. This phenomenon is much more important for high ($\geq$70) *J* values. Therefore, assignments become more and more difficult to perform. This type of study is more complex than the analysis of spherical tops like SF_6 [32, 33] or SeF_6 [34, 35] where *J* clusters are always much more distant from each other even for high *J* values (*J* around 70 or even higher).

Figure 5 is an overview of the ν_8 band. The ν_8 lines appear to be superimposed on a broad unresolved structure, which is probably mainly due to hot bands. Figures 6–8 concern detailed views of the ν_8 band and are less satisfactory than those for the ν_1 band. This spectrum being very dense and partially unresolved, the observed lines result from the superimposition of a large number of individual transitions. The disagreement between experiment and simulation spectra is even more visible in Fig. 8, i.e., for medium *J* values. This is mainly due to the fact that in this band the *P–Q–R* branches are much denser. As for the ν_1 band, the spectrum is perturbed by overlap with hot bands.

Figure 9 displays the observed and calculated reduced energy levels for the ν_1/ν_8 dyad. They are obtained by subtracting the scalar terms, i.e.,

$$E_{\text{red}} = E(J, n, \tilde{C}) - t^{2(0,0A_{1g},a_1)A_{1g}A_{1g}A_{1g}}_{\{0\}\{0\}} J(J+1) - t^{4(0,0A_{1g},a_1)A_{1g}A_{1g}A_{1g}}_{\{0\}\{0\}} J^2(J+1)^2. \quad [14]$$

In fact, all our tensorial constants could be written as infinite developments of the "usual" ones. Finally, we have compared our zeroth order parameters and the "usual" ones as given in Ref. (*25*). This correspondence is recalled here:

$$\begin{aligned} t^{2(0,0A_{1g},a_1)A_{1g}A_{1g}A_{1g}}_{\{0\}\{0\}} &= \frac{2B_0 + C_0}{3} + \cdots \\ t^{2(2,0E_g,a_1)A_{1g}A_{1g}A_{1g}}_{\{0\}\{0\}} &= \frac{C_0 - B_0}{2\sqrt{6}} + \cdots \\ t^{0(0,0A_{1g},a_1)F_{1u}F_{1u}E_g}_{\{3\}\{3\}} &= \frac{2(\nu_8 - \nu_1)}{3} + \cdots \\ t^{0(0,0A_{1g},a_1)F_{1u}F_{1u}A_{1g}}_{\{3\}\{3\}} &= \frac{2\nu_8 + \nu_1}{3} + \cdots . \end{aligned} \quad [15]$$

The above formulas result from contact transformations or perturbation theory and higher order terms can be neglected in first approximation. The correspondence is much more difficult to perform for higher-order tensorial parameters. This comes from the different construction of the rotational operators between the Dijon group (*36*) and the "usual" method.

Provided the preceding restrictions, we can deduce approximate values for the effective harmonic frequencies of the ν_1 and ν_8 modes given in Table 7. They are compared to previous values obtained from low-resolution spectroscopy (*18*). We can also recalculate approximate values of the ground state rotational constants (see Table 8) in comparison with those of Jurek *et al.* (*9*). Their C_0 constant was an approximate calculated value (see Eq. [5] of Ref. (*9*)) and their B_0 value is more precise. Our constants are in reasonable agreement with what was previously obtained.

TABLE 8
Ground State Rotational Constants in cm^{-1}

	Ref. [9]	This work†
C_0	0.090203503‡	0.0905136(30)
B_0	0.060861854(3)	0.06085483(30)

† One standard deviation in parentheses.
‡ Calculated value.

5. CONCLUSION

For this first rovibrational analysis of a C_{4v} molecule, we have used an effective Hamiltonian developed through the fourth order. The ν_1/ν_8 dyad of $SF_5{}^{35}Cl$ was analyzed using a new set of programs called C_{4v}TDS, in reference to the sets of programs called HTDS (*27*) and STDS (*30*) for XY_6 and XY_4 molecules, respectively. So we have reestimated the values of the effective harmonic frequencies and also those of ground state rotational constants of zeroth order. Moreover, some other rovibrational parameters have been determined. For the analysis of the $\nu_1(a_1)$ band, the root mean square obtained using 1346 data up to $J_{max} = 79$ is 0.00082 cm^{-1}. For the $\nu_8(e)$ band, the rms is 0.0011 cm^{-1} with 351 data up to $J_{max} = 19$. We have also used 406 GSCD data in the aim of improving the ground state parameters. The ground state rms is 0.00064 cm^{-1}. The rovibrational parameters obtained allow to reproduce the wavenumbers of both bands within the experimental precision. However, the agreement between calculated and experimental spectra is less good for the very dense ν_8 perpendicular band and is quite bad for high J values. This is mainly due to the numerous hot bands located in this spectral region. In order to improve this agreement, we could re-evaluate the ground state rotational constants thanks to a new pure rotational study. One other solution could also be to record the ν_8 band using jet FTIR spectroscopy with the aim of further suppressing hot bands. Moreover, stimulated Raman or CARS spectroscopy could also be investigated with natural SF_5Cl on some fundamental bands, for example ν_2.

ACKNOWLEDGMENTS

The authors thank Professor Hans Bürger very sincerely for providing us with the experimental spectrum and for helpful discussions. Support from the Région Bourgogne for the computer equipment of the Laboratoire de Physique de l'Université de Bourgogne is gratefully acknowledged.

REFERENCES

1. M. Quack, *Infrared Phys.* **29,** 441–466 (1989).
2. Y. He, J. Pochert, M. Quack, R. Ranz, and G. Seyfang, *Faraday Discuss.* **102,** 1–26 (1995).
3. K. K. Irikura, *J. Chem. Phys.* **102,** 5357–5367 (1995).
4. J. T. Herron, *Int. J. Chem. Kinet.* **19,** 129–142 (1987).
5. D. M. Manos and D. L. Flamm, *in* "Plasma Etching: An Introduction." Academic Press, Boston, 1989.
6. V. N. Maller and M. S. Naidu, *in* "Advances in High Voltage Insulation and Arc Interruption in SF_6 and Vacuum," Pergamon, Oxford, 1981.
7. M. E. Sitzmann, W. H. Gilligan, D. L. Ornellas, and J. S. Trasher, *J. Energ. Mat.* **8,** 352–374 (1990).
8. W. T. Sturges, T. J. Wallington, M. D. Hurley, K. P. Shine, K. Sihra, A. Engel, D. E. Oram, S. A. Penkett, R. Mulvaney, and C. A. M. Brenninkmeijer, *Science* **289,** 611–613 (2000).
9. P. Goulet and R. Jurek, *Europhys. Lett.* **15,** 485–490 (1991).
10. P. Goulet and R. Jurek, *Europhys. Lett.* **22,** 425–431 (1993).
11. R. Jurek, A. Poinsot, and P. Goulet, *J. Phys.* **47,** 645–648 (1986).
12. J. Bellet, R. Jurek, and J. Chanussot, *J. Mol. Spectrosc.* **78,** 16–30 (1979).
13. R. Jurek, J. Chanussot, and J. Bellet, *J. Phys.* **37,** 1129–1134 (1976).
14. J. Bellet, R. Jurek, and J. Chanussot, *C. R. Acad. Sci. Paris* **277,** 53–56 (1973).
15. P. Suzeau, R. Jurek, and J. Chanussot, *C. R. Acad. Sci. Paris* **276,** 729–732 (1973).
16. R. Jurek and J. Chanussot, *C. R. Acad. Sci. Paris* **272,** 941–944 (1971).
17. R. E. Noftle, R. R. Smardzewski, and W. B. Fox, *Inorg. Chem.* **16,** 3380–3381 (1977).
18. J. E. Griffiths, *Spectrochim. Acta Part A* **23,** 2145–2157 (1967).
19. L. H. Cross, H. L. Roberts, P. Goggin, and L. A. Woodward, *Trans. Faraday Soc.* **56,** 945–951 (1960).
20. R. R. Smardzewski, R. E. Noftle, and W. B. Fox, *J. Mol. Spectrosc.* **62,** 449–457 (1976).
21. W. V. F. Brooks, M. Eshaque, C. Lau, and J. Passmore, *Can. J. Chem.* **54,** 817–823 (1976).
22. A. C. Legon, *Trans. Faraday Soc.* **65,** 2595–2601 (1969).
23. P. N. Brier, *J. Mol. Spectrosc.* **125,** 233–242 (1987).
24. M. Rotger, V. Boudon, and M. Loëte, *J. Mol. Spectrosc.* **200,** 123–130 (2000).
25. M. Rotger, V. Boudon, and M. Loëte, *J. Mol. Spectrosc.* **200,** 131–137 (2000).
26. N. Cheblal, M. Loëte, and V. Boudon, *J. Mol. Spectrosc.* **197,** 222–231 (1999).
27. Ch. Wenger, V. Boudon, J. P. Champion, and G. Pierre, *J. Quant. Spectrosc. Radiat. Transfer* **66,** 1–16 (2000).
28. G. Guelachvili and K. Narahari Rao, "Handbook of Infrared Standards." Academic Press, San Diego, 1986.
29. J. P. Champion, M. Loëte, and G. Pierre, *in* "Spectroscopy of the Earth's Atmosphere and Interstellar Medium" (K. N. Rao and A. Weber, Eds.), pp. 339–422. Academic Press, San Diego, 1992.
30. Ch. Wenger and J. P. Champion, *J. Quant. Spectrosc. Radiat.* **59,** 471–480 (1998).
31. D. Papoušek and M. R. Aliev, "Molecular Vibrational–Rotational Spectra." Elsevier, New-York (1982).
32. O. Acef, C. Bordé, A. Clairon, G. Pierre, and B. Sartakov, *J. Mol. Spectrosc.* **199,** 188–204 (2000).
33. V. Boudon, G. Pierre, and H. Bürger, *J. Mol. Spectrosc.* **205,** 304–311 (2001).
34. M. Terki-Hassaine, G. Pierre, H. Bürger, and H. Willner, *J. Mol. Spectrosc.* **185,** 93–97 (1997).
35. M. Rotger, V. Boudon, H. Bürger, and H. Willner, *Chem. Phys. Lett.* **339,** 83–88 (2001).
36. J. Moret-Bailly, *Cah. Phys.* **15,** 237–316 (1961).

Journal of Molecular Spectroscopy **216,** 297–307 (2002)
doi:10.1006/jmsp.2002.8635

Spectroscopy of XY_2Z_2 (C_{2v}) Molecules: A Tensorial Formalism Adapted to the $O(3) \supset T_d \supset C_{2v}$ Chain. Application to the Ground State of SO_2F_2

M. Rotger, V. Boudon, and M. Loëte

Laboratoire de Physique de l'Université de Bourgogne, CNRS UMR 5027, 9, Av. Alain Savary, B.P. 47 870, F-21078 DIJON Cedex, France

E-mail: Maud.Rotger@u-bourgogne.fr, Vincent.Boudon@u-bourgogne.fr, Michel.Loete@u-bourgogne.fr

Received March 25, 2002; in revised form June 28, 2002

A tensorial formalism adapted to the case of quasi-spherical XY_2Z_2 asymmetric tops such as SO_2F_2 has been developed as an extension of the usual one for the tetrahedral molecules. We use the $O(3) \supset T_d \supset C_{2v}$ group chain. All the coupling coefficients and formulas for the computation of matrix elements are given for this chain. Such relations are then deduced in the C_{2v} group itself. We also present a development of the Hamiltonian, dipole moment, and polarizability operators for the molecules under consideration using this formalism. These operators are involved in the calculation of the energies and intensities of rovibrational transitions and are essential for spectrum simulations. Expressions for the matrix elements are derived for these operators. A first application to the ground state of SO_2F_2 is presented. Programs for spectrum simulation and fit using these methods are freely available at the URL http://www.u-bourgogne.fr/LPUB/c2vTDS.html.

Key Words: tensorial formalism; XY_2Z_2 quasi-spherical tops; SO_2F_2.

1. INTRODUCTION

The rotational spectroscopy of the quasi-spherical top molecule SO_2F_2 (sulfuryl fluoride) has been investigated recently by microwave Fourier transform spectroscopy and by millimeter-wave spectroscopy (*1*). Some fundamental rovibrational bands have also been recorded thanks to Fourier transform spectroscopy (*2*). However, the analysis of these spectra by conventional methods does not seem to be totally satisfying (*1*). The difficulties arise from the fact that SO_2F_2 corresponds to the specific case of an asymmetric rotor with nearly equal values of all three rotational constants A, B, and C. This species also possess some bands which are extremely close to each other and thus in strong interaction such as the $\nu_3/\nu_7/\nu_9$ triad and the ν_4/ν_5 dyad (*3*). This fact is also linked to the quasi-sphericity of the molecule, as we will show in the following.

In the aim of solving this problem, we propose a new tensorial formalism adapted to the case of C_{2v} asymmetric top molecules of type XY_2Z_2 as an extension of the usual formalism already developed in Dijon for tetrahedral XY_4 molecules in the $O(3) \supset T_d$ group chain (*4, 5*). Such an approach consists in a systematic development of all the rovibrational operators up to any order and for any kind of polyad scheme (*4*). Moreover, it has recently been successfully extended to different nonspherical top molecules such as CH_3D (C_{3v} symmetry (*6, 7*)), SF_5Cl (C_{4v} symmetry (*8–11*)), and C_2H_4 (D_{2h} symmetry (*12*)).

As SO_2F_2 is close to tetrahedral symmetry, we have chosen to work in the $O(3) \supset T_d \supset C_{2v}$ chain; i.e., we perform a reorientation of the $O(3) \supset T_d$ formalism into the C_{2v} subgroup.

In the first part of this article, we briefly recall the basic principles used for the XY_4 molecules and developed in Dijon thanks to the tensorial formalism. Then we extend these principles to the $O(3) \supset T_d \supset C_{2v}$ chain. Coupling coefficients and formulas for the computation of matrix elements of tensor operators are derived for this chain. Coupling coefficients are calculated for the C_{2v} group itself. We use these formulas for calculating the matrix elements of the Hamiltonian, dipole moment and polarizability operators. In the last section, we present a simulation of the pure rotational spectrum of SO_2F_2 in its ground state as a first application of this formalism. In the near future, we intend to use it for the treatment of other rovibrational polyads of this molecule.

2. TENSORIAL ALGEBRA

The methods developed here follow closely the ones we used for a quite similar problem: the orientation in the $O(3) \supset O_h \supset C_{4v}$ chain for XY_5Z molecules with C_{4v} symmetry (*8, 9*). We will thus follow the same scheme as in this reference. However, in the present case, a few simplifications occur, due to the fact that the C_{2v} point group has only nondegenerate irreducible representations.

2.1. Orientation in the $O(3) \supset T_d$ Chain

Let us first recall quickly the basic principles of the orientation in the chain $O(3) \supset T_d$ that is used for XY_4 tetrahedral molecules such as CH_4, CF_4, and SiH_4.

0022-2852/02 $35.00

This has been explained in detail in Refs. (*4, 13–15*), so we will only point out here the essential features of the method.

The $O(3)$ standard basis, say $|j,m\rangle$, is oriented into the T_d subgroup so that we obtain a new oriented basis through

$$|j,nC\sigma\rangle = \sum_m {}^{(j)}G^m_{nC\sigma}\,|j,m\rangle, \qquad [1]$$

where n is a multiplicity index distinguishing C identical irreducible representations of the T_d group within a given j block.

There are several possible methods for finding a G matrix that realizes this orientation. The one that has been retained in preceeding works (*13*) is based on the fact that the Hamiltonian is constructed as a linear combination of spherical tensors that are invariant in T_d:

$$H^{(A_1)} = \sum_k C_k H^{(k,A_1)}. \qquad [2]$$

The G matrix can be obtained by diagonalizing one of these operators. For reasons explained elsewhere (*14–16*), an operator of the type $H^{(4,A_1)}$ (rank four in $O(3)$) is chosen. If we write the matrix elements,

$$\begin{aligned}&\left\langle j,nC\sigma\middle|H^{(4,A_1)}\middle|j,nC\sigma\right\rangle\\ &\quad=\sum_{m,m',q}{}^{(j)}G^{nC\sigma\,(4)}_m G^q_{A_1}\,{}^{(j)}G^{m'}_{nC\sigma}\left\langle j,m\middle|H^{(4)}_q\middle|j,m'\right\rangle,\end{aligned} \qquad [3]$$

and if we apply the Wigner–Eckart theorem on both sides (that is, in T_d and in $O(3)$, respectively), and then simplify by the reduced matrix element $\langle j\|H^{(4)}\|j\rangle$, we can see that the equation above is equivalent to diagonalizing the matrix

$$A(j)^{m'}_m = (-1)^{j-m}\sum_q {}^{(4)}G^q_{A_1}\,\bar{V}\begin{pmatrix}4 & j & j\\ q & -m & m'\end{pmatrix}. \qquad [4]$$

The $\bar{V}$ are Wigner coefficients (*17, 18*). The eigenvectors of this matrix lead to the G matrix, provided that appropriate phase choices are made, as explained in Refs. (*13–15*).

This $|j,nC\sigma\rangle$-oriented basis is the starting point of our work since we will now realize a second reorientation in the C_{2v} subgroup.

In view of further applications to molecules, we follow Refs. (*19, 20*) to set the variances of irreducible tensors and kets. In the *molecule-fixed frame*, we take tensorial sets of type $|\ldots\rangle$ considered as contravariant: $\Psi^m_{(j)}$, and tensorial sets of type $\langle\ldots|$ considered as covariant: $\Psi^{(j)}_m$. The inverse convention is taken in the *laboratory-fixed frame*.

2.2. Orientation in the $O(3) \supset T_d \supset C_{2v}$ Chain

The C_{2v} point group has four symmetry elements. Its character and multiplication tables are recalled in Tables 1 and 2, respectively. Table 3 shows the decomposition of T_d irreducible representations (irreps) into C_{2v} irreps.

TABLE 1
Characters for the Irreducible Representations of C_{2v}

C_{2v}	I	C_2	σ_v	σ'_v
a_1	1	1	1	1
a_2	1	1	−1	−1
b_1	1	−1	1	−1
b_2	1	−1	−1	1

We also define here our notations: all tilded symbols ($\tilde{C}$, $\tilde{F},\ldots$) represent C_{2v} symbols (irreps, coupling coefficients, ...) and primed symbols (F', K', ...) represent oriented coupling coefficients in $T_d \supset C_{2v}$. We also denote the C_{2v} irreps by lower case letters (a_1, a_2, ...) to avoid any confusion with T_d irreps. In the following, $[C]$ is the dimension of the irrep C of T_d. We can notice that all irreps $\tilde{C}$ of C_{2v} have dimension 1 and, as a consequence, it is not necessary to define the components $\tilde{\sigma}$ of these irreps.

We can introduce a new $O(3) \supset T_d \supset C_{2v}$-oriented basis thanks to the following expression:

$$|j,nC,\tilde{C}\rangle = \sum_\sigma {}^{(C)}G'^{\sigma}_{\tilde{C}}\,|j,nC\sigma\rangle. \qquad [5]$$

If we call G' the matrix that realizes the orientation of the ($O(3) \supset$) T_d basis into the C_{2v} subgroup, we have for every element R of C_{2v} (which also pertains to T_d),

$$\begin{aligned}\left[\tilde{D}^{(\tilde{C})}(R)\right] &= \tilde{\chi}^{(\tilde{C})}(R)\\ &= \sum_{\sigma,\sigma'}{}^{(C)}G'^{\tilde{C}}_{\sigma'}\left[D^{(C)}(R)\right]^{\sigma'\,(C)}_{\sigma}G'^{\sigma}_{\tilde{C}},\end{aligned} \qquad [6]$$

for a given irreducible representation $\tilde{C}$ of C_{2v}. D and $\tilde{D}$ are the matrices of R in T_d and C_{2v}, respectively. All the D matrices being of dimension 1, they are equal to their character $\tilde{\chi}$.

To calculate the G' matrix we use the projection method as follows. We apply to the $|C,\sigma\rangle$ basis functions of T_d the projector (*21*)

$$P^{(\tilde{C})} = \frac{1}{[C_{2v}]}\sum_{R\in C_{2v}}\tilde{\chi}^{(\tilde{C})}(R)P_R, \qquad [7]$$

TABLE 2
Multiplication Table for the Irreducible Representations of C_{2v}

	a_1	a_2	b_1	b_2
a_1	a_1	a_2	b_1	b_2
a_2	a_2	a_1	b_2	b_1
b_1	b_1	b_2	a_1	a_2
b_2	b_2	b_1	a_2	a_1

TABLE 3
$T_d \supset C_{2v}$ Correlation Table

C	$\tilde{C}$
A_1	a_1
A_2	a_2
E	$a_1 + a_2$
F_1	$a_2 + b_1 + b_2$
F_2	$a_1 + b_1 + b_2$

where $[C_{2v}] = 4$ (number of elements in C_{2v}) and with

$$P_R|C,\sigma\rangle = \sum_{\sigma'} \left[D^{(C)}(R)\right]^{\sigma'}_{\sigma} |C,\sigma'\rangle, \qquad [8]$$

which defines the action of the symmetry element R on $|C,\sigma\rangle$. We have thus

$$|C,\tilde{C}\rangle = P^{(\tilde{C})}|C,\sigma\rangle. \qquad [9]$$

We are now able to calculate each G' value as given in Table 4. We can therefore build the oriented basis $|j,\ nC,\tilde{C}\rangle$.

In the following, we will put particular attention on the different phase choices to be made, since these are essential to obtain consistent phases for all the coupling coefficients and formulas developed hereafter.

In a general way, the contra–covariant change for symmetrized operators is made using the metric tensor (*19*)

$$\begin{aligned} T^{(C)}_{\tilde{C}} &= \varepsilon_C \begin{pmatrix} C \\ \tilde{C}\ \tilde{C}' \end{pmatrix} T^{\tilde{C}'}_{(C)}, \\ T^{\tilde{C}}_{(C)} &= \varepsilon'_C \begin{pmatrix} \tilde{C}'\ \tilde{C} \\ C \end{pmatrix} T^{(C)}_{\tilde{C}'}. \end{aligned} \qquad [10]$$

We adopt here Einstein's summation convention. ε_C and ε'_C are phase factors to be chosen. We choose here a real metric tensor and an involutive transformation; thus we have $\varepsilon_C = \varepsilon'_C$ and $\varepsilon^2_C = 1$. In order to match what has been done for the $O(3) \supset T_d$ chain, we define our F' oriented coupling coefficients in terms of the F ones of T_d (*13*) by

$$F'^{\begin{pmatrix} C_1 & C_2 & C_3 \\ \tilde{C}_1 & \tilde{C}_2 & \tilde{C}_3 \end{pmatrix}} = \sum_{\sigma_1,\sigma_2,\sigma_3} {}^{(C_1)}G'^{\sigma_1(C_2)}_{\tilde{C}_1} G'^{\sigma_2(C_3)}_{\tilde{C}_2} G'^{\sigma_3}_{\tilde{C}_3} F^{\begin{pmatrix} C_1 & C_2 & C_3 \\ \sigma_1 & \sigma_2 & \sigma_3 \end{pmatrix}}. \qquad [11]$$

As explained in Ref. (*19*), the various coupling coefficients for two irreducible tensors can be related by the general relations

$$\begin{aligned} &F'^{\begin{pmatrix} \tilde{C}_1 & \tilde{C}_2 & (C_3) \\ (C_1 & C_2) & \tilde{C}_3 \end{pmatrix}} \\ &= K(C_1C_2C_3) \begin{pmatrix} C_3 \\ \tilde{C}_3\ \tilde{C}'_3 \end{pmatrix} \begin{pmatrix} \tilde{C}'_1\ \tilde{C}_1 \\ C_1 \end{pmatrix} \begin{pmatrix} \tilde{C}'_2\ \tilde{C}_2 \\ C_2 \end{pmatrix} \\ &\quad \times F'^{\begin{pmatrix} (C_1 & C_2) & \tilde{C}'_3 \\ C'_1 & C'_2 & (C_3) \end{pmatrix}}, \end{aligned} \qquad [12]$$

$$\begin{aligned} &F'^{\begin{pmatrix} \tilde{C}_1 & \tilde{C}_2 & \tilde{C}_3 \\ (C_1 & C_2 & C_3) \end{pmatrix}} \\ &= K'(C_1C_2C_3) \begin{pmatrix} \tilde{C}'_1\ \tilde{C}_1 \\ C_1 \end{pmatrix} \begin{pmatrix} \tilde{C}'_2\ \tilde{C}_2 \\ C_2 \end{pmatrix} \begin{pmatrix} \tilde{C}'_3\ \tilde{C}_3 \\ C_3 \end{pmatrix} \\ &\quad \times F'^{\begin{pmatrix} (C_1 & C_2 & C_3) \\ \tilde{C}'_1 & \tilde{C}'_2 & \tilde{C}'_3 \end{pmatrix}}, \end{aligned} \qquad [13]$$

$$\begin{aligned} &F'^{\begin{pmatrix} (C_1 & C_2) & \tilde{C}_3 \\ C_1 & C_2 & (C_3) \end{pmatrix}} \\ &= \varepsilon_{C_3}\, e^{i\phi(C_1C_2C_3)}\, [C_3]^{\frac{1}{2}} \begin{pmatrix} \tilde{C}'_3\ \tilde{C}_3 \\ C_3 \end{pmatrix} F'^{\begin{pmatrix} (C_1 & C_2 & C_3) \\ \tilde{C}_1 & \tilde{C}_2 & \tilde{C}_3 \end{pmatrix}}, \end{aligned} \qquad [14]$$

$$\begin{aligned} &F'^{\begin{pmatrix} \tilde{C}_1 & \tilde{C}_2 & (\tilde{C}_3) \\ (C_1 & C_2) & \tilde{C}_3 \end{pmatrix}} \\ &= \varepsilon'_{C_3}\, e^{i\phi(C_1C_2C_3)}\, [C_3]^{\frac{1}{2}} \begin{pmatrix} C_3 \\ \tilde{C}_3\ \tilde{C}'_3 \end{pmatrix} F'^{\begin{pmatrix} \tilde{C}_1 & \tilde{C}_2 & \tilde{C}'_3 \\ (C_1 & C_2 & C_3) \end{pmatrix}}, \end{aligned} \qquad [15]$$

where $[C_3]$ is the dimension of the C_3 representation of T_d. For a consistent symmetry adaptation in $T_d \supset C_{2v}$, the phase factors $K(C_1C_2C_3)$, $K'(C_1C_2C_3)$, $e^{i\phi(C_1C_2C_3)}$, $e^{i\psi(C_1C_2C_3)}$ must be carefully chosen. We make here similar choices as in Ref. (*14*) in order to be consistent with the works on the $O(3) \supset T_d$ chain; that is,

$$\varepsilon_{C_3} = \varepsilon'_{C_3} = 1, \qquad [16]$$

$$K(C_1C_2C_3) = (-1)^{2C_3}, \quad K'(C_1C_2C_3) = 1, \qquad [17]$$

TABLE 4
The G' Coefficients for the $T_d \supset C_{2v}$-Orientation

C	σ	$\tilde{C}$	G'
A_1		a_1	1
A_2		a_2	1
E	1	a_1	1
E	2	a_2	1
F_1	x	b_1	$1/\sqrt{2}$
F_1	y	b_1	$-1/\sqrt{2}$
F_1	x	b_2	$1/\sqrt{2}$
F_1	y	b_2	$1/\sqrt{2}$
F_1	z	a_2	1
F_2	x	b_1	$1/\sqrt{2}$
F_2	y	b_1	$1/\sqrt{2}$
F_2	x	b_2	$1/\sqrt{2}$
F_2	y	b_2	$-1/\sqrt{2}$
F_2	z	a_1	1

$$e^{i\phi(C_1C_2C_3)} = (-1)^{2C_1}, \quad [18]$$

$$e^{i\psi(C_1C_2C_3)} = (-1)^{2C_2}. \quad [19]$$

The preceeding equations [12]–[15] reduce to relations similar to those between the Clebsch–Gordan and $3C-\sigma$ coefficients for $O(3)\supset T_d$. We have then

$$\begin{pmatrix} \tilde{C} & \tilde{C}' \\ C & \end{pmatrix} \equiv \begin{pmatrix} C \\ \tilde{C}\,\tilde{C}' \end{pmatrix} = (-1)^{2C}\begin{pmatrix} C \\ \tilde{C}'\,\tilde{C} \end{pmatrix}$$

$$= [C]^{\frac{1}{2}} F'^{\begin{pmatrix} C & A_1 & C \\ \tilde{C} & a_1 & \tilde{C}' \end{pmatrix}} = \delta_{\tilde{C},\tilde{C}'}, \quad [20]$$

and all the F' coefficients are real.

Within our $O(3)\supset T_d\supset C_{2v}$ chain the Wigner–Eckart theorem, for covariant quantities, can be written

$$\left\langle \Psi^{(C')}_{\tilde{C}'} \middle| T^{(\Gamma)}_{\tilde{\Gamma}} \middle| \Psi^{(C)}_{\tilde{C}} \right\rangle = F'^{\begin{pmatrix} \Gamma & C & C' \\ \tilde{\Gamma} & \tilde{C} & \tilde{C}' \end{pmatrix}} \langle C' \| T^{(\Gamma)} \| C \rangle \quad [21]$$

with the choice $e^{i\Phi_E}=1$ as in preceeding works (*14*).

2.3. $3\tilde{C}-\tilde{\sigma}$ Coefficients and the Wigner–Eckart Theorem in C_{2v}

We are now able to deduce $3\tilde{C}-\tilde{\sigma}$ coupling coefficients for the C_{2v} group itself. We follow a method given by Lulek in Refs. (*22, 23*) and used in Ref. (*14*). This method is based on the use of Racah's factorization lemma, which can be written here as

$$F'^{\begin{pmatrix} C_1 & C_2 & C_3 \\ \tilde{C}_1 & \tilde{C}_2 & \tilde{C}_3 \end{pmatrix}} = K'^{\begin{pmatrix} C_1 & C_2 & C_3 \\ (\tilde{C}_1 & \tilde{C}_2 & \tilde{C}_3) \end{pmatrix}} \times \tilde{F}(\tilde{C}_1\ \tilde{C}_2\ \tilde{C}_3), \quad [22]$$

where F' is one of our $T_d\supset C_{2v}$ oriented $3C$ coefficients, $\tilde{F}$ is a $3\tilde{C}-\tilde{\sigma}$ coefficient for C_{2v} and K' an $T_d\supset C_{2v}$ isoscalar factor. Again, the absence of $\tilde{\sigma}$ components for C_{2v} simplifies the notation.

The $3\tilde{C}-\tilde{\sigma}$ matrix being unitary, we have here simply

$$\left| K'^{\begin{pmatrix} C_1 & C_2 & C_3 \\ (\tilde{C}_1 & \tilde{C}_2 & \tilde{C}_3) \end{pmatrix}} \right|^2 = \left| F'^{\begin{pmatrix} C_1 & C_2 & C_3 \\ \tilde{C}_1 & \tilde{C}_2 & \tilde{C}_3 \end{pmatrix}} \right|^2. \quad [23]$$

This remark, along with Eq. [22], leads to the desired $3\tilde{C}-\tilde{\sigma}$ coefficients in a trivial way,

$$\tilde{F}(\tilde{C}_1\ \tilde{C}_2\ \tilde{C}_3), = \epsilon_{\tilde{C}_1\tilde{C}_2\tilde{C}_3} = 1, \quad [24]$$

where $\epsilon_{\tilde{C}_1\tilde{C}_2\tilde{C}_3}$ is an arbitrary phase factor that has been fixed to 1 for simplicity. In other words, this means that all our $\tilde{F}$ coefficients are equal to one if $\tilde{C}_1\otimes\tilde{C}_2=\tilde{C}_3$ and to zero otherwise. This makes the C_{2v} algebra extremely simple. This also implies that the F' and K' coefficients are identical and are left unchanged by any even permutation of their columns and that for an odd permutation they are multiplied by the factor

$$(-1)^{C_1+C_2+C_3}. \quad [25]$$

It follows immediately that the Wigner–Eckart theorem in C_{2v} can be expressed (for covariants sets) by the very simple relation

$$\left\langle \Psi^{(\tilde{C}')} \middle| T^{(\tilde{C}_0)} \middle| \Psi^{(\tilde{C})} \right\rangle = \left\langle \tilde{C}' \middle\| T^{(\tilde{C}_0)} \middle\| \tilde{C} \right\rangle, \quad [26]$$

again with $e^{i\Phi_E}=1$ (*14*).

We can also note a useful formula, which relates the reduced matrix elements in C_{2v} of a symmetry-adapted tensor to those in T_d,

$$\left\langle C'\tilde{C}' \middle\| T^{(C_0,\tilde{C}_0)} \middle\| C\tilde{C} \right\rangle = K'^{\begin{pmatrix} C_0 & C & C' \\ (\tilde{C}_0 & \tilde{C} & \tilde{C}') \end{pmatrix}} \left\langle C' \middle\| T^{(C_0)} \middle\| C \right\rangle, \quad [27]$$

as well as the formula relating reduced matrix elements in $O(3)$ or C_{2v} for an $O(3)\supset T_d\supset C_{2v}$-oriented tensor,

$$\left\langle j'n'C'\tilde{C}' \middle\| T^{(j_0,n_0C_0,\tilde{C}_0)} \middle\| jnC\tilde{C} \right\rangle$$

$$= (-1)^{j'} K'^{\begin{pmatrix} j_0 & j & j' \\ (n_0C_0 & nC & n'C') \end{pmatrix}} K'^{\begin{pmatrix} C_0 & C & C' \\ (\tilde{C}_0 & \tilde{C} & \tilde{C}') \end{pmatrix}} \left\langle j' \middle\| T^{(j_0)} \middle\| j \right\rangle. \quad [28]$$

2.4. Recoupling Coefficients for C_{2v}

We will now consider briefly the recoupling coefficients for C_{2v}. By analogy with what has been done by Fano and Racah (*17*) for $O(3)$ and in Refs. (*13, 14*) for $O(3)\supset T_d$, we can define $6\tilde{C}$ coefficients from the recoupling matrix for three irreducible representations by the relation

$$\| |\tilde{C}_1\rangle \times |\tilde{C}_2\rangle; \tilde{C}_{12}\rangle \times |\tilde{C}_3\rangle; \tilde{C}\rangle$$

$$= \sum_{\tilde{C}_{23}} \begin{Bmatrix} \tilde{C}_1 & \tilde{C}_2 & \tilde{C}_{12} \\ \tilde{C}_3 & \tilde{C} & \tilde{C}_{23} \end{Bmatrix} \| |\tilde{C}_1\rangle \times \|\tilde{C}_2\rangle \times |\tilde{C}_3\rangle; \tilde{C}_{23}\rangle; \tilde{C}\rangle. \quad [29]$$

Considering the very simple multiplication table for the C_{2v} irreps (see Table 2), it is clear that in fact there is always only one possibility for $\tilde{C}_{23}$ and thus the sum vanishes in the preceding formula. Expanding the two members of expression [29] and taking the very simple values of the $3C-\sigma$ [24] into account, we can deduce that the C_{2v} $6C$ symbols are equal to 1 if the following conditions are verified,

$$\begin{cases} \tilde{C}_1 \otimes \tilde{C}_{23} \supset \tilde{C}, \\ \tilde{C}_2 \otimes \tilde{C}_3 \supset \tilde{C}_{23}, \\ \tilde{C}_{12} \otimes \tilde{C}_3 \supset \tilde{C}, \\ \tilde{C}_1 \otimes \tilde{C}_2 \supset \tilde{C}_{12}, \end{cases} \quad [30]$$

and to 0 otherwise.

It is then possible to show that in the present case the reduced matrix elements of two coupled tensor operators of C_{2v} acting on the same space is just a product of two reduced matrix elements,

$$\langle \tilde{C}' \| [T^{(\tilde{C}_1)} \times T^{(\tilde{C}_2)}]^{(\tilde{C}_0)} \| \tilde{C} \rangle = \langle \tilde{C}' \| T^{(\tilde{C}_1)} \| \tilde{C}'' \rangle \langle \tilde{C}'' \| T^{(\tilde{C}_2)} \| \tilde{C} \rangle, \quad [31]$$

with $\tilde{C}''$ such that

$$\tilde{C}'' = \tilde{C}' \otimes C_1 = \tilde{C} \otimes \tilde{C}_2. \quad [32]$$

In the same way, we can define the $9\tilde{C}$ symbols by

$$\begin{aligned} &\| |\tilde{C}_1\rangle \times |\tilde{C}_2\rangle; \tilde{C}_{12}\rangle \times \| |\tilde{C}_3\rangle \times |\tilde{C}_4\rangle; \tilde{C}_{34}\rangle; \tilde{C}\rangle \\ &= \begin{Bmatrix} \tilde{C}_1 & \tilde{C}_2 & \tilde{C}_{12} \\ \tilde{C}_3 & \tilde{C}_4 & \tilde{C}_{34} \\ \tilde{C}_{13} & \tilde{C}_{24} & \tilde{C} \end{Bmatrix} \times \| |\tilde{C}_1\rangle \times |\tilde{C}_3\rangle; \tilde{C}_{13}\rangle \\ &\times \| |\tilde{C}_2\rangle \times |\tilde{C}_4\rangle; \tilde{C}_{24}\rangle; \tilde{C}\rangle. \end{aligned} \quad [33]$$

And again, the $9C$ values are trivial, since they are equal to 1 if the six following triangular conditions are verified,

$$\begin{cases} \tilde{C}_1 \otimes \tilde{C}_2 \supset \tilde{C}_{12}, \\ \tilde{C}_3 \otimes \tilde{C}_4 \supset \tilde{C}_{34}, \\ \tilde{C}_{13} \otimes \tilde{C}_4 \supset \tilde{C}, \\ \tilde{C}_1 \otimes \tilde{C}_3 \supset \tilde{C}_{13}, \\ \tilde{C}_2 \otimes \tilde{C}_4 \supset \tilde{C}_{24}, \\ \tilde{C}_{12} \otimes \tilde{C}_{34} \supset \tilde{C}, \end{cases} \quad [34]$$

and to zero otherwise.

This enables us to express the reduced matrix elements of two coupled tensor operators acting on two different spaces:

$$\begin{aligned} &\langle \tilde{C}'_1 \tilde{C}'_2, \tilde{C}' \| [T^{(\tilde{\Gamma}_1)} \times U^{(\tilde{\Gamma}_2)}]^{(\tilde{\Gamma}_0)} \| \tilde{C}_1 \tilde{C}_2, \tilde{C} \rangle \\ &= \langle \tilde{C}'_1 \| T^{(\tilde{\Gamma}_1)} \| \tilde{C}_1 \rangle \langle \tilde{C}'_2 \| U^{(\tilde{\Gamma}_2)} \| \tilde{C}_2 \rangle. \end{aligned} \quad [35]$$

3. GENERALITIES ABOUT HAMILTONIAN AND TRANSITION MOMENT OPERATORS

In this section, we recall briefly the basic principles of the expansion of the Hamiltonian and transition moment operators. This is valuable for any polyatomic molecule and can be found in detail for example in Ref. (*24*).

3.1. Transformed Operators

Successive Van Vleck contact transformations are generally applied to the Hamiltonian and transition moment operators. The aim of these contact transformations is to introduce appropriate basis functions in which the transformed Hamiltonian $\tilde{H}$ has a completely diagonal or block diagonal form with respect to some vibrational subspace. These subspaces of close vibrational levels correspond to the so-called polyads.

If A represents either H (Hamiltonian), μ (dipole moment) or α (polarizability), the transformed operator $\tilde{A}$ is given by:

$$\tilde{A} = TAT^{-1} = A + i[S, A] - \frac{1}{2}[S, [S, A]] + \cdots, \quad [36]$$

with $T = e^{iS}$. S is a Hermitian operator and is called the generator of the contact transformation. It has been shown that S is always a sum of rovibrational operators (*4*).

3.2. Dipole Moment

The dipole moment components in the laboratory-fixed frame (LFF) μ_Θ with $\Theta = X$, Y, or Z can be related to the components μ_θ with $\theta = x$, y or z in the molecule-fixed frame (MFF) by

$$\mu_\Theta = \sum_\theta \lambda_{\Theta,\theta} \mu_\theta, \quad [37]$$

where $\lambda_{\Theta,\theta}$ are the direction cosines.

In the small amplitude motion approximation one can expand each component μ_θ as a power series in the dimensionless normal coordinates $q_{s,\sigma}$ (where s is the oscillator index and the σ's are its components),

$$\begin{aligned} \mu_\theta = \mu_\theta^e &+ \sum_{s,\sigma} \left(\frac{\partial \mu_\theta}{\partial q_{s,\sigma}} \right)_e q_{s,\sigma} \\ &+ \frac{1}{2} \sum_{s,\sigma,s',\sigma'} \left(\frac{\partial^2 \mu_\theta}{\partial q_{s,\sigma} \partial q_{s',\sigma'}} \right) q_{s,\sigma} q_{s',\sigma'}, \end{aligned} \quad [38]$$

where μ_θ^e is the permanent dipole moment of the molecule if it exists. The other terms are induced by molecular vibrations.

One can show that the LFF components of the transformed dipole moment can be written in the symmetrized form (*4*) as follows:

$$\tilde{\mu}_\Theta = \frac{1}{2} \sum_\theta (\lambda_{\Theta,\theta} \tilde{\mu}_\theta + \tilde{\mu}_\theta \lambda_{\Theta,\theta}). \quad [39]$$

Like the contact transformation generator S, $\tilde{\mu}_\theta$, $\tilde{\mu}_\Theta$ are also sums of rovibrational operators, as implied by Eq. [36].

To establish the expressions of $\tilde{\mu}_\theta$ and $\tilde{\mu}_\Theta$, it is necessary to introduce in a first step the spherical components of the dipole moment operator. The LFF spherical components, denoted $\mu_m^{(1)}$, are related to the MFF ones $\mu_k^{(1)}$ through (*4*)

$$\mu_m^{(1)} = \sum_k \mathcal{D}_{km}^{(1)} \mu_k^{(1)}, \quad [40]$$

where the $\mathcal{D}_{km}^{(1)}$ are Wigner's harmonic functions (*25*) ($k, m = -1$, 0, or 1). The Cartesian and spherical components in both

frames are linked through the relations

$$\mu_\Theta = \sum_m \langle 1; m|\Theta\rangle \mu_m^{(1)}, \quad [41]$$

$$\mu_\theta = \sum_k \langle 1; k|\theta\rangle \mu_k^{(1)}, \quad [42]$$

where the $\langle 1; m|\Theta\rangle$ and $\langle 1; k|\theta\rangle$ are called Stone coefficients (*26*).

3.3. Polarizability

The application of an electric field E to the molecules induces a dipole moment, defined as

$$\mu_{\Theta_1} = \sum_{\Theta_2} \alpha_{\Theta_1\Theta_2} E_{\Theta_2}, \quad [43]$$

where $\alpha_{\Theta_1\Theta_2}$ is a LFF component of the polarizability tensor.

We can relate them to the MFF components $\alpha_{\theta_1\theta_2}$ through

$$\alpha_{\Theta_1\Theta_2} = \sum_{\theta_1,\theta_2} \lambda_{\Theta_1,\theta_1}\lambda_{\Theta_2,\theta_2}\alpha_{\theta_1\theta_2}, \quad [44]$$

where $\lambda_{\Theta_1,\theta_1}$ and $\lambda_{\Theta_2,\theta_2}$ are the direction cosines.

As for the dipole moment, we can develop the $\alpha_{\theta_1\theta_2}$ as a series of dimensionless normal coordinates such as

$$\alpha_{\theta_1\theta_2} = \alpha^e_{\theta_1\theta_2} + \sum_{s,\sigma}\left(\frac{\partial\alpha_{\theta_1\theta_2}}{\partial q_{s,\sigma}}\right)_e q_{s,\sigma} + \frac{1}{2}\sum_{s,\sigma,s',\sigma'}\left(\frac{\partial^2\alpha_{\theta_1\theta_2}}{\partial q_{s,\sigma}\partial q_{s',\sigma'}}\right)_e q_{s,\sigma}q_{s',\sigma'} + \cdots, \quad [45]$$

where $\alpha^e_{\theta_1\theta_2}$ is the permanent polarizability, if it exists. The other terms are induced by molecular vibrations.

Just as for the dipole moment, one has to consider the transformed polarizability and in the LFF we have

$$\tilde{\alpha}_{\Theta_1\Theta_2} = \frac{1}{2}\sum_\theta \left(\lambda_{\Theta_1,\theta_1}\lambda_{\Theta_2,\theta_2}\tilde{\alpha}_{\theta_1\theta_2} + \tilde{\alpha}_{\theta_1\theta_2}\lambda_{\Theta_1,\theta_1}\lambda_{\Theta_2,\theta_2}\right). \quad [46]$$

The spherical components in the LFF ($\alpha_m^{(L)}$) and in the MFF ($\alpha_k^{(L)}$) are linked through:

$$\alpha_m^{(L)} = \sum_k \mathcal{D}^{(L)}_{km}\alpha_k^{(L)}, \quad [47]$$

where L takes only the values 0 and 2. For the $\mathcal{D}^{(L)}_{km}$ Wigner's harmonics [25] $L=0$ implies $m,k=0$ and $L=2$ implies $m,k=0,\pm1,\pm2$.

Finally, we have

$$\alpha_{\Theta_1\Theta_2} = \sum_{L,m}\langle L; m|\Theta_1\Theta_2\rangle\alpha_m^{(L)}, \quad [48]$$

$$\alpha_{\theta_1\theta_2} = \sum_{L,k}\langle L; k|\theta_1\theta_2\rangle\alpha_k^{(L)}, \quad [49]$$

where the $\langle L; m|\Theta_1\Theta_2\rangle$ and $\langle L; k|\theta_1\theta_2\rangle$ are Stone coefficients (*26*).

4. TENSORIAL DEVELOPMENT OF THE HAMILTONIAN AND TRANSITION MOMENT OPERATORS FOR XY_2Z_2 (C_{2v}) ASYMMETRIC TOP MOLECULES

In this section, we will focus on the particularities of the tensorial expressions of the Hamiltonian and transition moments in the C_{2v} group. Table 5 shows the symmetries of the Hamiltonian, dipole moment and polarizability operators in the LFF and MFF for T_d and C_{2v} symmetry groups.

4.1. Expression of the Hamiltonian

The initial (or untransformed) Hamiltonian is expanded as a series of rovibrational operators which are denoted $T^{\Omega(K,n\Gamma,\tilde{\Gamma})\Gamma_1\Gamma_2\Gamma_v}_{\{n_s\}\{m_s\}}$,

$$H = \sum_{\text{all indexes}} t^{\Omega(K,n\Gamma,\tilde{\Gamma})\Gamma_1\Gamma_2\Gamma_v}_{\{n_s\}\{m_s\}} T^{\Omega(K,n\Gamma,\tilde{\Gamma})\Gamma_1\Gamma_2\Gamma_v}_{\{n_s\}\{m_s\}}, \quad [50]$$

with the coupled rovibrational operators

$$T^{\Omega(K,n\Gamma,\tilde{\Gamma})\Gamma_1\Gamma_2\Gamma_v}_{\{n_s\}\{m_s\}} = \left(R^{\Omega(K,n\Gamma,\tilde{\Gamma})} \otimes {}^{\varepsilon}V^{\Gamma_1\Gamma_2(\Gamma_v,\tilde{\Gamma})}_{\{n_s\}\{m_s\}}\right)^{(a_1)}, \quad [51]$$

where $\Omega \le 2$. The $t^{\Omega(K,n\Gamma,\tilde{\Gamma})\Gamma_1\Gamma_2\Gamma_v}_{\{n_s\}\{m_s\}}$ are the parameters of the model. The $R^{\Omega(K,n\Gamma)}$ (rotational) and ${}^{\varepsilon}V^{\Gamma_1\Gamma_2(\Gamma_v)}_{\{n_s\}\{m_s\}}$ (vibrational) operators are constructed exactly in the same way as in T_d (*5*). They are oriented in C_{2v} using

$$A^{(\Gamma,\tilde{\Gamma})} = \sum_\gamma {}^{(\Gamma)}G^{\gamma}_{\tilde{\Gamma}} A^{(\Gamma)}_\gamma. \quad [52]$$

The expression of the rotational and vibrational operators is detailed in Ref. (*4*). G' coefficients are given in Table 4. To ensure that H is unchanged under time reversal, the parity ε

TABLE 5

Symmetry of the Hamiltonian (H), Dipole Moment (μ) and Polarizability (α) Operators Expressed in the Molecular-Fixed Frame (MFF) and Laboratory-Fixed Frame (LFF) for Molecules Belonging to T_d and C_{2v} Symmetry Groups

	T_d		C_{2v}	
Operator	MFF	LFF	MFF	LFF
H	A_1	A_1	a_1	a_1
μ	F_2	A_2	$a_2 \oplus b_1 \oplus b_2$	a_2
α	$A_1 \oplus E \oplus F_2$	A_1	$3a_1 \oplus a_2 \oplus b_1 \oplus b_2$	a_1

of the vibrational operators in the conjugate momenta $p_{s,\sigma}$ is related to the rotational degree Ω through

$$\varepsilon = (-1)^{\Omega}. \qquad [53]$$

The order of the development is defined as $\Omega + \Omega_v - 2$, Ω_v being the degree of ${}^{\varepsilon}V^{\Gamma_1\Gamma_2(\Gamma_v)}_{\{n_s\}\{m_s\}}$ in the a^+ (creation) and a (annihilation) operators.

The transformed Hamiltonian has the same form as the initial one; that is,

$$\tilde{H} = \sum_{\text{all indexes}} \tilde{I}^{\Omega(K,n\Gamma,\tilde{\Gamma}')\Gamma_1\Gamma_2\Gamma_v}_{\{n_s\}\{m_s\}} T^{\Omega(K,n\Gamma,\tilde{\Gamma}')\Gamma_1\Gamma_2\Gamma_v}_{\{n_s\}\{m_s\}}, \qquad [54]$$

where the transformed parameter set $\{\tilde{I}^{\Omega(K,n\Gamma,\tilde{\Gamma}')\Gamma_1\Gamma_2\Gamma_v}_{\{n_s\}\{m_s\}}\}$ depends both on the initial parameter set denoted $\{I^{\Omega(K,n\Gamma,\tilde{\Gamma}')\Gamma_1\Gamma_2\Gamma_v}_{\{n_s\}\{m_s\}}\}$ and on the set of parameters of the contact transformation operator S.

In the following, we use the rovibrational coupled basis

$$\left|\left[\Psi^{(J,nC_r,\tilde{C}_r)}_r \otimes \Psi^{(C_v,\tilde{C}_v)}_v\right]^{(\tilde{C})}\right\rangle, \qquad [55]$$

where $\Psi^{(J,nC_r,\tilde{C}_r)}_r$ is the rotational basis and $\Psi^{(C_v,\tilde{C}_v)}_v$ the vibrational one, with

$$\left|\Psi^{(C_v,\tilde{C}_v)}_v\right\rangle = \left|\left[\left[\Psi^{(A_1)}_{v_1} \otimes \Psi^{(C_2)}_{v_2} \otimes \Psi^{(l_3,n_3C_3)}_{v_3}\right]^{(C_{23})} \otimes \Psi^{(l_4,n_4C_4)}_{v_4}\right]^{(C_v,\tilde{C}_v)}\right\rangle, \qquad [56]$$

where v_1, v_2, (v_3, l_3), and (v_4, l_4) are the harmonic oscillator quantum numbers for the XY_4 "parent" molecule and $\tilde{C}_v$ is the vibrational symmetry in the C_{2v} group as illustrated in Fig. 1 in the case of SO_2F_2. Contrary to the case of SF_6/SF_5Cl (*10*), no SX_4 tetrahedral "parent" molecule exists in the present case. Thus the left part of Fig. 1 is just indicative and serves to illustrate the polyad scheme. We can see that the ν_4/ν_5 dyad and the $\nu_3/\nu_7/\nu_9$ triad of SO_2F_2 are both very tight and can thus be considered as deriving from the ν_2 and ν_4 bands of a tetrahedral molecule, respectively (the symmetry correlation being of course correct; see Table 3). The splitting resulting from the $T_d \supset C_{2v}$ symmetry reduction is small and can be regarded as a perturbation. In the case of the ν_3 band of the "parent" molecule, the splitting into a $\nu_8/\nu_1/\nu_6$ triad while going from to T_d to C_{2v} is much bigger. However, if we consider the "tetrahedral" ν_1/ν_3 dyad as a whole which reduces into the $\nu_2/\nu_8/\nu_1/\nu_6$ tetrad, this $T_d \supset C_{2v}$ approach still seems suitable.

The Hamiltonian eigenfunctions are linear combinations of the rovibrational functions [55] and we denote them

$$\left|\Phi^{(J\tilde{C}\tilde{\alpha})}_M\right\rangle, \qquad [57]$$

where $\tilde{\alpha}$ numbers the energy levels in increasing order within a $(J, \tilde{C})$ block.

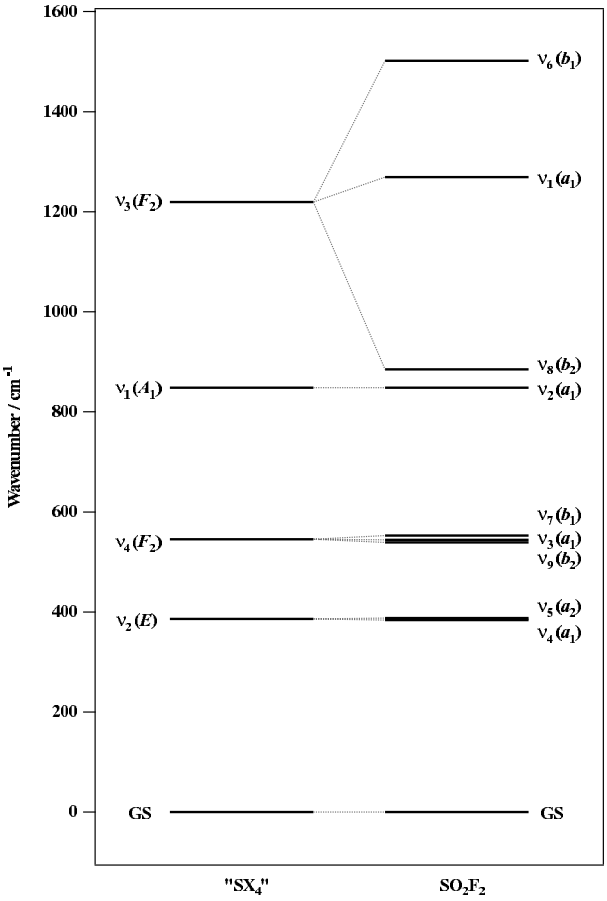

FIG. 1. Correlation between the vibrational fundamental levels of a hypothetical tetrahedral molecule "SX_4" and those of SO_2F_2.

The general expression of the matrix elements of the Hamiltonian operator is given in Appendix A.

4.2. Expression of the Dipole Moment

Each component of the initial dipole moment in the MFF is expanded as a series of purely vibrational operators,

$$\mu^{(\tilde{\Gamma}')}_{\theta} = \sum_{\text{all indexes}} \mu^{\Gamma_1\Gamma_2(\Gamma,\tilde{\Gamma}')}_{\{n_s\}\{m_s\}} V^{\Gamma_1\Gamma_2(\Gamma,\tilde{\Gamma}')}_{\{n_s\}\{m_s\}}, \qquad [58]$$

where the $\mu^{\Gamma_1\Gamma_2(\Gamma,\tilde{\Gamma}')}_{\{n_s\}\{m_s\}}$ are the dipole parameters and $\tilde{\Gamma}' = a_2, b_1$ or b_2 (see Table 5).

As S is a Hermitian operator and contains rovibrational operators, then, the transformed dipole moment must be expanded as a series of rovibrational operators by

$$\tilde{\mu}^{(\tilde{\Gamma}')}_{\theta} = \sum_{\{i\}} \tilde{\mu}^{\{i\}} M^{(\{i\},\tilde{\Gamma}')}_{\theta}, \qquad [59]$$

TABLE 6
Spin Statistical Weights in C_{2v}

$\tilde{C}$	a_1	a_2	b_1	b_2
g_i	1	1	3	3

with

$$M_\theta^{([i],\tilde{\Gamma})} = \left(R^{\Omega(K,\Gamma_r,\tilde{\Gamma}_r)} \otimes {}^{\varepsilon} V_{\{n_s\}\{m_s\}}^{\Gamma_1\Gamma_2(\Gamma_v,\tilde{\Gamma}_v)}\right)_\theta^{(\tilde{\Gamma})}, \quad [60]$$

and $\epsilon = (-1)^{\Omega}$. The order of the development is defined as $\Omega + \Omega_v - 1$. The LFF components of the transformed dipole moment are

$$\tilde{\mu}_\Theta^{(a_2)} = \sqrt{3}\sum_m \langle 1; m|\Theta\rangle \sum_{\{i\}} \tilde{\mu}^{\{i\}} \left[C^{(1,F_1,\tilde{\bar{\Gamma}})} \otimes M^{([i],\tilde{\Gamma})}\right]^{(a_2)}, \quad [61]$$

where $\tilde{\bar{\Gamma}} = a_2 \times \tilde{\Gamma}$ and $C^{(1,F_1,\tilde{\bar{\Gamma}})}$ is the direction cosine tensor. Θ is equal to X, Y or Z. The square brackets represent the symmetrized tensor product defined as

$$\left[A^{(\tilde{\Gamma}_1)} \otimes B^{(\tilde{\Gamma}_2)}\right]^{(\tilde{\Gamma})} = \frac{1}{2}\left(\left(A^{(\tilde{\Gamma}_1)} \otimes B^{(\tilde{\Gamma}_2)}\right)^{(\tilde{\Gamma})} + \left(B^{(\tilde{\Gamma}_2)} \otimes A^{(\tilde{\Gamma}_1)}\right)^{(\tilde{\Gamma})}\right). \quad [62]$$

The strength of a transition between the molecular rovibrational states Φ_i (with energy E_i) and Φ_f (with energy E_f) is calculated thanks to

$$S_{if} = K_{if} g_i e^{-\frac{hcE_i}{kT}} \sum_{M_i,M_f} |\langle \Phi_i|\tilde{\mu}_Z|\Phi_f\rangle|^2, \quad [63]$$

where K_{if} is a numerical coefficient and g_i is the spin statistical weight of state Φ_i. The values of spin statistical weights in XY_2Z_2 (C_{2v}) molecules with Y ligands having a $\frac{1}{2}$ spin and Z ligands having a spin equal to 1 are listed in Table 6. The sum is realized over the spherical components M_i and M_f of the two states in the LFF. Appendix A gives the general expression for the matrix elements of the transformed dipole moment operator.

4.3. Expression of the Polarizability

Each component of the initial polarizability in the MFF is expanded as a series of purely vibrational operators,

$$\alpha_\theta^{(\tilde{\Gamma})} = \sum_{\text{all indexes}} \alpha_{\{n_s\}\{m_s\}}^{\Gamma_1\Gamma_2(\Gamma,\tilde{\Gamma})} + V_{\{n_s\}\{m_s\}}^{\Gamma_1\Gamma_2(\Gamma,\tilde{\Gamma})}, \quad [64]$$

where the $\alpha_{\{n_s\}\{m_s\}}^{\Gamma_1\Gamma_2(\Gamma,\tilde{\Gamma})}$ are the polarizability parameters and θ is a component of the operator $\alpha^{(\tilde{\Gamma})}$.

For the same reasons as before, we can write the transformed polarizability as a series of rovibrational operators by

$$\tilde{\alpha}_\theta^{(\tilde{\Gamma})} = \sum_{\{i\}} \tilde{\alpha}^{([i],\tilde{\Gamma})} P_\theta^{([i],\tilde{\Gamma})}, \quad [65]$$

with

$$P_\theta^{([i],\tilde{\Gamma})} = \left(R^{\Omega(K,\Gamma_r,\tilde{\Gamma}_r)} \otimes {}^{\varepsilon} V_{\{n_s\}\{m_s\}}^{\Gamma_1\Gamma_2(\Gamma_v,\tilde{\Gamma}_v)}\right)_\theta^{(\tilde{\Gamma})}, \quad [66]$$

and $\epsilon = (-1)^{\Omega}$. The order of the development is defined as $\Omega + \Omega_v - 1$.

The LFF components of the transformed polarizability are

$$\begin{aligned}\tilde{\alpha}_{\Theta_1\Theta_2}^{(a_1)} = {} & \langle 0; 0|\Theta_1\Theta_2\rangle \sum_{\{i\}} \tilde{\alpha}^{\{i\}} \left[C^{(0,A_1,a_1)} \otimes P^{([i],a_1)}\right]^{(a_1)} \\ & + \sqrt{2}\sum_m \langle 2; m|\Theta_1\Theta_2\rangle \sum_{\{i\}} \tilde{\alpha}^{\{i\}} \left[C^{(2,E,\tilde{\Gamma}_v)} \otimes P^{([i],\tilde{\Gamma}_v)}\right]^{(a_1)} \\ & + \sqrt{3}\sum_m \langle 2; m|\Theta_1\Theta_2\rangle \sum_{\{i\}} \tilde{\alpha}^{\{i\}} \left[C^{(2,F_2,\tilde{\Gamma}'_v)} \otimes P^{([i],\tilde{\Gamma}'_v)}\right]^{(a_1)},\end{aligned} \quad [67]$$

where $\tilde{\Gamma}_v = a_1$ or a_2, $\tilde{\Gamma}'_v = a_1, b_1$ or b_2 and $\Theta_1, \Theta_2 = X, Y$ or Z. The first term represents the isotropic part of the polarizability and the two others constitute the anisotropic part.

The intensity of Raman transitions is expressed as

$$I_{if} = R_{if} g_i e^{-\frac{hcE_i}{kT}} \sum_{\Theta,\Theta'} \sum_{M_i,M_f} |\langle \Phi_i|\tilde{\alpha}_{\Theta,\Theta'}|\Phi_f\rangle|^2. \quad [68]$$

The general expression for the matrix elements of the transformed polarizability operator is given in Appendix A.

4.4. Selection Rules

The selection rules come directly from the expressions of the matrix elements given in Appendix A. They are given explicitly in Table 7. The rules concerning J comes from the non-zero condition of the K isoscalar factors.

TABLE 7
Selection Rules for the Hamiltonian ($\tilde{H}$), Dipole Moment ($\tilde{\mu}$), and Polarizability ($\tilde{\alpha}$) Operators: $\tilde{\alpha}^{(0)}$ and $\tilde{\alpha}^{(2)}$ Are the Isotropic and Anisotropic Parts of the Polarizability

	$\tilde{H}$	$\tilde{\mu}$	$\tilde{\alpha}^{(0)}$	$\tilde{\alpha}^{(2)}$
ΔJ	0	$0, \pm 1$	0	$0, \pm 1, \pm 2$
ΔM	0	$0, \pm 1$	0	$0, \pm 1, \pm 2$
$\tilde{C}'^a$	$\tilde{C}$	$\tilde{C} \otimes a_2$	$\tilde{C}$	$\tilde{C}$

[a] The matrix elements of an operator A are of the form $\langle C'|A|C\rangle$.

5. APPLICATION TO THE GROUND STATE OF SO_2F_2

In order to test the model developed in the present paper, we have performed a first application to the ground vibrational state of SO_2F_2. We present this analysis very briefly in this paragraph. A more detailed discussion along with a comparison with the results of the standard asymmetric-top model will be given in a forthcoming paper.

To perform spectrum analyses, we have built a software package called C_{2v}TDS. This program suite is based on the STDS package (*27*) designed for tetrahedral molecules. C_{2v}TDS implements the symmetry reorientation presented here and thus derives from STDS quite in the same way as C_{4v}TDS (*11*) (program suite for XY_5Z C_{4v} molecules) derives from HTDS (*28*) (program suite for octahedral molecules). C_{2v}TDS is freely available at the URL http://www.u-bourgogne.fr/LPUB/c2vTDS.html.

For this test, we used pure rotational microwave data provided to us by Dr. J. Demaison that correspond partly to the data from Ref. (*1*), with the addition of some new recent measurements. These data were analyzed using at least-squares fit procedure. The ground-state effective Hamiltonian was expanded up to order 4. We used 806 assigned lines for J values ranging between 1 and 99. The root mean square obtained for this fit is 2.4×10^{-6} cm^{-1}.

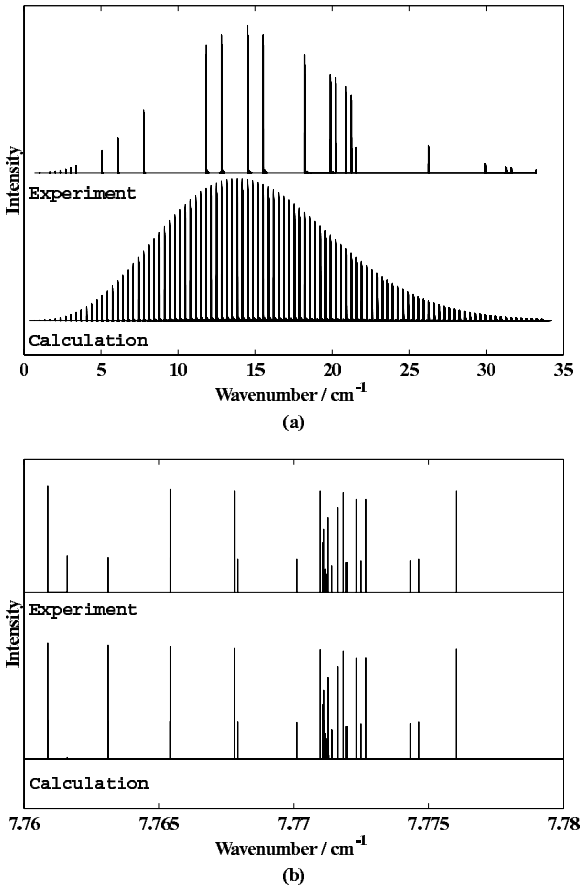

FIG. 2. Comparison between experimental and calculated stick spectra of the ground state of SO_2F_2. In the experimental stick spectrum, only lines that have been actually observed are plotted. (a) Overview. (b) Detail of the $R(22)$ cluster.

TABLE 8
Values of the Ground State Parameters

$\Omega(K, n\Gamma, \tilde{\Gamma})$	Value/cm^{-1}	
$2(0, 0A_1, a_1)$	0.1697286499(15)	
$2(2, 0E, a_1)$	$0.47533636(52) \times 10^{-3}$	
$2(2, 0F_2, a_1)$	$-0.9447632(28) \times 10^{-4}$	
$4(0, 0A_1, a_1)$	$-0.4465259(62) \times 10^{-7}$	
$4(2, 0E, a_1)$	$0.8491(20) \times 10^{-10}$	
$4(2, 0F_2, a_1)$	$-0.727849(82) \times 10^{-9}$	
$4(4, 0A_1, a_1)$	$-0.2578558(64) \times 10^{-8}$	
$4(4, 0E, a_1)$	$-0.66280(55) \times 10^{-10}$	
$4(4, 0F_2, a_1)$	0.640×10^{-9}	(fixed)
$6(0, 0A_1, a_1)$	$0.1723(10) \times 10^{-13}$	
$6(2, 0E, a_1)$	$-0.201(19) \times 10^{-15}$	
$6(2, 0F_2, a_1)$	$-0.158(37) \times 10^{-15}$	
$6(4, 0A_1, a_1)$	$-0.754(15) \times 10^{-15}$	
$6(4, 0E, a_1)$	$-0.200(14) \times 10^{-15}$	
$6(4, 0F_2, a_1)$	$-0.112(50) \times 10^{-15}$	
$6(6, 0A_1, a_1)$	$0.518(23) \times 10^{-15}$	
$6(6, 0E, a_1)$	$-0.140(11) \times 10^{-15}$	
$6(6, 0F_2, a_1)$	$-0.584(17) \times 10^{-15}$	
$6(6, 1F_2, a_1)$	$-0.2813(55) \times 10^{-15}$	

Figure 2a shows an overview of the observed and calculated data in the form of two stick spectra. One should notice that, as the intensities are extremely difficult to measure for a microwave spectrum, this figure displays in fact a calculated intensity for each measured frequency. Moreover, only some parts of the actual spectrum have been observed experimentally. Figure 2b shows the $R(22)$ cluster in more detail. The effective Hamiltonian parameters resulting from the present fit are given in Table 8 (where the standard deviation is given in parentheses, in the unit of the last two figures).

6. CONCLUSION

In order to study C_{2v} XY_2Z_2 molecules, we have developed a tensorial formalism adapted to the chain $O(3) \supset T_d \supset C_{2v}$ as an extension of what has already been done in Dijon in the case of $O(3) \supset T_d$. We have determined coupling and recoupling coefficients in this chain but also in the C_{2v} group itself. The Wigner–Eckart theorem with useful formulas for the computation of reduced matrix elements of tensor operators have been given. Special attention has been given to the various phase choices. The tensorial development of the Hamiltonian and transition moment operators has been realized and their matrix elements have been calculated. We have also presented a first application of this formalism to the spectroscopy of the ground-state of SO_2F_2 as a preliminary step.

We now intend to use this $O(3) \supset T_d \supset C_{2v}$ formalism for the global analysis of the $\nu_4/\nu_5/\nu_9/\nu_3/\nu_7$ pentad of this molecule, this polyad deriving from the ν_2/ν_4 dyad of the "parent" tetrahedral molecule (see Fig. 1). This pentad is composed of two interacting subpolyads, namely ν_5/ν_4 (coming from ν_2 of XY_4) and $\nu_9/\nu_3/\nu_7$ (coming from ν_3 of XY_4), which are both extremely intricate due to a very small $T_d \supset C_{2v}$ splitting. Our model should be well adapted in this case.

APPENDIX A

Matrix Elements for the Hamiltonian and Transition Moment Operators

In the following formulas, the $\langle \ldots \| \ldots \| \ldots \rangle$ are reduced matrix elements calculated in the $O(3)$ and T_d groups as in Ref. (*4*).

- Matrix elements of the Hamiltonian operator:

$$\begin{aligned}
&\left\langle \left[\Psi_{r'}^{(J',n'C'_r,\tilde{C}'_r)} \otimes \Psi_{v'}^{(C'_v,\tilde{C}'_v)}\right]^{(\tilde{C})} \middle| \left[R^{\Omega(K,n_r\Gamma_r,\tilde{\Gamma})} \otimes \varepsilon V_{\{n_s\}\{m_s\}}^{\Gamma_c\Gamma_a(\Gamma_v,\tilde{\Gamma})}\right]^{(a_1)} \right. \\
&\quad \left. \times \left| \left[\Psi_r^{(J,nC_r,\tilde{C}_r)} \otimes \Psi_v^{(C_v,\tilde{C}_v)}\right]^{(\tilde{C})} \right\rangle \right. \\
&= (-1)^J K' \begin{pmatrix} \Gamma_r & C_r & C'_r \\ \tilde{\Gamma} & \tilde{C}_r & \tilde{C}'_r \end{pmatrix} K' \begin{pmatrix} \Gamma_v & C_v & C'_v \\ \tilde{\Gamma} & \tilde{C}_v & \tilde{C}'_v \end{pmatrix} K \begin{pmatrix} K & J & J' \\ n_r\Gamma_r & nC_r & n'C'_r \end{pmatrix} \\
&\quad \times \left\langle \psi_{v'}^{(C'_v)} \middle\| \varepsilon V_{\{n_s\}\{m_s\}}^{\Gamma_c\Gamma_a(\Gamma_v)} \middle\| \Psi_v^{(C_v)} \right\rangle \left\langle \Psi_{r'}^{(J')} \middle\| R^{\Omega(K)} \middle\| \Psi_r^{(J)} \right\rangle \qquad \text{[A.69]}
\end{aligned}$$

- Matrix elements of the dipole moment operator ($\tilde{\bar{C}} = \tilde{C} \times a_2$ and $\tilde{\bar{\Gamma}} = \tilde{\Gamma} \times a_2$):

$$\begin{aligned}
&\left\langle \left[\Psi_{r'}^{(J',n'C'_r,\tilde{C}'_r)} \otimes \Psi_{v'}^{(C'_v,\tilde{C}'_v)}\right]^{(\tilde{\bar{C}})} \middle| \left[C^{(1,F_1,\tilde{\bar{\Gamma}})} \otimes M^{(\{i\},\tilde{\Gamma})}\right]^{(a_2)} \right. \\
&\quad \left. \times \left| \left[\Psi_r^{(J,nC_r,\tilde{C}_r)} \otimes \Psi_v^{(C_v,\tilde{C}_v)}\right]^{(\tilde{C})} \right\rangle \right. \\
&= \frac{1}{2} K' \begin{pmatrix} \Gamma_v & C_v & C'_v \\ \tilde{\Gamma}_v & \tilde{C}_v & \tilde{C}'_v \end{pmatrix} \left\langle J' \middle\| C^{(L)} \middle\| J \right\rangle \left\langle \Psi_{v'}^{(C'_v)} \middle\| \varepsilon V_{\{n_s\}\{m_s\}}^{\Gamma_c\Gamma_a(\Gamma_v)} \middle\| \Psi_v^{(C_v)} \right\rangle \\
&\quad \times \left\{ (-1)^{J+J'} \left\langle J \middle\| R^{\Omega(K)} \middle\| J \right\rangle \left[\sum_{n'',C''_r} K' \begin{pmatrix} C'_r & F_1 & C''_r \\ \tilde{C}'_r & \tilde{\Gamma} & \tilde{C}''_r \end{pmatrix} \right. \right. \\
&\quad \left. \times K' \begin{pmatrix} C''_r & \Gamma_r & C_r \\ \tilde{C}''_r & \tilde{\Gamma}_r & \tilde{C}_r \end{pmatrix} K \begin{pmatrix} 1 & J & J' \\ F_1 & n''C''_r & n'C'_r \end{pmatrix} K \begin{pmatrix} K & J & J \\ n_r\Gamma_r & nC_r & n''C''_r \end{pmatrix} \right] \\
&\quad + \left\langle J' \middle\| R^{\Omega(K)} \middle\| J' \right\rangle \left[\sum_{n'',C''_r} K' \begin{pmatrix} C''_r & F_1 & C_r \\ \tilde{C}''_r & \tilde{\Gamma} & \tilde{C}_r \end{pmatrix} K' \begin{pmatrix} C'_r & \Gamma_r & C''_r \\ \tilde{C}'_r & \tilde{\Gamma}_r & \tilde{C}''_r \end{pmatrix} \right. \\
&\quad \left. \left. \times K \begin{pmatrix} 1 & J & J' \\ F_1 & nC_r & n''C''_r \end{pmatrix} K \begin{pmatrix} K & J' & J' \\ n_r\Gamma_r & n''C''_r & n'C'_r \end{pmatrix} \right] \right\} \qquad \text{[A.70]}
\end{aligned}$$

- Matrix elements of the polarizability operator:

$$\begin{aligned}
&\left\langle \left[\Psi_{r'}^{(J',n'C'_r,\tilde{C}'_r)} \otimes \Psi_{v'}^{(C'_v,\tilde{C}'_v)}\right]^{(\tilde{C})} \middle| \left[C^{(L,\Gamma,\tilde{\Gamma})} \otimes P^{(\{i\},\tilde{\Gamma})}\right]^{(a_1)} \right. \\
&\quad \left. \times \left| \left[\Psi_r^{(J,nC_r,\tilde{C}_r)} \otimes \Psi_v^{(C_v,\tilde{C}_v)}\right]^{(\tilde{C})} \right\rangle \right. \\
&= \frac{1}{2} K' \begin{pmatrix} \Gamma_v & C_v & C'_v \\ \tilde{\Gamma}_v & \tilde{C}_v & \tilde{C}'_v \end{pmatrix} \left\langle J' \middle\| C^{(L)} \middle\| J \right\rangle \left\langle \Psi_{v'}^{(C'_v)} \middle\| \varepsilon V_{\{n_s\}\{m_s\}}^{\Gamma_c\Gamma_a(\Gamma_v)} \middle\| \Psi_v^{(C_v)} \right\rangle \\
&\quad \times \left\{ (-1)^{J+J'} \left\langle J \middle\| R^{\Omega(K)} \middle\| J \right\rangle \left[\sum_{n'',C''_r} K' \begin{pmatrix} C'_r & \Gamma & C''_r \\ \tilde{C}'_r & \tilde{\Gamma} & \tilde{C}''_r \end{pmatrix} \right. \right. \\
&\quad \left. \times K' \begin{pmatrix} C''_r & \Gamma_r & C_r \\ \tilde{C}''_r & \tilde{\Gamma}_r & \tilde{C}_r \end{pmatrix} K \begin{pmatrix} L & J & J' \\ \Gamma & n''C''_r & n'C'_r \end{pmatrix} K \begin{pmatrix} K & J & J \\ n_r\Gamma_r & nC_r & n''C''_r \end{pmatrix} \right] \\
&\quad + \left\langle J' \middle\| R^{\Omega(K)} \middle\| J' \right\rangle \left[\sum_{n'',C''_r} K' \begin{pmatrix} C''_r & \Gamma & C_r \\ \tilde{C}''_r & \tilde{\Gamma} & \tilde{C}_r \end{pmatrix} K' \begin{pmatrix} C'_r & \Gamma_r & C''_r \\ \tilde{C}'_r & \tilde{\Gamma}_r & \tilde{C}''_r \end{pmatrix} \right. \\
&\quad \left. \left. \times K \begin{pmatrix} L & J & J' \\ \Gamma & nC_r & n''C''_r \end{pmatrix} K \begin{pmatrix} K & J' & J' \\ n_r\Gamma_r & n''C''_r & n'C'_r \end{pmatrix} \right] \right\} \qquad \text{[A.71]}
\end{aligned}$$

ACKNOWLEDGMENTS

The authors thank Dr. Jean Demaison (PhLAM Laboratory, University of Lille I, France) for providing the SO_2F_2 experimental data. Support from the Région Bourgogne for the computer equipment of the Laboratoire de Physique de l'Université de Bourgogne is gratefully acknowledged.

REFERENCES

1. K. Sarka, J. Demaison, L. Margulès, I. Merke, N. Heineking, H. Bürger, and H. Rulland, *J. Mol. Spectrosc.* **200,** 55–64 (2000).
2. H. Bürger, H. Ruland, I. Merke, K. Sarka, L. Margulès, and J. Demaison, *J. Mol. Spectrosc.* **203,** 268–272 (2000).
3. H. Bürger, J. Demaison, F. Hegelund, L. Margulès, and I. Merke, *J. Mol. Struct.* **612,** 133–141 (2002).
4. J.-P. Champion, M. Loëte, and G. Pierre, *in* "Spectroscopy of the Earth's Atmosphere and Interstellar Medium" (K. N. Rao and A. Weber, Eds.), pp. 339–422. Academic Press, San Diego, 1992.
5. N. Cheblal, M. Loëte, and V. Boudon, *J. Mol. Spectrosc.* **197,** 222–231 (1999).
6. A. Nikitin, J.-P. Champion, and Vl. G. Tyuterev, *J. Mol. Spectrosc.* **182,** 72–84 (1997).
7. A. Nikitin, L. R. Brown, L. Féjard, J.-P. Champion, and Vl. G. Tyuterev, *submitted for publication.*
8. M. Rotger, V. Boudon, and M. Loëte, *J. Mol. Spectrosc.* **200,** 123–130 (2000).
9. M. Rotger, V. Boudon, and M. Loëte, *J. Mol. Spectrosc.* **200,** 131–137 (2000).
10. M. Rotger, A. Decrette, V. Boudon, M. Loëte, S. Sander, and H. Willner, *J. Mol. Spectrosc.* **208,** 169–179 (2001).
11. Ch. Wenger, M. Rotger, and V. Boudon, *J. Quant. Spectrosc. Radiat. Transfer* **74,** 621–636 (2002).
12. B. G. Sartakov, J. Oomens, J. Reuss, and A. Fayt, *J. Mol. Spectrosc.* **185,** 31–47 (1997).
13. J.-P. Champion, G. Pierre, F. Michelot, and J. Moret-Bailly, *Can. J. Phys.* **55,** 512–520 (1977).
14. V. Boudon and F. Michelot, *J. Mol. Spectrosc.* **165,** 554–579 (1994).

15. M. Rey, V. Boudon, Ch. Wenger, G. Pierre, and B. Sartakov, in preparation (2002).
16. B. I. Zhilinskiĭ, V. I. Perevalov, and Vl. G. Tyuterev, "Méthode des opérateurs tensoriels irréductubles et théorie des spectres des molécules," 1986 [Translated from Russian].
17. U. Fano and G. Racah, "Irreducible Tensorial Sets." Academic Press, New York, 1959.
18. M. Rotenberg, R. Bivins, N. Metropolis, and J. K. Wooten, Jr., "The 3*j* and 6*j* Symbols." The Technology Press, M.I.T., Cambridge, MA, 1959.
19. F. Michelot, "Hamiltonien effectif des molécules semi-rigides non-linéaires dans un état électronique non-dégénéré. Application au calcul des énergies hyperfines des toupies sphériques." Thèse d'état, Dijon, 1980.
20. F. Michelot, B. Bobin, and J. Moret-Bailly, *J. Mol. Spectrosc.* **76,** 374–411 (1979).
21. M. Hamermesh, "Group Theory and Its Application to Physical Problems." Addison–Wesley, Reading, MA, 1962.
22. B. Lulek, T. Lulek, and B. Szczepaniak, *Acta Phys. Polon. A* **54,** 545–559 (1978).
23. B. Lulek and T. Lulek, *Acta Phys. Polon. A* **54,** 561–572 (1978).
24. D. Papoušek and M. Aliev, "Molecular Vibrational–Rotational Spectra." Elsevier, New York, 1982.
25. A. Edmonds, "Angular Momentum in Quantum Mechanics." Princeton Univ. Press, Princeton, NJ, 1957.
26. A. J. Stone, *Mol. Phys.* **29,** 1461–1471 (1975).
27. Ch. Wenger and J.-P. Champion, *J. Quant. Spectrosc. Radiat. Transfer* **59,** 471–480 (1998).
28. Ch. Wenger, V. Boudon, J.-P. Champion, and G. Pierre, *J. Quant. Spectrosc. Radiat. Transfer* **66,** 1–16 (2000).

Available online at www.sciencedirect.com
SCIENCE DIRECT®
Journal of Molecular Spectroscopy 222 (2003) 172–179
Journal of MOLECULAR SPECTROSCOPY
www.elsevier.com/locate/jms

The ground state rotational spectrum of SO_2F_2☆

M. Rotger,[a,*] V. Boudon,[a] M. Loëte,[a,*] L. Margulès,[b] J. Demaison,[b] H. Mäder,[c] G. Winnewisser,[d] and H.S.P. Müller[d]

[a] *Laboratoire de Physique de l'Université de Bourgogne, CNRS UMR 5027, 9, Avenue Alain Savary, B.P. 47 870, F-21078 Dijon Cedex, France*
[b] *Laboratoire de Physique, Atomes et Molécules, CNRS UMR 8523, Université de Lille I, Bât. P5, 59655 Villeneuve d'Ascq Cedex, France*
[c] *Institut für Physikalische Chemie, Universität Kiel, Olshausenstr. 40, D-24098 Kiel, Germany*
[d] *I. Physikalisches Institut, Universität zu Köln, D-50937 Köln, Germany*

Received 1 April 2003; in revised form 11 June 2003

Abstract

The analysis of the ground state rotational spectrum of SO_2F_2 [K. Sarka, J. Demaison, L. Margulès, I. Merke, N. Heineking, H. Bürger, H. Ruland, J. Mol. Spectrosc. 200 (2000) 55] has been performed with the Watson's Hamiltonian up to sextic terms but shows some limits due to the *A* and *S* reductions. Since SO_2F_2 is a quasi-spherical top, it can also be regarded as derived from an hypothetical XY_4 molecule. Thus we have developed a new tensorial formalism in the $O(3) \supset T_d \supset C_{2v}$ group chain (M. Rotger, V. Boudon, M. Loëte, J. Mol. Spectrosc. 216 (2002) 297]. We test it on the ground state of this molecule using the same experimental data (10 GHz–1 THz region, *J* up to 99). Both fits are comparable even if the formalisms are slightly different. This paper intends to establish a link between the classical approach and the tensorial formalism. In particular, our tensorial parameters at a given order of the development are related to the usual ones. Programs for spectrum simulation and fit using these methods are named C_{2v}TDS. They are freely available at the URL: `http://www.u-bourgogne.fr/LPUB/c2vTDS.html`.

PACS: 33.15.Mt; 33.20.Sn; 33.20.Bx

Keywords: Microwave spectroscopy; Tensorial formalism; XY_2Z_2; Asymmetric tops

1. Introduction

The ground state rotational spectrum of sulfuryl fluoride, SO_2F_2, has been recently investigated [1]. In parallel to this work, the rovibrational spectra of some fundamental bands are being analyzed. The results for the isolated $\nu_8(b_2)$ band centered at 887.2 cm^{-1} have already been published [2] as well as those for the $\nu_3(a_1)/\nu_7(b_1)/\nu_9(b_2)$ triad around 550 cm^{-1} [3].

However the analyses are not satisfactory and in particular the *A* (asymmetric) and *S* (symmetric) reductions proposed by Watson [4] fail in the ground state analysis. The best results are obtained using the so-called 6 reduction. In fact, the *A*, *B*, and *C* rotational constants have very close values and in this case the *A* and *S* reductions lead to non-perturbative unitary transformations of the Hamiltonian [5].

In this paper, we will use another approach. According to the rotational constants values, in first approximation we can consider the SO_2F_2 molecule as a spherical top derived from an hypothetical SY_4 molecule.

For this we have developed an adapted tensorial formalism in the $O(3) \supset T_d \supset C_{2v}$ chain [6]. It is an extension of the usual formalism used in Dijon for XY_4 [7] spherical tops with tetrahedral symmetry.

This theory is presented here and is applied to the analysis of the ground state. Results are compared to the previous analysis. In addition the tensorial and Watson's models are compared and relations between the parameters of both models are established.

☆ Supplementary data associated with this article can be found at doi:10.1016/S0022-2852(03)00215-7

* Corresponding authors. Fax: +33-3-80-39-59-71.
E-mail address: Maud.Rotger@u-bourgogne.fr (M. Rotger).
URL: http://www.u-bourgogne.fr/LPUB/Equipe2A/Spectroscopy/spectro.html.

0022-2852/$ - see front matter © 2003 Elsevier Inc. All rights reserved.
doi:10.1016/S0022-2852(03)00215-7

2. Experimental details

The sample is the same as previously used [1]. In Kiel, the spectra were recorded in the frequency range from about 8–14 GHz, employing a Fourier transform microwave spectrometer for the X/Ku-band with automatic scan facility [8] and a waveguide-cell of quadratic cross-section and 12 m length [9]. Ambient temperature and sample pressures of about 0.3–0.6 Pa (2–4 mTorr) were used throughout. The transition frequencies were determined from a least-squares analysis of the transient emission signals, in most cases at an accuracy of better than 5 kHz.

The Cologne Terahertz spectrometer was used between 545 and 945 GHz. The radiation sources are Russian phase-locked backward-wave oscillators (BWOs). The detector is a magnetically tuned LHe cooled InSb hot electron bolometer. Further details of the spectrometer are given in [10]. The accuracy of the measurements is 30 up to 100 kHz for weak lines.

In Lille, a FIR laser sideband spectrometer [11] was used to cover selected regions between 600 and 1000 GHz. The output of a MW synthetizer (2–18 GHz) and that of an optically pumped FIR laser were mixed on a Schottky diode to generate terahertz sideband radiation which was detected by a heterodyne receiver. The laser was locked permitting an accuracy better than 300 kHz. In addition, the lines below 473 GHz were measured with a source-modulated spectrometer employing phase-locked French Thomson-CSF BWOs. The signal was detected with a LHe cooled InSb bolometer. In general, the accuracy of the measurements was better than 50 kHz.

3. Theory

3.1. The Hamiltonian operator

3.1.1. Watson's form

The usual sextic rotational Hamiltonian for an asymmetric rotor (which we call H_{Watson} or "Watsonian") can be written in terms of the operators J^2, J_Z, and $J_\pm = J_X \pm iJ_Y$ as follows [12]:

$$\begin{aligned} H_{\text{Watson}} = {} & B_{200}J^2 + B_{020}J_Z^2 + T_{400}(J^2)^2 + T_{220}J^2J_Z^2 \\ & + T_{040}J_Z^4 + \Phi_{600}(J^2)^3 + \Phi_{420}(J^2)^2J_Z^2 \\ & + \Phi_{240}J^2J_Z^4 + \Phi_{060}J_Z^6 + \frac{1}{2}[B_{002} + T_{202}J^2 \\ & + T_{022}J_Z^2 + \Phi_{402}(J^2)^2 + \Phi_{222}J^2J_Z^2 \\ & + \Phi_{024}J_Z^4, J_+^2 + J_-^2]_+ + \frac{1}{2}[T_{004} + \Phi_{204}J^2 \\ & + \Phi_{024}J_Z^2, J_+^4 + J_-^4]_+ + \Phi_{006}(J_+^6 + J_-^6) \end{aligned} \tag{1}$$

with

$$\begin{cases} B_{200} = \frac{B+C}{2}, \\ B_{020} = \frac{2A-B-C}{2}, \\ B_{002} = \frac{B-C}{4}, \end{cases} \tag{2}$$

in the I^r representation.

The use of capital letters (X, Y, Z) to label the angular momentum components in Eq. (1) is different from the standard notation and will be explained later.

In the S reduction [1], one quartic parameter, T, and three sextic parameters, Φ, are constrained to zero: $T_{022} = \Phi_{222} = \Phi_{042} = \Phi_{024} = 0$.

3.1.2. Distorted tetrahedron form

Let us now introduce our tensorial Hamiltonian for a distorted tetrahedral molecule.

The theoretical model described below to develop the Hamiltonian operator is based on the tensorial formalism and vibrational extrapolation methods used in Dijon. These methods have already been explained for example in [7,13–15]. We only recall here the basic principles and their applications to the case of XY_2Z_2 molecules [6] belonging to the C_{2v} group.

The background of the model is based on the idea of considering XY_2Z_2 molecules as distorted XY_4 molecules, by substitution of two ligands. Practically, this means that we start from the $O(3) \supset T_d$ formalism used for tetrahedral species [7] and make a symmetry reduction (or reorientation) into the C_{2v} subgroup. This procedure has been detailed in [6]. In the following, all the C_{2v} oriented tensor operators will be denoted in the form:

$$T^{(\ldots,\Gamma,\widetilde{\Gamma})},$$

with Γ ($= A_1, A_2, E, F_1, F_2$) and $\widetilde{\Gamma}$ ($= a_1, a_2, b_1, b_2$) denoting T_d and C_{2v} irreducible representations (irreps), respectively. This way of handling XY_2Z_2 molecules has some consequences on the labelling of Hamiltonian and transition moment parameters. The energy level labels are also different from the "usual" ones used in the standard treatment of asymmetric tops, as it will be detailed in Section 3.1.5.

If we consider an XY_2Z_2 molecule in its vibrational ground state, the Hamiltonian operator can be put in the following form (after performing some contact transformations):

$$H_{\text{Moret-Bailly}} = \sum_{\text{all indices}} t^{\Omega(K,n\Gamma,\widetilde{\Gamma})}\beta R^{\Omega(K,n\Gamma,\widetilde{\Gamma})}, \tag{3}$$

which we have called $H_{\text{Moret-Bailly}}$ since it is based on the rotational operators R defined by Moret-Bailly [16,17].

In Eq. (3), the $t^{\Omega(K,n\Gamma,\Gamma)}$ are the parameters to be determined and β is a numerical factor such that:

$$\beta = \begin{cases} \left(-\frac{\sqrt{3}}{4}\right)^{\Omega/2} & \text{if } (K,n\Gamma) = (0,0A_1), \\ 1 & \text{otherwise.} \end{cases} \tag{4}$$

$R^{\Omega(K,n\Gamma,\widetilde{\Gamma})}$ is the rotational operator of degree Ω. The order of each individual term is defined as $\Omega - 2$.

Let us summarize here the construction of the $R^{\Omega(K,n\Gamma,\Gamma)}$ rotational operators. Further details can be found in [6,7]. A convenient classification of a complete set of rotational tensors requires two indices: the degree Ω in the angular momentum components and the tensorial rank K. This basic tensor as defined by Moret-Bailly [16,17] is denoted by

$$R^{1(1)} = 2J^{(1)},$$

where $J^{(1)}$ is the angular momentum vector. The general tensor $R^{\Omega(K)}$ is defined according to the following recursive expressions given by Zhilinskiĭ [18]

$$R^{\Omega(K)} = R^{\Omega-K(0)} \times R^{K(K)}, \tag{5}$$

where

$$R^{\Omega-K(0)} = ((R^{1(1)} \times R^{1(1)})^{(0)})^{(\Omega-K)/2} = (R^{2(0)})^{(\Omega-K)/2} \tag{6}$$

and

$$R^{K(K)} = (R^{K-1(K-1)} \times R^{1(1)})^{(K)}. \tag{7}$$

In the T_d group, $R^{\Omega(K,n\Gamma)}_{\sigma}$ is the general form for a rotational tensor. Γ is an irrep of this group, σ a component of Γ and n is an index of multiplicity. They are linked to $O(3)$ tensors (5) thanks to the G coefficients [19,20]

$$R^{\Omega(K,n\Gamma)}_{\sigma} = \sum_{M}^{(K)} G^{M}_{n\Gamma\sigma} R^{\Omega(K)}_{M}. \tag{8}$$

Finally, the preceeding rotational tensor is re-oriented from T_d into our subgroup (C_{2v}) and is denoted $R^{\Omega(K,n\Gamma,\Gamma)}$, where $\widetilde{\Gamma}$ is a C_{2v} irrep. This re-orientation is done using the G' coefficients [6,21]:

$$R^{\Omega(K,n\widetilde{\Gamma},\Gamma)} = \sum_{\sigma}^{(\Gamma)} G^{\widetilde{\Gamma}\sigma}_{\Gamma} R^{\Omega(K,n\Gamma)}_{\sigma}. \tag{9}$$

3.1.3. Principal axes

Let us first consider only terms of order 0 (i.e., degree 2 in J_x, J_y, J_z) in (3)

$$H_{\text{Moret-Bailly}} = t_1 \beta R^{(2,0A_1,a_1)} + t_2 R^{(2,0E,a_1)} + t_3 R^{(2,0F_2,a_1)} + \cdots \tag{10}$$

In term of J_x, J_y, and J_z operators and according to (5)–(9), this leads to the following equation

$$\begin{aligned} H_{\text{Moret-Bailly}} = {} & \left(t_1 - 2\sqrt{\frac{2}{3}}t_2\right)J_x^2 + \left(t_1 - 2\sqrt{\frac{2}{3}}t_2\right)J_y^2 \\ & + \left(t_1 + 4\sqrt{\frac{2}{3}}t_2\right)J_z^2 + 2\sqrt{2}t_3(J_xJ_y \\ & + J_yJ_x) + \cdots, \end{aligned} \tag{11}$$

where x, y, and z denote the components in the axis system of the tetrahedral molecule (see Fig. 1).

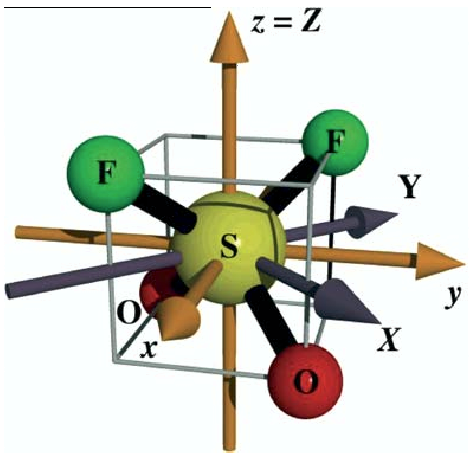

Fig. 1. The molecular axis frames in T_d and C_{2v}.

At the same order of development, the Watsonian can be written

$$\begin{aligned} H_{\text{Watson}} = {} & (B_{200} + 2B_{002})J_X^2 + (B_{200} - 2B_{002})J_Y^2 \\ & + (B_{020} + B_{200})J_Z^2 + \cdots \end{aligned} \tag{12}$$

We can see that our oriented Hamiltonian contains an additional term proportional to $J_xJ_y + J_yJ_x$. This can be easily understood because $H_{\text{Moret-Bailly}}$ has been derived from the reorientation of the tetrahedral Hamiltonian. For this one, the (x, y, z) axis frame that is used (see Fig. 1) is not the principal axis system of the "distorted" C_{2v} molecule. Thus, a coordinate change has to be made in order to eliminate the $J_xJ_y + J_yJ_x$ cross-term.

In term of angular momentum operators, this leads to the following relations for the components of the J angular momentum:

$$\begin{cases} J_X = -\frac{1}{\sqrt{2}}(J_x - J_y), \\ J_Y = \frac{1}{\sqrt{2}}(J_x + J_y), \\ J_Z = J_z \end{cases} \tag{13}$$

or

$$\begin{cases} J_x = -\frac{1}{\sqrt{2}}(J_X - J_Y), \\ J_y = \frac{1}{\sqrt{2}}(J_X + J_Y), \\ J_z = J_Z. \end{cases} \tag{14}$$

A correct phase choice for the J_X component has been made to be in agreement with the signs of the usual rotational constants. In other words, our C_{2v} molecular axis frame (or ($OXYZ$) frame) is deduced from the ($Oxyz$) molecular axis of the T_d group by a rotation of an angle equals to $\pi/4$ about the OZ axis as shown on Fig. 1.

3.1.4. Comparison of the two models

In the aim of comparing the two models, we give hereafter the expression of both Hamiltonians taken in the same ($Oxyz$) molecular frame, up to order 2 (i.e.,

degree 4 in J_x, J_y, J_z). By applying transformation (13) to Eq. (1), we get :

$$\begin{aligned}H_{\text{Watson}} &= B_{200}J^2 + B_{020}J_z^2 - 2B_{002}(J_xJ_y + J_yJ_x)\\ &+ T_{400}\left(J_x^2+J_y^2+J_z^2\right)\left(J_x^2+J_y^2+J_z^2\right)\\ &+ \frac{T_{220}}{2}\left[\left(J_x^2+J_y^2+J_z^2\right)J_z^2 + J_z^2\left(J_x^2+J_y^2+J_z^2\right)\right]\\ &+ T_{040}J_z^4 - T_{202}\left[\left(J_x^2+J_y^2+J_z^2\right)(J_xJ_y+J_yJ_x)\right.\\ &\left.+ (J_xJ_y+J_yJ_x)\left(J_x^2+J_y^2+J_z^2\right)\right]\\ &- T_{022}\left[J_z^2(J_xJ_y+J_yJ_x) + (J_xJ_y+J_yJ_x)J_z^2\right]\\ &- 2T_{004}\left[J_y^4 - J_y^2J_x^2 - J_x^2J_y^2 + J_x^4\right]\\ &+ 2T_{004}\left(J_xJ_yJ_xJ_y + J_yJ_xJ_yJ_x + J_xJ_y^2J_x + J_yJ_x^2J_y\right),\end{aligned} \tag{15}$$

to be compared with:

$$\begin{aligned}&H_{\text{Moret-Bailly}}\\ &= t_1\left(J_x^2+J_y^2+J_z^2\right) + \frac{4}{3}t_2\left(2J_z^2 - J_x^2 - J_y^2\right)\\ &+ 2\sqrt{2}t_3(J_xJ_y+J_yJ_x) + t_4\left(J_x^2+J_y^2+J_z^2\right)\left(J_x^2+J_y^2+J_z^2\right)\\ &- \frac{8\sqrt{2}}{6}t_5\left[\left(2J_z^2 - J_x^2 - J_y^2\right)\left(J_x^2+J_y^2+J_z^2\right)\right.\\ &\left.+ \left(J_x^2+J_y^2+J_z^2\right)\left(2J_z^2 - J_x^2 - J_y^2\right)\right]\\ &- \frac{8\sqrt{2}}{2\sqrt{3}}t_6\left[(J_xJ_y+J_yJ_x)\left(J_x^2+J_y^2+J_z^2\right)\right.\\ &\left.+ \left(J_x^2+J_y^2+J_z^2\right)(J_xJ_y+J_yJ_x)\right]\\ &+ \frac{8\sqrt{2}}{\sqrt{15}}t_7\left[5J_x^4 + 5J_y^4 + 5J_z^4 - 3\left(J_x^2+J_y^2+J_z^2\right)\right.\\ &\left.\times\left(J_x^2+J_y^2+J_z^2\right) + J_x^2+J_y^2+J_z^2\right]\\ &+ \frac{8\sqrt{2}}{\sqrt{21}}t_8\left[J_x^4 + J_y^4 - 2J_z^4 - 6\left(J_x^2J_y^2 + J_y^2J_x^2\right)\right]\\ &+ \frac{8\sqrt{2}}{\sqrt{21}}t_8\left[3\left(J_x^2J_z^2 + J_z^2J_x^2 + J_y^2J_z^2 + J_z^2J_y^2\right)\right.\\ &\left.+ 5J_x^2 + 5J_y^2 - 10J_z^2\right]\\ &+ \frac{8\sqrt{2}}{\sqrt{7}}t_9\left[3J_z^2(J_xJ_y+J_yJ_x) + 3(J_xJ_y+J_yJ_x)J_z^2\right]\\ &- \frac{8\sqrt{2}}{\sqrt{7}}t_9\left[\left(J_x^3J_y + J_yJ_x^3\right) - \left(J_yJ_x^3 + J_x^3J_y\right)\right.\\ &\left.- 4(J_xJ_y+J_yJ_x)\right].\end{aligned} \tag{16}$$

It is not possible to fit all quartic constants in both models using terms up to the order 2 only [1,6]. In order to identify these two expressions and also to be able to compare the results with experimental values, we use the so-called S reduction for H_{Watson} [1]. In this reduction, $T_{022} = 0$ which clearly corresponds to $t_9 = 0$ in $H_{\text{Moret-Bailly}}$. This ensures a full consistency between the two expressions. So, we get:

$$\begin{cases} t_1 = B_{200} + \frac{1}{3}B_{020} + \frac{2}{5}T_{004} - \frac{1}{15}T_{040} + \cdots\\ t_2 = \frac{\sqrt{6}}{84}(7B_{020} - 30T_{004} - 5T_{040}) + \cdots\\ t_3 = -\frac{1}{2}\sqrt{2}B_{002} + \cdots\\ t_4 = -\frac{8}{15}T_{004} + \frac{1}{5}T_{040} + \frac{1}{3}T_{220} + T_{400} + \cdots\\ t_5 = -\frac{\sqrt{2}}{112}(8T_{004} + 6T_{040} + 7T_{220}) + \cdots\\ t_6 = \frac{\sqrt{6}}{8}T_{202} + \cdots\\ t_7 = -\frac{\sqrt{30}}{240}(6T_{004} - T_{040}) + \cdots\\ t_8 = -\frac{\sqrt{42}}{336}(6T_{004} + T_{040}) + \cdots \end{cases} \tag{17}$$

In the reverse way, we obtain:

$$\begin{cases} B_{002} = -\sqrt{2}t_3 + \cdots\\ B_{020} = 2\sqrt{6}t_2 - \frac{40}{7}\sqrt{42}t_8 + \cdots\\ B_{200} = t_1 - \frac{2}{3}\sqrt{6}t_2 + \frac{8}{15}\sqrt{30}t_7 + \frac{40}{21}\sqrt{42}t_8 + \cdots\\ T_{400} = -D_J = t_4 + \frac{8}{3}\sqrt{2}t_5 - \frac{4}{15}\sqrt{30}t_7 - \frac{88}{21}\sqrt{42}t_8 + \cdots\\ T_{220} = -D_{JK} = -8\sqrt{2}t_5 - \frac{8}{3}\sqrt{30}t_7 + \frac{88}{21}\sqrt{42}t_8 + \cdots\\ T_{040} = -D_K = 4\sqrt{30}t_7 - 4\sqrt{42}t_8 + \ldots\\ T_{202} = d_1 = \frac{4}{3}\sqrt{6}t_6 + \cdots\\ T_{004} = d_2 = -\frac{2}{3}\sqrt{30}t_7 - \frac{2}{3}\sqrt{42}t_8 + \cdots \end{cases} \tag{18}$$

The dots indicate that these expressions are only approximate. The main reason is that Moret-Bailly's rotational operators are not homogeneous polynomials in J_x, J_y and J_z. $R^{\Omega(K)}$ terms contain monomials in J_x, J_y, J_z of maximum degree Ω. For instance, we can see that the term $R^{4(4,A_1,a_1)}$ with parameter t_7 in (16) contains also monomials of degree 2. Thus, the dots in the above expressions will contain additional contributions from $\Omega = 6, 8, \ldots$.

3.1.5. Matrix elements of the tensorial Hamiltonian

The matrix elements of a pure rotational operator are calculated in the following pure rotational basis

$$\left|\Psi^{(J,nC_r,\widetilde{C}_r)}\right\rangle. \tag{19}$$

Expression of the matrix elements of the Hamiltonian from [6] is simplified in the following manner for purely rotational operators:

$$\begin{aligned}&\left\langle \Psi^{(J',n'C'_r,\widetilde{C}'_r)}\left|R^{\Omega(K,n_r\Gamma_r,\widetilde{\Gamma})}\right|\Psi^{(J,nC_r,\widetilde{C}_r)}\right\rangle\\ &= K'\begin{pmatrix}\Gamma_r & C_r & C'_r\\ \widetilde{\Gamma} & \widetilde{C}_r & \widetilde{C}'_r\end{pmatrix}K\begin{pmatrix}K & J & J'\\ n_r\Gamma_r & nC_r & n'C'_r\end{pmatrix}\\ &\times\left\langle\Psi^{(J')}\left\|R^{\Omega(K)}\right\|\Psi^{(J)}\right\rangle.\end{aligned} \tag{20}$$

All the rovibrational levels are described by $(J, \widetilde{\alpha}, \widetilde{C})$ labels where $\widetilde{\alpha}$ is a numbering index for levels that have the same C_{2v} symmetry within a J block. This labelling is related to our group chain choice which considers XY_2Z_2 molecules like near-spherical tops.

In this way, the usual asymmetric-top K_a, K_c labels are hidden and related to the $\widetilde{C}$ symmetry. Thus, the (ΔK_a, ΔK_c) nomenclature does not occur in our transition labels.

3.1.6. Intensity calculations for the tensorial model

The strength of a transition between the molecular rovibrational states Φ_i (with energy E_i) and Φ_f (with energy E_f) is calculated using

Table 1
Rotational and centrifugal distortion constants in MHz of SO_2F_2 in S and 6 reductions

		S reduction		6 reduction
A		5134.877276(93)	A	5134.876906(51)
B		5073.078278(60)	B	5073.078441(36)
C		5057.056659(69)	C	5057.055567(36)
D_J	$\times 10^3$	1.478671(14)	D_J $\times 10^3$	1.497054(26)
D_{JK}	$\times 10^3$	−1.529510(51)	D_{JK} $\times 10^3$	−1.64148(15)
D_K	$\times 10^3$	1.850506(50)	D_K $\times 10^3$	1.94409(13)
d_1	$\times 10^6$	−30.212(17)	d_1 $\times 10^6$	−30.1838(46)
d_2	$\times 10^3$	0.1372017(39)	R_5 $\times 10^3$	−0.16272(22)
			R_6 $\times 10^3$	0.146508(13)
H_J	$\times 10^9$	0.44338(95)	H_J $\times 10^9$	0.71538(67)
H_{JK}	$\times 10^9$	0.565(11)	H_{JK} $\times 10^9$	−1.5585(24)
H_{KJ}	$\times 10^9$	0.141(21)	H_{KJ} $\times 10^9$	2.351(12)
H_K	$\times 10^9$	−0.730(18)	H_K $\times 10^9$	−1.005(13)
h_1	$\times 10^9$	0.5891(34)	h_1 $\times 10^9$	−0.1012(10)
h_2	$\times 10^{12}$	95.05(90)	h_2 $\times 10^{12}$	−57.00(55)
h_3	$\times 10^9$	−0.67251(96)	h_3 $\times 10^{12}$	13.86(93)
L_{JJK}	$\times 10^{15}$	−59.23(97)		
L_{JK}	$\times 10^{12}$	−0.1431(24)		
L_{KKJ}	$\times 10^{15}$	−65.3(2.5)		
l_1	$\times 10^{15}$	−8.44(21)		
l_3	$\times 10^{15}$	7.73(12)		
σ^a	kHz	26		21
RMS	kHz	102.85		79.27

[a] Standard deviation of the fit calculated from the median of absolute residuals.

Table 2
Values of the ground state parameters with our tensorial formalism ($H_{\text{Moret-Bailly}}$)

t_i	$\Omega(K, n\Gamma, \widetilde{\Gamma})$	Value/MHz	
		Best fit	$t_9 = 0$ Reduction
t_1	$2(0, 0A_1, a_1)$	5088.337142(42)	5088.337190(42)
t_2	$2(2, 0E, a_1)$	14.250186(12)	14.250245(12)
t_3	$2(2, 0F_2, a_1)$	−2.832303(8)	−2.832273(8)
t_4	$4(0, 0A_1, a_1)$	−0.001338723(13)	−0.001338742(14)
t_5	$4(2, 0E, a_1)$	$2.835(3) \times 10^{-6}$	$5.0518(36) \times 10^{-6}$
t_6	$4(2, 0F_2, a_1)$	$-2.03114(28) \times 10^{-5}$	$-9.2687(26) \times 10^{-6}$
t_7	$4(4, 0A_1, a_1)$	$-7.68568(13) \times 10^{-5}$	$-7.35454(13) \times 10^{-5}$
t_8	$4(4, 0E, a_1)$	$-1.9084(12) \times 10^{-6}$	$-1.3551(12) \times 10^{-6}$
t_9	$4(4, 0F_2, a_1)$	1.689×10^{-5} (fixed)	0 (fixed)
t_{10}	$6(0, 0A_1, a_1)$	$5.235(17) \times 10^{-10}$	$5.256(17) \times 10^{-10}$
t_{11}	$6(2, 0E, a_1)$	$-1.5(3) \times 10^{-12}$	$-6.08(32) \times 10^{-12}$
t_{12}	$6(2, 0F_2, a_1)$	$-5.61(1.23) \times 10^{-12}$	$-1.751(10) \times 10^{-10}$
t_{13}	$6(4, 0A_1, a_1)$	$-1.87(63) \times 10^{-11}$	$-1.34(6) \times 10^{-11}$
t_{14}	$6(4, 0E, a_1)$	$-7.5(5.71) \times 10^{-13}$	$7.5(5.7) \times 10^{-13}$
t_{15}	$6(4, 0F_2, a_1)$	$-2.72(16) \times 10^{-11}$	$1.352(13) \times 10^{-10}$
t_{16}	$6(6, 0A_1, a_1)$	$1.02(8) \times 10^{-11}$	$1.1(9) \times 10^{-12}$
t_{17}	$6(6, 0E, a_1)$	$-1.08(3) \times 10^{-11}$	$-4.80(39) \times 10^{-12}$
t_{18}	$6(6, 0F_2, a_1)$	$-3.355(51) \times 10^{-11}$	$-2.69(42) \times 10^{-11}$
t_{19}	$6(6, 1F_2, a_1)$	$-1.986(16) \times 10^{-11}$	$-1.1762(14) \times 10^{-10}$
σ^a	kHz	23.29	23.47
RMS	kHz	69.87	72.85

[a] Standard deviation of the fit calculated from the median of absolute residuals.

$$S_{if} = K_{if} g_i e^{-(hcE_i)/kT} \sum_{M_i,M_f} |\langle \Phi_i | \tilde{\mu}_{\mathscr{Z}} | \Phi_f \rangle|^2, \quad (21)$$

where K_{if} is a numerical coefficient and g_i is the spin statistical weight of state Φ_i. The values of spin statistical weights in XY_2Z_2 (C_{2v}) molecules, with Y ligands having spin $\frac{1}{2}$ and Z ligands having a spin equal to 1 are listed in Table (6) of [6]. The sum is realized over the spherical components M_i and M_f of the two states in the Laboratory-Fixed Frame (LFF). $\mu_{\mathscr{Z}}$ is the $\mathscr{Z}$ component of the dipole moment in the ($\mathscr{O}\mathscr{X}\mathscr{Y}\mathscr{Z}$) LFF.

In order to calculate transition intensities, we have limited the development of the dipole moment operator through the zeroth order only using the methods explained in [6]. This reference also gives the expression of the matrix elements of the dipole moment operator.

4. Analysis and discussion

First, the assigned transitions (1071) were fitted to the Watsonian using I^r representation in the S and 6 reductions. The results are given in Table 1. Inspection of this table shows that all the determinable sextic centrifugal distortion constants are well determined and that the standard deviation of the fit in the 6 reduction is slightly smaller although the number of fitted parameters is smaller (16 instead of 20). It confirms the conclusion of [1] that, in the particular case of SO_2F_2, it is preferable to use a non-reduced Hamiltonian (at least up to quartic terms). It is also worth noting that the rotational constants have a smaller standard deviation in the 6 reduction and that the sextic constants are significantly different in the S and 6 reductions (another indication that the reduction parameter is too large).

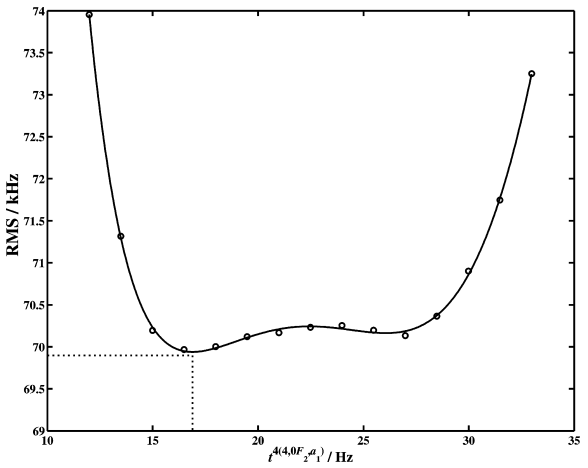

Fig. 2. The root mean square versus the values of the $t^{A(4,0F_2,a_1)}$ parameter.

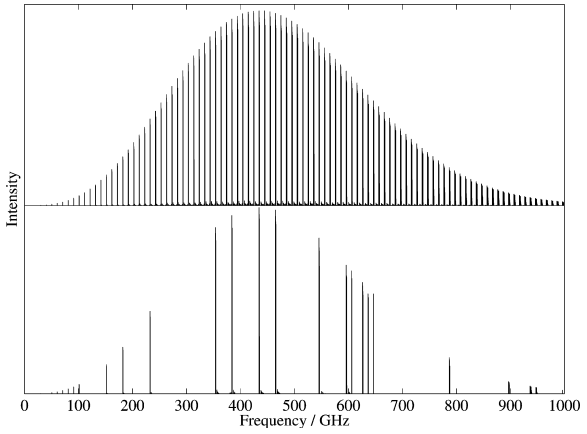

Fig. 3. Overview stick spectrum of the ground state of SO_2F_2: experiment and simulation.

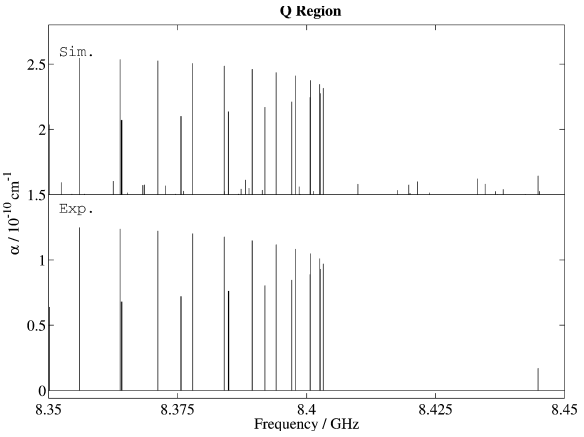

Fig. 4. Q region of the ground state of SO_2F_2: experiment and simulation.

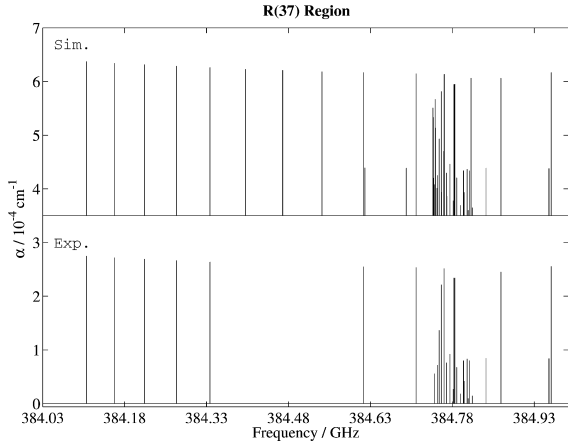

Fig. 5. $R(37)$ cluster of the ground state of SO_2F_2: experiment and simulation.

We have then performed an analysis of the ground state of SO_2F_2 using the tensorial model described above. For this, $\mathscr{H}_{\{\text{Moret-Bailly}\}}$ has been developed to the fourth order. Preliminary simulations of this region were obtained starting from the rotational parameters of Sarka et al. [1] and in taking the same value for A_0, B_0, and C_0 rotational constants. In the I^r representation, we obtain the following relations for our t_1, t_2 and t_3 tensorial parameters using (2) and (17)

$$t_1 \simeq \frac{A_0+B_0+C_0}{3}, \quad t_2 \simeq \frac{\sqrt{6}}{12}\left(A_0-\frac{B_0}{2}-\frac{C_0}{2}\right), \quad t_3 \simeq \frac{C_0-B_0}{4\sqrt{2}}. \tag{22}$$

A first simulation enabled us to begin the assignments and the fit procedure for low J values. More and more parameters have been successively released and the whole spectrum has been simulated. At the end, all the 1071 available transitions (see above) were used. So 18 parameters were adjusted together and the final standard deviation is equal to 23.29 kHz. The resulting parameters are listed in Table 2. Only one parameter, namely $t_9 = t^{4(4,0F_2,A_1)}$, is fixed because of an ambiguity problem. Its value is choosen as shown in Fig. 2 in the aim of decreasing the root mean square. Several root mean squares have been calculated for different values of the $t^{4(4,0F_2,A_1)}$ parameter. This curve has been fitted by a polynomial and the minimum has been found. The last column of this table also gives the values of our parameter in $t_9 = 0$ reduction.

Figs. 3–5 show synthetic spectra calculated with the parameters of the fit listed in Table 2. The detailed views show very good agreement between the simulation and the experiment.

In the experimental stick spectrum, only lines that have been actually observed are plotted. Fig. 7 displays the calculated and observed reduced energy levels for the ground state (observed levels are levels reached by observed transitions). They are obtained by subtracting the scalar terms, i.e.,

$$E_{\text{red}} = E(J,\tilde{\alpha},\tilde{C}) - t^{2(0,0A_1,A_1)}J(J+1) - t^{4(0,0A_1,A_1)}J^2(J+1)^2. \tag{23}$$

The Fig. 6 show the observed minus the calculated frequencies versus J. These residual values are quite similar in both models versus J.

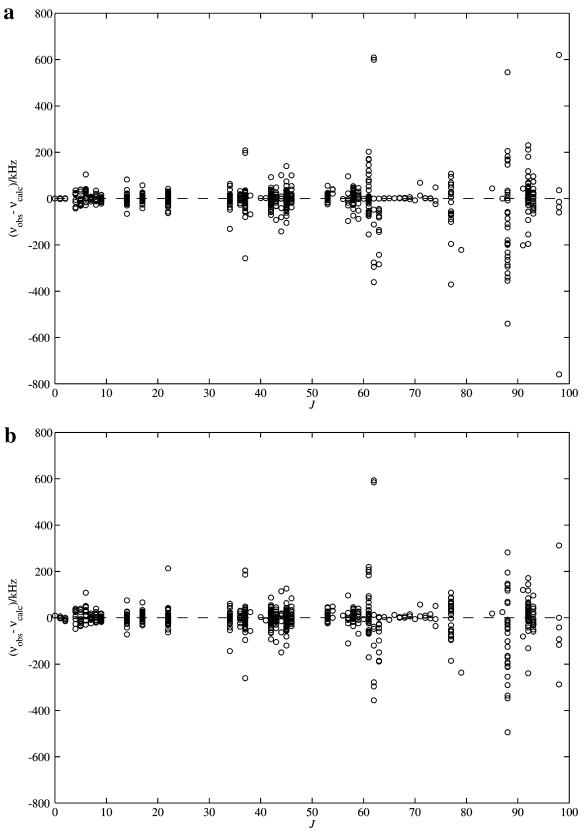

Fig. 6. Observed minus calculated wavenumbers versus J with the Watsonian (a) and Moret-Bailly's Hamiltonian (b).

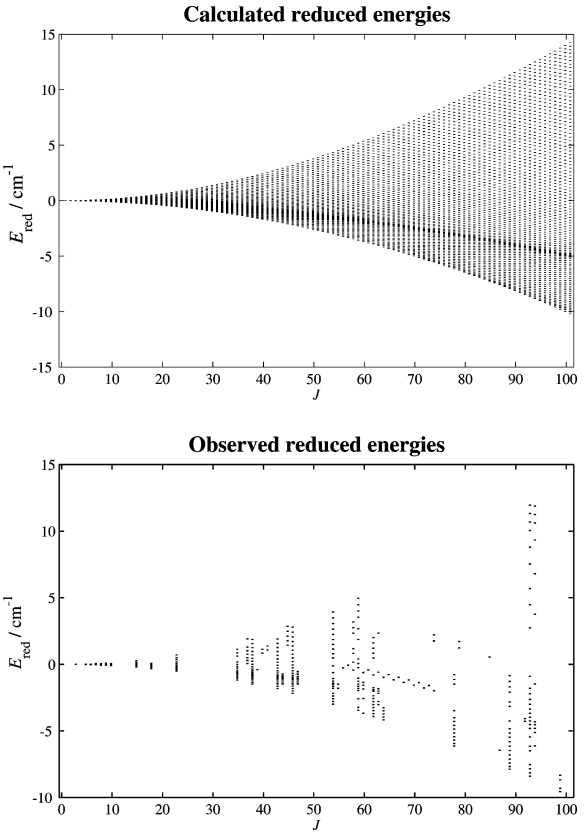

Fig. 7. Observed and calculated energies for the ground state of SO_2F_2 using the Moret-Bailly's model.

Table 3
Fitted values of the ground state parameters up to the quartic order with the tensorial model ($H_{\text{Moret-Bailly}}$)

t_i	$\Omega(K,n\Gamma,\tilde{\Gamma})$	Value/MHz
t_1	$2(0,0A_1,a_1)$	5088.3097(18)
t_2	$2(2,0E,a_1)$	14.2468(5)
t_3	$2(2,0F_2,a_1)$	−2.8291(3)
t_4	$4(0,0A_1,a_1)$	$-0.133101(28)\times10^{-2}$
t_5	$4(2,0E,a_1)$	$4.530(75)\times10^{-6}$
t_6	$4(2,0F_2,a_1)$	$-7.657(39)\times10^{-6}$
t_7	$4(4,0A_1,a_1)$	$-7.2906(30)\times10^{-5}$
t_8	$4(4,0E,a_1)$	$-3.64(25)\times10^{-7}$
t_9	$4(4,0F_2,a_1)$	0 (fixed)

Table 4
Fitted values of the ground state parameters up to the quartic order with the Watson model compared to those obtained according to relation (18) and Table 3

Watson's Par.	Value/MHz	"Calc."/MHz
A	$5.1348351(28)\times10^{3}$	$5.1348394(51)\times10^{3}$
B	$5.0730374(21)\times10^{3}$	$5.0730466(35)\times10^{3}$
C	$5.0570357(24)\times10^{3}$	$5.0570424(35)\times10^{3}$
$D_J=-T_{400}$	$1.47055(19)\times10^{-3}$	$1.2052(13)\times10^{-3}$
$D_{JK}=-T_{220}$	$-1.53611(37)\times10^{-3}$	$-1.0037(20)\times10^{-3}$
$D_K=-T_{040}$	$1.85278(97)\times10^{-3}$	$1.5879(13)\times10^{-3}$
$d_1=T_{202}$	$-24.374(94)\times10^{-6}$	$-25.01(13)\times10^{-6}$
$d_2=T_{004}$	$13.3326(53)\times10^{-5}$	$26.779(22)\times10^{-5}$
$R_5=\frac{1}{2}T_{022}$	0 (fixed)	0

In the aim of comparing the parameters obtained with the two models with the correspondence formula (17),(18), we decide to do in the both case a fit till order 2 only. So these fits are not the best ones but they are just performed to verify our relations of correspondence. In Tables 3 and 4, we give fitted values up to the quartic parameters in both models and according to relations (18), we recalculate the Watson's parameters. The values are in reasonably good agreement. We must keep in mind that our relations (18) are only approximate.

5. Conclusion

We have first presented the two theoretical models which have enabled us to analyze the ground state of the SO_2F_2 quasi-spherical top. Then, we give the two corresponding sets of parameters and relations between them. They clearly show an approximate numerical link between the two formalisms. We can conclude at this stage of comparison that both models give similar results in the analysis independently from the J values. A complete table of measured and assigned transitions in both models is available on the journal's home page. Our analysis has been performed thanks to the C_{2v} TDS software, which can be freely downloaded at the URL: `http://www.u-bourgogne.fr/LPUB/c2vTDS.html`.

Our next challenge is to apply the tensorial model to the $\nu_9(b_2)/\nu_7(b_1)/\nu_3(a_1)$ triad and particularly to the $\nu_4(a_1)/\nu_5(a_2)$ dyad where problems concerning the choice of axes are encountered with Watson's formalism.

Acknowledgments

The authors wish to thank Dr. Jean-Marie Flaud (LPPM, 91405 Orsay Cedex, France) for helpful discussions in Prague in September 2002. Support from the Région Bourgogne for the computer equipment of the Laboratoire de Physique de l'Université de Bourgogne is gratefully acknowledged. The work in Köln has been supported in part by the Deutsche Forschungsgemeinschaft (DFG) via grant SFB 494 and by special funding from the Land Nordrhein-Westfalen. L.M. acknowledges the Alexander von Humboldt-Stiftung for his stipend.

References

[1] K. Sarka, J. Demaison, L. Margulès, I. Merke, N. Heineking, H. Bürger, H. Ruland, J. Mol. Spectrosc. 200 (2000) 55–64.
[2] H. Bürger, H. Ruland, I. Merke, K. Sarka, L. Margulès, J. Demaison, J. Mol. Spectrosc. 203 (2000) 268–272.
[3] H. Bürger, J. Demaison, F. Hegelund, L. Margulès, I. Merke, J. Mol. Struct. 612 (2002) 133–141.
[4] J.K.G. Watson, in: J.R. Durig (Ed.), Vibrational Spectra and Structure, vol. 6, Elsevier, Amsterdam, 1977, pp. 1–89.
[5] A. Mekhtiev, J.T. Hougen, J. Mol. Spectrosc. 199 (2000) 284–301.
[6] M. Rotger, V. Boudon, M. Loëte, J. Mol. Spectrosc. 216 (2002) 297–307.
[7] J.-P. Champion, M. Loëte, G. Pierre, in: K.N. Rao, A. Weber (Eds.), Spectroscopy of the Earth's Atmosphere and Interstellar Medium, Academic Press Inc., San Diego, 1992, pp. 339–422.
[8] M. Krüger, H. Harder, C. Gerke, H. Dreizler, Z. Naturforsch. A 48 (1993) 737–738.
[9] C. Gerke, unpublished results (Kiel).
[10] G. Winnewisser, A.F. Krupnov, M. Yu Tretyakov, M. Liedtke, F. Lewen, A.A. Saleck, R. Schieder, A.P. Shkaev, S.V. Volokhov, J. Mol. Spectrosc. 165 (1994) 294–300.
[11] D. Boucher, R. Bocquet, J. Burie, W.D. Chen, J. Phys. III (France) 4 (1994) 1467–1480.
[12] D. Papoušek, M.R. Aliev, Molecular Vibrational–Rotational Spectra, Elsevier, Amsterdam/New York, 1982.
[13] N. Cheblal, M. Loëte, V. Boudon, J. Mol. Spectrosc. 197 (1999) 222–231.
[14] Ch. Wenger, V. Boudon, J.-P. Champion, G. Pierre, J. Quant. Spectrosc. Radiat. Transfer 66 (2000) 1–16.
[15] Ch. Wenger, J.-P. Champion, J. Quant. Spectrosc. Radiat. Transfer 59 (1998) 471–480.
[16] J. Moret-Bailly, Cah. Phys. 15 (1961) 237–316.
[17] J. Moret-Bailly, J. Mol. Spectrosc. 15 (1965) 344–354.
[18] B.I. Zhilinskiĭ, Opt. Spectrosc. (USSR) 51 (1981) 262–263.
[19] J.-P. Champion, G. Pierre, F. Michelot, J. Moret-Bailly, Can. J. Phys. 55 (1977) 512–520.
[20] M. Rey, V. Boudon, Ch. Wenger, G. Pierre, B. Sartakov, J. Mol. Spectrosc. 219 (2003) 313–325.
[21] M. Rotger, A. Decrette, V. Boudon, M. Loëte, S. Sander, H. Willner, J. Mol. Spectrosc. 208 (2001) 169–179.

QUATRIÈME PARTIE

Chapitre

2

Bases de Données Spectroscopiques

Publications P17, P24, P25

2.1 Introduction

Des bases de données ont été développées dans le but d'une part de conserver les valeurs des paramètres et les attributions des analyses effectuées aussi bien pour les toupies sphériques (bases de données existant déjà) que pour les toupies symétriques et asymétriques mais aussi pour donner à la communauté scientifique la possibilité de prédire des spectres de ces molécules dans différentes conditions expérimentales et pour différentes régions spectrales.

Ces bases de données et programmes sont librement utilisables par la communauté scientifique et remisent à jour régulièrement.

2.2 Résultats

Différents modèles issus du modèle toupie sphérique ont été mis au point (voir le chapitre précédent) et ont donc permis le développement de trois nouvelles bases de données. Il s'agit de :

- C_{4v}TDS pour les molécules symétriques de type XY_5Z,
- C_{2v}TDS pour les molécules asymétriques de type XY_2Z_2,
- D_{2h}TDS pour les molécules asymétriques de type X_2Y_4.

Seules existaient initialement les bases de données STDS et HTDS pour le toupies sphériques (groupes de symétrie T_d et O_h). Ces nouvelles bases ont été développées dans le même esprit que les précédentes. Récemment des efforts ont été faits pour les rendre compatibles avec le format HITRAN. Pour illustration de ce travail, je donne ci-après une seule version de ce type d'article sur la base de données C_{4v}TDS. Un travail analogue a été fait pour les bases de données C_{2v}TDS et D_{2h}TDS.

2.3 Perspectives

En matière de bases de données, des efforts importants sont à faire afin de les rendre plus interactives et plus abordables pour le commun des mortels. Une interface graphique va être développée prochainement par Ch. Wenger afin de rendre les résultats scientifiques et notamment la prédiction de spectres plus accessibles à tous.

Une perspective importante est de généraliser ces bases de données en y incluant par exemple l'effet Stark, notamment pour le groupe de symétrie D_{2h} (voir plus de détails dans le chapitre suivant).

2.4 Article-clé

Est reproduit ici l'article type sur les bases de données et notamment celui pour le groupe de symétrie C_{4v}.

– [**P17 :** *J. Quant. Spectrosc. Rad. Transfer*, **74**, 621–636 (2002)] présente les chaînes de programmes pour simuler les spectres d'absorption infrarouge de molécules symétriques de type XY_5Z. Des articles identiques ont été rédigés pour les groupes C_{2v} et D_{2h}.

PERGAMON

Journal of Quantitative Spectroscopy & Radiative Transfer 74 (2002) 621–636

Journal of Quantitative Spectroscopy & Radiative Transfer

www.elsevier.com/locate/jqsrt

C_{4v} Top Data System (C_{4v} TDS) software for infrared spectrum simulation of XY_5Z symmetric molecules

Ch. Wenger, M. Rotger*, V. Boudon

Laboratoire de Physique de l'Université de Bourgogne, UMR CNRS 5027, 9, Avenue Alain Savary, BP 47870, F-21078 Dijon Cedex, France

Received 1 October 2001; accepted 29 November 2001

Abstract

The *Highly spherical Top Data System* program suite developed in Dijon has been extended in the aim of studying any rovibrational band or polyad of XY_5Z (C_{4v}) symmetric top molecules. We work in the $O(3) \supset O_h \supset C_{4v}$ chain because most of these species result from the substitution of one ligand of the corresponding spherical tops and thus are relatively close to octahedral symmetry. The choice of this group chain has consequences in the way in which it is used to specify the input parameters of the programs for Hamiltonian and transition moment model calculations. One example concerning the ν_1/ν_8 dyad of the $SF_5{}^{35}Cl$ molecule is presented. As before, this suite consists of a series of FORTRAN programs called as scripts. The whole package is freely accessible through ftp (user anonymous) at jupiter.u-bourgogne.fr or through the World Wide Web at http://www.u-bourgogne.fr/LPUB/c4vTDS.html.

Keywords: Symmetric molecules; Tensorial formalism; Vibrational extrapolation

1. Introduction

In a previous paper [1], we described *Highly spherical Top Data System* (HTDS) for the simulation of XY_6 spherical top spectra. This package can be used for the calculation of any band or polyad of such molecules. It is itself derived from the *Spherical Top Data System* (STDS) package developed in Dijon for XY_4 molecules [2].

In this article, we present a derived version of HTDS, named C_{4v}TDS (C_{4v} *Top Data System*) dedicated to the study of XY_5Z symmetric molecules belonging to the C_{4v} point group. This extension was first motivated by the possibility of studying rovibrational bands of $SF_5{}^{35}Cl$ and similar molecules, whose high-resolution spectroscopy is quite unexplored. In a previous paper [3], we have described our preliminary analysis of the ν_1/ν_8 dyad of $SF_5{}^{35}Cl$ using the C_{4v}TDS programs.

* Corresponding author. Tel.: +33-380395967; fax: +33-380395971.
E-mail address: maud.rotger@u-bourgogne.fr (M. Rotger).

0022-4073/02/$ - see front matter
PII: S0022-4073(01)00275-8

This case will therefore be largely used in the examples given in the present paper. The principal characteristics of C_{4v}TDS are:

- A full treatment in the C_{4v} group is made.
- All XY_5Z molecules are considered as being derived from an XY_6 "parent" molecule. For example, SF_5Cl is associated to the SF_6 spherical top. For this reason, we work in the $O(3) \supset O_h \supset C_{4v}$ chain [4,5]. However, we should mention here that there are other ways to treat symmetric or asymmetric top molecules using tensorial formalism, in particular without using an intermediate group (like O_h here) [6,7].
- A given polyad of an XY_5Z molecule corresponds to a certain vibrational level (or polyad) of the XY_6 "parent" molecule under consideration. So it is this XY_6 level (or polyad) which is fully specified by the user in the command-line arguments.
- Just as for STDS and HTDS, C_{4v}TDS uses both vibrational extrapolation and tensorial formalism techniques, which allow a systematic treatment of all types of interactions for any polyad system and up to any order of the development.
- The package includes programs necessary to fit the experimental data with Hamiltonian parameters.

C_{4v}TDS thus constitutes a complement to STDS and HTDS for people who requires to study XY_5Z molecule spectra.

The C_{4v}TDS package presented here is intended to provide direct access to the theoretical results achieved in high-resolution research on XY_5Z molecules as well as the tools for studying new spectra. It is freely accessible by anonymous `ftp` at the Internet address

`jupiter.u-bourgogne.fr`

or through the World Wide Web at

`http://www.u-bourgogne.fr/LPUB/c4vTDS.html`

C_{4v}TDS is designed for UNIX workstations (including Macintosh computers running under MacOS X), for PC computers running under LINUX and also for Macintosh computers (MacOS 8.x and 9.x). It consists of a complete set of FORTRAN routines managed by UNIX scripts (MPW scripts for the MacOS 8.x/9.x versions). The aim of this paper is to provide the user, nonexpert in the theory of XY_5Z symmetric top molecules, all information needed to exploit efficiently the software package.

2. General comments about symmetric molecules and their spectra

2.1. Remarkable spectroscopic features

XY_5Z molecules [8–14] possess 11 normal modes of vibration: five stretching modes named $\nu_1(a_1)$, $\nu_2(a_1)$, $\nu_4(a_1)$, $\nu_5(b_1)$ and $\nu_8(e)$, and six bending modes that are $\nu_3(a_1)$, $\nu_6(b_1)$, $\nu_7(b_2)$, $\nu_9(e)$, $\nu_{10}(e)$ and $\nu_{11}(e)$. All these bands are Raman active, and only $\nu_5(b_1)$, $\nu_6(b_1)$ and $\nu_7(b_2)$ bands are infrared inactive.

To achieve the analysis of rovibrational spectra of these molecules, we have proposed a new tensorial formalism [4,5] adapted to the case of C_{4v} symmetric tops. As already mentioned above,

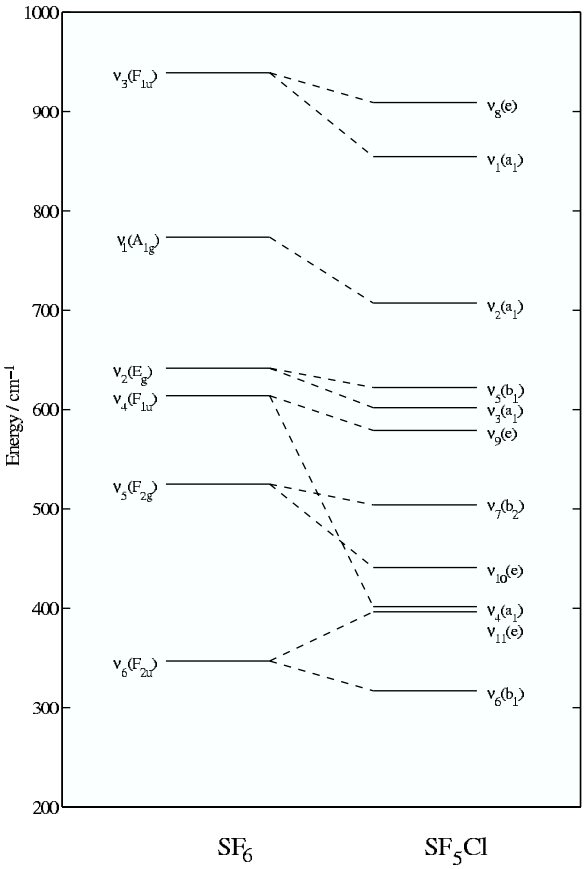

Fig. 1. $SF_6 \rightarrow SF_5Cl$ correlation scheme.

it is an extension of the usual formalism already developed in Dijon for octahedral XY_6 molecules [1,15] in the $O(3) \supset O_h$ group chain. We work in the $O(3) \supset O_h \supset C_{4v}$ chain because XY_5Z symmetric tops result from the substitution of one ligand of the corresponding spherical top and thus are relatively closer to octahedral symmetry. For example, SF_5Cl has a vibrational level scheme [16], as illustrated in Fig. 1, quite similar to that of the SF_6 molecule. For instance, the ν_1/ν_8 dyad is correlated to the strong ν_3 fundamental band of SF_6. In this way, each rovibrational "polyad" of SF_5Cl is related to a certain band of the XY_6 "parent" molecule.

2.2. Theory

The theoretical model used in C_{4v}TDS is based on the tensorial formalism and vibrational extrapolation methods developed in Dijon [15,17]. We choose the following notation:

- Γ $(=A_{1\tau}, A_{2\tau}, E_\tau, F_{1\tau}, F_{2\tau}, \tau = g$ or $u)$ denotes O_h irreducible representations (irreps), and
- $\tilde{\Gamma}(=a_1, a_2, b_1, b_2, e)$ is used for C_{4v} irreps.

More generally, tilded letters like $\tilde{C}$ denote C_{4v} representations.

Let us consider an XY_5Z molecule whose XY_6 "parent" species has its vibrational levels grouped in a series of polyads designed by P_k ($k=0,\ldots,n,\ldots$), P_0 being the ground state (GS). The XY_5Z Hamiltonian can be developed as a sum of operators specific to each polyad as

$$\mathscr{H}=\mathscr{H}_{\{P_0\equiv \mathrm{GS}\}}+\mathscr{H}_{\{P_1\}}+\cdots+\mathscr{H}_{\{P_k\}}+\cdots+\mathscr{H}_{\{P_{n-1}\}}+\mathscr{H}_{\{P_n\}}+\cdots. \tag{1}$$

The effective Hamiltonian for polyad P_n is obtained by projection in the corresponding subspace,

$$\begin{aligned} H^{\langle P_n\rangle} &= P^{\langle P_n\rangle}\mathscr{H}P^{\langle P_n\rangle}, \\ &= H^{\langle P_n\rangle}_{\{\mathrm{GS}\}}+H^{\langle P_n\rangle}_{\{P_1\}}+\cdots+H^{\langle P_n\rangle}_{\{P_k\}}+\cdots+H^{\langle P_n\rangle}_{\{P_{n-1}\}}+H^{\langle P_n\rangle}_{\{P_n\}}. \end{aligned} \tag{2}$$

The different terms are written as

$$\mathscr{H}_{\{P_k\}}=\sum_{\text{all indexes}} t^{\Omega(K_g,n\Gamma_g,\tilde{\Gamma})\Gamma_{1\mu}\Gamma_{2\mu}\Gamma_{vg}}_{\{n_s\}\{m_s\}}\beta\times\left(R^{\Omega(K_g,n\Gamma_g,\tilde{\Gamma})}\otimes^{\varepsilon} V^{\Gamma_{1\mu}\Gamma_{2\mu}(\Gamma_{vg},\tilde{\Gamma})}_{\{n_s\}\{m_s\}}\right)^{(a_1)}. \tag{3}$$

In this equation, $t^{\Omega(K_g,n\Gamma_g,\tilde{\Gamma})\Gamma_{1\mu}\Gamma_{2\mu}\Gamma_{vg}}_{\{n_s\}\{m_s\}}$ are the parameters to be determined. $R^{\Omega(K_g,n\Gamma_g,\tilde{\Gamma})}$ and ${}^{\varepsilon}V^{\Gamma_{1\mu}\Gamma_{2\mu}(\Gamma_{vg},\tilde{\Gamma})}_{\{n_s\}\{m_s\}}$ are rotational and vibrational operators of respective degrees Ω (maximum degree in the rotational angular momentum components J_x, J_y and J_z) and Ω_v (degree in the creation and annihilation operators). The order of each individual term is $\Omega+\Omega_v-2$. Their construction is described in Ref. [17]. β is a numerical factor equal to $\sqrt{[\Gamma_1]}(-\sqrt{3}/4)^{\Omega/2}$ if $(K_g,n\Gamma_g)=(0,0A_{1g})$ and equal to 1 otherwise. We can notice that R and V operators are first reoriented into the C_{4v} group and then coupled together [4]. Let us just recall here that any operator A ($=R,V,\ldots$) that is symmetrized in O_h can be reoriented into the C_{4v} subgroup thanks to the G' matrix [4]:

$$A^{(C,\tilde{C})}_{\tilde{\sigma}}=\sum_{\sigma}{}^{(C)}G^{\prime\sigma}_{\tilde{C}\tilde{\sigma}}A^{(C)}_{\sigma}. \tag{4}$$

Such a Hamiltonian development scheme enables the treatment of any polyad system. In this work, and as an example, we will use the two following effective Hamiltonians:

- The ground state effective Hamiltonian

$$H^{\langle \mathrm{GS}\rangle}=H^{\langle \mathrm{GS}\rangle}_{\{\mathrm{GS}\}}. \tag{5}$$

- The ν_1/ν_8 stretching dyad effective Hamiltonian

$$H^{\langle \nu_1/\nu_8\rangle}=H^{\langle \nu_1/\nu_8\rangle}_{\{\mathrm{GS}\}}+H^{\langle \nu_1/\nu_8\rangle}_{\{\nu_1/\nu_8\}}, \tag{6}$$

recalling that the ν_1/ν_8 dyad comes from the splitting of the ν_3 band of the XY_6 "parent" molecule; thus $\mathscr{H}_{\{\nu_1/\nu_8\}}$ is constructed using ${}^{\varepsilon}V^{\Gamma_{1\mu}\Gamma_{2\mu}(\Gamma_{vg},\tilde{\Gamma})}_{\{3\}\{3\}}$ vibrational operators which involve $a_3^{+(F_{1u})}$ and $a_3^{(F_{1u})}$, creation and annihilation operators [17].

The matrix elements are calculated in the coupled basis

$$\left|\left[\Psi_r^{(J,nC_r,\tilde{C}_r)}\otimes\Psi_v^{(C_v,\tilde{C}_v)}\right]^{(\tilde{C})}_{\tilde{\sigma}}\right\rangle \tag{7}$$

with

$$|\Psi_v^{(C_v,\tilde{C}_v)}\rangle = |[[[[\Psi_{v_1}^{(A_{1g})} \otimes \Psi_{v_2}^{(l_2,C_2)}] \otimes \Psi_{v_3}^{(l_3,n_3C_3)}]^{(C_{23})} \otimes \Psi_{v_4}^{(l_4,n_4C_4)}]^{(C_{234})} \otimes \Psi_{v_5}^{(l_5,n_5C_5)}]^{(C_{2345})} \otimes \Psi_{v_6}^{(l_6,n_6C_6)}]^{(C_v,\tilde{C}_v)}\rangle. \quad (8)$$

$v_1,\ldots,v_6$ are vibration quantum numbers for the XY_6 "parent" molecule. $\tilde{C}_v$ is the vibrational symmetry in C_{4v}:

$$D^{(C_v)} \supset \tilde{D}^{(\tilde{C}_v)}. \quad (9)$$

Expressions of the matrix elements are given in Ref. [5]. All the rovibrational levels are described by $(J, \tilde{\alpha}, \tilde{C})$ labels where $\tilde{\alpha}$ is a numbering index for levels that have the same C_{4v} symmetry within a J block. This labelling is related to our group chain choice which considers XY_5Z molecules like near-spherical tops. In this way, the usual K quantum number is hidden and related to $\tilde{\alpha}$ and the $\tilde{C}$ symmetry. So, the K values do not appear explicitly in our labels and the ΔK nomenclature does not occur in our transition labels.

In order to perform intensity calculations, the dipole moment (for absorption spectra) operator is expanded in a similar way. This is described in detail in one of our previous papers [5] and is thus not explained here.

3. Description of the C_{4v}TDS package

In this paper, we describe the UNIX version of C_{4v}TDS. Users interested in the Mac OS 8.x/9.x version should visit the C_{4v}TDS Web site:

http://www.u-bourgogne.fr/LPUB/c4vTDS.html

Once properly installed, the C_{4v}TDS package has the directory structure described in Fig. 2 (assuming that the installation directory is named C_{4v}TDS). The subdirectories contain the following files:

- `bin`: executable files created by the `compile` script.
- `ctrp`: examples of files containing constraints for parameter fits.
- `exp`: some experimental files (line frequencies and assignments).
- `gtd`: symmetrization coefficients ${}^{(J)}G^m_{nC\sigma}$ (see Ref. [17]) till $J = 199$. This upper limit value is a recent modification also done in STDS and HTDS [18].
- `jobs`: examples of jobs for spectrum calculations and experimental data fits.
- `para`: parameter files for all the molecules and band systems presently included in the package.
- `prog`: scripts for compilation, program sources and some other files used by the scripts.

The calculation jobs (in `jobs`) are arranged by molecule. Their names are in the form

```
job_cal_NameOfTheBandSystem.
```

For example, `.../jobs/SF535Cl/job_cal_nu1nu8` calculates the ν_1/ν_8 dyad of $SF_5{}^{35}Cl$. For the moment, only this case is given in this data bank but other rovibrational studies are planned and will be added in future updates.

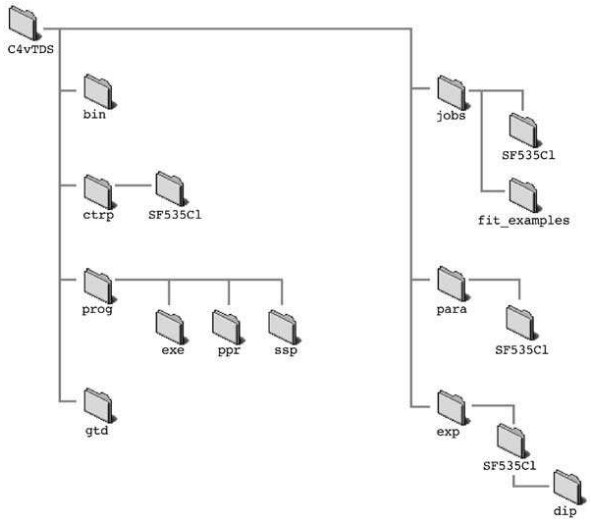

Fig. 2. The directory structure of C_{4v}TDS.

4. Calculating spectra with C_{4v}TDS

The general structure of a job for spectrum calculation is given in Fig. 3. A commented example (for the ν_1/ν_8 dyad of $SF_5{}^{35}Cl$) is given in Table 1. First of all, the eigenvalues (energies) and eigenstates of the effective Hamiltonian are calculated for the upper and lower polyad (here a polyad can be a single vibrational state as well as a complex vibrational system). Then the transition moments for the transitions between these two polyads are evaluated and finally, the spectrum (line frequencies and intensities) is calculated for specific conditions (frequency range, temperature, etc). Let us first describe the Hamiltonian energy calculation.

The first program used is `hmodel` which determines the operators to be used in the Hamiltonian development for the vibrational levels and polyad scheme considered and up to the development order specified. The general command-line syntax for `hmodel` can be summarized as follows:

$$
\begin{array}{llllllllllll}
\texttt{hmodel} & Pn & \texttt{N1} & \texttt{D}k_0 & 0\,0\,0\,0\,0\,0 & \backslash & & & & & & \\
 & & \texttt{N}m_1 & \texttt{D}k_1 & v^1_{1_1} & \ldots & v^1_{6_1} & \ldots & v^{m_1}_{1_1} & \ldots & v^{m_1}_{6_1} & \backslash \\
 & & \ldots & \ldots & \ldots & \ldots & \ldots & \ldots & \ldots & \ldots & \ldots & \backslash \\
 & & \texttt{N}m_i & \texttt{D}k_i & v^1_{1_i} & \ldots & v^1_{6_i} & \ldots & v^{m_i}_{1_i} & \ldots & v^{m_i}_{6_i} & \backslash \\
 & & \ldots & \ldots & \ldots & \ldots & \ldots & \ldots & \ldots & \ldots & \ldots & \backslash \\
 & & \texttt{N}m_n & \texttt{D}k_n & v^1_{1_n} & \ldots & v^1_{6_n} & \ldots & v^{m_n}_{1_n} & \ldots & v^{m_n}_{6_n} &
\end{array}
$$

The first argument must be the letter P immediately followed by an integer number n. This one indicates the running number of the polyad to consider. This argument is followed by $n+1$ lines describing polyads $P_0,\ldots,P_i,\ldots,P_n$. Each line consists of the following:

- The number m_i of vibrational states for polyad P_i (following letter `N`).
- The order of development (following letter `D`) of $\mathscr{H}_{\{P_i\}}$.

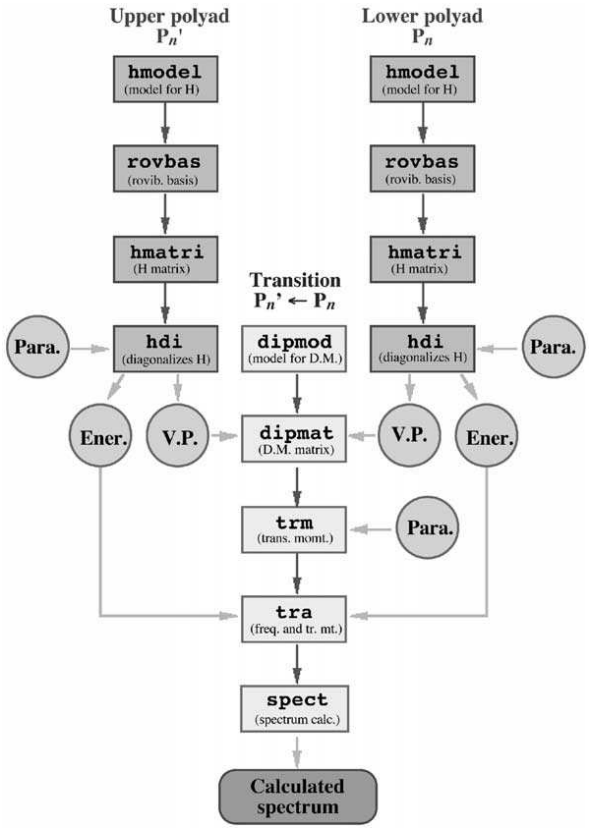

Fig. 3. Schematic description of the spectrum calculation.

- m_i sets of six vibrational quantum numbers $(v_1, v_2, v_3, v_4, v_5, v_6)$ defining the m_i vibrational states of polyad P_i of the XY_6 "parent" molecule.

The rovibrational basis (Eq. (7)) is then calculated by `rovbas` for $J = 0,\ldots,J_{\max}$. The matrix elements of the Hamiltonian operators constructed by `hmodel` are calculated by `hmatri` in this basis. Finally, `hdi` uses the Hamiltonian parameter values to construct the Hamiltonian matrix and then diagonalizes it.

The model and matrix elements of the dipole moment are calculated in a similar way by `dipmod` and `dipmat` for absorption spectra. The syntax for `dipmod` follows the same principles as for `hmodel`. This time, both the lower and upper polyads must be fully specified on the command-line (see example in Table 1). Programs `trm` and `tra` calculate the transition moments.

The final step is made by `spect` that calculates the line frequencies and intensities in the frequency range $[f_{\min}, f_{\max}]$ and for rotational and vibrational temperatures $T_{\rm rot}$ and $T_{\rm vib}$, respectively. The command-line syntax for `spect` is

`spect` $f_{\min} f_{\max} T_{\rm rot} T_{\rm vib} I_{\min}$

Table 1
Example of a job for spectrum calculation: the ν_1/ν_8 dyad of $SF_5{}^{35}Cl$. Some comments are given on the right

```
#! /bin/sh
 set -v
##
## Calculation of the absorption spectrum
## of the nu1/nu8 dyad of SF535Cl
##
BASD=.../.../C4vTDS                                  ⇒ C4v TDS installation directory.
#
  SCRD=$BASD/prog/exe
  PARD=$BASD/para
##
## Jmax values.
##                                                   ⇒ Maximum J value for lower level.
 JPinf_p=80                                         ⇒ Maximum J value for upper level.
 JPsup_p=79                                         ⇒ Maximum J value for the calculated
 JPsupminf_p=79                                       spectrum.
##
## Parameter file.
##
 PARA=$PARD/SF535Cl/Pa_001000m000000                ⇒ Parameters for H and μ.
##
##
########################################
##
## Hamiltonian matrix elements.
##
## Lower Polyad.
##
 $SCRD/passx hmodel P0 N1 D2   0 0 0 0 0 0
##                                                  ⇒ Hamiltonian model for lower polyad.
$SCRD/passx rovbas P0 N1 D2 $JPinf_p
##                                                  ⇒ Rovibrational basis for lower polyad.
 $SCRD/passx hmatri P0 N1 D2 $JPinf_p
##                                                  ⇒ H matrix elements for lower polyad.
 $SCRD/passx hdi P0 N1 D2 $JPinf_p $PARA
##                                                  ⇒ Diagonalization of H for lower polyad.
## Upper Polyad.
##
 $SCRD/passx hmodel P1 N1 D2 0 0 0 0 0 0   \
                       N1 D4 0 0 1 0 0 0
##                                                  ⇒ Hamiltonian model for upper polyad.
 $SCRD/passx rovbas P1 N1 D24 $JPsup_p
##                                                  ⇒ Rovibrational basis for upper polyad.
 $SCRD/passx hmatri P1 N1 D24 $JPsup_p
##                                                  ⇒ H matrix elements for upper polyad.
 $SCRD/passx hdi P1 N1 D24 $JPsup_p $PARA
##                                                  ⇒ Diagonalization of H for upper polyad.
## Dipole moment matrix elements.
```

Table 1. (*continued*)

```
##
## Upper - lower level transition.
##
 $SCRD/passx dipmod P1 N1   0 0 0 0 0 0 \
                      N1   0 0 1 0 0 0    \
                    P0 N1   0 0 0 0 0 0    \          ⇒ Dipole moment model.
                    D0
##
 $SCRD/passx dipmat P1 N1 P0 N1 D0 \
                    $JPsupminf_p                      ⇒ Dipole moment matrix elements.
##
## Transition moment.
##
 $SCRD/passx trm     P1 N1 P0 N1 D0     \
              $JPsupminf_p $PARA dip                  ⇒ Transition moments.
##
 $SCRD/passx tra     P1     P0     D0 \
              $JPsupminf_p                            ⇒ Frequencies and transition moments.
##
## Spectrum calculation.
##
 $SCRD/passx spect  840.  870.  203.  203.  0.001
 mv spectr.t spect_nu1.t
 mv spectr.xy spect_nu1.xy
##                                                   ⇒ Spectrum calculation for the ν1 band.
 $SCRD/passx spect   900.  920.  203.  203.  0.001
 mv spectr.t spect_nu8.t
 mv spectr.xy spect_nu8.xy                            ⇒ Spectrum calculation for the ν8 band.
##
 rm DI* EN* FN* HA* MD* MH* TR* VP*
```

$I_{\min}$ is the intensity threshold (all lines with intensity lower than $I_{\min}$ are not written in the output file). The main output file is `spectr.t`. An example is given in Table 2. The beginning of this file recalls the parameter values, the vibrational states involved and the calculation conditions. Then, the list of calculated transitions is given. Each line is identified by the lower $(J'', \tilde{C}'', \tilde{\alpha}'')$ labels and upper $(J', \tilde{C}', \tilde{\alpha}')$ quantum numbers, where $\tilde{\alpha}$ is a numbering index for levels that have the same C_{4v} $(\tilde{C})$ symmetry within a J block. This labelling is related to our group chain choice which considers XY_5Z molecules like near-spherical tops. In each case, the $(J, \tilde{C}, \tilde{\alpha})$ sets are followed by a vibrational identification consisting of the number of the vibrational state and representing the projection of the "true" vibrational wavefunction in a percentage, on the specified normal mode basis.

Table 2
Example of the spectr.t output file. See text for comments

```
Hamiltonian Parameters in Tetrahedral Formalism

 2103 Data ; Jmax 79 ; St Dev previous  0.847 , predicted  0.847
12. 12. 8. 8. 12.        .5    Spin Statistics , Spin Y
   nu1   nu2   nu3   nu4   nu5   nu6   (J=0)    B0    D0
  771.0  677.2  713.3  258.0  320.0  127.0  .70741108E-01  .1607683D-07
  37    8.d-20    7    Para Number ; Model Accuracy Parameters
  SF5Cl 000000 Order 2 et 001000 Order 4
lundi 30 octobre 2000 10:18:43        Hmn Frdm      Value/cm-1      St.Dev./cm-1
   1 2(0,0A1g a1) 000000A1g 000000A1g A1g a1 02    354 0.70741106556E-01 0.1187955E-05
   2 2(2,0 Eg a1) 000000A1g 000000A1g A1g a1 02    223 0.60540777672E-02 0.5476388E-06
... ... ... ... ... ... ... ... ...
  36 4(4,0F2g b2) 001000F1u 001000F1u F2g b2 24      0 0.00000000000E+00 0.0000000E+00
  37 4(4,0F2g e ) 001000F1u 001000F1u F2g e  24      0 0.00000000000E+00 0.0000000E+00

Transition Moment Parameters in Tetrahedral Formalism

*
*
*
  1 Arbitrary Units
  2  1d-1
Unpublished Work
*
  1 0(0,0A1g a1) 000000A1g 001000F1u F1u a1 10      0.10000000000E+01 0.0000000E+00
  2 0(0,0A1g a1) 000000A1g 001000F1u F1u e  10      0.10000000000E+01 0.0000000E+00

 2 Upper Vibrational States

    #         v1         v2         v3         v4         v5         v6         Cv
    1 |[[[[0(0,0A1g)*0(0,0A1g)*1(1,0F1u)]F1u*0(0,0A1g)]F1u*0(0,0A1g)]F1u*0(0,0A1g)]F1u,a1>
    2 |[[[[0(0,0A1g)* 0(0,0A1g)*1(1,0F1u)]F1u* 0(0,0A1g)]F1u*0(0,0A1g)]F1u*0(0,0A1g)]F1u,e>

 1 Lower Vibrational States

    #         v1         v2         v3         v4         v5         v6         Cv
    1 |[[[[0(0,0A1g)*0(0,0A1g)*0(0,0A1g)]A1g*0(0,0A1g)]A1g*0(0,0A1g)]A1g*0(0,0A1g)]A1g,a1>

Spectroscopic Data Calculated through J=79
Imposed Frequency Range:         900.000000 -        920.000000
Vibrational Temperature: 203.00 Kelvin
Rotational Temperature:  203.00 Kelvin
Intensity Lower Limit 0.10E-02    Arbitrary Units

  Calculated Transitions

    Frequency Intensity      J" C" n" #vib"  J C n #vib  Lower Energy

    910.542277 8.33E-03 P   1 e   1 1 100%  0 e  1 2 100%        0.151369
    910.601811 2.50E-02 Q   1 a2  1 1 100%  1 a1 1 2 100%        0.121710
... ... ... ... ... ... ... ... ...
    909.921163 2.16E-02 P  80 e 39 1 100% 79 e 118 2 100%    572.539330
    910.686313 2.10E-02 P  80 e 40 1 100% 79 e 119 2 100%    581.960120
Number of Calculated Transitions    25626
First Transition      ->    900.006442 4.36E-03 P 78 e
Strongest Transition ->     910.605530 3.42E-01 Q 32 a1
Last Transition       ->    919.996548 5.51E-02 R 71 e
Effective Jo range    ->  0 - 80
Strongest Tr at Jmax  ->    910.484208 8.15E-02 Q 79 a2
Intensity summations:
0.16E+04  Arbitrary Units           with threshold = 0.10E-02
0.16E+04 Arbitrary Units            without threshold
```

5. Fitting parameters with C_{4v}TDS

The C_{4v}TDS package also provides the possibility to fit Hamiltonian parameters using experimental data. The general procedure is described in Fig. 4. This necessitates an assignment file containing lines of the following form (the format must be respected):

```
2012  850.983220+15.000000    0.002000          35 a2 3 34 a1 3 SFC nu1
2013  850.987318+15.000000    0.002000          35 e  5 34 e  5 SFC nu1
2014  850.992755+15.000000    0.002000          35 b2 3 34 b1 3 SFC nu1
```

Each line has the following structure:

Columns 1–6: running index on experimental lines.
Columns 9–18: experimental line wavenumber.
Column 20: the plus sign indicates that the line has been assigned and fitted. If any other character is placed here, then this indicates that the line has been assigned, but will not be fitted and will thus not be taken into account by the programs.

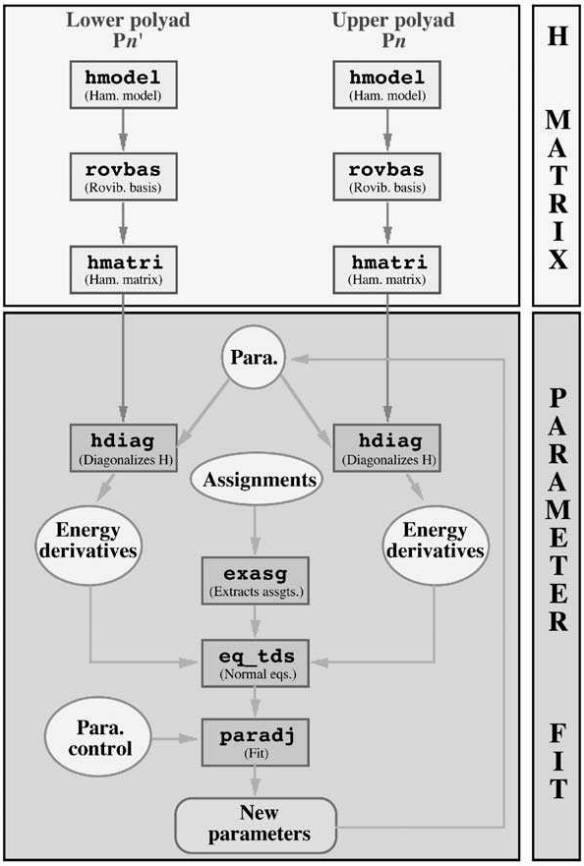

Fig. 4. Schematic description of the parameter fit.

Columns 24–31: experimental line intensity.

Columns 36–43: experimental precision on line position.

Columns 53–70: assignment in the form of $J''\tilde{C}''\tilde{\alpha}''$ (lower level) and $J'\tilde{C}'\tilde{\alpha}'$ (upper level). Each experimental line can be assigned to several theoretical transitions if necessary.

Columns 72–83: character chain used to extract desired assignment lines.

Practically, two jobs must be used. The first job is used to calculate the Hamiltonian operators matrix elements (up to the desired order). This is done using `hmodel`, `rovbas` and `hmatri` for both lower and upper polyad, just as explained in the preceding section. In `jobs/fit_examples`, some examples of such jobs are given. Their names are in the following form:

```
job_hme_NameOfTheMolecule_NameOfTheBandSystem.
```

In the same directory, one can find examples of the second type of job (fit job) required, named in the following form:

```
job_fit_NameOfTheMolecule_NameOfTheBandSystem.
```

This second job performs an iteration to determine a new parameter set. It is organized as follows. The first program used is `hdiag`. It diagonalizes the Hamiltonian matrix for the lower and upper polyad using the Hamiltonian initial parameter file. The difference between `hdi` (see preceding section) and `hdiag` is that the latter also calculates energy derivatives with respect to the parameters.

The job `exasg` is used to extract the desired lines in the assignment file (see above) using a specified character chain. Then, `eq_tds` calculates the normal equations and `paradj` determines the new parameter set. Further iterations can be done simply by renaming the output parameter file (its name is indicated at the end of the job) with a command line like (Unix version)

```
mv OutputParameterFile InputParameterFile
```

and by running the job again.

A commented example of a fit job is given in Table 3.

6. Hardware and software requirements

The C_{4v}TDS package includes source codes of all the executables. A FORTRAN compiler is necessary to generate these executable files using the installation script (for Macintosh under 8.x and 9.x systems, the C_{4v}TDS version contains executables).

In principle, since almost only standard statements and UNIX commands are used, C_{4v}TDS should be suitable for most UNIX workstations. It has been carefully tested on the following platforms: HP 9000/7xx operating under HP-UX 10.20, IBM RS/6000 operating under AIX 4.3, DEC alpha operating under OSF1 4.0 and SUN UltraSPARC operating under Solaris 5.8. A PC LINUX and a Macintosch version of the package are also available. The user should refer to the `c4vtds_README` file for more detailed instructions. SGI workstations can also run the C_{4v}TDS package with a few modifications. The authors can be contacted for such technical questions.

The minimum configuration for C_{4v}TDS is 64 Mbytes RAM and 200 Mbytes of free disk space for the creation of temporary files of the most complex calculations.

Table 3
Example of a job for parameter fit: the ν_1/ν_8 dyad of $SF_5{}^{35}Cl$. Some comments are given on the right

```
#! /bin/sh
 set -v
## Example of parameter fitting :
##  nu1/nu8 of SF535Cl.
##
 BASD=.../.../C4vTDS
#                                        ⇒   C4vTDS installation directory.
 SCRD=$BASD/prog/exe
 PARD=$BASD/para
 EXPD=$BASD/exp
 CTRD=$BASD/ctrp
##
## Jmax values.
##
 JPlow=80                                ⇒   Maximum J value for lower level.
 JPupp=79                                ⇒   Maximum J value for upper level.
 JPupp_low=79                            ⇒   Maximum J value for the calculated spectrum.
##
## Parameter file.
##
 PARAGS=$PARD/SF535Cl/Pa_000000m000000
 PARA18=$PARD/SF535Cl/Pa_001000m000000
##                                       ⇒   Parameters for H.
## Assignment files.
##
 ASG0=$EXPD/SF535Cl/dip/Burger_GSCD.exp  ⇒   Files containing experimental assigned lines.
 ASG1=$EXPD/SF535Cl/dip/Burger_nu1.exp
 ASG8=$EXPD/SF535Cl/dip/Burger_nu8.exp
##
## Parameter constrain file.
##                                       ⇒   File defining the constraints on parameters.
 CLF=$CTRD/SF535Cl/001000
##
########################################
##
## Hamiltonian diagonalization.
##
## 000000 level.
##
 $SCRD/passx hdiag P0 N1 D2 $JPlow $PARAGS
##                                       ⇒   Diagonalization of H for lower polyad.
## 001000 level.
##                                       ⇒   Diagonalization of H for upper polyad.
 $SCRD/passx hdiag P1 N1 D24 $JPupp $PARA18
##
## nu1/nu8 + GSCD fit.
##
 $SCRD/exasg 'SFC GSCD' $ASG0
 mv ASG_EXP ASG_GS                       ⇒   Extraction of assigned lines.
 cp ASG_GS assignments.t
```

Table 3 (*continued*)

```
##
 $SCRD/passx eq_tds P0 P0 p p ir $JPupp_low $PARAGS
 mv normal_eq.t    NQ_GS       ⇒       Calculation of normal equations for the ground-state.
 mv prediction_mix.t  Pred_GS
##
 $SCRD/exasg 'SFC nu1' $ASG1
 mv ASG_EXP ASG_nu1
 cp ASG_nu1 assignments.t
##
##
 $SCRD/passx eq_tds P1 P0 p p ir $JPupp_low $PARA18
 mv normal_eq.t    NQ_nu1
 mv prediction_mix.t  Pred_nu1
##                            ⇒       Calculation of normal equations for the ν1 band.
 $SCRD/exasg 'SFC nu8' $ASG8
 mv ASG_EXP ASG_nu8
 cp ASG_nu8 assignments.t
##
 $SCRD/passx eq_tds P1 P0 p p ir $JPupp_low $PARA18
 mv normal_eq.t    NQ_nu8
 mv prediction_mix.t  Pred_nu8
##                            ⇒       Calculation of normal equations for the ν8 band.
##############################
##
## New Hamiltonian parameter estimates.
##
 cp $CLF CL_H_001000
 $SCRD/passx paradj H CL_H_001000 NQ_GS NQ_nu1 NQ_nu8
##                            ⇒       New estimate of parameters.
 \rm NQ_nu8_adj
 \rm NQ_GS NQ_nu1 NQ_nu8
##
 \rm assignments.t
 \rm ASG* CL* ED* HA* VP*
###
### The new parameter file is :
###
###    NQ_GS_adj
###    NQ_nu1nu8_adj
###
```

7. Getting, installing and running C_{4v}TDS

The C_{4v}TDS computer package can be accessed directly either by anonymous `ftp` at the Internet address

jupiter.u-bourgogne.fr

Table 4
Instructions to get and install C_{4v}TDS on UNIX systems*

1	Create a local directory to be used as the C4vTDS installation directory.
2	Login by `ftp`, user `anonymous`, on `jupiter.u-bourgogne.fr`.
3	Get (`binary` mode) the remote file `dist/C4vTDS_UNIX/c4vtds_199.tar.gz` into the local directory.
4	Quit ftp and start installation using `gunzip < c4vtds_199.tar.gz | tar xvf -`.
5	Continue installation following instructions in file "`c4vtds_README`".

*To get the PC LINUX version, follow the same procedure using the file `dist/C4vTDS_UNIX/c4vtds_199_PC.tar.gz` instead of `dist/C4vTDS_UNIX/c4vtds_199.tar.gz`.

in the directory /`dist/C4vTDS_UNIX` for Unix systems including MacOS X and in /`dist/C4vTDS_Mac` for MacOS 8.x and 9.x systems or through the world wide web at the URL

`http://www.u-bourgogne.fr/LPUB/c4vTDS.html`.

As mentioned above, three versions are available: a general UNIX, a specific PC LINUX version and a Macintosh version. The UNIX version consists of a single compressed file in the standard `tar.gz` format. Its size is 14 Mbytes. The Mac version is a compressed file in the `sit.hqx` format. Its size is 20 Mbytes. Instructions to get and install C_{4v}TDS (UNIX version) are given in Table 4.

For the UNIX version, the execution of the instructions given in Table 4 automatically creates the appropriate directories and files according to the structure given in Fig. 2 and explained in Section 3. The final step of the installation is achieved using the included compiling script (refer to file `c4vtds_README`).

During the execution of the jobs (spectrum calculation or parameter fit), the various steps are displayed in the session window. The sequences of routines previously described exchange data through temporary files created in the working directory. Since these files are automatically deleted after use, it is highly recommended to work in a dedicated directory (distinct from the C4vTDS installation directory), in order to avoid undesired removal of permanent files.

Although the use of C_{4v}TDS does not require any particular knowledge in theory nor in programming, users are freely allowed to modify any of the files (source codes, parameter files or executable scripts). Of course, this is not recommended to users who are not experts in the theory of symmetric tops or in computer programming. The authors may be contacted for further information and developments on the present package.

8. Conclusion and perspectives

Untill now, the C_{4v}TDS package has been tested only on the ν_1/ν_8 dyad of $SF_5{}^{35}Cl$. But the user who requires to use other conditions or molecules than the one provided has just to modify the jobs. This offers the greatest flexibility and an enormous amount of possibilities. The polyad scheme being entirely specified by the user, it is not linked to any particular molecule. Apart from this, the advantages of C_{4v}TDS compared to other databases containing essentially experimental or precalculated data (fixed number of transitions) are the same as for HTDS. Extrapolations to high J values (till 199 [18]), although they obviously have a limited reliability, are possible and can be very helpful at least for qualitative predictions. C_{4v}TDS can also be used for theoretical studies of

vibration-rotation features in XY_5Z molecules simply by using appropriate parameter files to represent specific molecular quantum systems. Moreover, C_{4v}TDS includes programs for Hamiltonian parameter fitting. This allows the use of C_{4v}TDS with the user's own data.

The study of other rovibrational bands of XY_5Z ($SF_5Cl, SF_5Br, IOF_5, \ldots$) molecules is planned and thus C_{4v}TDS should be updated consequently in the future.

Acknowledgements

Support from the Région Bourgogne for the computer equipment of the Laboratoire de Physique de l'Université de Bourgogne is gratefully acknowledged. We thank Pr. G. Pierre and Pr. J.-P. Champion for helpful discussions. C_{4v}TDS benefited from many contributors (experimentalists and theoreticians) who are also sincerely thanked.

References

[1] Wenger Ch, Boudon V, Champion J-P, Pierre G. JQSRT 2000;66:1–16.
[2] Wenger Ch, Champion J-P. JQSRT 1998;59:471–80.
[3] Rotger M, Boudon V, Decrette A, Loëte M, Sander S, Willner H. J Mol Spectrosc 2001;208:169–79.
[4] Rotger M, Boudon V, Loëte M. J Mol Spectrosc 2000;200:123–30.
[5] Rotger M, Boudon V, Loëte M. J Mol Spectrosc 2000;200:131–7.
[6] Nikitin A, Champion J-P, Tyuterev VG. J Mol Spectrosc 1997;182:72–84.
[7] Sartakov BG, Oomens J, Reuss J, Fayt A. J Mol Spectrosc 1997;185:31–47.
[8] Noftle RE, Smardzewski RR, Fox WB. Inorg Chem 1977;16:3380–1.
[9] Griffiths JE. Spectrochim Acta A 1967;23:2145–57.
[10] Cross LH, Roberts HL, Goggin P, Woodward LA. Trans Faraday Soc 1960;56:945–51.
[11] Smardzewski RR, Noftle RE, Fox WB. J Mol Spectrosc 1976;62:449–57.
[12] Brooks WVF, Eshaque M, Lau C, Passmore J. Can J Chem 1976;54:817–23.
[13] Legon AC. Trans Farad Soc 1969;65:2595–601.
[14] Brier PN. J Mol Spectrosc 1987;125:233–42.
[15] Cheblal N, Boudon V, Loëte M. J Mol Spectrosc 1999;197:222–31.
[16] Jurek R, Poinsot A, Goulet P. J Phys 1986;47:645–8.
[17] Champion J-P, Loëte L, Pierre G. In: Narahari Rao K, Weber A, editors. Spectroscopy of the Earth's atmosphere and interstellar medium. San Diego: Academic Press, 1992. p. 339–422.
[18] Wenger Ch, Rey M, Sartakov BG, Boudon V, Pierre G. in preparation.

Cinquième partie

Spectroscopie des Molécules Piégées dans des Solides

Cinquième partie

Chapitre

1

Spectroscopie des Molécules piégées dans des Zéolithes

Publication P20

1.1 Introduction

Une discussion avec les membres du groupe "Adsorption sur Solides Poreux" du Laboratoire LRRS (J.-P. Bellat, J.-M. Simon, G. Weber, ...) est à l'origine de cette thématique. En effet, ces derniers utilisent la spectroscopie infrarouge comme outil de diagnostic afin de mieux comprendre les interactions molécules–solides microporeux et notamment le phénomène d'adsorption. La compréhension de ce phénomème est une clé importante pour de nombreux enjeux industriels notamment en matière de dépollution de rejets gazeux.

De ces expériences faites par nos collègues chimistes est né un besoin de leur part en matière d'interprétation de spectres, d'où l'idée de cette collaboration entre chimistes et physiciens. D'un commun accord, il a été décidé que la molécule-test serait la molécule C_2H_4. Celle-ci est la plus simple des chaînes carbonées de la famille des hydrocarbures saturés.

1.2 Résultats

Tout en nous appuyant sur les compétences dijonnaises, nous avons mis en place un modèle pour l'hamiltonien et les moments de transition de molécules de type X_2Y_4. Afin de tenir compte de l'environnement zéolithique, nous devrons en plus traduire théoriquement l'interaction molécule-solide. Cette interaction peut prendre différents aspects :

- L'aspect de confinement dû à la cage zéolithique,
- L'effet du champ électrique très important régnant à l'intérieur des cavités zéolithiques ou effet Stark.

C'est ce dernier effet que nous avons entrepris de modéliser et qui constitue une partie importante de la thèse de Wilfried Raballand. Pour cela, nous avons ajouté à l'hamiltonien de la molécule isolée les termes créés par l'interaction de cette molécule avec un champ électrique. Cet effet sera traité d'une manière perturbative et nous nous limiterons aux effets dus au moment dipolaire électrique et à la polarisabilité. Dans ces conditions, l'hamiltonien Stark s'écrit :

$$H_S = \widetilde{H} + {}^{\mu}\widetilde{H}_S + {}^{\alpha}\widetilde{H}_S, \tag{V.1.1}$$

où

$$\begin{aligned} {}^{\mu}\widetilde{H}_S &= -\vec{\mu}\cdot\vec{E}, \\ {}^{\alpha}\widetilde{H}_S &= -\overline{\overline{\alpha}} : \vec{E} : \vec{E}. \end{aligned} \tag{V.1.2}$$

Nous considérerons pour le moment le cas où le champ électrique extérieur est statique et sa direction est parallèle à l'axe OZ du repère fixe du laboratoire. Nous prédisons actuellement les éclatements Stark. Ces prédictions de déplacements sont en accord avec les valeurs calculées par T. Oka pour la bande ν_7 de la molécule C_2H_4. Une publication va être prochainement soumise sur ce sujet.

1.3 Perspectives

La molécule d'éthylène, seule, présente un intérêt planétologique puisqu'elle est présente dans l'atmosphère de Titan. De ce fait, des collaborations avec des astronomes sont envisageables. Des spectres calibrés en intensité enregistrés par J. Vander Auwera à Bruxelles vont être analysés dès que possible.

Cette molécule intéresse également le groupe d'expérimentateurs de notre laboratoire travaillant sur le contrôle cohérent afin d'essayer de l'aligner à l'aide d'une source femtoseconde. Une collaboration vient de commencer et vise dans un premier temps la détermination purement expérimentale de la polarisabilité dans l'état vibrationnel de base. La technique employée donne de plus accès au spectre Raman purement rotationnel de cette molécule centrosymétrique.

Pour tenir compte de l'effet Stark, nous avons supposé que le champ électrique gardait toujours la même direction. Bien évidemment, cette situation peut changer notamment en orientation, ce qu'il est facile de modifier théoriquement dans notre modèle. Il faudra également envisager à plus long terme de traiter le cas d'un champ électrique multipolaire ce qui n'a jamais été fait et dont la symétrie serait liée à la symétrie des canaux ou des intersections de la zéolithe.

En matière de bases de données, nous devrions pouvoir développer des bases permettant de prédire des spectres Stark pour ce type de molécules asymétriques, ce qui n'a jamais été fait jusqu'à présent.

L'environnement de la molécule peut changer suivant le type de zéolithes dans laquelle elle est placée. Pour tenir compte de ce confinement plus ou moins important, il est indispensable de coupler théoriquement la géométrie de la cavité avec celle de la molécule. Ce travail s'inscrit dans la lignée de ce qu'a fait T. Momose au Japon. Il a en effet étudié entre autres des molécules de méthane placées dans du para-hydrogène solide.

1.4 Articles-clés

Est reproduit ici le premier article de cette thématique, article théorique décrivant l'hamiltonien et les moments de transition pour la molécule isolée et en utilisant les techniques tensorielles dijonnaises.

– [**P20 :** *J. Mol. Spectrosc.*, **217**, 239–248 (2002)] présente un formalisme tensoriel pour l'hamiltonien et les moments de transition pour des molécules de type X_2Y_4 appartenant au groupe de symétrie D_{2h}.

ACADEMIC PRESS

Available online at www.sciencedirect.com

SCIENCE DIRECT®

Journal of Molecular Spectroscopy 217 (2003) 239–248

Journal of MOLECULAR SPECTROSCOPY

www.elsevier.com/locate/jms

Spectroscopy of X_2Y_4 (D_{2h}) molecules: tensorial formalism adapted to the $O(3) \supset D_{2h}$ chain, Hamiltonian and transition moment operators

W. Raballand, M. Rotger,* V. Boudon, and M. Loëte

Laboratoire de Physique de l'Université de Bourgogne, UMR CNRS 5027, 9, Avenue Alain Savary, B.P. 47 870, F-21078 Dijon Cedex, France

Received 23 July 2002; in revised form 3 October 2002

Abstract

A tensorial formalism adapted to the case of the X_2Y_4 molecules with D_{2h} symmetry has been developed in the same way as in the previous works on XY_4 (T_d) and XY_6 (O_h) spherical tops and XY_5Z (C_{4v}) symmetric tops. Here, we use the $O(3) \supset D_{2h}$ group chain. All the coupling coefficients and formulas for the computation of matrix elements are given for this chain and used in the case of the Hamiltonian and transition moment operators.

Keywords: D_{2h}; Tensorial formalism; X_2Y_4; Ethylene

1. Introduction

High-resolution rovibrational spectroscopy of X_2Y_4 molecules has already been widely studied in infrared absorption, more particularly in the case of ethylene [1] and other C_2Y_4 species. The interest in ethylene is specially founded on the discovery of this species in planetary atmospheres like Jupiter, Saturn and its satellite Titan, and more recently Neptune. C_2H_4 is part of the chemical processes involving methane [2]. The study of halogenated derivatives of ethylene becomes even more important. Species such as $C_2F_xCl_y$ belong to the CFC (*chlorofluorocarbons*) pollutants family. They contribute to destroy the ozone layer when released in the atmosphere. More generally, one can imagine to study other particular species such as Si_2Y_4.

In this work, we establish a tensorial formalism adapted to the case of the D_{2h} symmetry group. It is based on principles already used and applied in Dijon for the XY_4, XY_3Z, XY_6, and XY_5Z molecules, with T_d [3], C_{3v} [4], O_h [5], and C_{4v}[6–8] symmetry, respectively. One important advantage of this method is that it enables the systematic development of the Hamiltonian and transition moment (dipole moment and polarizability) operators up to any order. As a consequence, the model constructed in this way also allows to treat easily the vibrational polyads present in molecular spectra (such as for molecules with T_d [3,9] or C_{3v} [4,10] symmetry). A first approach of such a formalism has been undertaken by Sartakov et al. [11] and applied to several bands of ethylene. The present paper is devoted to clarify and complete this previous work by focusing on all technical details in order to be coherent with the usual techniques of the Dijon group.

In the first part of this paper, we study the link between the D_{2h} symmetry group and the vibrational modes of the ethylene molecule.

Then we also recall the principles that we extend to the $O(3) \supset D_{2h}$ chain. Coupling coefficients and formulas for the computation of matrix elements of tensor operators are derived for this chain.

In the last part, we use these formulas for calculating the reduced matrix elements of the Hamiltonian and the transition moment operators.

*Corresponding author. Fax: +33-380395971.

E-mail addresses: Wilfried.Raballand@u-bourgogne.fr (W. Raballand), maud.rotger@u-bourgogne.fr (M. Rotger).

0022-2852/03/$ - see front matter © 2003 Elsevier Science (USA). All rights reserved.
doi:10.1016/S0022-2852(02)00038-3

2. Symmetry and vibrational modes

2.1. The D_{2h} group

We consider here molecules pertaining to the D_{2h} group. This group is directly deduced from the direct product of D_2 by the C_I group: $D_{2h} = D_2 \otimes C_I$, with $C_I = \{E, I\}$, I being the space inversion. Its symmetry elements are those of D_2 to which are added their products by inversion, $E \times I = I$ and $C_2(i) \times I = \sigma(jk)$, where $i, j, k = x, y, z$. So the group has eight symmetry elements:

$$E,\ C_2(z),\ C_2(y),\ C_2(x),\ I,\ \sigma(xy),\ \sigma(xz),\ \sigma(yz).$$

In the same way, the irreducible representations (irreps) are those of D_2 indexed by their parity g or u

$$A_g,\ B_{1g},\ B_{2g},\ B_{3g},\ A_u,\ B_{1u},\ B_{2u},\ B_{3u}.$$

The characters for the irreps of D_{2h} are obtained as follows: if C is an irrep and R a symmetry element of D_2, then we have: $\chi^{(C_g)}(R) = \chi^{(C_u)}(R)$; $\chi^{(C_g)}(R \times I) = \chi^{(C_g)}(R)$ and $\chi^{(C_u)}(R \times I) = -\chi^{(C_u)}(R)$. The multiplication rules for the irreps of D_{2h} are the same as for D_2. We only need to apply the parity rules: $g \times g = u \times u = g$ and $g \times u = u \times g = u$. We recall the character and multiplication tables of D_2 in Tables 1 and 2.

In Table 3, we recall the symmetry properties of the components of various useful tensors: translation (T) and rotation (R) vectors, dipole moment (μ), and polarizability (α).

2.2. Usual conventions

The starting point of our work is the choice of the molecular axis frame. The usual conventions differ in the choice of the axis which is parallel to the double bond (see Fig. 1).

We have to choose between two commonly used conventions. The first one is based on the Mulliken's notation [12], which obey the IUPAC (International Union of Pure and Applied Chemistry) recommendations by taking the z axis. In this case, the vibrational representation for an X_2Y_4 molecule is

$$\Gamma_V = 3A_g \oplus B_{2g} \oplus 2B_{3g} \oplus A_u \oplus 2B_{1u} \oplus 2B_{2u} \oplus B_{3u}. \quad (1)$$

Let us consider the case of ethylene, C_2H_4, as an example. The moments of inertia of the molecule being expressed as a function of the mass and coordinates of the carbon $(m_C; x_{fC}, y_C, z_C)$ and hydrogen atoms $(m_H; x_H, y_H, z_H)$:

$$\begin{aligned} I_{xx} &= 2m_C z_C^2 + 4m_H(y_H^2 + z_H^2), \\ I_{yy} &= 2m_C z_C^2 + 4m_H z_H^2, \\ I_{zz} &= 4m_H y_H^2, \end{aligned} \quad (2)$$

and the x_H, y_H, z_H, x_C, y_C, and z_C lengths having the same order of magnitude, but since $m_C = 12m_H$, we get $I_{xx} > I_{yy} > I_{zz}$ and thus in terms of usual rotational constants

$$B_{\alpha\alpha} = \frac{\hbar^2}{2hcI_{\alpha\alpha}} \Rightarrow B_x < B_y < B_z. \quad (3)$$

We can classify the molecule as an asymmetric oblate top (in the z direction with this convention). With the usual A, B, and C notation, by convention, $A > B > C$, and

$$B_x \equiv C; \quad B_y \equiv B; \quad B_z \equiv A. \quad (4)$$

Thus, the IUPAC recommendations lead to a I^r identification [13] for C_2H_4.

The second convention uses the notations that Herzberg defined in his works [14] by taking the x axis parallel to the double bond. We get this time

$$\Gamma_V = 3A_g \oplus 2B_{1g} \oplus B_{2g} \oplus A_u \oplus B_{1u} \oplus 2B_{2u} \oplus 2B_{3u}. \quad (5)$$

According this frame choice, we obtain: $I_{xx} < I_{yy} < I_{zz}$ or $B_x > B_y > B_z$, which gives us

$$B_x \equiv A; \quad B_y \equiv B; \quad B_z \equiv C. \quad (6)$$

Thus we have a III^r identification for C_2H_4, according to the Herzberg's convention.

Table 1
Characters for the irreductible representations of D_2

D_2	E	$C_2(z)$	$C_2(y)$	$C_2(x)$
A	1	1	1	1
B_1	1	1	−1	−1
B_2	1	−1	1	−1
B_3	1	−1	−1	1

Table 2
Multiplication of the irreductible representations of D_2

D_2	A	B_1	B_2	B_3
A	A	B_1	B_2	B_3
B_1	B_1	A	B_3	B_2
B_2	B_2	B_3	A	B_1
B_3	B_3	B_2	B_1	A

Table 3
Useful components in the D_{2h} group

Component(s)		Component(s)	
A_g	α_{xx}, α_{yy}, α_{zz}	A_u	
B_{1g}	R_z, α_{xy}	B_{1u}	T_z, μ_z
B_{2g}	R_y, α_{xz}	B_{2u}	T_y, μ_y
B_{3g}	R_x, α_{yz}	B_{3u}	T_x, μ_x

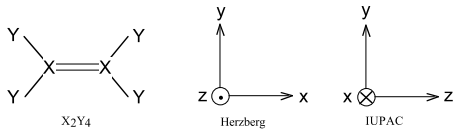

Fig. 1. Molecular axis frames.

2.3. Vibrational normal modes

Table 4 recalls the symmetries of the 12 vibrational modes of an X_2Y_4 molecule using the two conventions described above. Table 5 exemplifies the case of the ethylene (C_2H_4) molecule.

We can notice that the exchange of the z and x axes between the two conventions causes an exchange of the B_1 and B_3 symmetries. In this present study, we work with the Herzberg's convention, which is the most used in the literature.

2.4. Infrared and Raman spectroscopy

The intensity of infrared absorption spectroscopy transitions depends on the matrix element of the dipole moment tensor taken between an initial state $|i\rangle$ and a final state $|f\rangle$ with the selection rule

$$\Gamma_f = \Gamma(\vec{\mu}) \otimes \Gamma_i.$$

As $\vec{\mu}$ is a polar vector, the only active vibrational levels (for transitions from the ground state) in absorption spectroscopy (see Table 3) are those with symmetry

B_{1u}, B_{2u} or B_{3u}.

Table 4
Vibrational modes of X_2Y_4 molecules

Mode	Herzberg	IUPAC
ν_1	A_g	A_g
ν_2	A_g	A_g
ν_3	A_g	A_g
ν_4	A_u	A_u
ν_5	B_{1g}	B_{1u}
ν_6	B_{1g}	B_{1u}
ν_7	B_{1u}	B_{2g}
ν_8	B_{2g}	B_{2u}
ν_9	B_{2u}	B_{2u}
ν_{10}	B_{2u}	B_{3g}
ν_{11}	B_{3u}	B_{3g}
ν_{12}	B_{3u}	B_{3u}

Table 5
The vibrational modes of ethylene [15]

Frequency (cm^{-1})	Vibration	Herzberg (mode, sym.)	IUPAC (mode, sym.)
826	CH_2 rocking	ν_{10}, B_{2u}	ν_9, B_{2u}
943	CH_2 wagging	ν_8, B_{2g}	ν_7, B_{2g}
949.3	CH_2 wagging	ν_7, B_{1u}	ν_{12}, B_{3u}
1023	Torsion	ν_4, A_u	ν_4, A_u
1222	CH_2 rocking	ν_6, B_{1g}	ν_{11}, B_{3g}
1342.2	HCH bend	ν_3, A_g	ν_3, A_g
1443.5	HCH bend	ν_{12}, B_{3u}	ν_6, B_{1u}
1622.9	C–C stretch	ν_2, A_g	ν_2, A_g
2988.7	C–H stretch	ν_{11}, B_{3u}	ν_5, B_{1u}
3026.2	C–H stretch	ν_1, A_g	ν_1, A_g
3103.5	C–H stretch	ν_5, B_{1g}	ν_{10}, B_{3g}
3105.5	C–H stretch	ν_9, B_{2u}	ν_8, B_{2u}

In the same way, the Raman intensities depend on the $\langle i|\alpha|f\rangle$ matrix elements of the polarizability tensor. The only active vibrational levels in Raman spectroscopy are those with symmetry

A_g, B_{1g}, B_{2g} or B_{3g}.

We can notice that the ν_4 (A_u) symmetry mode is inactive both in Raman and in infrared absorption spectroscopy. However, it can be detected thanks to its interactions with the other modes.

3. Tensorial formalism for the D_{2h} group

As we intend to express tensorial operators such as the Hamiltonian, the dipole moment or the polarizability tensor, we must orient the $O(3)$ vectors basis into the D_{2h} subgroup and then formulate the tensorial algebra in the new symmetry. In the aim of simplifying the explanations, we can first limit us to the D_2 group, since the extension to D_{2h} is simply deduced by adding the inversion. Consequently, we first consider the $SO(3) \supset D_2$ group chain.

3.1. Orientation in the $SO(3) \supset D_2$ chain

The $SO(3)$ standard basis can be oriented in a subgroup through the relation

$$|J, nC\sigma\rangle = P^{(C)}_{\sigma}|J, M\rangle = \sum_{M} {}^{(J)}G^{M}_{nC}|J, M\rangle, \tag{7}$$

where C is an irrep of the subgroup, n its multiplicity index, and σ a component. The G coefficients are elements of the passage matrix from $SO(3)$ into the subgroup. The $P^{(C)}_{\sigma}$ projectors are expressed by the relations [16]:

$$P^{(C)}_{\sigma}|J, M\rangle = \frac{[C]}{[D_2]} \sum_{R \in D_2} [D^{(C)}(R)]^{\sigma}_{\sigma} P_R |J, M\rangle, \tag{8}$$

$$P_R|J, M\rangle = \sum_{M'} [\mathscr{D}^{(J)}(R)]^{M'}_{M} |J, M'\rangle, \tag{9}$$

where R is a symmetry element and $D(R)$ the corresponding matrix. $[\mathscr{D}^{(J)}(R)]^{M'}_{M}$ and $[D^{(C)}(R)]^{\sigma}_{\sigma}$ are matrix elements.

The order of the D_2 group is $[D_2] = 4$. Its 4 irreps (A, B_1, B_2, B_3) have dimension $[C] = 1$ (see Table 1), so

$$[D^{(C)}(R)]^{\sigma}_{\sigma} = \chi^{(C)}(R) \tag{10}$$

(i.e., the matrices are identical to the characters). If we do the substitution of (9) and (10) into (8), we obtain the relation

$$P^{(C)} = \frac{1}{4} \sum_{R \in D_2} \chi^{(C)}(R) \sum_{M'} [\mathscr{D}^{(J)}(R)]^{M'}_{M} |J, M'\rangle. \tag{11}$$

We define $[\mathscr{D}^{(J)}(R)]^{M'}_{M}$ ($SO(3)$ rotations matrix) as usual [17]

Table 6
Euler angles for the D_2 elements

C	α	β	γ
E	0	0	0
$C_2(x)$	π	π	0
$C_2(y)$	0	π	0
$C_2(z)$	π	0	0

$$[\mathscr{D}^{(J)}(R)]^{M'}_{M} = \langle J, M'|D(\alpha,\beta,\gamma)|J, M\rangle \tag{12}$$

with

$$D(\alpha,\beta,\gamma) = e^{\frac{i\gamma}{\hbar}J_z} e^{\frac{i\beta}{\hbar}J_y} e^{\frac{i\alpha}{\hbar}J_z},$$

where α,β,γ are the Euler angles for the R symmetry element (see Table 6).

Expliciting $D(\alpha,\beta,\gamma)$, we can write [17]

$$[\mathscr{D}^{(J)}(R)]^{M'}_{M} = e^{iM'\gamma}[d^{(J)}(\beta)]^{M'}_{M} e^{iM\alpha}. \tag{13}$$

We have some simple expressions of the $[d^{(J)}(\beta)]^{M'}_{M}$ Wigner functions for $\beta = 0$ or π [17]:

$$\begin{aligned} [d^{(J)}(0)]^{M'}_{M} &= \delta_{M',M}, \\ [d^{(J)}(\pi)]^{M'}_{M} &= (-1)^{J+M}\delta_{M',-M} \end{aligned} \tag{14}$$

and by substitution in (13)

$$\sum_{M'}[\mathscr{D}^{(J)}(R)]^{M'}_{M}|J, M'\rangle = \begin{cases} e^{iM(\alpha+\gamma)}|J, M\rangle & \text{if } \beta = 0, \\ (-1)^{J+M}e^{iM(\alpha-\gamma)}|J, -M\rangle & \text{if } \beta = \pi. \end{cases} \tag{15}$$

This allows us to calculate the $P^{(C)}$ projectors in Eq. (8) and by this way the D_2 basis vectors (7). They are noted $|J, nC\rangle$:

$$\begin{aligned} |J, nA\rangle &= \frac{1}{4}[1 + (-1)^M]|J, M\rangle \\ &\quad + \frac{1}{4}(-1)^J[(-1)^M + 1]|J, -M\rangle, \\ |J, nB_1\rangle &= \frac{1}{4}[1 + (-1)^M]|J, M\rangle \\ &\quad - \frac{1}{4}(-1)^J[(-1)^M + 1]|J, -M\rangle, \\ |J, nB_2\rangle &= \frac{1}{4}[1 - (-1)^M]|J, M\rangle \\ &\quad + \frac{1}{4}(-1)^J[(-1)^M - 1]|J, -M\rangle, \\ |J, nB_3\rangle &= \frac{1}{4}[1 - (-1)^M]|J, M\rangle \\ &\quad - \frac{1}{4}(-1)^J[(-1)^M - 1]|J, -M\rangle. \end{aligned} \tag{16}$$

The n multiplicity index is associated to $|M|$ (i.e., n always corresponds to a particular value of $|M|$).

From Eqs. (7) and (16), we obtain the values of the G coefficients. For a given couple of J and M, they are equal to the components of the $|J, nC\rangle$ normalized vector. Table 7 gives the ${}^{(J)}G^{M}_{nC}$ coefficients for $M > 0$ and the sign of the corresponding ${}^{(J)}G^{-M}_{nC}$ coefficients.

Table 7
${}^{(J)}G^{M}_{nC}$ and sign of ${}^{(J)}G^{-M}_{nC}$ coefficients ($M > 0$)

M	J	A	B_1	B_2	B_3
$=0$	Even	1	0	0	0
$=0$	Odd	0	1	0	0
$\neq 0$ Even	Even	$\frac{1}{\sqrt{2}}, +$	$\frac{1}{\sqrt{2}}, -$	0	0
$\neq 0$ Even	Odd	$\frac{1}{\sqrt{2}}, -$	$\frac{1}{\sqrt{2}}, +$	0	0
$\neq 0$ Odd	Even	0	0	$\frac{1}{\sqrt{2}}, -$	$\frac{1}{\sqrt{2}}, +$
$\neq 0$ Odd	Odd	0	0	$\frac{1}{\sqrt{2}}, +$	$\frac{1}{\sqrt{2}}, -$

We have used the phase convention ${}^{(J)}G^{M}_{nC} > 0$ $\forall M \geqslant 0$ and we have

$${}^{(J)}G^{-M}_{nC} = (-1)^{(J+M)}\Xi_C{}^{(J)}G^{M}_{nC}. \tag{17}$$

Taking into account our conventions, the ${}^{(J)}G^{M}_{nC}$ values calculated here lead to

$$\Xi_C = \begin{cases} +1 & \text{for } C = A, B_2, \\ -1 & \text{for } C = B_1, B_3. \end{cases} \tag{18}$$

Our method leads to the same coefficients that Sartakov et al. [11] proposed in their paper.

Table 8 gives the reduction of the $SO(3)$ irreps into D_2 for the lowest J values. The first row contains the $|M|$ value and the sign of ${}^{(J)}G^{-M}_{nC}$ ($M > 0$).

More generally, for a particular value of J, we have the associated representation

$$\Gamma_J = p(A + B_1 + B_2 + B_3) + q(B_1 + B_2 + B_3) + (1 - q)A \tag{19}$$

with $J = 2p + q$ and both p and q are integers. The multiplicity of a C representation (the number of possible values of $|M|$) increases with J.

We can now build the $3C$ coefficients (equivalent to the Wigner $3J$ coefficients [18]) oriented according to the $O(3) \supset D_2$ chain

$$F^{(J_1\ J_2\ J_3)}_{n_1C_1\ n_2C_2\ n_3C_3} = \sum_{M_1,M_2,M_3} {}^{(J_1)}G^{M_1}_{n_1C_1}\,{}^{(J_2)}G^{M_2}_{n_2C_2} \times {}^{(J_3)}G^{M_3}_{n_3C_3}\,\overline{V}\begin{pmatrix} J_1 & J_2 & J_3 \\ M_1 & M_2 & M_3 \end{pmatrix}, \tag{20}$$

where the $\overline{V}$s are Racah coefficients deduced from the Wigner $3J$ coefficients by the relation [19]

Table 8
Symmetry of the $|J, nC\rangle$ vectors

$\lvert M\rvert$, sign of ${}^{(J)}G^{-M}_{nC}$	0	1, −	1, +	2, −	2, +	3, −	3, +	⋯
$J = 0$	A							
$J = 1$	B_1	B_3	B_2					
$J = 2$	A	B_2	B_3	B_1	A			
$J = 3$	B_1	B_3	B_2	A	B_1	B_3	B_2	
⋮								

$$\overline{V}\begin{pmatrix} J_1 & J_2 & J_3 \\ M_1 & M_2 & M_3 \end{pmatrix} = (-1)^{J_1+J_2+J_3}\begin{pmatrix} J_1 & J_2 & J_3 \\ M_1 & M_2 & M_3 \end{pmatrix}. \tag{21}$$

3.2. Tensorial algebra in the D_2 group

In the aim of expressing the tensorial relations in the D_2 group, we must calculate all its specific coupling coefficients. The steps of this calculation are the same as for any other symmetry group, so we can base ourselves on the methods already used for T_d [3], O_h [5] or C_{4v} [6], for example.

We start from the Racah's factorization lemma

$$F^{\begin{pmatrix} J_1 & J_2 & J_3 \\ n_1C_1 & n_2C_2 & n_3C_3 \end{pmatrix}} = K^{\begin{pmatrix} J_1 & J_2 & J_3 \\ (n_1C_1 & n_2C_2 & n_3C_3) \end{pmatrix}} F^{(C_1C_2C_3)}, \tag{22}$$

where K is the isoscalar factor for the $SO(3) \supset D_2$ chain and $F^{(C_1C_2C_3)}$ the $3C-\sigma$ coefficient of the D_2 group. The $3C-\sigma$ coefficients can be calculated by the method that Lulek et al. developed in [6,20]

$$\begin{aligned} F^{(C_1C_2C_3)} &= \frac{\epsilon_{C_1C_2C_3}}{\sqrt{N_{J_1n_1C_1,J_2n_2C_2,J_3n_3C_3}}} F^{\begin{pmatrix} J_1 & J_2 & J_3 \\ n_1C_1 & n_2C_2 & n_3C_3 \end{pmatrix}} \\ &= \pm\epsilon_{C_1C_2C_3} \end{aligned} \tag{23}$$

with $\epsilon_{C_1C_2C_3}$ a phase factor and

$$\begin{aligned} N_{J_1n_1C_1,J_2n_2C_2,J_3n_3C_3} &= \left|K^{\begin{pmatrix} J_1 & J_2 & J_3 \\ (n_1C_1 & n_2C_2 & n_3C_3) \end{pmatrix}}\right|^2 \\ &= \left|F^{\begin{pmatrix} J_1 & J_2 & J_3 \\ n_1C_1 & n_2C_2 & n_3C_3 \end{pmatrix}}\right|^2. \end{aligned} \tag{24}$$

In the calculation of the $3C$ coefficients, we take the minimal value of J for which the symmetry is present: 0 for A and 1 for B_1, B_2, and B_3.

In the following, we will also need the oriented metric tensor defined by

$$\begin{pmatrix} J \\ nC\,n'C' \end{pmatrix} = \sum_{m,m'} \begin{pmatrix} J \\ m\,m' \end{pmatrix}^{(J)} G^m_{nC}{}^{(J)} G^{m'}_{n'C'}, \tag{25}$$

where

$$\begin{pmatrix} J \\ m\,m' \end{pmatrix} = (-1)^{J-m}\delta_{m',-m} \tag{26}$$

is the $SO(3)$ metric tensor [21]. Consequently, through (18), we obtain

$$\begin{pmatrix} J \\ nC\,n'C' \end{pmatrix} = \sum_m \Xi_C{}^{(J)} G^m_{nC}{}^{(J)} G^m_{n'C'} = \delta_{n,n'}\delta_{C,C'}\Xi_C. \tag{27}$$

If we consider the relation that exists between K and its conjugate K^* as in [21], we can show that

$$\begin{aligned} &\epsilon^2_{C_1C_2C_3} = \Xi_{C_1}\Xi_{C_2}\Xi_{C_3} = 1 \\ &\forall C_1, C_2, C_3 \text{ such as } C_1 \otimes C_2 = C_3. \end{aligned} \tag{28}$$

So we deduce that $F^{(C_1C_2C_3)} = \pm 1$.

Table 9
Values of the $\epsilon_{C_1C_2C_3}$ phase factors

$C_1C_2C_3$	AAA	AB_1B_1	AB_2B_2
$\epsilon_{C_1C_2C_3}$	1	−1	1

$C_1C_2C_3$	AB_3B_3	$B_1B_2B_3$	$B_3B_2B_1$
$\epsilon_{C_1C_2C_3}$	−1	1	−1

We choose to fix the phase factor $\epsilon_{C_1C_2C_3}$ such that

$$F^{(C_1C_2C_3)} = +1 \quad \forall (C_1, C_2, C_3), \tag{29}$$

which involves

$$K^{\begin{pmatrix} J_1 & J_2 & J_3 \\ (n_1C_1 & n_2C_2 & n_3C_3) \end{pmatrix}} = F^{\begin{pmatrix} J_1 & J_2 & J_3 \\ n_1C_1 & n_2C_2 & n_3C_3 \end{pmatrix}}. \tag{30}$$

To determine whether $\epsilon_{C_1C_2C_3}$ is equal to +1 or to −1, it is necessary to calculate the oriented $3C$ coefficients. According to (23), $\epsilon_{C_1C_2C_3}$ has the same sign as the oriented F. The phase factors that we obtain are given in Table 9. They are left unchanged by any even permutation of the representations.

In this way, we can find the expressions of the $6C$, $9C$ and $12C$ recoupling coefficients [19]. The $6C$ coefficients are defined by the relation

$$\begin{Bmatrix} C_1 & C_2 & C_{12} \\ C_3 & C & C_{23} \end{Bmatrix} = \frac{F^{(C_1C_{23}C)}F^{(C_2C_3C_{23})}F^{(C_{12}C_3C)}}{F^{(C_1C_2C_{12})}}. \tag{31}$$

The existing coefficients are equal to

$$\begin{Bmatrix} C_1 & C_2 & C_{12} \\ C_3 & C & C_{23} \end{Bmatrix} = 1 \tag{32}$$

with the following conditions:

$$\begin{aligned} &C_1 \otimes C_{23} = C, \quad C_2 \otimes C_3 = C_{23}, \\ &C_{12} \otimes C_3 = C, \quad C_1 \otimes C_2 = C_{12}. \end{aligned} \tag{33}$$

So these recoupling coefficients can be expressed by a product of Kronecker delta functions

$$\begin{aligned} \begin{Bmatrix} C_1 & C_2 & C_{12} \\ C_3 & C & C_{23} \end{Bmatrix} &= \delta_{C_1\times C_{23},C}\delta_{C_2\times C_3,C_{23}} \\ &\quad \times \delta_{C_{12}\times C_3,C}\delta_{C_1\times C_2,C_{12}}. \end{aligned} \tag{34}$$

The $9C$ and $12C$ coefficients can be calculated from the $6C$ ones through the usual formulas [6]. They are equal to 1 if the selection rules on the representations are respected and 0 otherwise. For example, we can express the $9C$ coefficients by

$$\begin{aligned} \begin{Bmatrix} C_1 & C_2 & C_{12} \\ C_3 & C_4 & C_{34} \\ C_{13} & C_{24} & C \end{Bmatrix} &= \delta_{C_1\times C_2,C_{12}}\delta_{C_1\times C_3,C_{13}}\delta_{C_2\times C_4,C_{24}} \\ &\quad \times \delta_{C_3\times C_4,C_{34}}\delta_{C_1\times C_2\times C_3\times C_4,C}. \end{aligned} \tag{35}$$

3.3. Calculation of matrix elements

In the $SO(3) \supset D_2$ group chain, we can express the Wigner–Eckart relation through the general form [22]:

$$\langle \Psi^{(J')}_{n'C'} | T^{(k)}_{n_0C_0} | \Psi^{(J)}_{nC} \rangle = \epsilon_{J'}(-1)^{2J'} K(k,J,J') e^{-i\psi(k,J,J')} \times \begin{pmatrix} nC\, n''C'' \\ J' \end{pmatrix} F^{(k \quad J \quad J')}_{n_0C_0 \; nC \; n''C''} e^{i\phi_E} \times \langle J' \| T^{(k)} \| J \rangle, \tag{36}$$

where $\langle J' \| T^{(k)} \| J \rangle$ is the reduced matrix element of the operator T and

$$\begin{pmatrix} nC\, n'C' \\ J \end{pmatrix} = \begin{pmatrix} J \\ nC\, n'C' \end{pmatrix} = \delta_{n,n'} \delta_{C,C'} \Xi_C. \tag{37}$$

In the calculation of the matrix elements of T, we keep the choices used by Michelot [22]:

$$\epsilon_{J'} = 1, \quad K(k,J,J') = (-1)^{2J'}, \qquad e^{i\phi_E} = 1, \quad e^{i\psi(k,J,J')} = (-1)^{2J}. \tag{38}$$

In our case, J and J' are integers, so these coefficients are all equal to 1. Relation (36) is reduced to

$$\langle \Psi^{(J')}_{n'C'} | T^{(k)}_{n_0C_0} | \Psi^{(J)}_{nC} \rangle = \Xi_C F^{(k \quad J \quad J')}_{n_0C_0 \; nC \; n'C'} \langle J' \| T^{(k)} \| J \rangle. \tag{39}$$

In the same way, we can express the Wigner–Eckart theorem in the D_2 group itself

$$\langle \Psi^{(C')} | T^{(C_0)} | \Psi^{(C)} \rangle = F^{(C_0CC')} \langle C' \| T^{(C_0)} \| C \rangle = \langle C' \| T^{(C_0)} \| C \rangle. \tag{40}$$

We can now calculate the reduced matrix elements of two coupled tensor operators acting on the same space through the relation

$$\langle C' \| [T^{(C_1)} \otimes T^{(C_2)}]^{(C_0)} \| C \rangle = \sum_{C''} (-1)^{C_1+C_2+C+C'} [C_0]^{1/2} \begin{Bmatrix} C_1 & C_2 & C_0 \\ C & C' & C'' \end{Bmatrix} \times \langle C' \| T^{(C_1)} \| C'' \rangle \langle C'' \| T^{(C_2)} \| C \rangle \tag{41}$$

with in the D_2 group

$$(-1)^{C_1+C_2+C+C'} = 1, \quad [C_0]^{1/2} = 1. \tag{42}$$

So we obtain

$$\langle C' \| [T^{(C_1)} \otimes T^{(C_2)}]^{(C_0)} \| C \rangle = \delta_{C_1 \times C_2 \times C, C'} \delta_{C_0 \times C, C'} \delta_{C_1 \times C_2, C_0} \langle C' \| T^{(C_1)} \| C_2 \times C \rangle \times \langle C_2 \times C \| T^{(C_2)} \| C \rangle. \tag{43}$$

And we can finally write the reduced matrix elements of two coupled tensor operators acting on two different spaces

$$\langle C'_1 C'_2, C' \| [T^{(\Gamma_1)} \otimes U^{(\Gamma_2)}]^{(\Gamma_0)} \| C_1 C_2, C \rangle = ([C][C'][\Gamma_0])^{1/2} \begin{Bmatrix} \Gamma_1 & C_1 & C'_1 \\ \Gamma_2 & C_2 & C'_2 \\ \Gamma_0 & C & C' \end{Bmatrix} \times \langle C'_1 \| T^{(\Gamma_1)} \| C_1 \rangle \langle C'_2 \| U^{(\Gamma_2)} \| C_2 \rangle, \tag{44}$$

where

$$([C][C'][\Gamma_0])^{1/2} = 1,$$

$$\begin{Bmatrix} \Gamma_1 & C_1 & C'_1 \\ \Gamma_2 & C_2 & C'_2 \\ \Gamma_0 & C & C' \end{Bmatrix} = \delta_{\Gamma_1 \times C_1, C'_1} \delta_{\Gamma_1 \times \Gamma_2, \Gamma_0} \delta_{C_1 \times C_2, C} \times \delta_{\Gamma_2 \times C_2, C'_2} \delta_{\Gamma_1 \times C_1 \times \Gamma_2 \times C_2, C'}, \tag{45}$$

which gives us

$$\langle C'_1 C'_2, C' \| [T^{(\Gamma_1)} \otimes U^{(\Gamma_2)}]^{(\Gamma_0)} \| C_1 C_2, C \rangle = \delta_{\Gamma_1 \times C_1, C'_1} \delta_{\Gamma_1 \times \Gamma_2, \Gamma_0} \delta_{C_1 \times C_2, C} \delta_{\Gamma_2 \times C_2, C'_2} \delta_{\Gamma_1 \times C_1 \times \Gamma_2 \times C_2, C'} \times \langle C'_1 \| T^{(\Gamma_1)} \| C_1 \rangle \langle C'_2 \| U^{(\Gamma_2)} \| C_2 \rangle. \tag{46}$$

3.4. Extension to the $O(3) \supset D_{2h}$ Chain

The tensorial algebra we developed here for the $SO(3) \supset D_2$ chain can be easily extended to the $O(3) \supset D_{2h}$ chain using some simple rules. The values of the different coefficients depend on the parity index in a trivial way. For example

$$^{(J\tau)}G^M_{nC_\tau} = {}^{(J)}G^M_{nC}, \; \Xi_{C_\tau} = \Xi_C, \qquad F^{(J_1\tau_1 \quad J_2\tau_2 \quad J_3\tau_3)}_{n_1C_1\tau_1 \; n_2C_2\tau_2 \; n_3C_3\tau_3} = F^{(J_1 \quad J_2 \quad J_3)}_{n_1C_1 \; n_2C_2 \; n_3C_3}, \tag{47}$$

where $\tau_i = g$ or u. Just as for the irreps, we must introduce selection rules on the parity. For instance, the triangular conditions for F coefficients become

$$C_{1\tau_1} \otimes C_{2\tau_2} = C_{3\tau_3} \Longleftrightarrow \begin{cases} C_1 \otimes C_2 = C_3, \\ \tau_1 \otimes \tau_2 = \tau_3. \end{cases} \tag{48}$$

4. Tensorial formalism for the X_2Y_4 (D_{2h}) molecules

In this section, we will focus on the tensorial expressions of the Hamiltonian and transition moments operators in the D_{2h} group. They are based on the expansion of these operators according to the usual principles [7,13]. We show in Table 10 the symmetries of the Hamiltonian, dipole moment, and polarizability operators in the LFF (Laboratory-Fixed Frame) and MFF (Molecule-Fixed Frame) for our group.

Successive Van Vleck contact transformations are generally applied to the Hamiltonian and transition

Table 10
Symmetry of the Hamiltonian, dipole moment, and polarizability operators expressed in the MFF and LFF for molecules belonging to the D_{2h} symmetry group

Operator	MFF	LFF
H	A_g	A_g
μ	$B_{1u} \oplus B_{2u} \oplus B_{3u}$	A_u
α	$3A_g \oplus B_{1g} \oplus B_{2g} \oplus B_{3g}$	A_g

moment operators. The aim of these contact transformations is to introduce appropriate basis functions in which the transformed Hamiltonian $\tilde{H}$ has a completely diagonal or block diagonal form with respect to some vibrational subspace. These subspaces of close vibrational levels correspond to the so-called polyads.

If A represents either H (Hamiltonian), μ (dipole moment) or α (polarizability), the transformed operator $\tilde{A}$ is given by

$$\tilde{A} = TAT^{-1} = A + \mathrm{i}[S,A] - \frac{1}{2}[S,[S,A]] + \cdots \tag{49}$$

with $T = \mathrm{e}^{\mathrm{i}S}$. S is a Hermitian operator and is called the generator of contact transformation. It has been shown that S is always a sum of rovibrational operators [3].

4.1. Expression of the Hamiltonian

The Hamiltonian is expanded as a series of rovibrational operators which are noted $T^{\Omega(K,n\Gamma_r)\Gamma_1\Gamma_2\Gamma_v}_{\{n_s\}\{m_s\}}$

$$H = \sum_{\text{all indexes}} t^{\Omega(K,n\Gamma_r)\Gamma_1\Gamma_2\Gamma_v}_{\{n_s\}\{m_s\}} T^{\Omega(K,n\Gamma_r)\Gamma_1\Gamma_2\Gamma_v}_{\{n_s\}\{m_s\}} \tag{50}$$

with the coupled rovibrational operators

$$T^{\Omega(K,n\Gamma_r)\Gamma_1\Gamma_2\Gamma_v}_{\{n_s\}\{m_s\}} = \beta[R^{\Omega(K,n\Gamma_r)} \otimes {}^{\varepsilon}V^{\Gamma_1\Gamma_2\Gamma_v}_{\{n_s\}\{m_s\}}]^{(A_g)}, \tag{51}$$

where $\Omega \geqslant 2$ and β is a numerical factor. The $t^{\Omega(K,n\Gamma_r)\Gamma_1\Gamma_2\Gamma_v}_{\{n_s\}\{m_s\}}$ are the parameters of our model.

The $R^{\Omega(K,n\Gamma_r)}$ (rotational) and ${}^{\varepsilon}V^{\Gamma_1\Gamma_2\Gamma_v}_{\{n_s\}\{m_s\}}$ (vibrational) operators are constructed in the same way as in C_{4v} [7] or O_h [5]. This construction is detailed for the T_d group in [3]. To ensure that H is unchanged under time reversal, the parity ϵ of the vibrational operators in the conjugate moment $p_{s,\sigma}$ is related to the rotational degree Ω through

$$\epsilon = (-1)^{\Omega}. \tag{52}$$

The order of the development is defined as

$$\sum_s (n_s + m_s) + \Omega - 2, \tag{53}$$

n_s and m_s being the degree of ${}^{\varepsilon}V^{\Gamma_1\Gamma_2\Gamma_v}_{\{n_s\}\{m_s\}}$ in the a^+ (creation) and a (annihilation) operators, respectively.

In the following, we use the rovibrational coupled basis

$$|[\Psi^{(J,n_rC_r)}_r \otimes \Psi^{(\{v_s\}C_v)}_v]\rangle, \tag{54}$$

where $\Psi^{(J,n_rC_r)}_r$ is the rotational basis and $\Psi^{(\{v_s\}C_v)}_v$ the vibrational one, with

$$|\Psi^{(\{v_s\}C_v)}_v\rangle = |[\Psi^{(A_g)}_{v_1} \otimes \cdots \otimes \Psi^{(B_{3u})}_{v_{12}}]^{(C_v)}\rangle, \tag{55}$$

where $v_1, v_2, \ldots, v_{12}$ are the harmonic oscillator quantum numbers for the X_2Y_4 molecule and C_v is the vibrational symmetry in the D_{2h} group.

The Hamiltonian eigenfunctions are linear combinations of such rovibrational functions and we denote them

$$|\Phi^{(JC\alpha)}_M\rangle, \tag{56}$$

where α numbers the energy levels in increasing order within a (JC) block.

The general expression of the matrix elements of the Hamiltonian operator is given in Appendix A. In Table 11, we give the correspondence between some of our parameters and the "classical" ones, for the ground state and the ν_4/ν_7 dyad of C_2H_4 [23].

4.2. Expression of the dipole moment

For a general discussion about transition operators, the reader can refer for instance to [5]. We only outline here the results that are specific to our D_{2h} case.

Table 11
Correspondance between our parameters and the usual ones

Level	Parameter $t^{\Omega(K,n\Gamma)\Gamma_1\Gamma_2\Gamma_v}_{\{n_s\}\{m_s\}}$						Value[a] (cm^{-1})	Classical formalism[b]
	$\Omega(K,n\Gamma)$	$\{n_s\}$	Γ_1	$\{m_s\}$	Γ_2	Γ_v		
G.S.	$2(0,0A_g)$	$\{0\}$	A_g	$\{0\}$	A_g	A_g	2.23124088334	$\frac{1}{3}(A_0+B_0+C_0)$
	$2(2,0A_g)$	$\{0\}$	A_g	$\{0\}$	A_g	A_g	0.80630444089	$-\frac{\sqrt{3}}{12\sqrt{2}}(C_0+B_0-2A_0)$
	$2(2,1A_g)$	$\{0\}$	A_g	$\{0\}$	A_g	A_g	$-3.05842262095\times10^{-2}$	$\frac{1}{4\sqrt{2}}(C_0-B_0)$
ν_4	$0(0,0A_g)$	$\{\nu_4\}$	A_u	$\{\nu_4\}$	A_u	A_g	$0.10255893000\times10^{+4}$	ω_4
	$2(0,0A_g)$	$\{\nu_4\}$	A_u	$\{\nu_4\}$	A_u	A_g	$-0.94627833334\times10^{-2}$	$\frac{1}{3}(\Delta A_4+\Delta B_4+\Delta C_4)$
	$2(2,0A_g)$	$\{\nu_4\}$	A_u	$\{\nu_4\}$	A_u	A_g	$-0.49731306432\times10^{-2}$	$-\frac{\sqrt{3}}{12\sqrt{2}}(\Delta C_4+\Delta B_4-2\Delta A_4)$
	$2(2,1A_g)$	$\{\nu_4\}$	A_u	$\{\nu_4\}$	A_u	A_g	$0.51092177251\times10^{-3}$	$\frac{1}{4\sqrt{2}}(\Delta C_4-\Delta B_4)$
ν_7	$0(0,0A_g)$	$\{\nu_7\}$	B_{1u}	$\{\nu_7\}$	B_{1u}	A_g	$0.94877090520\times10^{+3}$	ω_7
	$2(0,0A_g)$	$\{\nu_7\}$	B_{1u}	$\{\nu_7\}$	B_{1u}	A_g	$0.19376500000\times10^{-2}$	$\frac{1}{3}(\Delta A_7+\Delta B_7+\Delta C_7)$
	$2(2,0A_g)$	$\{\nu_7\}$	B_{1u}	$\{\nu_7\}$	B_{1u}	A_g	$0.67550497195\times10^{-3}$	$-\frac{\sqrt{3}}{12\sqrt{2}}(\Delta C_7+\Delta B_7-2\Delta A_7)$
	$2(2,1A_g)$	$\{\nu_7\}$	B_{1u}	$\{\nu_7\}$	B_{1u}	A_g	$0.20211056350\times10^{-3}$	$\frac{1}{4\sqrt{2}}(\Delta C_7-\Delta B_7)$
ν_4/ν_7	$1(1,0B_{1g})$	$\{\nu_4\}$	A_u	$\{\nu_7\}$	B_{1u}	B_{1g}	?	$\frac{1}{2}\zeta^{xz}_{4,7}$

[a] The numerical values are calculated with the rotational constants found in [23].
[b] A_0, B_0 and C_0 are the ground state constants and $\Delta A_i = A(v_i=1) - A_0$, $\Delta B_i = B(v_i=1) - B_0$, and $\Delta C_i = C(v_i=1) - C_0$.

Each component of the initial (untransformed) dipole moment in the MFF is expanded as a series of purely vibrational operators

$$\mu_\theta^{(\Gamma)} = \sum_{\text{all indexes}} \mu_{\{n_s\}\{m_s\}}^{\Gamma_1\Gamma_2\Gamma_v} + V_{\{n_s\}\{m_s\}}^{\Gamma_1\Gamma_2\Gamma_v}, \tag{57}$$

where the $\mu_{\{n_s\}\{m_s\}}^{\Gamma_1\Gamma_2\Gamma_v}$ are the dipole parameters and θ is a component of the operator $\mu^{(\Gamma)}$.

Then, the transformed dipole moment must be expanded as a series of rovibrational operators by [3,5]

$$\tilde{\mu}_\theta^{(\Gamma)} = \sum_{\{i\}} \tilde{\mu}^{\{i\},\Gamma} M_\theta^{(\{i\},\Gamma)}, \tag{58}$$

with

$$M_\theta^{(\{i\},\Gamma)} = \left(R^{\Omega(K,n\Gamma_r)} \otimes {}^{\varepsilon}V_{\{n_s\}\{m_s\}}^{\Gamma_1\Gamma_2\Gamma_v}\right)_\theta^{(\Gamma)} \tag{59}$$

and $\epsilon = (-1)^\Omega$. The order of the development is

$$\sum_s (n_s + m_s) + \Omega - 1. \tag{60}$$

The LFF components of the transformed dipole moment are

$$\begin{aligned}\tilde{\mu}_\Theta^{(A_u)} = \sum_m \langle 1;\ m|\Theta\rangle \Bigg\{ &\sum_{\{i\}} \tilde{\mu}^{\{i\},B_{1g}} [C^{(1_g,B_{1g})} \otimes M^{(\{i\},B_{1u})}]^{(A_u)} \\ &+ \sum_{\{i\}} \tilde{\mu}^{\{i\},B_{2g}} [C^{(1_g,B_{2g})} \otimes M^{(\{i\},B_{2u})}]^{(A_u)} \\ &+ \sum_{\{i\}} \tilde{\mu}^{\{i\},B_{3g}} [C^{(1_g,B_{3g})} \otimes M^{(\{i\},B_{3u})}]^{(A_u)} \Bigg\},\end{aligned} \tag{61}$$

where $\langle 1;\ m|\Theta\rangle$ is a Stone coefficient given in [3] and $C^{(1_g,\Gamma)}$ is the direction cosine tensor. The Θ component is equal to X, Y, or Z. The square brackets represent the symmetrized tensor product defined as

$$[A^{(\Gamma_1)} \otimes B^{(\Gamma_2)}]^{(\Gamma)} = \frac{1}{2}\left((A^{(\Gamma_1)} \otimes B^{(\Gamma_2)})^{(\Gamma)} + (B^{(\Gamma_2)} \otimes A^{(\Gamma_1)})^{(\Gamma)}\right). \tag{62}$$

The strength of a transition between the molecular rovibrational states Φ_i (with energy E_i) and Φ_f (with energy E_f) is calculated thanks to the relation

$$S_{if} = K_{if} g_i e^{-(hcE_i/k_BT)} \sum_{M_i,M_f} |\langle \Phi_i|\tilde{\mu}_Z|\Phi_f\rangle|^2, \tag{63}$$

where K_{if} is a numerical coefficient and g_i is the spin statistical weight of state Φ_i. The values of spin statistic weights in X_2Y_4 (D_{2h}) molecules with Y ligands having a $\frac{1}{2}$ spin and X atoms having a null spin are listed in Table 12.

Table 12
Spin statistic weights in D_{2h}

C	A_g	B_{1g}	B_{2g}	B_{3g}
g_i	7	3	3	3

C	A_u	B_{1u}	B_{2u}	B_{3u}
g_i	7	3	3	3

Appendix A gives the general expression for the matrix elements of the dipole moment operator.

4.3. Expression of the polarizability

Each component of the initial (untransformed) polarizability in the MFF is expanded as a series of purely vibrational operators

$$\alpha_\theta^{(\Gamma)} = \sum_{\text{all indexes}} \alpha_{\{n_s\}\{m_s\}}^{\Gamma_1\Gamma_2\Gamma_v} + V_{\{n_s\}\{m_s\}}^{\Gamma_1\Gamma_2\Gamma_v}, \tag{64}$$

where the $\alpha_{\{n_s\}\{m_s\}}^{\Gamma_1\Gamma_2\Gamma_v}$ are the polarizability parameters.

In the same way as before, we can write the transformed polarizability as a series of rovibrational operators by

$$\tilde{\alpha}_\theta^{(\Gamma)} = \sum_{\{i\}} \tilde{\alpha}^{\{i\},\Gamma} P_\theta^{(\{i\},\Gamma)}, \tag{65}$$

with

$$P_\theta^{(\{i\},\Gamma)} = \left(R^{\Omega(K,n\Gamma_r)} \otimes {}^{\varepsilon}V_{\{n_s\}\{m_s\}}^{\Gamma_1\Gamma_2\Gamma_v}\right)_\theta^{(\Gamma)} \tag{66}$$

and $\epsilon = (-1)^\Omega$. The order of the development is

$$\sum_s (n_s + m_s) + \Omega - 1. \tag{67}$$

The LFF components of the transformed polarizability are

$$\begin{aligned}\tilde{\alpha}_{\Theta_1\Theta_2}^{(A_g)} = \langle 0;\ 0|\Theta_1\Theta_2\rangle &\sum_{\{i\}} \tilde{\alpha}^{\{i\},A_g} [C^{(0_g,0A_g)} \otimes P^{(\{i\},A_g)}]^{(A_g)} \\ &+ \sum_m \langle 2;\ m|\Theta_1\Theta_2\rangle \\ &\times \Bigg\{ \sum_{\{i\}} \tilde{\alpha}^{\{i\},0A_g} [C^{(2_g,0A_g)} \otimes P^{(\{i\},A_g)}]^{(A_g)} \\ &+ \sum_{\{i\}} \tilde{\alpha}^{\{i\},1A_g} [C^{(2_g,1A_g)} \otimes P^{(\{i\},A_g)}]^{(A_g)} \\ &+ \sum_{\{i\}} \tilde{\alpha}^{\{i\},B_{1g}} [C^{(2_g,0B_{1g})} \otimes P^{(\{i\},B_{1g})}]^{(A_g)} \\ &+ \sum_{\{i\}} \tilde{\alpha}^{\{i\},B_{2g}} [C^{(2_g,0B_{2g})} \otimes P^{(\{i\},B_{2g})}]^{(A_g)} \\ &+ \sum_{\{i\}} \tilde{\alpha}^{\{i\},B_{3g}} [C^{(2_g,0B_{3g})} \otimes P^{(\{i\},B_{3g})}]^{(A_g)} \Bigg\},\end{aligned} \tag{68}$$

where $\langle J;\ m|\Theta_1\Theta_2\rangle$ is the Stone coefficient [3] and the Θ_1 and Θ_2 components are equal to X, Y or Z.

The intensity of Raman transitions is expressed as

$$I_{if} = R_{if} g_i e^{-(hcE_i/k_BT)} \sum_{\Theta,\Theta'} \sum_{M_i,M_f} |\langle \Phi_i|\tilde{\alpha}_{\Theta,\Theta'}|\Phi_f\rangle|^2. \tag{69}$$

The general expression for the matrix elements of the transformed polarizability operator is given in Appendix A.

4.4. Selection rules

The selection rules (see Table 13) come directly from the expressions of the matrix elements given in Appen-

Table 13
Selection rules for the Hamiltonian, dipole moment, and polarizability operators

	H	μ	$\alpha^{(0)}$	$\alpha^{(2)}$
ΔJ	0	$0,\pm1$	0	$0,\pm1,\pm2$
ΔM	0	$0,\pm1$	0	$0,\pm1,\pm2$
C'	C	$C\otimes A_u$	C	C

dix A. In the matrix element expressions, C' is the symmetry of the bra corresponding to a ket with symmetry C. The rules concerning J come from the nonzero condition of the K isoscalar factors.

5. Conclusion

To study the ethylene molecule, or more generally the X_2Y_4 (D_{2h}) molecules, we have developed a tensorial formalism adapted to the $O(3)\supset D_{2h}$ chain as an other extension of what has already been done in Dijon in the case of $O(3)\supset T_d, O_h$. We have determined coupling and recoupling coefficients in this chain but also in D_{2h} itself. The Wigner–Eckart theorem with useful formulas for the computation of reduced matrix elements of tensor operators have been given. The tensorial algebra in our group being constructed, we have proposed a method to expand the Hamiltonian and the transition moments operators for X_2Y_4 (D_{2h}) asymmetric top molecules using this tensorial formalism. The formulas necessary to calculate the matrix elements of these operators have been given as well as the related selection rules. Similarly to the HTDS software developed in Dijon for the calculation of XY_6 molecular spectra, we have written a new one for the case of X_2Y_4 molecules; it uses the formulas derived in the present paper for frequency and intensity calculations. Readers interested in using these programs can contact the authors.

Acknowledgments

Support from the Région Bourgogne for the computer equipment of the Laboratoire de Physique de l'Université de Bourgogne is gratefully acknowledged.

Appendix A.

A.1. Matrix elements of the Hamiltonian operator

$$\begin{aligned}&\langle[\Psi_r^{(J',n_r'C_r')}\otimes\Psi_v^{(\{v_s'\}C_v')}]^{(C')}\|[(R^{\Omega(K,n\Gamma)}\\&\quad\otimes{}^{\epsilon}V^{\Gamma_1\Gamma_2(\Gamma)}_{\{n_s\}\{m_s\}})^{(A_g)}\|\Psi_r^{(J,n_rC_r)}\otimes\Psi_v^{(\{v_s\}C_v)}]^{(C)}\rangle\\&=\delta_{J,J'}\delta_{\Gamma\times C_r,C_r'}\delta_{\Gamma\times C_v,C_v'}\delta_{C_r\times C_v,C}\delta_{C,C'}\Xi_{C_r}\\&\quad\times K^{(K\quad J\quad J')}_{(n\Gamma\quad n_rC_r\quad n_r'C_r')}\langle\Psi_r^{(J)}\|R^{\Omega(K)}\|\Psi_r^{(J)}\rangle\\&\quad\times\langle\Psi_v^{(\{v_s'\}C_v')}\|{}^{\epsilon}V^{\Gamma_1\Gamma_2(\Gamma)}_{\{n_s\}\{m_s\}}\|\Psi_v^{(\{v_s\}C_v)}\rangle.\end{aligned}\tag{A.1}$$

A.2. Matrix elements of the dipole moment operator

$$\begin{aligned}&\langle[\Psi_r^{(J',n_r'C_r')}\otimes\Psi_v^{(\{v_s'\}C_v')}]^{(C')}\|[C^{(1_g,\Gamma_g)}\\&\quad\otimes M^{(\{i\},\Gamma_u)}]^{(A_u)}\|\Psi_r^{(J,n_rC_r)}\otimes\Psi_v^{(\{v_s\}C_v)}]^{(C)}\rangle\\&=\frac{1}{2}\delta_{C,C'}\langle\Psi_r^{(J')}\|C^{(1_g,\Gamma_g)}\|\Psi_r^{(J)}\rangle\\&\quad\times\langle\Psi_v^{(\{v_s'\}C_v')}\|{}^{\epsilon}V^{\Gamma_1\Gamma_2(\Gamma_v)}_{\{n_s\}\{m_s\}}\|\Psi_v^{(\{v_s\}C_v)}\rangle\\&\quad\times\sum_{n_r''C_r''}[\Xi_{C_r}\,\Xi_C\,\delta_{\Gamma_r\times C_r,C_r''}\,\delta_{\Gamma_v\times C_v,C_v'}\\&\quad\times K^{(1\quad J\quad J')}_{(0\Gamma\quad n_r''C_r''\quad n_r'C_r')}K^{(K\quad J\quad J)}_{(n\Gamma_r\quad n_rC_r\quad n_r''C_r'')}\\&\quad\times\langle\Psi_r^{(J)}\|R^{\Omega(K)}\|\Psi_r^{(J)}\rangle\\&\quad+\Xi_{C_r''}\,\Xi_{\Gamma\times C}\delta_{\Gamma_r\times C_r'',C_r'}\,\delta_{\Gamma_v\times C_v,C_v'}\\&\quad\times K^{(1\quad J\quad J')}_{(0\Gamma\quad n_rC_r\quad n_r''C_r'')}K^{(K\quad J'\quad J')}_{(n\Gamma_r\quad n_r''C_r''\quad n_r'C_r')}\\&\quad\times\langle\Psi_r^{(J')}\|R^{\Omega(K)}\|\Psi_r^{(J')}\rangle].\end{aligned}\tag{A.2}$$

A.3. Matrix elements of the polarizability operator

$$\begin{aligned}&\langle[\Psi_r^{(J',n_r'C_r')}\otimes\Psi_v^{(\{v_s'\}C_v')}]^{(C')}\|[C^{(L_g,n_\alpha\Gamma_g)}\\&\quad\otimes P^{(\{i\},\Gamma_g)}]^{(A_g)}\|\Psi_r^{(J,n_rC_r)}\otimes\Psi_v^{(\{v_s\}C_v)}]^{(C)}\rangle\\&=\frac{1}{2}\delta_{C,C'}\langle\Psi_r^{(J')}\|C^{(L_g,n_\alpha\Gamma_g)}\|\Psi_r^{(J)}\rangle\\&\quad\times\langle\Psi_v^{(\{v_s'\}C_v')}\|{}^{\epsilon}V^{\Gamma_1\Gamma_2(\Gamma_v)}_{\{n_s\}\{m_s\}}\|\Psi_v^{(\{v_s\}C_v)}\rangle\\&\quad\times\sum_{n_r''C_r''}[\Xi_{C_r}\,\Xi_C\,\delta_{\Gamma_r\times C_r,C_r''}\,\delta_{\Gamma_v\times C_v,C_v'}\\&\quad\times K^{(L\quad J\quad J')}_{(n_\alpha\Gamma\quad n_r''C_r''\quad n_r'C_r')}K^{(K\quad J\quad J)}_{(n\Gamma_r\quad n_rC_r\quad n_r''C_r'')}\\&\quad\times\langle\Psi_r^{(J)}\|R^{\Omega(K)}\|\Psi_r^{(J)}\rangle\\&\quad+\Xi_{C_r''}\,\Xi_{\Gamma\times C}\,\delta_{\Gamma_r\times C_r'',C_r'}\,\delta_{\Gamma_v\times C_v,C_v'}\\&\quad\times K^{(L\quad J\quad J')}_{(n_\alpha\Gamma\quad n_rC_r\quad n_r''C_r'')}K^{(K\quad J'\quad J')}_{(n\Gamma_r\quad n_r''C_r''\quad n_r'C_r')}\\&\quad\times\langle\Psi_r^{(J')}\|R^{\Omega(K)}\|\Psi_r^{(J')}\rangle].\end{aligned}\tag{A.3}$$

References

[1] W.E. Blass, J.J. Hillman, A. Fayt, S.J. Daunt, L.R. Senesac, A.C. Ewing, L.W. Jennings, J.S. Hager, S.L. Mahan, D.C. Reuter, M. Sirota, J. Quant. Spectrosc. Radiat. Transfer 71 (2001) 47–60.
[2] K. Lodders, B. Fegley Jr., Icarus 155 (2002) 393–424.
[3] J.-P. Champion, M. Loëte, G. Pierre, in: K.N. Rao, A. Weber (Eds.), Spectroscopy of the Earth's Atmosphere and Interstellar Medium, Academic Press, San Diego, CA, 1992, pp. 339–422.
[4] A. Nikitin, J.-P. Champion, Vl.G. Tyuterev, J. Mol. Spectrosc. 182 (1997) 72–84.
[5] N. Cheblal, M. Loëte, V. Boudon, J. Mol. Spectrosc. 197 (1999) 222–231.
[6] M. Rotger, V. Boudon, M. Loëte, J. Mol. Spectrosc. 200 (2000) 123–130.
[7] M. Rotger, V. Boudon, M. Loëte, J. Mol. Spectrosc. 200 (2000) 131–137.

[8] M. Rotger, A. Decrette, V. Boudon, M. Loëte, S. Sander, H. Willner, J. Mol. Spectrosc. 208 (2001) 169–179.
[9] J.-C. Hilico, O. Robert, M. Loëte, S. Toumi, A.S. Pine, L.R. Brown, J. Mol. Spectrosc. 208 (2001) 1–13.
[10] A. Nikitin, L.R. Brown, L. Féjard, J.-P. Champion, Vl. G. Tyuterev, J. Mol. Spectrosc. 216 (2002), in press.
[11] B.G. Sartakov, J. Oomens, J. Reuss, A. Fayt, J. Mol. Spectrosc. 185 (1997) 31–47.
[12] R.S. Mulliken, J. Chem. Phys. 23 (1955) 1997–2011.
[13] D. Papoušek, M.R. Aliev, Molecular Vibrational–Rotational Spectra, Elsevier, New York, 1982.
[14] G. Herzberg, Infrared and Raman Spectra of Polyatomic Molecules, Von Nostrand, New York, 1945.
[15] A.J. Merer, R.S. Mulliken, Chem. Rev. 69 (1969) 639.
[16] M. Hamermesh, Group Theory and its Application to Physical Problems, Addison-Wesley, Reading, MA, 1962.
[17] A.R. Edmonds, Angular Momentum in Quantum Mechanics, Princeton University Press, Princeton, NJ, 1982.
[18] M. Rotenberg, N. Metropolis, R. Bivins, J.K. Wooten Jr., The 3-**j** and 6-**j** Symbols, The Technology Press, Cambridge, MA, 1959.
[19] U. Fano, G. Racah, Irreductible Tensorial Sets, Academic Press, New York, 1959.
[20] B. Lulek, T. Lulek, B. Szczepaniak, Acta Phys. Pol. A 54 (5) (1978) 545–559.
[21] V. Boudon, F. Michelot, J. Mol. Spectrosc. 165 (1994) 554–579.
[22] F. Michelot, Thèse d'état, Dijon, 1980.
[23] E. Rusinek, H. Fichoux, M. Khelkhal, F. Herlemont, J. Legrand, A. Fayt, J. Mol. Spectrosc. 189 (1998) 64–73.

Sixième partie

Conclusion

Dans ce rapport, j'ai tenté de résumer mes activités d'enseignant-chercheur au cours des quatorze dernières années (1990–2004) au laboratoire SMIL qui a été restructuré en 1995 et est ensuite devenu Laboratoire de Physique de l'Université de Bourgogne.

Au tout début de ce document, j'ai rappelé brièvement mes études ainsi que mes propres réalisations en matière d'enseignement et de recherche. J'y mentionne également les activités d'interêt général ainsi que les encadrements d'étudiants.

Comme on a pu le voir dans ce manuscrit, au cours de mes premières années de Maître de Conférences je me suis initiée à la spectroscopie surtout expérimentale puis ensuite, je me suis impliquée dans le développement de nouveaux modèles théoriques et dans l'analyse de spectres. Il existait depuis longtemps au laboratoire un savoir faire en matière d'hamiltonien, de moments de transition et d'effet Stark pour les toupies sphériques. Je l'ai étendu à des toupies symétriques et asymétriques.

Ainsi, deux nouvelles voies sont en train d'être explorées. D'une part, la spectroscopie des toupies quasi-sphériques pour lesquelles les modèles "classiques" montrent leurs limites et d'autre part, la spectroscopie des molécules piégées dans des solides microporeux, sujet porteur au niveau des applications. La première thématique est d'intérêt purement théorique et relie les techniques dijonnaises aux techniques usuelles, la seconde présente un challenge industriel important en matière de dépollution de l'air. Il s'agit d'utiliser la spectroscopie comme un outil de diagnostic optique pour mieux comprendre les phénomènes d'adsorption de molécules dans des solides afin de capturer les polluants atmosphériques.

La partie concernant la spectroscopie des molécules piégées dans des solides doit beaucoup au travail de DEA puis de thèse réalisé par W. Raballand à partir de 2002 et qui se terminera à la rentrée 2005.

J'ai par ailleurs mis l'accent sur la diffusion des résultats auprès de la communauté scientifique à travers la mise en place de trois nouvelles bases de données.

Dans l'avenir, il reste du travail tant expérimental que théorique.

La mise en place d'un jet fente du même type que celui fonctionnant à Zürich devrait permettre l'extension de l'expérience diode-laser à l'enregistrement de portions de spectres de molécules lourdes telles que SF_5Cl ou les hexacarbonyles de métaux de transition.

Du point de vue théorique, l'approche quasi-sphérique a montré sa faisabilité, elle peut désormais être appliquée à l'analyse d'autres polyades de SO_2F_2 ou à d'autres molécules (IOF_5, H_2SO_4, ...)

L'interprétation des spectres de molécules placées dans des zéolithes est en cours. La polarisabilité est une grandeur qui y joue un rôle très important. Une collaboration a été établie avec les expérimentateurs du groupe de spectroscopie résolue en temps afin d'en déterminer ses composantes. L'effet Stark est en partie modélisé pour l'éthylène. La confrontation du modèle avec des spectres basse résolution d'éthylène dans des zéolithes est à faire.

Des bases de données prédictives de l'effet Stark pour des molécules asymétriques devront être mises en place à l'image de ce qu'il existe déjà en l'absence de champ. C'est un aspect important car peu de données précises sont disponibles actuellement sur la polarisabilité et sur le moment dipolaire.

Septième partie

Annexe : Liste des Travaux

Thèse de doctorat

"Contribution à l'étude d'un laser Nd-YAG industriel de puissance. Réalisation d'un lambdamètre pour lasers impulsionnels",
M. Rotger,
Thèse, Dijon, (**1990**).

Articles dans des revues à comité de lecture

[**P1**] " Résonateur Optique de Type Cavité Optique en Anneau",
H. Berger, J.-P. Boquillon, J. Moret-Bailly, B. Taisne and M. Rotger,
*Brevêt déposé le 28/11/***1989** *au nom de l'ARDT.*

[**P2**] "Choix d'un Interféromètre pour Mesurer la Longueur d'Onde de Lasers Impulsionnels Monomodes",
M. Rotger, R. Chaux, H. Berger and J. Moret-Bailly,
Journal d'Optique, **5**, 193–202, (**1990**).

[**P3**] "Non-Linear Raman Spectroscopy in Gases",
B. Lavorel, G. Millot, M. Rotger, G. Rouille, H. Berger and H.W. Schrötter,
Journal of Molecular Structure, **273**, 49–59, (**1992**).

[**P4**] "High-Resolution Photoacoustic Raman Spectroscopy of Gases",
M. Rotger, B. Lavorel and R. Chaux,
Journal of Raman Spectroscopy, **23**, 303–309, (**1992**).

[**P5**] "Stimulated Raman and CARS Spectroscopy of ν_1 and $2\nu_2$ Bands of $^{12}CF_4$",
A. Tabyaoui, B. Lavorel, R. Saint-Loup and M. Rotger,
Journal of Raman Spectroscopy, **25**, 255–260, (**1994**).

[**P6**] "Spectroscopy of Hexafluorides with an Odd Number of Electrons. The Vibronic Bands of IrF_6",
V. Boudon, M. Rotger and D. Avignant,
Journal of Molecular Spectroscopy, **175**, 327–339, (**1996**).

[**P7**] "Spontaneous Raman Scattering Spectrum of Gaseous IrF_6 in the Ground Electronic State",
M. Rotger, V. Boudon, A.T. Nguyen and D. Avignant,
Journal of Raman Spectroscopy, **27**, 145–148, (**1996**).

[**P8**] "Theoretical Comparison of the Three Most Widely Used Resonators for High Power Nd-YAG Lasers",
M. Rotger and V. Boudon,
Journal d'Optique, **27**(3), 121–128, (**1996**).

[**P9**] "Ultraviolet Absorption Spectrum of Gaseous IrF_6 in the 200–500 nm Region",
V. Boudon, M. Rotger and D. Avignant,
Spectrochimica Acta A, **52**, 1175–1182, (**1996**).

[**P10**] "Absorption Spectrum of the $f(A_{1g}) \leftarrow X(E_g)$, $a(F_{2g})$ Electronic Transition of OsF_6",
M. Rotger, V. Boudon and H. Selig,
Spectrochimica Acta A, **53**, 991–994 (**1997**).

[**P11**] "*Ab Initio* Calculations and High Resolution Spectroscopy of the Bending Pentad of SiH_2D_2 in the 10-16 μm Region"
M. Rotger, V. Boudon, B. Lavorel, S. Sommer, H. Bürger, J. Breidung, W. Thiel, M. Bétrencourt and J.-C. Deroche,
Journal of Molecular Spectroscopy, **192**, 294–308 (**1998**).

[P12] "Absorption Spectrum of the $a(E'_{2g}) \leftarrow X(G'_g)$ and $b(G'_g) \leftarrow X(G'_g)$ Electronic Transitions of ReF_6",
M. Rotger, V. Boudon and H. Selig,
Spectrochimica Acta A, **55**, 1575–1584 (**1999**).

[P13] "Spectroscopy of XY_5Z (C_{4v}) Molecules. A Tensorial Formalism Adapted to the $O(3) \supset O_h \supset C_{4v}$ Chain ",
M. Rotger, V. Boudon and M. Loëte,
Journal of Molecular Spectroscopy, **200**, 123–130 (**2000**).

[P14] "Spectroscopy of XY_5Z (C_{4v}) Molecules. Development of the Hamiltonian and of the Transition Moment Operators Using a Tensorial Formalism ",
M. Rotger, V. Boudon and M. Loëte,
Journal of Molecular Spectroscopy, **200**, 131–137 (**2000**).

[P15] "High Resolution Spectroscopy and Analysis of the ν_4 Band of $^{80}SeF_6$",
M. Rotger, V. Boudon, H. Bürger and H. Willner,
Chemical Physics Letters, **339**, 83–88 (**2001**).

[P16] "High Resolution Spectroscopy and Analysis of the ν_1/ν_8 Dyad of $SF_5{}^{35}Cl$",
M. Rotger, A. Decrette, V. Boudon, M. Loëte, S. Sander and H. Willner,
Journal of Molecular Spectroscopy, **208**, 169–179 (**2001**).

[P17] "C_{4v} Top Data System (C_{4v}TDS) Software for Infrared Spectrum Simulation of XY_5Z Symmetric Molecules",
Ch. Wenger, M. Rotger and V. Boudon,
Journal of Quantitative Spectroscopy and Radiative Transfer, **74**, 621–636 (**2002**).

[P18] "High Resolution Spectroscopy of the ν_3 Band of WF_6 and ReF_6 in a Supersonic Jet",
V. Boudon, M. Rotger, Y. He, H. Hollenstein, M. Quack and U. Schmitt,
Journal of Chemical Physics, **117**, 3196–3207 (**2002**).
Supplément: Document EPAPS No. E-JCPSA6-116-005222, "Four Tables Containing the Observed and Calculated Transition Wavenumbers for WF_6".
Cf. `http://www.aip.org/pubservs/epaps.html`.

[P19] "Spectroscopy of XY_2Z_2 (C_{2v}) Molecules: A Tensorial Formalism Adapted to the $O(3) \supset T_d \supset C_{2v}$ Chain. Application to the Ground State of SO_2F_2",
M. Rotger, V. Boudon and M. Loëte,
Journal of Molecular Spectroscopy, **216**, 297–307 (numéro spécial en l'honneur de H. Bürger, **2002**).

[P20] "Spectroscopy of X_2Y_4 (D_{2h}) Molecules: Tensorial Formalism Adapted to the $O(3) \supset D_{2h}$ Chain, Hamiltonian and Transition Moment Operators",
W. Raballand, M. Rotger, V. Boudon and M. Loëte,
Journal of Molecular Spectroscopy, **217**, 239–248 (**2003**).

[P21] "The Ground State Rotational Spectrum of SO_2F_2",
M. Rotger, V. Boudon, M. Loëte, L. Margulès, J. Demaison, H. Mäder, G. Winnewisser and H. S. P. Müller,
Journal of Molecular Spectroscopy, **222**, 172–179 (**2003**).
Supplément: "Complete Table of Measured and Assigned Transitions".
Cf. `http://www.sciencedirect.com/science/journal/00222852`.

[P22] "Diode Laser Spectroscopy of the ν_8 Band of the SF_5Cl Molecule",
W. Raballand, N. Benoit, M. Rotger and V. Boudon,
Spectrochimica Acta A, **60**, 3403–3412 (**2003**) (numéro spécial à l'occasion de *TDLS 2003: 4th*

International Conference on Tunable Diode Laser Spectroscopy, 14-18/07 **2003**, Zermatt, Suisse).

[**P23**] "Symmetry-Adapted Tensorial Formalism to Model Rovibrational and Rovibronic Spectra of Molecules Pertaining to Various Point Groups",
V. Boudon, J.-P. Champion, T. Gabard, M. Loëte, F. Michelot, G. Pierre, M. Rotger, Ch. Wenger and M. Rey,
Journal of Molecular Spectroscopy, **228**, 620–634 (**2004**).

[**P24**] "C_{2v} Top Data System (C_{2v}TDS) Software for Infrared Spectrum Simulation of XY_2Z_2 Asymmetric Molecules. Some Improvements to the TDS Packages",
Ch. Wenger, M. Rotger and V. Boudon,
Journal of Quantitative Spectroscopy and Radiative Transfer, **accepté**, (**2004**).

[**P25**] "D_{2h} Top Data System (D_{2h}TDS) Software for Infrared and Raman Spectrum Simulation of X_2Y_4 Asymmetric Molecules.",
Ch. Wenger, W. Raballand, M. Rotger and V. Boudon,
Journal of Quantitative Spectroscopy and Radiative Transfer, **accepté**, (**2005**).

Article à soumettre prochainement

[**P26**] "Stark Hamiltonian for X_2Y_4 (D_{2h}) Molecules using Tensorial Techniques",
W. Raballand, M. Rotger, V. Boudon and M. Loëte,
Journal of Molecular Spectroscopy, **à soumettre**, (début **2005**).

Actes de colloques

[**A1**] "Open-Shell Octahedral Molecules: A First Insight into the Full Rovibronic Problem",
V. Boudon, M. Rey, M. Rotger and M. Loëte,
Proceedings of SPIE, *XIVth Symposium on High Resolution Molecular Spectroscopy, HighRus 2003*, (06-11/07 2003, Krasnoïarsk – Yenisseisk – Krasnoïarsk, Russie), **5311**, 1–13 (**2003**).

Conférences invitées

[**I1**] "*13th International Conference on Raman Spectroscopy*", **1992**, Würzburg (Allemagne) :
"High Resolution Raman Spectroscopies. Recent Performances and Limits of SRS, CARS and PARS"
H. Berger, B. Lavorel, G. Millot, M. Rotger, R. Saint-Loup, R. Chaux and G. Rouillé.

[**I2**] "*Journées de Spectroscopie Moléculaire*", **2004**, Dunkerque :
"De la Toupie Sphérique à la Toupie Asymétrique"
M. Rotger.

Posters présentés lors de colloques

[**C1**] "*Colloque International sur le Soudage et la Fusion par Faisceau d'Electrons et Lasers*", 26-30/09 **1988**, Cannes (France), **un poster** présenté :

- "Laser YAG Industriel de Puissance : Situation Actuelle et Perspectives",
  M. Rotger and B. Taisne.

[**C2**] "*12th Colloquium on High Resolution Molecular Spectroscopy*", 9-13/09 **1991**, Dijon (France), **un poster** présenté :

- "High Resolution Photoacoustic Raman Spectroscopy of Gases",
  M. Rotger, B. Lavorel, R. Chaux and R. Saint-Loup.

[C3] "*12th Colloquium on High Resolution Infrared and Microwave Spectroscopy*", 7-11/09 **1992**, Dobris (République Tchèque), **un poster** présenté :

- "Bideuterated Silane SiH_2D_2 by CARS Experiment",
  M. Betrencourt, J.-C. Deroche, B. Lavorel and M. Rotger

[C4] "*13th Colloquium on High Resolution Molecular Spectroscopy*", 13-17/09 **1993**, Riccione (Italie), **deux posters** présentés :

- "Polarization CARS Spectroscopy of the ν_5 Band of SiH_2D_2",
  M. Rotger, B. Lavorel, M. Betrencourt, J.-C. Deroche and H. Bürger.
- "Analysis of the SiH_2D_2 Pentad near 12 μm",
  M. Betrencourt, J.-C. Deroche, M. Rotger, B. Lavorel, S. Sommer and H. Bürger

[C5] "*14th Colloquium on High Resolution Molecular Spectroscopy*", 11-15/09 **1995**, Dijon (France), **un poster** présenté :

- "Spectroscopy of the Ground and Excited Electronic States of IrF_6",
  V. Boudon and M. Rotger.

[C6] "*15th Colloquium on High Resolution Molecular Spectroscopy*", 31/08-05/09 **1997**, Glasgow (Royaume-Uni), **un poster** présenté :

- "High Resolution Spectroscopy of the ν_3 Band of WF_6 in a Supersonic Jet",
  V. Boudon, M. Rotger, Y. He, U. Schmitt and M. Quack.

[C7] "*3^{ième} Colloque Journées de Spectroscopie Moléculaire*", 07-08/07 **1998** à Reims (France), **un poster** présenté :

- "Calculs *Ab Initio* et Spectroscopie Haute Résolution de la Pentade de Pliage de SiH_2D_2 dans la Région 10-16 μm",
  M. Rotger, V. Boudon, B. Lavorel, S. Sommer, H. Bürger, J. Breidung, W. Thiel, M. Bétrencourt et J.-C. Deroche.

[C8] "*Praha 98 : 15th Conference on High Resolution Molecular Spectroscopy*", 30/08-03/09 **1998**, Prague (Rép. Tchèque), **un poster** présenté :

- "*Ab Initio* Calculations and High Resolution Spectroscopy of the Bending Pentad of SiH_2D_2 in the 10-16 μm Region",
  M. Rotger, V. Boudon, B. Lavorel, S. Sommer, H. Bürger, J. Breidung, W. Thiel, M. Bétrencourt and J.-C. Deroche.

[C9] "*Fourteenth Winter Fluorine Conference*", 17-22/01 **1999**, St. Petersburg Beach (Floride, USA), **un poster** présenté :

- "Absorption Spectrum of the $a(E'_{2g}) \leftarrow X(G'_g)$ and $b(G'_g) \leftarrow X(G'_g)$ Electronic Transitions of ReF_6",
  M. Rotger, V. Boudon and H. Selig.

[C10] "*16th Colloquium on High Resolution Molecular Spectroscopy*", 06-10/09 **1999**, Dijon (France), **quatre posters** présentés :

- "High Resolution Infrared Spectroscopic Study of the ν_3 Band of ReF_6 in a Supersonic Jet Expansion",
  V. Boudon, M. Rotger, Y. He, H. Hollenstein, M. Quack and U. Schmitt.
- "Spectroscopy of XY_5Z (C_{4v}) Symmetric Top Molecules : A Tensorial Formalism Adapted to the Chain $O(3) \supset O_h \supset C_{4v}$ Chain",
  M. Rotger, V. Boudon and M. Loëte.
- "Transition Moments for the XY_5Z (C_{4v}) Symmetric Top Using the Tensorial Formalism",
  M. Rotger, V. Boudon and M. Loëte.
- "Spontaneous Raman Spectroscopy of Closed and Open-Shell Transition-Metal Fluorides",
  M. Rotger, M. Rey, V. Boudon, M. Loëte, A. Lorriaux and H. Selig.

[C11] "*Praha 2000 : 16th Conference on High Resolution Molecular Spectroscopy*", 03-07/09 **2000**, Prague (Rép. Tchèque), **un poster** présenté :

- "C_{4v}TDS Software and its application to the ν_1/ν_8 Dyad of $SF_5{}^{35}Cl$",
  M. Rotger, A. Decrette, V. Boudon, M. Loëte, H. Bürger, S. Sander and H. Willner.

[C12] "*17th Colloquium on High Resolution Molecular Spectroscopy*", 09-13/09 **2001**, Nimègue (Pays-Bas), **trois posters** présentés :

- "High-Resolution Spectroscopy and Analysis of the ν_4 Band of $^{80}SeF_6$",
  M. Rotger, V. Boudon, H. Bürger and H. Willner.
- "Spectroscopy of XY_2Z_2 (C_{2v}) Asymmetric Top Molecules: A Tensorial Formalism Adapted to the $O(3) \supset T_d \supset C_{2v}$ Chain",
  M. Rotger, V. Boudon and M. Loëte.
- "Transition Moments for XY_2Z_2 (C_{2v}) Asymmetric Top Using The Tensorial Formalism – C_{2v} Top Data System Software",
  M. Rotger, V. Boudon and M. Loëte.

[C13] "*Praha 2002 : 17th Conference on High Resolution Molecular Spectroscopy*", 01-05/09 **2002**, Prague (Rép. Tchèque), **deux posters** présentés :

- "Study of Quasi-Spherical XY_2Z_2 Molecules Using Symmetry-Adapted Tensorial Formalism: Application to SO_2F_2",
  M. Rotger, V. Boudon and M. Loëte.
- "Spectroscopy of the Ethylene Molecule: A Tensorial Formalism Adapted to the $O(3) \supset D_{2h}$ Chain",
  W. Raballand, M. Rotger, V. Boudon and M. Loëte.

[C14] "TDLS 2003: 4th International Conference on Tunable Diode Laser Spectroscopy", 14-18/07 **2003**, Zermatt (Suisse), **un poster** présenté :

- "Diode Laser Spectroscopy of the ν_5 band of the SF_5Cl Molecule",
  W. Raballand, N. Benoit, M. Rotger and V. Boudon.

[C15] "*18th Colloquium on High Resolution Molecular Spectroscopy*", 08-12/09 **2003**, Dijon (France), **cinq posters** présentés :

- "Stark Spectroscopy of the Ethylene Molecule: Tensorial Formalism for Spectrum Simulations",
  W. Raballand, M. Rotger, V. Boudon and M. Loëte.
- "D_{2h} Top Data System (D_{2h}TDS) Software for Spectrum Simulation of X_2Y_2 Asymmetric Molecules",
  W. Raballand, Ch. Wenger, M. Rotger, V. Boudon and M. Loëte.
- "Spectroscopy of Octahedral Molecules in a Degenerate Electronic State: Detailed Investigation of the 720 cm^{-1} Region of Jet-Cooled ReF_6",
  M. Rey, V. Boudon, M. Rotger, M. Loëte, H. Hollenstein and M. Quack.
- "*Ab Initio* Calculations on the SF_5Cl Molecule",
  N. Zvereva, M. Rotger, V. Boudon and M. Loëte.
- "The Ground State Rotational Spectrum of SO_2F_2",
  M. Rotger, V. Boudon, M. Loëte, L. Margulès, J. Demaison, H. Mäder, G. Winnewisser and H. S. P. Müller.

[C16] "*Journées de Spectroscopie Moléculaire*", 01/06-03/06 **2004**, Dunkerque (France), **un poster présenté** :

- "Spectroscopie Stark de la Molécule d'Ethylène : Formalisme Tensoriel et Simulation de Spectres",
  W. Raballand, M. Rotger, V. Boudon and M. Loëte.

[C17] "*18th International Conference on High Resolution Molecular Spectroscopy*", 08-12/09 **2004**, Prague ((Rép. Tchèque),), **trois posters** présentés :

- "Symmetry Adapted Tensorial Formalism for the Spectroscopy of the SO_2F_2 Quasi-Spherical Top: Application to the Bending Triad",
  M. Rotger, V. Boudon, N. Zvereva-Loëte and M. Loëte.
- "Rovibrational Parameters for the Ground State and the $\nu_3/\nu_7/\nu_9$ Triad of the SO_2F_2 Asymmetric Molecule",
  M. Rotger, V. Boudon, N. Zvereva-Loëte and M. Loëte.
- "Stark Effect Using Tensorial Formalism in the D_{2h} Group: Applications to the C_2H_4 Molecule",
  M. Rotger, V. Boudon, N. Zvereva-Loëte and M. Loëte.

Communications orales présentées lors de colloques

[O1] "*56th Ohio State University International Symposium on Molecular Spectroscopy*", 11-15/06 **2001**, Columbus, Ohio (USA) : **une communication** présentée :

- "Extension of the STDS/HTDS Software to Rovibronic Spectroscopy and to Lower Symmetry Problems",
  V. Boudon, M. Rey, M. Rotger and M. Loëte. *Présentée par V.* Boudon,
  Mini-symposium "*Spectroscopic Freeware*".

[O2] "*57th Ohio State University International Symposium on Molecular Spectroscopy*", 17-21/06 **2002**, Columbus, Ohio (USA) : **une communication** présentée :

- "Study of Distorted Spherical Tops Using Symmetry-Adapted Tensorial Formalism: Application to SF_5Cl and SO_2F_2",
  M. Rotger, V. Boudon and M. Loëte. *Présentée par M.* Rotger.

[O3] "*Séminaire National de Spectroscopie – SNS'02*", 15-17/12 **2002**, Saïda (Algérie) : **une communication** présentée :

- "STDS, HTDS, C_{2v}TDS, C_{4v}TDS, MIRS, GROUP : Un Ensemble de Logiciels Développés pour la Spectroscopie Moléculaire",
  Ch. Wenger, V. Boudon, M. Rotger, M. Rey, J.-P. Champion, A. Nikitin and G. Pierre. *Présentée par Ch. Wenger.*

[O4] "*58th Ohio State University International Symposium on Molecular Spectroscopy*", 16-20/06 **2003**, Columbus, Ohio (USA) : **deux communications** présentées :

- "The Ground State Rotational Spectrum of SO_2F_2",
  M. Rotger, V. Boudon, M. Loëte, L. Margulès, J. Demaison, H. Mäder, G. Winnewisser and H. S. P. Müller. *Présentée par M.* Rotger.
- "Spectroscopy of X_2Y_4 (D_{2h}) Molecules: Tensorial Formalism Adapted to the $O(3) \supset D_{2h}$ Chain, Hamiltonian and Transition Moment Operators. Application to the ν_{12} and ν_2 Bands of C_2H_4",
  M. Rotger, W. Raballand, V. Boudon and M. Loëte. *Présentée par M.* Rotger.

[O5] "*Bunsentagung 2004*", 20-22/05 **2004**, Dresden (Allemagne) : **une communication** présentée :

- "Rovibronic Spectroscopy of some Open-Shell Spherical Top Molecules: ReF_6",
  M. Rey, V. Boudon, M. Rotger, M. M. Loëte, H. Hollenstein and M. Quack. *Présentée par M.* Quack.

[O6] "*59th Ohio State University International Symposium on Molecular Spectroscopy*", 21-25/06 **2004**, Columbus, Ohio (USA) : **trois communications** présentées :

- "The Use of Tensorial Formalism in Molecular Spectroscopy: Advantadges and Recent Advances",

V. Boudon, J.-P. Champion, T. Gabard, M. Loëte, F. Michelot, G. Pierre, M. Rotger and Ch. Wenger. *Présentée par V.* Boudon.

– "Stark Effect Using Tensirial formalism in the D_{2h} Group: Application to the C_2H_4 Molecule",
W. Raballand, M. Rotger, V. Boudon and M. Loëte. *Présentée par M.* Rotger.

– "Symmetry-Adapted Tensorial Formalism for the Spectroscopy of the SO_2F_2 Quasi-Spherical Top: Application to the Bending Triad",
M. Rotger, V. Boudon M. Loëte and N. Zvereva-Loëte. *Présentée par M.* Rotger.

Séminaires et communications orales diverses

[**S1**] **Séminaire** présenté au *Laboratorium für Physikalische Chemie* de *l'Ecole Polytechnique Fédérale de Zürich* (Suisse) le 10/07/**1996** à l'invitation du Pr. M. Quack.
"Spectroscopy of Transition-Metal Hexafluorides",
M. Rotger and V. Boudon. *Présenté par V.* Boudon et M. Rotger.

[**S2**] **Séminaire** présenté à la *Société COMURHEX* (Pierrelatte) le 06/11/**2002** à l'invitation de Mme C. Belhomme et de Mr. B. Morel.
"Eléments de Spectroscopie Moléculaire",
M. Rotger et V. Boudon. *Présenté par M.* Rotger *et V.* Boudon.